Model systems for exploring new therapeutic interventions and disease mechanisms in spinal muscular atrophies (SMAs)

James N. Sleigh

Hertford College

University of Oxford

Supervisor: Professor Kevin Talbot

Co-supervisor: Professor Dame Kay E. Davies

Past Supervisor: Professor David B. Sattelle

Thesis submitted for the degree of Doctor of Philosophy

Trinity Term 2012

Abstract

Model systems for exploring new therapeutic interventions and disease mechanisms in spinal muscular atrophies (SMAs)

James N. Sleigh, Hertford College, University of Oxford

Submitted for the degree of Doctor of Philosophy, Trinity Term, 2012

Spinal muscular atrophy (SMA) and Charcot-Marie-Tooth disease type 2D (CMT2D)/distal SMA type V (dSMAV) are two incurable neuromuscular disorders that predominantly manifest during childhood and adolescence. Both conditions are caused by mutations in widely and constitutively expressed genes that encode proteins with essential housekeeping functions, yet display specific lower motor neuron pathology. SMA results from recessive inactivating mutations in the *survival motor neuron 1* (*SMN1*) gene, while CMT2D/dSMAV manifests due to dominant point mutations in the glycyl-tRNA synthetase (GlyRS) gene, *GARS*. Using a number of different model systems, ranging from *Caenorhabditis elegans* to the mouse, this thesis aimed to identify potential novel therapeutic compounds for SMA, and to increase our understanding of the mechanisms underlying both diseases. I characterised a novel *C. elegans* allele, which possesses a point mutation in the worm *SMN1* orthologue, *smn-1*, and showed its potential for large-scale screening by highlighting 4-aminopyridine in a screen for compounds able to improve the mutant motility defect. Previously, the gene encoding three isoforms of chondrolectin (*Chodl*) was shown to be alternatively spliced in the spinal cord of SMA mice before disease onset. I performed functional analyses of the three isoforms in neuronal cells with experimentally reduced Smn levels, and determined that the dysregulation of *Chodl* likely reflects a combination of compensatory mechanism and contributor to pathology, rather than mis-splicing. Finally, working with two *Gars* mutant mice and a new *Drosophila* model, I have implicated semaphorin-plexin pathways and axonal guidance in the GlyRS toxic gain-of-function disease mechanism of CMT2D/dSMAV.

Declaration

The work presented in this thesis was conducted by the author (James N. Sleigh) unless stated otherwise. The research was carried out during 2009-2012 at the MRC Functional Genomics Unit, Department of Physiology, Anatomy and Genetics, University of Oxford, UK and The Jackson Laboratory, Bar Harbor ME, USA. No part of this thesis has been submitted for any other degree at this or any other university or institute of learning.

Acknowledgements

First and foremost, I would like to thank Prof. David B. Sattelle, Prof. Kevin Talbot, and Prof. Dame Kay E. Davies for their constant encouragement of my work. I have learnt a vast amount from all three supervisors, and I will always be grateful to them for permitting me the independence to make the DPhil my own. I am equally indebted to Dr. M. Zameel Cader and Dr. Robert W. Burgess for their rewarding and inspiring collaboration, and allowing me to broaden my scientific horizons. I would also like to thank Prof. Thomas H. Gillingwater, Dr. Simon H. Parson, and all members of Gillingwater and Parson Groups for teaching me some invaluable techniques.

The MRC Functional Genomics Unit and The Jackson Laboratory have both provided a supportive and intellectually stimulating setting for my DPhil. In particular, I would like to thank the following people for their encouragement, expertise, and, above all, patience: Dr. Neza Alfazema, Dr. Andrew R. Bassett, Dr. Esther B. Becker, Dr. Angeliki Biba, Dr. Laurent P. Bogdanik, Dr. Steven D. Buckingham, Dr. Carmen H. Coxon, Dr. Andrew K. Jones, Dr. Peter L. Oliver, Dr. Kevin L. Seburn, and Dr. Tamara M. Sirey.

I must also acknowledge the MRC for funding my three year DPhil, the Jennifer Trust for Spinal Muscular Atrophy for their Research Correspondent Scholarship, and the Society of Biology for their Travelling Fellowship. The fellowship, combined with grants from Hertford College and the Department of Physiology, Anatomy and Genetics at the University of Oxford gave me the fantastic opportunity to work in the Burgess Laboratory at The Jackson Laboratory.

The work presented in chapter 3 would not have been possible without Dr. Steven D. Buckingham's brilliant, time-saving software, Dr. Behrooz Esmaeili's knowledge of the *C. elegans* nervous system, and the generation of the worm model by Dr. Mohan Viswanathan, Dr. Edwin Cuppen, and Dr. Bethany M. Westlund.

The work of chapter 5 was done in close collaboration with Dr. Stuart J. Grice, who performed all of the experiments involving *Drosophila*. I would like to say a very big thank you to Stuart for sharing his work and providing great advice, motivation, and all the pints. The WHEP-deletion cell secretion work was performed by Weiwei He and Xiang-Lei Yang.

Finally, without the love and support of my girls, Amelia, Azara-Jane, Helen, and Kathleen, none of this would have been possible - I will be forever in your debt.

This thesis is dedicated to my late father, Nicholas Wilfred Sleigh (1956-2007), who helped foster the scientist in me.

Table of contents

List of figures and tables

Abbreviations

4-AP	4-aminopyridine
AChR	acetylcholine receptor
ANOVA	analysis of variance
ARS	aminoacyl-tRNA synthetase
CHODL	chondrolectin
CLEC	C-type lectin
CMT	Charcot-Marie-Tooth
CMT2D	CMT disease type 2D
CTLD	C-type lectin-like domain
DLG	discs large
DMEM	Dulbecco's Modified Eagle Medium
DMSO	dimethyl sulphoxide
dSMAV	distal SMA type V
EV	empty vector
FBS	foetal bovine serum
GABA	gamma-aminobutyric acid
GAPDH	glyceraldehyde 3-phosphate dehydrogenase
GARS	GlyRS gene
GlyRS	glycyl-tRNA synthetase
HRP	horseradish peroxidase
MTT	thiazolyl blue tetrazolium bromide
NCV	nerve conduction velocity
Neu5Ac	N-acetylneuraminic acid

NINDS	National Institute of Neurological Disorders and Stroke
NMJ	neuromuscular junction
NS	not significant
PFA	paraformaldehyde
qPCR	quantitative RT-PCR
RNAi	RNA interference
RT	room temperature
RT-PCR	reverse transcription-PCR
SDS	sodium dodecyl sulphate
SEM	standard error of the mean
siRNA	short interfering RNA
SMA	spinal muscular atrophy
SMN	survival motor neuron
SNb/d	segmental nerve b/d
snRNA	small nuclear RNA
snRNP	small nuclear ribonucleoprotein
SP	signal peptide
TMD	transmembrane domain
TN	transverse nerve
Tris-HCl	tris(hydroxymethyl)aminomethane hydrochloride
TRPC3	transient receptor potential cation channel, type C3

1. Introduction

With a combined frequency of at least 1 in 3,000, human neuromuscular diseases pose a major physical, emotional, and financial burden on patients, their families, and society (Emery 1991). Neuromuscular disorders are estimated to cost ≈ €30,000 per person every year, which in Europe alone, amounted to ≈ €7.7 billion in 2010 (Olesen *et al.* 2012). They often present abruptly with dramatic progressive decline in motor function and lead to premature death. Despite improvements in diagnosis resulting from the identification of causative disease genes, the underlying pathological mechanisms remain largely elusive and physical therapy with palliative care is frequently the only available treatment option.

In this thesis, I will present work on two neuromuscular diseases, spinal muscular atrophy (SMA) and Charcot-Marie-Tooth disease type 2D (CMT2D)/distal SMA type V (dSMAV), both of which display predominantly lower motor neuron pathology and are caused by mutations in highly conserved housekeeping genes that encode proteins vital for cellular viability. In this chapter, I will provide an overview of SMA followed by CMT2D, reviewing salient features of each disease, highlighting some of the available animal models, and discussing possible disease mechanisms. Chapters 3 and 4 focus on SMA, and describe a new *Caenorhabditis elegans* model for SMA and assess the role that a protein called chondrolectin may be playing in early stages of the disease, respectively. I then move on to CMT2D in chapter 5, and, using various different models including two available mouse mutants, identify novel features of disease pathology and a potential mechanism to explain the neuronal specificity seen in the disease.

With permission from The Company of Biologists, large parts of the sections on SMA in the following chapter, excluding those discussing invertebrate models, are adapted from

the published review article Sleigh JN, Gillingwater TH, Talbot K. 2011. The contribution of mouse models to understanding the pathogenesis of spinal muscular atrophy. Dis Model Mech *4: 457-67. By permission of John Wiley and Sons, the discussion of invertebrate models of SMA is adapted from the published review article Grice SJ, Sleigh JN, Liu JL, Sattelle DB. 2011. Invertebrate models of spinal muscular atrophy: insights into mechanisms and potential therapeutics.* Bioessays *33: 956-65. As the first author and joint first author of the above two publications, I took the lead on writing the sections that are included in this thesis.*

1.1 Spinal muscular atrophy

Spinal muscular atrophy (SMA), characterised by the selective degeneration of spinal cord lower motor neurons leading to proximal muscle wasting and paralysis, is an autosomal recessive disease affecting ≈ 1 in 6-10,000 live births (Ogino & Wilson 2002, Pearn 1978, Prior *et al.* 2010). Although there is a wide spectrum of clinical severity based on age of onset and motor ability (types I-IV, Table 1.1), in its commonest and most severe form (type I), SMA leads to death from respiratory muscle weakness in infancy (Lunn & Wang 2008, Munsat & Davies 1992). Most patients with non-fatal forms of SMA are considerably disabled and there is an urgent need for treatments that slow or arrest progression.

SMA type	Age at onset	Life expectancy	Motor milestones achieved
I (Werdnig-Hoffman disease)	< 6 months	< 2 years	Cannot sit unaided
II (intermediate form)	6-18 months	10-40 years	Cannot stand unaided
III (Kugelberg-Welander disease)	> 18 months	Normal	Walk short distances unaided
IV (adult-onset form)	20-30 years	Normal	Walk normally

Table 1.1. Classification of SMA.

1.1.1 The genetics of SMA

SMA is caused by attenuated function of the survival motor neuron (SMN) protein. Due to an intrachromosomal duplication event on chromosome 5q13, humans possess two copies of the *SMN* gene, *SMN1* and *SMN2* (Figure 1.1), that are 99.9% identical at the sequence level (Lefebvre *et al.* 1995, Monani *et al.* 1999). Deletion or gene conversion events render SMA patients homozygously null for *SMN1*, while they retain a variable number of *SMN2* copies. A critical C-to-T transition 6 base pairs into exon 7 of *SMN2* causes aberrant splicing of 80-90% of transcripts, causing them to lack exon 7 (*SMNΔ7*) and therefore produce a protein product with reduced function and stability (Lorson & Androphy 2000, Lorson *et al.* 1999, Monani *et al.* 1999). SMN levels generally correlate with disease severity (Coovert *et al.* 1997, Lefebvre *et al.* 1997), and because complete loss of SMN is lethal, SMA only arises as a disease in humans due to the presence of *SMN2*, which provides sufficient residual full-length protein for cellular viability (Feldkötter *et al.* 2002, Mailman *et al.* 2002, McAndrew *et al.* 1997). SMA is therefore a disease of low levels of SMN protein and not total ablation, a situation that any model system, either *in vitro* or *in vivo*, must reproduce in order to provide meaningful insights.

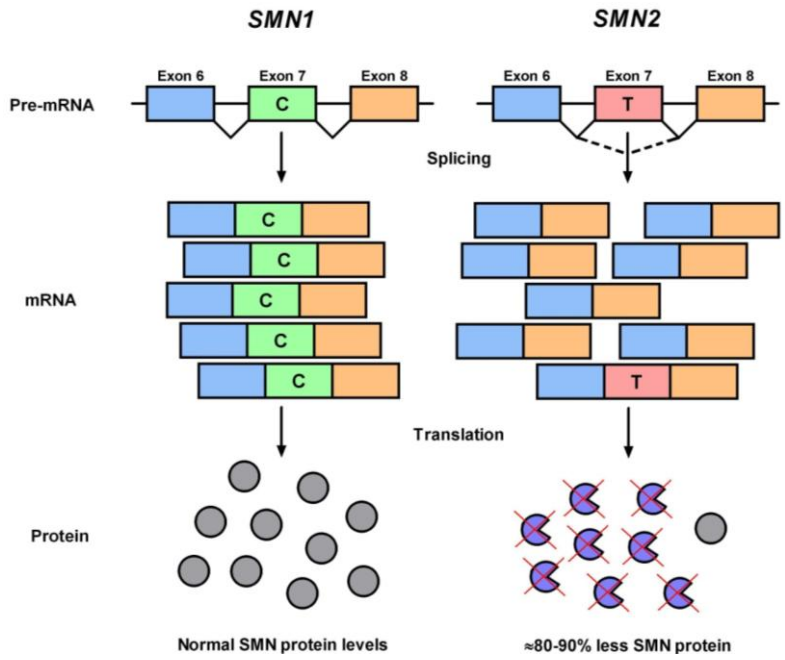

Figure 1.1. SMA genetics. Humans have two, almost identical, genes encoding SMN protein: *SMN1* and *SMN2* (Lefebvre *et al.* 1995). *SMN1* produces fully functional, full-length SMN protein, whereas *SMN2*, due to a translationally silent C-to-T transition, predominantly produces transcripts lacking exon 7 (80-90%), resulting in a truncated and unstable protein (Lorson & Androphy 2000, Monani *et al.* 1999). Mutations in *SMN1* lead to SMA, while loss of *SMN2* alone has no adverse effect (Burghes 1997). Since *SMN2* produces small amounts of SMN protein, *SMN2* copy number inversely correlates with disease severity (Mailman *et al.* 2002, McAndrew *et al.* 1997). SMA is thus a disease of low SMN levels and not absence, which is universally cell lethal. Figure adapted from Burghes & Beattie (2009).

1.1.2 SMN protein function

SMN is widely and constitutively found and has been implicated in a number of fundamental cellular processes including axonal transport (Pagliardini *et al.* 2000, Rossoll *et al.* 2003, Zhang *et al.* 2003), transcription (Pellizzoni *et al.* 2001b), small nucleolar ribonucleoprotein biogenesis (Pellizzoni *et al.* 2001a), and stem cell maintenance (Grice & Liu 2011); nonetheless, its unequivocal housekeeping function is to assemble and process small nuclear ribonucleoproteins (snRNPs) (Fischer *et al.* 1997, Liu *et al.* 1997, Pellizzoni *et al.* 1998, Meister *et al.* 2001, Pellizzoni *et al.* 2002). In this process, SMN self-

oligomerises and interacts with Gemins 2-8 and unrip forming the SMN complex (Figure 1.2A), which ensures the specific and efficient assembly of a stable heptameric ring of Sm proteins (forming the Sm core) onto newly exported small nuclear ribonucleic acids (snRNAs) (Pellizzoni 2007). After further maturation steps, the resulting snRNPs are exported into the nucleus and function in the catalytic removal of introns from pre-mRNA transcripts in the process of splicing (Pellizzoni *et al.* 2002). Depending on the class of intron removed, there are two principal types of spliceosomal snRNP assembled by the SMN complex: those found in the major spliceosome, which processes almost all eukaryotic introns, and those that splice all other introns as part of the minor spliceosome (Patel & Steitz 2003). Five snRNPs consisting of the snRNAs U1, U2, U4, U5, and U6 and many other proteins including the Sm core constitute the major spliceosome, whereas the minor spliceosome makes use of different snRNAs (U5, U11, U12, U4atac, and U6atac) and distinct regulatory sequences (Patel & Steitz 2003).

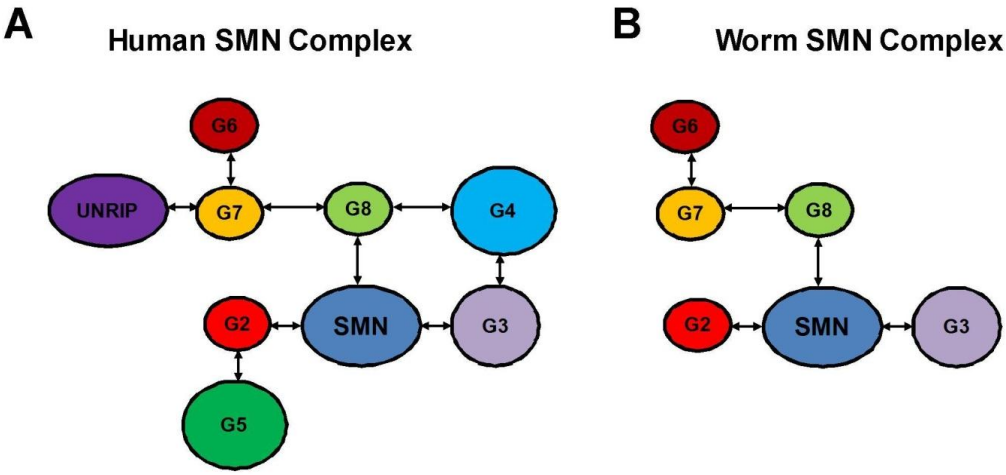

Figure 1.2. The SMN complex. Schematics of the interactions between core protein components of the SMN complex in humans (A) and *C. elegans* (B). The exact stoichiometry and number of sub-complexes of the constituent components is not known. Gemin proteins are labelled with the letter G and relevant number. Figure adapted from Grice *et al.* (2011), Kroiss *et al.* (2008), and Otter *et al.* (2007).

1.1.3 Models for SMA

Given the fundamental cellular role of SMN, the *SMN* gene is highly conserved. The effects of SMN protein depletion have therefore been modeled in diverse organisms, including the invertebrates *C. elegans* (Briese *et al.* 2009, Miguel-Aliaga *et al.* 1999, Sleigh *et al.* 2011a) and *Drosophila* (Chan *et al.* 2003, Chang *et al.* 2008, Grice & Liu 2011, Miguel-Aliaga *et al.* 2000), and the vertebrates *Danio rerio* (Boon *et al.* 2009, Carrel *et al.* 2006, McWhorter *et al.* 2003, Oprea *et al.* 2008, Winkler *et al.* 2005) and *Mus musculus* (Hsieh-Li *et al.* 2000, Le *et al.* 2005, Monani *et al.* 2000, Schrank *et al.* 1997, Sleigh *et al.* 2011b). All species used to model SMA possess only a single copy of the *SMN* gene, the homozygous deletion of which leads to lethality when any maternally contributed protein or mRNA becomes depleted. I will now focus on *C. elegans* and mouse models of the disease.

1.1.3.1 *C. elegans* as a model for SMA

C. elegans is a small (1.0-1.5 mm), optically transparent, hermaphroditic nematode worm with fast generation time (≈ 3 days), large reproductive capacity (250-300 offspring), and short lifespan (≈ 3 weeks), so it can be quickly and cheaply cultured in the laboratory. After hatching from eggs, worms develop through four larval stages (L1-L4) before reaching adulthood. *C. elegans* was the first complex animal to have its genome sequenced (The *C. elegans* Sequencing Consortium 1998). Its entire cell lineage has been reconstructed, which includes 302 neurons and 95 body wall muscles, and it remains the only organism for which a complete nervous system wiring diagram is available (White *et al.* 1986). There is a surprisingly high level of genetic conservation between humans and the worm (Culetto & Sattelle 2000, Harris *et al.* 2004, Rubin *et al.* 2000), which is essential for the dissection of pathological mechanisms of disease and the identification of

compounds with the potential to treat them. Importantly, despite differences in neuromuscular development and architecture, the mechanism of synaptic transmission at the *C. elegans* neuromuscular junction (NMJ) is largely similar to that of humans. The excitatory neurotransmitter at the nematode NMJ is acetylcholine, so there is a great deal of homology with pre- and post-synaptic human proteins (Rand 2007), for instance genes encoding acetylcholine receptor (AChR) subunits (Jones & Sattelle 2004), acetylcholinesterase (Johnson & Russell 1983, Kolson & Russell 1985), choline acetyltransferase (Rand & Russell 1985), choline transporter (Okuda *et al.* 2000), and vesicular acetylcholine transporter (Alfonso *et al.* 1993) are all conserved in worms. Accordingly, *C. elegans* has been used to model numerous nervous system and neuromuscular disorders, and is a common tool for large-scale screening of genetic knockdown and chemical compound libraries (Dimitriadi & Hart 2010, Sleigh & Sattelle 2010).

1.1.3.1.1 *C. elegans SMN*

The *C. elegans SMN* orthologue, *smn-1*, was first putatively identified due to its high sequence similarity with the terminal regions of human and fission yeast *SMN* (Talbot *et al.* 1997). Similar to the situation in humans, *smn-1* is expressed in most cells throughout development and its protein product localises to both the nucleus and cytoplasm (Miguel-Aliaga *et al.* 1999). *In vitro*, SMN-1 retains the potential to self-oligomerise, bind to RNA, and interact with known SMN-binding partners such as worm Gemin2 (SMI-1) and the RNA processing protein fibrillarin (FIB-1), indicating that functional capability is conserved (Bertrandy *et al.* 1999, Burt *et al.* 2006, Miguel-Aliaga *et al.* 1999). Similar to in the mouse, the spatiotemporal patterns of SMN-1 and SMI-1 largely overlap and complete depletion of either protein results in embryonic lethality (Burt *et al.* 2006,

Jablonka *et al.* 2001, Jablonka *et al.* 2002). In addition to Gemin2, four of the remaining six Gemin proteins (3, 6, 7, and 8) have orthologues in *C. elegans* (Figure 1.2B), and the Sm protein-binding region of SMN-1 is highly conserved (Bertrandy *et al.* 1999, Kroiss *et al.* 2008).

1.1.3.1.2 The *C. elegans smn-1* null mutant

The first *C. elegans smn-1* allele, *smn-1(ok355),* is a genetic null that possesses a deletion removing all but 87 bp at the 3' end of the gene (Briese *et al.* 2009). Since *smn-1* deletion is homozygous lethal, the *ok355* allele is maintained using a balancer chromosome that allows the differentiation of genotypes using green fluorescent protein (GFP). Maternally loaded SMN-1 from the heterozygous parental generation allows early larval development to proceed as normal. At later stages, the null mutant displays defects in growth and fertility, possesses a pale, starved appearance, and dies before adulthood. Moreover, neuromuscular function rapidly and progressively declines in early larval stages; specifically, both swimming (thrashing) rate in solution and pharyngeal pumping rate (feeding behaviour) become significantly reduced. Nevertheless, *smn-1(ok355)* animals are indistinguishable from wild type for up to two days post-hatching, suggesting both that muscles are successfully targeted and reached by developing motor neurons (likely due to maternal SMN-1 contribution) and that SMN-1 plays a vital role in later development and adult life, as indicated in mice (Briese *et al.* 2009, Jablonka *et al.* 2000).

1.1.3.1.3 Genome-scale modifier screens of invertebrate SMN loss-of-function defects

The power of using invertebrate models to study human neuromuscular disease was recently exemplified in a collaborative effort based at Harvard Medical School using

Drosophila and *C. elegans* models of SMA in tandem to identify novel disease-relevant genetic pathways. The theory behind using two invertebrates separated by ≈ 500 million years of evolution is that modifier genes identified in both species are more likely to be conserved in humans.

Using the Exelixis collection of transposon-induced mutations, Chang *et al.* first performed a genome-scale (≈ 50% coverage) screen for enhancers and suppressors of the larval lethal phenotype of a *Drosophila smn* mutant (Chang *et al.* 2008). In total, 27 genes were highlighted, nearly all of which were subsequently confirmed to modify a second phenotype of NMJ degeneration, a pathological hallmark of SMA in humans that is also observed in zebrafish and mice (Boon *et al.* 2009, Kariya *et al.* 2008, Martínez-Hernández *et al.* 2012, Murray *et al.* 2008). Anne C. Hart and colleagues then used the worm null mutant in a genome-wide RNA interference (RNAi) screen to identify modifiers of the growth defect (Dimitriadi *et al.* 2010). Genes highlighted by this screen and orthologues of hits from the fly screen were subsequently re-tested for rescue of both the pharyngeal pumping and growth defects. Orthologues of the genes identified in *C. elegans* were simultaneously assayed at the *Drosophila* NMJ. In all, fifteen genes were designated as cross-species modifiers, the majority of which were concordant between models, i.e. an enhancer in the fly was also an enhancer in the worm, improving confidence in the reliability of the results. Crucially, reduced function of invertebrate orthologues of Plastin 3, the only human genetic modifier of SMA identified other than *SMN2* (Oprea *et al.* 2008), exacerbated SMN loss-of-function defects, serving as a proof-of-principle that modifiers can be successfully identified in invertebrates (Dimitriadi *et al.* 2010). Plastin 3 levels have since been shown to modify the phenotype of both zebrafish and mouse models of SMA (Ackermann *et al.* 2013, Hao le *et al.* 2012). Interestingly, the screen highlighted a number of conserved genes involved in endocytosis and mRNA regulation

pathways, suggesting that these processes may be particularly crucial for motor neuron integrity in SMA. In a separate study, two additional RNA-binding splicing factors have also been implicated in transmission at the *C. elegans* synapse (Loria *et al.* 2003). Together, this suggests that dysregulated RNA processing in motor neurons may play a pivotal role in the reduced synaptic neurotransmission seen in SMA models and could thus be of particular significance to SMA pathogenesis.

1.1.3.2 Mouse models of SMA

Since the essential elements of the organisation of neuromuscular function are conserved across ≈ 50 million years of evolution between mice and humans, mouse models are probably best placed to answer fundamental questions about SMN biology in the nervous system and the pathogenesis of SMA. Indeed, the development, structure, and function of the mouse NMJ very closely resemble that of the human neuromuscular synapse. Mouse models not only allow the dissection of biological processes and assessment of gene and protein function in a mammalian context, but are a useful preclinical tool for testing potential therapies. Thus, an ideal mouse model of SMA should faithfully recapitulate the cellular levels of SMN protein seen in patients in order to preserve the relative selectivity for motor neuron degeneration. Levels that are too low, such as can be found in models involving tissue-specific ablation of *Smn* (Frugier *et al.* 2000), will simply induce cell death through disrupting the constitutive cellular function of Smn, providing limited insight into motor neuron vulnerability. The level of *Smn* expression should ideally also be titrated to ensure that the mouse lives long enough for phenotypic analysis and therapeutic trials.

1.1.3.2.1 *SMN2* transgenic mice

Mice possess a single *Smn* gene that has 82% amino acid identity with its human orthologue and a similar expression pattern (Bergin *et al.* 1997, DiDonato *et al.* 1997, Viollet *et al.* 1997). Homozygous *Smn* deletion results in massive embryonic cell death before implantation (Schrank *et al.* 1997). Heterozygous null mice lack a marked clinical phenotype, though some reports suggest that there is histologically detectable, age-dependent loss of neuromuscular integrity (Balabanian *et al.* 2007, Jablonka *et al.* 2000, Schrank *et al.* 1997). A number of different strategies have been employed to produce models that recapitulate the human genotype (summarised in Sleigh *et al.* (2011b), with further information at http://jaxmice.jax.org/list/ra1733.html). Two groups showed that expression of a human *SMN2* transgene on the *Smn* null background rescues embryonic lethality, and that transgene copy number modifies severity (Hsieh-Li *et al.* 2000, Monani *et al.* 2000). Mice carrying one or two copies of *SMN2* (*Smn*$^{-/-}$; *SMN2*$^{+/+}$) are indistinguishable from controls at birth but die before postnatal day 7 (P7). Mice with four or more copies of *SMN2* show complete rescue and a normal lifespan, indicating that modestly enhancing levels of full-length SMN from the *SMN2* gene can prevent SMA, confirming the idea that enhancing *SMN2* expression is a potential therapeutic strategy.

1.1.3.2.2 Modifications to the severe *Smn*$^{-/-}$; *SMN2*$^{+/+}$ mouse

Introduction of a second transgene containing human SMNΔ7 cDNA into the *Smn*$^{-/-}$; *SMN2*$^{+/+}$ model extends lifespan from 6 to 13 days (Le *et al.* 2005). Initially generated to assess potential SMNΔ7 toxicity (Kerr *et al.* 2000), the 'SMNΔ7' model (*Smn*$^{-/-}$; *SMN2*$^{+/+}$; *SMNΔ7*$^{+/+}$), which is still in effect a model of severe postnatal SMA, is thought to be milder due to the formation of heterologous complexes between full-length SMN and SMNΔ7, which might stabilise SMN and affect its turnover. The *Smn*$^{-/-}$; *SMN2*$^{+/+}$ mouse and its modification, the SMNΔ7 mouse, have become the most widely used SMA models

(see Figure 1.3 for some of the major symptomatic events observed during their development). A number of other transgenes containing point mutations in *SMN1* (A2G, A111G) have also been introduced into the *Smn*$^{-/-}$; *SMN2*$^{+/+}$ model, resulting in increased lifespan (Monani *et al.* 2003, Workman *et al.* 2009). However, unlike *SMN2*, which generates a small amount of full-length protein, none of the other transgenes rescue the embryonic lethality caused by *Smn* deletion, indicating that full-length SMN is an absolute requirement for function of the SMN complex. Using a slightly different approach to reduce Smn levels, a knock-in allele that disturbs endogenous *Smn* splicing (*Smn*$^{2B/-}$), similar to human *SMN2*, was shown to result in more moderate severity, with a few animals living longer than a month (Bowerman *et al.* 2009).

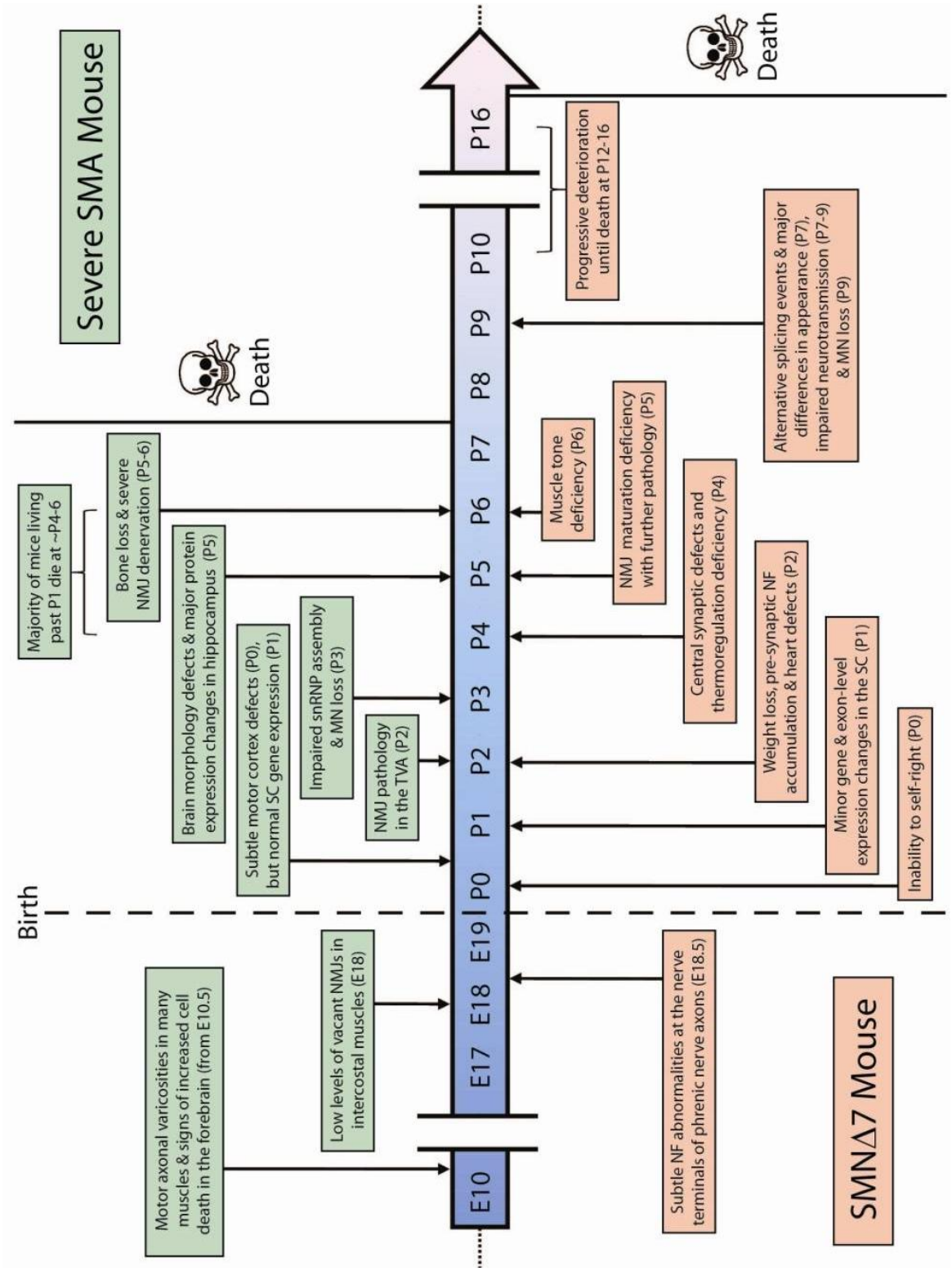

Figure 1.3. Timeline illustrating major cellular and symptomatic events during the embryonic and postnatal development of *Smn*$^{-/-}$; *SMN2*$^{+/+}$ and SMNΔ7 mouse models of SMA. MN motor neuron, NF neurofilament, SC spinal cord, snRNP small nuclear ribonucleoprotein, TVA transversus abdominis. Figure taken with permission from The Company of Biologists from Sleigh *et al.* (2011b).

1.1.3.2.3 Cre-loxP models

Targeting of genomic DNA using the Cre-loxP recombination system to perform deletion of *Smn* exon 7 from a conditional (floxed) allele (Smn^{F7}) should theoretically result in the sole production of SmnΔ7 and complete absence of full-length Smn in the presence of Cre recombinase. Indeed, crossing these mice with tissue-specific Cre mouse lines effectively produces complete cellular knockdown of *Smn* in target tissues (Cifuentes-Diaz *et al.* 2001, Cifuentes-Diaz *et al.* 2002, Frugier *et al.* 2000, Nicole *et al.* 2003, Vitte *et al.* 2004). The complete absence of functional Smn, which never occurs in patients, suggests that these models provide only limited insights into the pathogenesis of SMA; however, the absence of convincing data regarding whether complete ablation of full-length Smn is achieved at a range of time points precludes a definitive judgement. A more recently published study in which endogenous Smn was conditionally depleted in motor neuron progenitor cells, but importantly low SMN levels remained due to the presence of transgenic human *SMN2*, provides a potentially better model of the disease (Park *et al.* 2010). However, the presence of normal levels of Smn in tissues other than motor neurons appears to result in an unexpectedly mild phenotype, hinting that SMA might be more subject to systemic effects than previously appreciated.

1.1.4 Selective vulnerability of lower motor neurons in SMA

The central role of SMN in such a fundamental cellular process as snRNP biogenesis provides an adequate explanation as to why complete absence of the protein is universally lethal, and why there is evidence for non-motor neuron pathology in the most severe forms of the disease where SMN depletion is most drastic (Figure 1.4). However, why lower motor neurons appear to be preferentially susceptible to a reduction in SMN remains the central conundrum of SMA research. A number of theories have been posited to explain

this selectivity (Figure 1.5). It is possible that the motor nerves require relatively more snRNP assembly than other cell types and are therefore uniquely susceptible to a global splicing deficiency, or that disturbed splicing of one or a subset of lower motor neuron-specific genes triggers cellular degeneration. More simply, SMN protein levels may be lower in the lower motor nerves, due to a neuron-specific negative feedback loop affecting *SMN2* exon 7 inclusion, disrupting a common cellular function (Jodelka *et al.* 2010, Ruggiu *et al.* 2012). Alternatively, SMN might have a distinct motor neuron-specific role, as suggested by the presence of SMN in protein complexes in the axon that have a different makeup than the canonical SMN complex that is involved in snRNP assembly (Briese *et al.*, 2005; Rossoll and Bassell, 2009). Moreover, it is plausible that all of the above explanations could contribute to pathology.

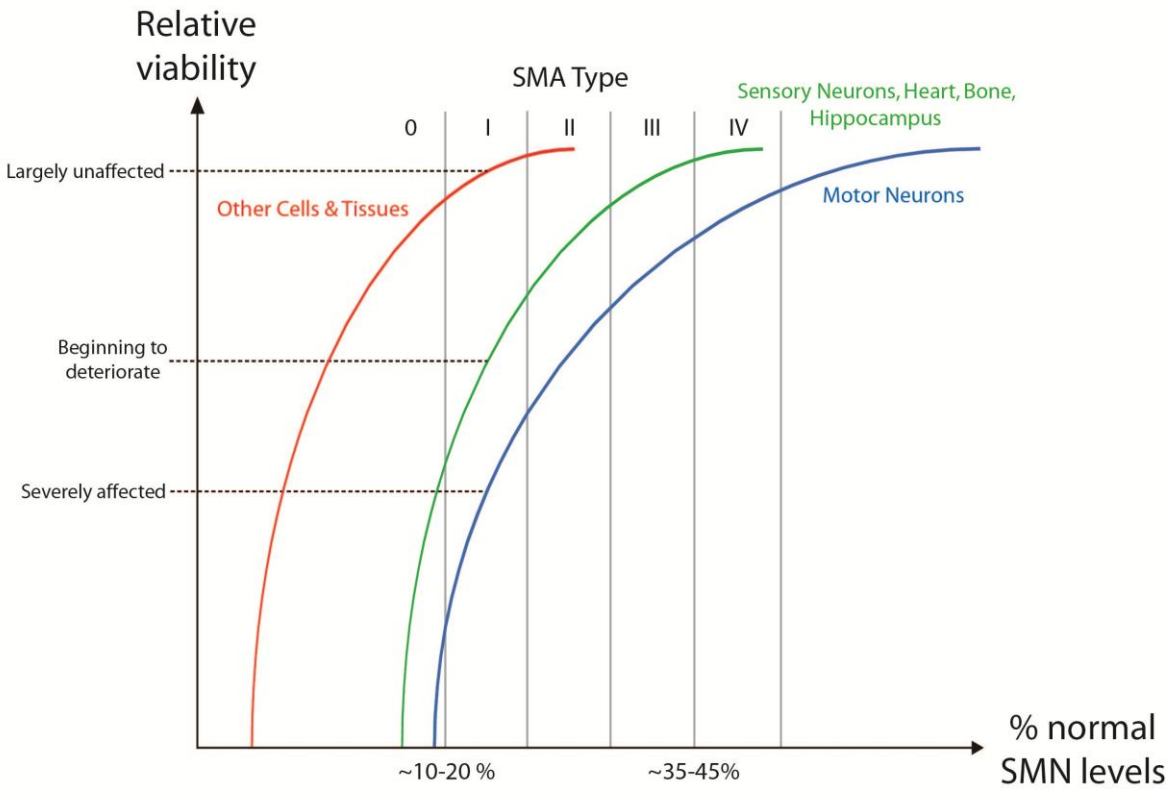

Figure 1.4. The threshold hypothesis of SMA. In the most severe SMA patients, pathology does not appear to be restricted to the lower motor neurons (Anagnostou *et al.* 2005, Khatri *et al.* 2008, Rudnik-Schöneborn *et al.* 2003, Rudnik-Schöneborn *et al.* 2008). Along with growing evidence in mouse models that this is indeed the case (Bevan *et al.* 2010, Heier *et al.* 2010, Mutsaers *et al.* 2011, Shababi *et al.* 2010, Shanmugarajan *et al.* 2009, Somers *et al.* 2012, Wishart *et al.* 2010), this suggests that there is a differential susceptibility of cell types and tissues to SMN reduction. Motor neurons are most severely affected by SMN depletion and are thus at one end of a vulnerability-resistance spectrum. As protein levels are further reduced, additional tissues such as bone, heart, and sensory neurons become affected, while other cells and tissues remain unaffected. For example, at ≈ 10-20% of normal SMN levels, as seen in type I SMA patients, motor neurons are severely affected, the heart and brain show partial involvement, while many organs remain relatively unperturbed. Figure taken with permission from The Company of Biologists from Sleigh *et al.* (2011b).

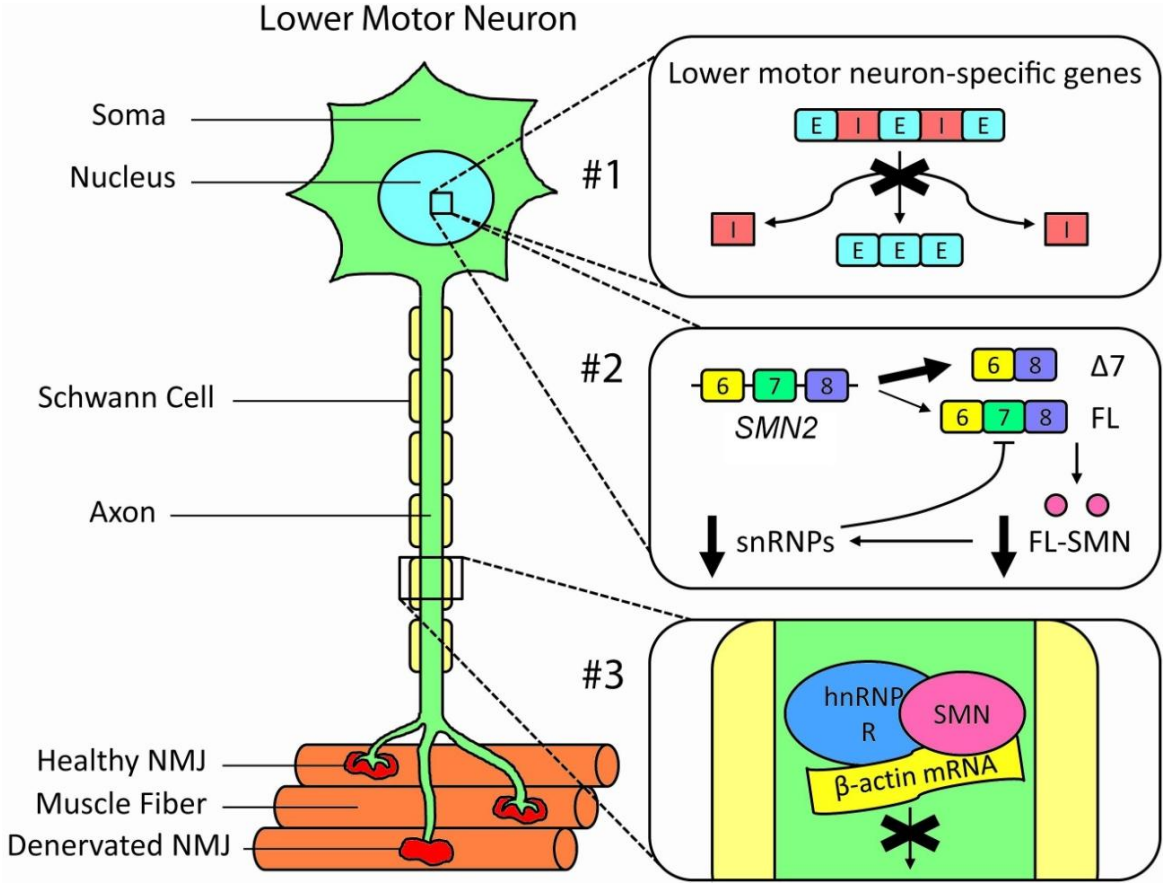

Figure 1.5. Major hypotheses for the selective vulnerability of lower motor neurons to low SMN levels. The reason for lower motor neuron sensitivity to SMN protein depletion is unknown. Three plausible hypotheses for this specificity have been suggested. SMA may arise due to one or a combination of the following: **#1)** SMN is involved in the generation of the spliceosome and plays a role in pre-mRNA splicing (Fischer *et al.* 1997, Pellizzoni *et al.* 1998). Recent evidence suggests that SMA is not a general splicing disorder, yet alternative splicing of a subset of key lower motor neuron-specific genes may cause these cells to degenerate (Bäumer *et al.* 2009). E, exon; I, intron. **#2)** Inefficient inclusion of *SMN2* exon 7 has recently been identified as an intrinsic property of motor neurons under normal conditions (Ruggiu *et al.* 2012). Furthermore, when SMN levels are diminished this inclusion becomes even less efficient (Jodelka *et al.* 2010, Ruggiu *et al.* 2012). This negative feedback loop, where low SMN levels lead to a reduction in snRNP levels, which in turn decreases *SMN2* exon 7 incorporation further reducing the amount of available SMN protein, appears to be specific to SMA motor neurons (Ruggiu *et al.* 2012). Thus, the motor neuron specificity seen in SMA may be due to the levels of available functional SMN being lower in these neuronal cells than any other cell type, leading to disruption of the canonical function of SMN in the lower motor nerves alone. Δ7, truncated mRNA; FL, full-length mRNA; FL-SMN, full-length, functional SMN protein.

#3) SMN has been shown to play a potential role in a number of non-canonical functions. If depletion of SMN below a particular point were to completely disrupt a lower motor neuron-specific function of the protein, such as axonal transport of mRNA from the cell body to the synapse (Rossoll *et al.* 2003), while having no or little effect on its general housekeeping function, this could explain the cell/tissue specificity. The non-motor neuronal pathology seen in more severe forms of the disease is likely explained by SMN levels being reduced past an additional threshold that begins to affect the canonical function of the protein in different cell and tissues types (see Figure 1.4).

1.1.4.1 SMA: a disorder of splicing regulation?

The evidence for a tight linkage between SMA and functional impairment of snRNP assembly is significant yet incomplete. SMA-causing *SMN1* mutations have been shown to affect SMN interaction with Sm proteins (Bühler *et al.* 1999, Pellizzoni *et al.* 1999) and snRNP assembly activity generally correlates with SMN levels in SMA patient cells (Gabanella *et al.* 2007, Wan *et al.* 2005). The first study to demonstrate a direct link between snRNP biogenesis and SMA pathology showed that defects in *Xenopus laevis* or zebrafish embryos caused by a reduction of SMN or Gemin2 can be rescued by injection of purified snRNPs (Winkler *et al.* 2005). However, a number of SMA-causing *SMN1* mutations, including one found in a type I SMA patient, display no defect in snRNP assembly activity (Shpargel & Matera 2005) and, despite impairment of snRNP synthesis, endogenous snRNP/snRNA levels were found to be unaltered in type I SMA patient-derived fibroblasts, a chicken cell line, and a *Drosophila* mutant all with severely reduced SMN levels (Gabanella *et al.* 2007, Rajendra *et al.* 2007, Wan *et al.* 2005). Moreover, despite a significant difference in lifespan between the $Smn^{-/-}$; $SMN2^{+/+}$ and SMNΔ7 mouse models (≈ 9 days) there is no difference in snRNP assembly activity (Gabanella *et al.* 2007), suggesting that an additional function of the protein is differentially affected. Consistent with this, the role of SMN in snRNP biogenesis can be separated in *Drosophila*

from motility and survival defects caused by SMN deficiency (Praveen *et al.* 2012). Similarly in zebrafish, the role of SMN in snRNP biogenesis can be dissociated from a motor axon function (Carrel *et al.* 2006). It should be noted that snRNAs not associated with Sm cores are unstable (Sauterer *et al.* 1988), so snRNA levels are similar to snRNP levels.

Steady-state snRNA levels in spinal cord extracts of P3 $Smn^{-/-}$; $SMN2^{+/+}$ mice were also only marginally reduced in spite of a ten-fold decrease in snRNP assembly activity (Gabanella *et al.* 2007). This apparent contradiction indicates that cells possess an excess capacity to assemble snRNPs, such that reducing SMN levels has only a modest effect. However, levels of a subset of snRNAs belonging to the minor splicing pathway (U11 and U12) were significantly reduced in the brain and spinal cord of $Smn^{-/-}$; $SMN2^{+/+}$ mice (Gabanella *et al.* 2007). U11 snRNA levels were also lowered in the kidney, suggesting that reduced SMN levels can unevenly affect the profile of snRNPs in a tissue-specific fashion. This preferential reduction in minor snRNAs has since been confirmed in a number of different models and tissues (Praveen *et al.* 2012, Workman *et al.* 2009, Zhang *et al.* 2008).

The association between disease severity and snRNP assembly activity has been shown in a range of mouse models (Gabanella *et al.* 2007, Workman *et al.* 2009). In mouse spinal cord, snRNP biogenesis is most prominent in the central nervous system during embryogenesis and early postnatal development, correlating with levels of SMN (Gabanella *et al.* 2005). The spatiotemporal expression patterns of *Smn* and *Gemin2* are closely co-regulated, and the subclinical motor neuron loss seen in *Smn* heterozygous mice is accelerated in $Smn^{+/-}$; $Gemin2^{+/-}$ heterozygotes, which is associated with a reduction in snRNP assembly (Jablonka *et al.* 2001, Jablonka *et al.* 2002).

It is clear that the formation of snRNPs is affected by SMN reduction. However, the functional consequences of this disturbed assembly and how this contributes to SMA pathology are much less clear. If a failure of snRNP assembly is the pathological lesion that leads to selective motor neuron death, this would be predicted to cause dysfunctional splicing across a wide range of pre-mRNA transcripts, at or before disease onset, and also to result in aberrant transcripts not normally seen in tissues in physiological states. Evidence suggests that there is two-fold increase in the error rate of splice-site pairing in phenotypically normal fibroblasts from severe type I SMA patients (Fox-Walsh & Hertel 2009). Furthermore, increased intron-inclusion has been reported in a number of systems upon SMN depletion (Boulisfane *et al.* 2011, Campion *et al.* 2010, Zhang *et al.* 2008). Nonetheless, defective splicing of a motor neuronal gene at or before disease onset has yet to be identified. In end-stage (P13) SMNΔ7 mice, Zhang *et al.* (2008) used exon-level microarrays to identify widespread tissue-specific splicing abnormalities, even in histologically normal tissues such as kidney. This curious finding suggests a lack of congruence between splicing abnormalities and cellular pathology and, given that the mice used were moribund, may simply be a non-specific response to tissue injury. A longitudinal study of exon-level changes in the spinal cord of both $Smn^{-/-}$; $SMN2^{+/+}$ and SMNΔ7 mice at pre-symptomatic and late-symptomatic stages suggests that the vast majority of alternative splicing events are actually a late feature of disease and are thus unlikely to play a causative role in SMA pathology (Bäumer *et al.* 2009). Only a small number of transcripts were altered compared to control mice at the pre-symptomatic stage and all were shifts were to known isoforms. Additionally, the introns processed by the minor spliceosome were not preferentially affected, as might be expected if the specific reduction of minor spliceosomal snRNPs had a direct effect on splicing. Nevertheless, the

role of the small number of genes that are alternatively spliced early on in the disease should be further assessed.

1.1.4.2 Evidence for a motor neuron-specific function of SMN

Throughout evolution proteins often develop multiple functions. Besides its role in snRNP assembly, there is considerable evidence to suggest that the SMN protein plays a part in a wide range of different cellular processes (Grice & Liu 2011, Pagliardini *et al.* 2000, Pellizzoni *et al.* 2001a, Pellizzoni *et al.* 2001b, Rossoll *et al.* 2003). Consistent with this, SMN is able to bind to a large number of proteins that possess diverse functions (Rossoll & Bassell 2009), some of which may be specific to neuronal cells. Disruption of a lower motor neuron-specific function of SMN could serve to explain, at least in part, the characteristic pathology observed in SMA (Briese *et al.* 2005, Burghes & Beattie 2009, Fallini *et al.* 2012).

SMN is usually found in both the cytoplasm and the nucleus (Francis *et al.* 1998, Liu & Dreyfuss 1996). In rat spinal cord motor neurons, the protein has been shown to localise to dendrites and axons (Béchade *et al.* 1999, Pagliardini *et al.* 2000), and in human motor neurons, SMN appears to shift from the nucleus to the cytoplasm with clear localisation in axons during axonogenesis and axonal sprouting (Giavazzi *et al.* 2006). In mouse primary motor neuronal cultures, Smn can be found at the growth cones of neurites, independent of its SMN complex partner Gemin2 (Jablonka *et al.* 2001). *Smn* is expressed in growth cone-like structures in immortalised neuronal P19 cells (Fan & Simard 2002). Live cell imaging experiments have shown that SMN is able to rapidly shuttle back and forth along processes of primary neuronal cultures and that this is dependent on the cytoskeleton (Fallini *et al.* 2010, Zhang *et al.* 2003). Furthermore, the SMN granules found in the axons of primary motor neurons do not colocalise with Sm proteins, key

components of the canonical SMN complex (Zhang *et al.* 2006). Cellular compartmentalisation of proteins is absolutely essential for survival. Thus, it is highly unlikely that the SMN protein is travelling along neuronal processes and localising to growth cones without this serving a particular purpose.

Reduced SMN levels cause defects in neurite and axon outgrowth in a number of different cell lines and animal models (Chang *et al.* 2011, Jablonka *et al.* 2007, Kwon *et al.* 2011, Liu *et al.* 2011, McWhorter *et al.* 2003, Ning *et al.* 2010, Nölle *et al.* 2011, Shafey *et al.* 2008, van Bergeijk *et al.* 2007, Ymlahi-Ouazzani *et al.* 2010). SMN has been shown to facilitate the localisation of two mRNAs, *β-actin* and *candidate plasticity-related gene 15* (*cpg15*), to growth cones (Akten *et al.* 2011, Rossoll *et al.* 2003). β-actin is a structural component of growth cones thought to be a primary mediator of neuronal actin dynamics (Bassell *et al.* 1998), whereas Cpg15 is involved in outgrowth of neurites and axon branching, amongst other things (Fujino *et al.* 2008, Javaherian & Cline 2005). Poly(A) mRNA levels are also reduced in the axons of primary motor neurons with reduced Smn (Fallini *et al.* 2011). Local axonal translation of *β-actin* mRNA was recently shown to be deficient in Smn-depleted primary neuron cultures (Rathod *et al.* 2012), and the reduced levels of β-actin mRNA and protein in growth cones correlate with diminished growth cone size and shorter axons (Rossoll *et al.* 2003). SMN is known to bind to a number of *β-actin* mRNA-binding proteins including hnRNP R (Rossoll *et al.* 2003, Rossoll *et al.* 2002) and HuD (Akten *et al.* 2011, Fallini *et al.* 2011, Hubers *et al.* 2011), and these interactions are thought to be required for localisation of *β-actin* mRNA into axons and growth cones (Glinka *et al.* 2010). It is believed that the enrichment of mRNAs in axons and growth cones with subsequent local protein translation is important for axon outgrowth, maintenance, and repair (Jung *et al.* 2011, Jung *et al.* 2012, Satkauskas & Bagnard 2007). It is therefore hypothesised that the reduced levels of specific mRNAs in

important regions of the lower motor neurons may at least contribute to the characteristic SMA pathology. Together, there is a significant body of work indicating that, in addition to its canonical role in snRNP assembly, SMN does indeed possess a motor neuron-specific function. Nevertheless, the question of how SMN depletion causes such a specific detrimental effect on the lower motor nerves remains to be answered.

1.2 Charcot-Marie-Tooth disease/distal hereditary motor neuropathy

The Charcot-Marie-Tooth (CMT) diseases, also known as hereditary sensory and motor neuropathies (HSMNs), are a heterogeneous group of conditions that are characterised by distal motor and sensory dysfunction with progressive muscle atrophy predominantly in the hands and feet (Reilly *et al.* 2011). CMT diseases can be divided into type 1 forms that are typified by demyelination and reduced nerve conduction velocity (NCV), type 2 forms, which display axon loss and deficient synaptic transmission, and intermediate CMT that shares features of the two. The distal hereditary motor neuropathies (dHMNs), also known as distal SMAs (dSMAs), are a set of diseases that display predominantly motor neuropathy with relatively little sensory involvement compared to CMT disease (Rossor *et al.* 2012). Nevertheless, there is considerable overlap in the clinical manifestation between the CMT diseases and dHMNs, and the same mutations can cause both phenotypes. This suggests that there is a disease continuum, which is likely affected by a number of genetic modifiers. When grouped together, there are over 40 associated genetic loci, and inheritance can be dominant, recessive, or X-linked (www.molgen.ua.ac.be/CMTMutations/Home/IPN.cfm). In total, these neuropathies affect ≈ 1 in 2,500 people, making them one of the most common inherited neurological disorders (Skre 1974).

1.2.1 CMT disease type 2D/dSMA type V

Charcot-Marie-Tooth disease type 2D (CMT2D) and distal spinal muscular atrophy type V (dSMAV) are axonal neuropathies caused by dominant mutations in the *GARS* gene (Antonellis *et al.* 2003, Del Bo *et al.* 2006, Dubourg *et al.* 2006, Eskuri *et al.* 2012, James *et al.* 2006, Sivakumar *et al.* 2005). Both diseases result in weakness and muscle atrophy predominantly in the distal, upper extremities, with mild-to-moderate sensory involvement in CMT2D. Symptom onset usually begins in the second decade of life, but infantile presentation has also been reported (Eskuri *et al.* 2012, James *et al.* 2006). For simplicity, throughout this thesis, I will refer to mutations in the *GARS* gene causing CMT2D and not both diseases.

1.2.1.1 The genetics of CMT2D

CMT2D is caused by inherited mutations in *GARS* (Antonellis *et al.* 2003). Through different translation start sites, the *GARS* gene encodes two isoforms (mitochondrial and cytoplasmic) of the highly conserved, non-redundant, homodimeric glycyl-tRNA synthetase (GlyRS) (Chang & Wang 2004, Chihara *et al.* 2007, Mudge *et al.* 1998, Turner *et al.* 2000). All disease-associated mutations are located downstream of the 54 amino acid mitochondrial targeting sequence, and have been shown to cluster around the dimer interface (He *et al.* 2011, Motley *et al.* 2010). GlyRS is one of over 35 human aminoacyl-tRNA synthetases (ARSs), which are an ancient class of enzymes that ligate specific amino acids to their corresponding transfer RNAs (tRNAs) in an ATP-dependent reaction (Ibba & Soll 2000). The resulting charged tRNA is then primed for use by ribosomes in protein translation. In particular, GlyRS charges glycine. Similar to *SMN1*, *GARS* is a widely and constitutively expressed gene that is absolutely vital for life, and analogous to

the situation in SMA, it is unknown how mutations in an essential gene, result in the selective vulnerability and degeneration of the peripheral nerves.

1.2.1.2 Mouse models of CMT2D

Two mouse models with *Gars* mutations leading to dominantly inherited neuropathy have been reported. The first, $Gars^{Nmf249/+}$, is a spontaneous mutant identified at The Jackson Laboratory, Maine, USA, and characterised by Robert W. Burgess and colleagues (Seburn *et al.* 2006). The mutation, a CC-to-AAATA replacement, leads to the in-frame substitution of a proline to a lysine and tyrosine at residue 278, hence the mouse sometimes being referred to as the *P278KY* allele. The mouse protein annotation includes the mitochondrial targeting sequence whereas the human protein does not (nor the *Drosophila* protein), therefore the *P278KY* allele is equivalent to P234KY in human GlyRS. At 5 weeks, $Gars^{Nmf249/+}$ mice display significant motor and sensory axon loss, reduced NCV and muscle force, and frank NMJ denervation. On a C57BL/6J genetic background, many mice die around 6-8 weeks, but some survive well into adulthood and these figures are background-dependent, indicative of modifying loci.

The second mutation in *Gars* was identified in an *N*-ethyl-*N*-nitrosourea mutagenesis screen at the MRC Mammalian Genetics Unit in Harwell, UK, and subsequently characterised by a team headed by Elizabeth M. Fisher (Achilli *et al.* 2009). A T-to-C point mutation leads to a cysteine to arginine alteration at residue 201 (C201R), which is equivalent to C157R in the human protein. On a C3H background, $Gars^{C201R/+}$ mice have a normal lifespan, diminished muscle force, a mild NMJ phenotype, slowed NCV, and reduced peripheral axon diameter. Heterozygous mice are less severe than $Gars^{Nmf249/+}$ mice, but the relatively mild phenotype is worsened on the C57BL/6J genetic background. $Gars^{C201R/C201R}$ mice are able to survive, albeit in a fairly debilitated state, up

to P15 and P17 on C57BL/6J and C3H backgrounds, respectively (Achilli *et al.* 2009), whereas homozygous *Nmf249* mice are embryonic lethal (Seburn *et al.* 2006).

1.2.1.3 Using *Drosophila* to model CMT2D

Ever since Thomas Hunt Morgan chose *Drosophila melanogaster* to study the chromosomal theory of inheritance, the fruit fly has become an important model organism for researching genetics, development, and physiology. We now have a considerable arsenal of genetic libraries and techniques (Dietzl *et al.* 2007, Duffy 2002, Gong & Golic 2003, Parks *et al.* 2004, Theodosiou & Xu 1998), and an extensive knowledge of synapse structure, neurotransmission, synaptic plasticity, and muscle physiology at the larval NMJ (Collins & DiAntonio 2007, Peron *et al.* 2009, Schuster 2006, Wu *et al.* 2010). Crucially, the process of neurotransmission in *Drosophila* is fundamentally akin to that at the human NMJ; however, the fly neuromuscular connection relies on glutamate to transmit information from motor nerves to muscle (Jan & Jan 1976). Moreover, unlike human post-synaptic AChRs, which permit sodium and potassium ion exchange, fly glutamate receptors are voltage-dependent calcium channels that give rise to post-synaptic potentials graded in amplitude and duration, as opposed to all-or-nothing action potentials. This has been seen as a major limitation of using *Drosophila* larvae to study the neuromuscular system. Nonetheless, it is becoming increasingly apparent that pathways underpinning neuronal development and a large number of molecules at the larval NMJ, including active zone scaffolding proteins (Brucker *et al.* 2012, Wagh *et al.* 2006), post-synaptic structural proteins (Sanford *et al.* 2004), and cell adhesion proteins (Giagtzoglou *et al.* 2009), are conserved between flies and mammals (Budnik & Salinas 2011, Goda & Davis 2003, Wu *et al.* 2010). Consequently, *Drosophila* is well placed to play an important role in improving the understanding of human neuromuscular disorders (Lloyd & Taylor 2010,

Reiter & Bier 2002). An assertion reaffirmed by ≈ 75% of known human disease genes having a highly conserved fly orthologue (Reiter *et al.* 2001, Rubin *et al.* 2000).

GlyRS function has also been studied using *Drosophila*. Fly *gars* shares a high degree of orthology with the human gene, and the vast majority of mutations identified in patients affect conserved amino acids (Motley *et al.* 2010). In a screen using the mosaic analysis with a repressible cell marker (MARCM) system to generate positively labeled homozygous mutant clones in olfactory projection neurons in the *Drosophila* brain, *gars* was identified to be involved in terminal arborisation of axons and dendrites (Chihara *et al.* 2007). Loss of *gars* function was fully rescued with wild type human *GARS* but not $GARS^{E71G}$ or $GARS^{L129P}$, while transgene expression caused no overt phenotype in wild type neurons. This work in *Drosophila* is consistent with a loss-of-function disease mechanism, as opposed to that of a dominant-negative effect or a toxic gain-of-function. However, this recessive loss-of-function in single neurons of genetically mosaic animals does not reflect well human CMT - a dominantly inherited disease where mutant GlyRS is present in all tissues. Nevertheless, this work still contributes to the debate about the disease mechanism of CMT2D.

1.2.1.4 The CMT2D disease mechanism

Dominant mutations in human and mouse *GARS* result in a dominantly inherited neuropathy; however, until recently it was unclear whether the disease results from a pathological gain-of-function, a partial loss-of-function, a dominant-negative mechanism, or a combination from the three. Heterozygous deletion of *Gars* using a gene-trap insertion allele (*XM256*) causing a 50% reduction in gene expression has no effect on mouse lifespan or NMJ morphology, indicating that the disease is unlikely to be caused by haploinsufficiency (Seburn *et al.* 2006). Moreover, the *in vitro* aminoacylation activity of

GlyRS^{P278KY} (Seburn *et al.* 2006), and the charging capacity of brain lysates from *Gars*$^{C201R/+}$ mice are unaffected (Achilli *et al.* 2009), arguing against a canonical loss-of-function. This lack of congruence between functional capacity and disease severity is corroborated by evidence suggesting that additional *GARS* mutations differentially affect aminoacylation (Nangle *et al.* 2007, Xie *et al.* 2007). Nevertheless, both the *C201R* and *Nmf249* mutations are unable to complement *XM256* loss-of-function resulting in embryonic lethality, indicating that a secondary GlyRS function could be perturbed. To determine whether this is indeed the case or if the neuropathy is due to a toxic gain-of-function, wild type human *GARS* was overexpressed in *Gars*$^{Nmf249/+}$ and *Gars*$^{C201R/+}$ mice (Motley *et al.* 2011). Consistent with the latter, wild type *GARS* overexpression had minimal effects on the disease phenotype, and toxicity was dependent on the mutant protein dose. Nonetheless, clues as to the identity of this toxic gain-of-function disease mechanism linking *GARS* mutations to lower motor neuron pathology are lacking.

1.3 Aims of this work

My DPhil thesis is devoted to using a range of cellular and animal models to explore novel therapies and disease mechanisms in monogenic *SMN1*-associated SMA, and CMT2D. The three principal aims were:

1. To characterise a novel *C. elegans smn-1* point mutant, and assess its utility as a screening platform by using it to screen a library of 1,040 chemical compounds for drugs that can ameliorate defective motility. It is hoped that substances identified by the screening process may assist in accelerating SMA drug development (chapter 3).

2. To investigate the effects of the different isoforms of chondrolectin in Smn-depleted neuronal cells, and, through this, be able to comment on the role of snRNP biogenesis and splicing in the disease (chapter 4).
3. To identify novel features of CMT2D disease pathology and the GlyRS toxic gain-of-function disease mechanism using a range of model systems including the two existing mouse mutants and a novel fly model generated by Dr. Stuart J. Grice (chapter 5).

2. Materials and methods

By permission of Oxford University Press, the C. elegans*-specific methods presented in this chapter are taken from the published article Sleigh JN, Buckingham SD, Esmaeili B, Viswanathan M, Cuppen E, Westlund BM, Sattelle DB. 2011. A novel* Caenorhabditis elegans *allele,* smn-1(cb131)*, mimicking a mild form of spinal muscular atrophy, provides a convenient drug screening platform highlighting new and pre-approved compounds.* Hum Mol Genet *20: 245-60. As the first author of the above publication, I took the lead on writing the sections that are included in this thesis.*

2.1 General methods

Mouse handling and experiments were performed in accordance with the UK Home Office Animals (Scientific Procedures) Act (1986) and approved by the University of Oxford Ethical Review Panel. All reagents were obtained from Sigma unless otherwise stated.

2.1.1 DNA extraction and standard PCR

Cells were collected in 1.5 ml eppendorf tubes using 1X phosphate buffered saline (PBS, 137 mM NaCl, 10 mM Na_2HPO_4, 2.7 mM KCl, 2 mM KH_2PO_4), spun at 4,000 x *g* for 2 min, resuspended in DNA extraction buffer (200 mM NaCl, 100 mM tris(hydroxymethyl)aminomethane-hydrochloride (Tris-HCl) [pH 7.5], 5 mM ethylenediaminetetraacetic acid [pH 8.0], 0.2% (w/v) sodium dodecyl sulphate (SDS)) with 3 µl freshly added 20 µg/ml proteinase K (Roche), and left at 55˚C overnight. To extract DNA from mouse tissue, no centrifugation step was required. The following day, samples were spun at 16,000 x *g* for 10 min, the supernatants collected, and an equal volume of isopropanol added. DNA was pelleted at 16,000 x *g* for 10 min, air-dried for 5-

10 min and then resuspended in 50 µl H_2O. 15-25 ng genomic DNA was used per 20 µl PCR with *Taq* DNA polymerase. *Chodl* primer sequences for a product of 701 bp: forward 5'-CCAGACACGCCCACGGTGTC-3' and reverse 5'-GGCGTTCATGCCACAGCAGC-3'. Cycling conditions: 95˚C for 3 min, 35 x [95˚C 30 sec, 64˚C 30 sec, 72˚C 1 min], 72˚C 2 min. PCR products were separated on a 1.5% (w/v) agarose gel.

2.1.2 RNA extraction and reverse transcription-PCR (RT-PCR)

RNA was extracted from cells, snap frozen mouse tissues, and *Drosophila* larvae using an RNeasy Mini Kit (QIAGEN) following the manufacturer's instructions. In each reverse transcription reaction, 1.5 µg RNA/15 µl reaction was added. cDNA was diluted 1/10 and 1 µl was used per 20 µl PCR with *Taq* DNA polymerase. RT-PCR primers can be found in Table 2.1. Cycling conditions: 95˚C for 3 min, 34 x [95˚C 30 sec, 61˚C/64˚C 30 sec, 72˚C 1 min], 72˚C 2 min. RT-PCR products were separated on a 1.5% (w/v) agarose gel.

Target	Product (bp)	Forward primer 5'-3'	Reverse primer 5'-3'
Chodl	723	GCATCGCCTCACTCTTGCTGG	GCAACATCTGGAAACAGCAGG
Gapdh	486	GTATGTCGTGGAGTCTACTGG	TACTTGGCAGGTTTCTCCAGG

Table 2.1. Primers used for RT-PCR.

2.1.3 Quantitative RT-PCR (qPCR)

SuperScript III Reverse Transcriptase (Invitrogen) was used to create cDNA. 0.2 µg cell RNA, 0.15 µg mouse muscle RNA and 0.6-2.0 µg *Drosophila* larvae RNA/30 µl reverse transcription reaction was used. Mouse muscle cDNA was pre-amplified in a 50 µl reaction using a Taqman Preamp Master Mix Kit (Invitrogen). mRNA levels were assessed by qPCR using 1 µl of a 1/10 dilution of the cell and *Drosophila* cDNA or 1 µl of a 1/25 dilution of the pre-amplified mouse muscle cDNA in 20 µl reactions using SYBR Green

(Applied Biosystems) and a StepOnePlus real-time PCR machine (Applied Biosystems). Details of the primers used for qPCR can be found in Table 2.2. Cycling conditions: 95˚C 10 min, 40 x [95˚C 15 sec, 60˚C 1 min], 95˚C 15 sec. Three technical replicates per reaction were performed. Primers were used at 200 nm, after optimisation of concentration to minimise primer-dimer formation and yield low Ct values. Primer efficiencies were estimated by performing qPCR on serial dilutions of at least two independent cDNA samples, plotting Ct values on the Y-axis against log-transformed cDNA inputs, and using the slope of the line of regression in the following equation: $(10^{-1/slope} - 1) \times 100$. *Glyceraldehyde 3-phosphate dehydrogenase* (*Gapdh*) and *actin 5C* (*Act5C*) were used as reference genes for mouse and *Drosophila* samples, respectively. Relative gene expression was calculated using the comparative Ct (ΔΔCt) method: $\Delta Ct = Ct_{\textit{gene of interest}} - Ct_{\textit{Gapdh/Act5C}}$, and $\Delta\Delta Ct = \Delta Ct_{\text{experimental sample}} - \Delta Ct_{\text{control sample}}$, with relative expression given using the formula $2^{-\Delta\Delta Ct}$. Ct values were adjusted for primer efficiency using the following formula: Ct value x (log(2 x primer efficiency/100)/log(2)).

Target	Organism	Forward primer 5'-3'	Reverse primer 5'-3'
Act5c	*Drosophila*	TTATGCCCTTCCCCATGC	GAAAGAGTAACCGCGCTCG
Chrne	Mouse	GCAGCTTTTACCGAGAATGG	CGTCAGTTTCTCCAGGACC
Chrng	Mouse	GGCAGAAATGCACAGTGG	CAGGTACTTGCTGATGAGTGG
Gapdh	Mouse	TGTGTCCGTCGTGGATCTGA	CCTGCTTCACCACCTTCTTGA
Nrp-1	Mouse	AGCTGGACCAACCACACC	AGTGGTGCCTCCTGTGAGC
plexB	*Drosophila*	GCGTTTTCATCGTTAGCGC	CATTCGACAAGGAGCCTGC
Sema-2a	*Drosophila*	GCTCGTCGTTGACAAAATTCG	TAAATGCGACCCAGATTGGTGC
Sema3a	Mouse	AGAATGCTGCCTCGCTCG	GTCTTGTGCGCCTCTTTG
Sema3c	Mouse	ATATGTGGGGAGCAAAGACC	GATCTTTGCCAGCCATTTTGC
Smn	Mouse	CCAGAAGAAAACCTGCCAAGAA	CACTTGTCACCAACTTTCCACTGT

Table 2.2. Primers used for qPCR.

2.1.4 Protein extraction

Cells were collected into 1.5 ml eppendorf tubes using PBS, spun at 4,000 x *g* for 2 min, re-suspended in 50 µl radioimmunoprecipitation assay (RIPA) lysis buffer (150 mM NaCl, 50 mM Tris-HCl [pH 7.5], 1% (v/v) sodium deoxycholate, 1% (v/v) Triton X-100, 0.1% (w/v) SDS) with freshly added 1.5% (v/v) protease inhibitor cocktail, and left on ice for 30 min. Cells were spun at 3,800 x *g* for 10 min and the supernatant transferred to fresh tubes, which were then stored at -80˚C. Protein concentration was quantified using a Pierce BCA Protein Assay Kit (Thermo Scientific), as per the manufacturer's instructions.

2.1.5 Western blotting

Approximately equal amounts of protein (10-20 µg) from each sample were boiled for 5 min in Laemmli sample buffer (Bio-Rad) with 5% (v/v) β-mercaptoethanol, and separated by 10% (w/v) SDS polyacrylamide gel electrophoresis. Resolved gels were transferred to 0.2 µm nitrocellulose membranes (Millipore), which were then blocked for 1 h in 5% (w/v) milk powder in PBS, and incubated overnight with primary antibody (Table 2.3) in 5% (w/v) milk in PBS-triton (PBS-T, 0.1% (v/v) Triton X-100 in PBS) at 4˚C on a rocker. The following day, membranes were washed three times for 10 min in PBS-T, probed with horseradish peroxidase (HRP)-conjugated secondary antibodies (Amersham) at 1/5000 in PBS-T with 5% (w/v) milk for 2 h, and washed three times for 10 min in PBS-T. Signal was detected using enhanced chemiluminescence reagents (Amersham) according to the manufacturer's instructions. For probing with a second primary antibody, membranes were stripped at 55˚C for 30 min in stripping buffer (100 mM β-mercaptoethanol, 62.5 mM Tris-HCl [pH 6.8], 2% (w/v) SDS), washed three times for 10 min with PBS-T, and the probing process repeated starting with blocking for 1 h in 5% (w/v) milk in PBS. Densitometric quantification was performed using the Gels tool of ImageJ

(http://rsbweb.nih.gov/ij/). The loading control (β-tubulin for all Westerns) band density of each sample was normalised to the same single sample to produce a normalisation factor. The density of each Smn band was then multiplied by the normalisation factor for each individual sample. These values were then used to calculate the percentage Smn levels relative to an experimental control condition (the first bar in each graph).

Antibody	Manufacturer	Catalogue #	Dilution
Rabbit polyclonal anti-β-tubulin	Abcam	ab15568	1/5000
Mouse monoclonal anti-FLAG	Sigma Aldrich	F1804	1/1000
Rabbit polyclonal anti-GlyRS	Nangle *et al.* 2007	N/A	1/1000
Mouse monoclonal anti-Smn	BD Biosciences	610646	1/5000

Table 2.3. Antibodies used for Western blotting.

2.1.6 Cloning of 3xFLAG-Chodl cDNA constructs

1 µg RNA extracted from the tibialis anterior muscle of a young mouse was reverse transcribed in a 15 µl reaction using Taq-Man Reverse Transcription Reagents (Applied Biosystems). Chodl cDNA was then amplified in a 25 µl PCR with KOD Hot Start DNA Polymerase (Novagen) using sequence-specific primers with added 5' HindIII and XbaI restriction sites (Table 2.4). All PCRs used the following cycling conditions: 95˚C for 2 min, 40 x [95˚C 20 sec, 62˚C/60˚C/64˚C 10 sec, 70˚C 20 sec], 70˚C 2 min. PCR products were digested for 2 h at 37˚C with HindIII and XbaI (New England Biolabs), and column-purified using a PCR purification kit (QIAGEN). The p3xFLAG-CMV-7.1 expression vector (E7533) was cut using the same restriction enzymes, which were then heat-inactivated for 20 min at 65˚C. To prevent recircularisation, the digested vector was treated with 1 µl calf intestinal phosphatase (New England Biolabs) for 1.5 h at 37˚C, and gel-purified. 50 ng of vector and an equimolar amount of insert were ligated using T4 ligase

(New England Biolabs) in a 20 µl reaction for 15 min at room temperature (RT). 3xFLAG-Chodl-003 was created using 3xFLAG-Chodl-001 due to lack of isoform 003 detection in the tissue used. Plasmid maxi-preps (QIAGEN) were prepared according to manufacturer's instructions, and constructs were gel-purified and verified by DNA sequencing using CMV_F 5'-GAGCTCGTTTAGTGAACCGTC-3' and mChodl_Seq_F 5'-ACCAGTGGTCTGATGGAAGC-3'.

Primer	Sequence 5'-3'	Annealing Temp (˚C)
Chodl-001-003_F	GCAAGCTTATGATCCGCATCGCCTCACTCTTGC	60-64
Chodl-001_R	GGAAGGAAAGTGGCATGGAGGTATAATCTAGATATA	62
Chodl-002_R	CCAAAATAACTCTCCTTCCCTTAACTAGTCTAGATATA	60
Chodl-003_R	CCAGATGTTGCATAAAAGGTAATCTAGATATA	64

Table 2.4. Cloning primer sequences.

2.1.7 pEGFP-N1-Smn site-directed mutagenesis

Site-directed mutagenesis of a pEGFP-N1-Smn vector (Clontech) was performed using a QuikChange Site-Directed Mutagenesis Kit (Agilent). Primers were designed according to the manufacturer's instructions, and high-performance liquid chromatography-purified (Table 2.5). Over two rounds of mutagenesis, three base pair changes were incorporated into the target sequence of Smn short interfering RNA (siRNA) 74016. Cycling conditions: 95˚C for 30 min, 18 x [95˚C 30 sec, 55˚C 1 min, 70˚C 9 min], 70˚C 2 min. The mutated construct was gel-purified and verified by sequencing using CMV_F.

Primer	Sequence 5'-3'
Smn_mut_1a	CTTTCCCCGACATGTGAAGTTGCTAATAGTAC
Smn_mut_1b	GTACTATTAGCAACTTCACATGTCGGGGAAAG
Smn_mut_2a	CGACATGTGAAGTTGCAAATAGTACAGAACAGAACACTCAGG
Smn_mut_2b	CCTGAGTGTTCTGTTCTGTACTATTTGCAACTTCACATGTCG

Table 2.5. Mutagenesis primer sequences.

2.1.8 Statistical analysis

When normally distributed, data sets were statistically analysed using either an unpaired *t*-test with Welch's correction or a one-way analysis of variance (ANOVA) with Bonferroni's multiple comparison test. If the data did not pass normality testing, the non-parametric Mann-Whitney *U* test or Kruskal-Wallis test with Dunn's multiple comparison test were used. The Log-rank (Mantel-Cox) and Gehan-Breslow-Wilcoxon tests were used to analyse the *C. elegans* survival and pyridostigmine bromide paralysis data. For regression analysis, linear regression was performed and R^2 values calculated. Pearson's product-moment correlation coefficient (R) was calculated to assess correlation. GraphPad Prism 5 software was used for all statistical analyses. Means + standard error of the means (SEMs) are plotted for all graphs unless otherwise stated.

2.2 *C. elegans*-specific methods

2.2.1 *C. elegans* strains

Worm strains were maintained under standard conditions on *Escherichia coli* OP50 (Brenner 1974). The following strains were used: N2 Bristol wild type, NW1229 *[evIs111[F25B3.3::GFP; dpy-20(+)]]*, LL2058 *[smn-1(cb131) I]*, LL2073 *[smn-1(cb131) I]* (4x outcrossed), LM99 *[smn-1(ok355) I/hT2[bli-4(e937) let-?(q782) qIs48] (I;III)]*,

LM123 *[smn-1(cb131) I; evIs111]*, LM124 *[smn-1(cb131) smn-1(ok355) I]*, LM125 *[smn-1(cb131) I/hT2[bli-4(e937) let-?(q782) qIs48] (I;III)]*, and ZZ26 *[unc-63(x26) I]*.

2.2.2 Isolation of the *smn-1(cb131)* allele

C. elegans bearing the *smn-1* mutant allele *cb131* were isolated from a frozen clonal library of ethyl methane sulphonate-mutagenised animals as previously described (Cuppen *et al.* 2007). Briefly, the *smn-1* open reading frame was amplified by nested PCR from genomic DNA isolated from animals within individual wells of the library. PCR products generated from each library sample were sequenced (using M13 primers) and the data were analysed using LIMSTILL software (http://limstill.niob.knaw.nl/) to identify missense mutations in *smn-1*. The *smn-1* mutant allele *cb131* was identified using this technique. *cb131* contains a G-to-A mutation at nucleotide 79 of the *smn-1* open reading frame and is predicted to encode the mutant protein SMN-1^{D27N}. LL2058 animals homozygous for *cb131* were successfully isolated following resuscitation of the cryopreserved library sample. LL2058 was outcrossed four times to wild type animals producing LL2073; the presence of the mutant allele was determined by sequencing the *smn-1* locus at each step. Nested primers were used to screen for *cb131* (Table 2.6).

Primer	Sequence 5'-3'
smnF1	CATGGATATCGTGAGACTGG
smnF2	TGTAAAACGACGGCCAGTGCAGGCACTCATCAAATG
smnR3	AGGAAACAGCTATGACCATTCCAACTTCGAGATTATCAGC
smnR4	CCGCAATAGCTTCTTCATTC

Table 2.6. Nested primer sequences used to screen for *cb131*. M13 primer sites are underlined.

2.2.3 Body length, development, and lifespan assays

For body length measurements, gravid adults were bleached with sodium hypochlorite to obtain embryos, which were then plated at 23.5˚C for 48 ± 1 h. Pictures were taken of age-synchronised animals so that length along the midline from head to tail could be measured using ImageJ. To assess the rate of development, L4 stage animals were passaged to fresh plates and left at 23.5˚C for 24 ± 1 h. Five of the resulting young adults were passaged to a new plate, allowed to lay eggs at 23.5˚C for 2 h and then removed. The developmental stage of the progeny was assessed at 24, 48, and 72 h post-removal of adults. Over 650 animals per strain were assayed over three independent experiments. Animals were categorised as L1-L2, L3, L4, or young adult based on size and morphological features (Wood 1988). For lifespan assays, eggs laid by non-starved adults at RT were passaged to *E. coli*-seeded plates and stored at 23.5˚C. Survival of individual animals was observed each day at roughly the same time. Animals were scored as dead when unresponsive to prodding of the head and tail with a pick in combination with complete cessation of pharyngeal pumping. Animals were transferred to new plates at least every other day to reduce the chances of contamination.

2.2.4 Egg-laying assays

For characterisation of egg-laying behaviour, L4 stage animals were transferred to fresh plates and left to mature for 24 ± 1 h at 23.5˚C. To quantify the number of eggs laid, young adults were singled to individual plates with or without *E. coli*. The number of eggs laid in 2 h at 23.5˚C was then counted. Eggs of all shapes, sizes, and densities were counted. Mechanical stimulation can inhibit egg-laying so care was taken not to cause excessive vibration during the assay. To assess the number of eggs retained within the uterus, age-synchronised young adults were transferred to small quantities of 10 mM sodium azide in a 35 mm plate containing multiple thin agar pads. Animals were viewed under a Leica

M205 C stereo microscope. For bleaching assays, animals were passaged to individual microtitre wells containing 50 µl 20% (v/v) sodium hypochlorite solution and left for 5-10 min before counting the dispersed eggs. 30 animals were assayed per strain over three independent experiments. For brood size assays, L4 stage animals were individually passaged to fresh plates and left at 23.5˚C overnight. The following day, the resulting adults were singled to new plates, and eggs and hatchlings counted. This was repeated each day until egg-laying ceased. To calculate the percentage of eggs that successfully hatched, 50-100 eggs laid by age-synchronised young adults were transferred to a new plate and then checked the following day to see if they were still present.

2.2.5 Pharyngeal pumping and thrashing assays

For pharyngeal pumping assays, age-synchronised animals were passaged to freshly seeded plates and left for 10-20 min before assaying. Animals were filmed for 10 s using an XLI 2 Mpixel camera attached to a Nikon SMZ 1000 dissecting microscope at 12 frames/s and then videos were played back at a slower rate to allow counting of pumps. The number of pumps was multiplied by six to get an estimate per min. A single pump was scored as a complete backward and forward movement of the terminal bulb grinder. Only animals found within the circumference of food and that were rhythmically and consistently pumping were assayed. For thrashing assays, animals age-synchronised using sodium hypochlorite were picked to individual wells containing 100 µl PBS and left for 10 min. Every other thrash was counted for 30 s and then multiplied by four to obtain an estimate per min. A single thrash was defined as a complete change in direction of the body down the midline. Animals that lingered on well sides or were motionless for ≥ 10 s were discarded from the analysis.

2.2.6 Muscle and nervous system morphology

To visualise musculature using Nomarski microscopy, young adults age-synchronised by hypochlorite bleaching (two days post-L1) were mounted in 30 µl M9 on microscope slides and observed using a Zeiss Axioplan 2 microscope with mounted AxioCam. For phalloidin staining of F-actin, adapted from (Shaham 2006), staged young adults were washed off plates into microfuge tubes, frozen in liquid nitrogen and lyophilised using a DNA 120 SpeedVac (Thermo Savant) for 10 min at RT. Two units of Alexa Fluor 488 phalloidin (Invitrogen) per strain were simultaneously freeze-dried to remove the methanol solvent. 20 µl chilled acetone was then added to the nematodes for 5 min, followed by air drying for 5 min. Meanwhile, 20 µl S-mix (0.2 M sodium phosphate, 0.001 M $MgCl_2$, 0.001% (w/v) SDS) was mixed with the phalloidin and used to stain F-actin for 30 min at RT. Animals were then twice washed with PBBT (0.5% (w/v) bovine serum albumin, 0.5% (v/v) Tween-20 in PBS), mounted on microscope slides in a small amount of ProLong Gold antifade reagent (Invitrogen) and visualised using a Zeiss LSM 510 META laser scanning microscope. To perform ventral nerve cord neuron counts and assess nervous system morphology, age-synchronised young adults were immobilised in 30 µl 10 M levamisole and viewed using a Zeiss Axioplan 2 microscope. Musculature and nervous system morphology were observed independently three times in 10-15 age-synchronised young adults.

2.2.7 Pyridostigmine bromide paralysis assays

L4 stage larvae were passaged to new plates and left for 24 ± 1 h at 23.5˚C. The resulting young adults were then transferred to freshly poured plates containing 100 mM pyridostigmine bromide. Drug plates were seeded with 30 µl bacteria 30-60 min before the assay. Paralysis percentages were calculated by viewing animals at 30 min intervals for 6 h

post-plating. Animals were considered paralysed when unresponsive within 5 s to gentle prodding of the head and tail with a pick.

2.2.8 Automated thrashing assays

Animals were age-synchronised by bleaching and placed at 23.5˚C for 72 ± 1 h to reach the adult stage. They were then washed into plastic reservoirs with PBS and 200 µl of this nematode suspension subsequently added to individual wells of a 96-well plate. At various time points in suspension, thrashing rates of animals in individual wells were assessed using an automated phenotyping system (Buckingham & Sattelle 2009), which was adapted for the 96-well plate format. For the primary screen, 200 µl PBS containing *smn-1(cb131)* animals was pipetted into individual wells containing 2 µl of drug dissolved in dimethyl sulphoxide (DMSO) at a concentration of 1 mM, resulting in a final concentration for each drug of 10 µM. After gentle mixing, animals were left and assayed for thrashing rate after 4 and 6 h. For the dose-response assays, 200 µl PBS containing either *smn-1(cb131)* or wild type animals was pipetted into wells with the top 64 hits, resulting in concentrations of 50, 25, 12.5, 6.25, 3.13, 1.56, and 0.78 µM in DMSO. For both the primary screen and dose-response assays, the outer two columns of each plate contained 1% (v/v) DMSO controls.

2.2.9 Screen analysis

For the primary screen, median thrashing rates calculated from the 16 control wells in the outer two columns of each plate were subtracted from the individual well thrashing rates to give the difference in thrashing rate compared to the median control value. Median control values were calculated on a plate by plate basis in order to reduce the effects of inter-plate variation (the range of plate medians over three trials at 4 and 6 h = 58.9 and 39.0, SEM =

3.1 and 1.6). The differences in thrashing were calculated at each time point (4 and 6 h), and for each replicate. The median of the three replicates was then taken as the screen score. The arbitrary cut-off criteria, chosen so as to identify the top ≈ 5% of compounds, were a difference of ≥ +3.65 thrashes/min at 4 h and ≥ +7.3 at 6 h. For the dose-response assays, dose-dependency curves and non-linear regression coefficients (R^2) were calculated from the raw data (n = 3/compound/concentration) generated from three independent experiments. Selection criteria for the dose-response assays were a positive trend in the data, $R^2 > 0.1$, and a point along the line of regression ≥ 7.3 at both 4 and 6 h. The screening selection criteria were designed to identify and rank candidate compounds with potential for further testing.

2.2.10 Drug validation assays

Thrashing assays were performed in the same manner as the screen, using optimal concentrations taken from the dose-response assays. For egg-laying experiments, 10-15 L4 stage *smn-1(cb131)* animals were passaged to new plates with 50 µM compounds in the medium and left for 24 ± 1 h at 23.5˚C. These plates were freshly seeded with *E. coli* also containing compounds at 50 µM. 15-20 eggs were then transferred to new drug plates and left for 72 ± 1 h at 23.5˚C. These age-synchronised young adults were then assayed for the number of eggs laid in 2 h on plates seeded with 10 µl *E. coli* containing compounds at the same concentration. For the body length, pharyngeal pumping, and lifespan assays using *smn-1(ok355)*, 15-20 eggs were passaged to plates containing compounds and left for 72 ± 1 h at 23.5˚C. Young adults from these plates were then picked to new drug plates, left for 5 h at 23.5˚C to lay eggs and removed. After 48 ± 1 h from first passaging the young adults, progeny not expressing *GFP* (i.e. homozygous *smn-1* animals) were transferred to new plates and assayed for body length, pumping rate, and survival (1 day post-L1).

Assays were performed on subsequent days at approximately the same time. N-acetylneuraminic acid (Neu5Ac, from bovine milk 98%) used in these assays was purchased from Fisher Scientific.

2.3 Cell culture-specific methods

2.3.1 Cell culture

Mouse NSC-34 (motor neuronal) and C2C12 (myoblastic) cells were maintained in Dulbecco's Modified Eagle Medium (DMEM) with 4.5 g/L D-glucose and pyruvate (Invitrogen) supplemented with 10% (v/v) heat-inactivated foetal bovine serum (FBS, Invitrogen). Cells were kept at 37˚C in a 5% (v/v) CO_2 humidified atmosphere and subcultured every 4-6 days when ≈ 70-90% confluent.

2.3.2 Transfection

NSC-34 cells were grown in 24-well plates in 1 ml DMEM with 10% (v/v) FBS. For experiments performed 72 and 96 h post-transfection, cells were plated at ≈ 5.0 x 10^4 and 2.5 x 10^4 cells/well, respectively. 24 h post-plating, 600 µl media was removed from each well, and the cells treated with 1-1.5 µl Lipofectamine 2000 Transfection Reagent (Invitrogen) and a final concentration of 25-100 nm siRNA and 0.05-0.5 µg DNA in 100 µl OPTI-MEM Reduced Serum Medium with L-glutamine and HEPES (Invitrogen). 24 h post-transfection, the media was replaced with 1 ml DMEM plus 10% (v/v) FBS. Silencer Select pre-designed siRNAs targeting *Smn* were ordered from Applied Biosystems (Table 2.7), and Silencer Select Negative Control #1 siRNA was used as a control.

siRNA	Sequence 5'-3'
Smn s74016	CGACCUGUGAAGUAGCUAATT
Smn s74017	GCAUUUACCCAGCUACUATT
Smn s74018	GGUUUAUACUGGAUAUGGATT

Table 2.7. Silencer Select pre-designed siRNA sequences.

2.3.3 Magnetofection

Transfection of C2C12 cells with Lipofectamine was inefficient, so a second method that relies on magnetism was used. C2C12 cells were plated at 2.5 x 10^4 cells/well in 24-well plates that were treated for 45 min at RT with 0.1% (w/v) gelatin (Milipore) in ultrapure H_2O. After 24 h, the media was replaced with 400 µl differentiation media (DMEM supplemented with 2% (v/v) horse serum). 1 µg cDNA constructs able to express either wild type or mutant *P234KY* human *GARS* were incubated with 3 µl NeuroMag beads (Oz Biosciences) in 100 µl DMEM with no supplements for 15-20 min. 100 µl DNA:NeuroMag complexes was added to cells, which were then magnetofected for 20 min at 37˚C using a magnetic plate (Oz Biosciences). The differentiation media was replaced with 1 ml fresh media after 24 h.

2.3.4 Immunocytochemistry

Cells were grown in wells of a 24-well plate on 13 mm circular coverslips coated for 10 min with 10 µg/ml poly-D-lysine (BD Biosciences). Coverslips were removed with forceps, rinsed in a few drops of PBS, and fixed with freshly prepared 4% (w/v) paraformaldehyde (PFA, Electron Microscopy Sciences) in PBS for 15 min. The PFA was aspirated from the cells, which were then bathed for 10 min in PBS, permeabilised with a few drops of 0.3% (v/v) Triton X-100 in PBS for 20 min, washed three times for 5 min in

PBS, and blocked for 1 h in 5% (w/v) milk in PBS. Primary antibodies in 150-200 µl 5% (w/v) milk in PBS were then added to the cells and left overnight at 4˚C. Anti-β-tubulin was used at 1/500, and anti-Smn at 1/200 (Table 2.3). The following day, cells were washed three times with PBS for 10 min, and incubated for 2 h at RT with secondary antibodies (Alexa Fluor 488/594 goat anti-Rabbit and Alexa Fluor 488/594 goat anti-mouse, Invitrogen) at 1/1000 in PBS. Cells were washed three times for 10 min with PBS, mounted using Vectashield Mounting Medium with DAPI (Vector Laboratories), and imaged using a Zeiss LSM 510 META laser scanning microscope.

2.3.5 MTT viability assay

The enzymatic cleavage of thiazolyl blue tetrazolium bromide (MTT) can be used as a proxy for cell viability (Denizot & Lang 1986, Mosmann 1983): soluble, yellow MTT is converted to insoluble, purple formazan crystals by dehydrogenase enzymes in functioning mitochondria. Media was aspirated from cells, which were then incubated for 30-50 min at 37˚C with 200 µl PBS and 25 µl 5 mg/ml MTT in PBS. The assay was terminated and the formazan solubilised using 600 µl DMSO. To aid solubilisation the plate was put in the 37˚C shaker for 5-15 min. 500 µl of this solution was then transferred to a new 24-well plate to stop residue in the wells affecting the absorbance reading. At least three wells without cells were processed in parallel. Absorbance of each well was measured at a wavelength of 570 nm using a FLUOstar OPTIMA plate reader (BMG Labtech). The absorbance of each well was recorded at least three times and a mean average taken. To calculate relative viability, the mean absorbance of the wells lacking cells was subtracted from the mean recording for each individual well. This individual value was then used to calculate viability relative to the mean average across all the wells of a control treatment (the first bar in each graph).

2.3.6 Trypan blue exclusion assay

The cells and media of each well were removed to 1.5 ml eppendorf tubes. Cells were pelleted at 7,000 x *g* for 2 min, the supernatant carefully removed, and the cells then resuspended in 100 µl 0.4% (w/v) trypan blue:serum-free DMEM (1:1). 10 µl of this cell suspension was then applied to a haemocytometer, and viewed using an Olympus CK2 inverted microscope with 10x objective lens. The percentage of viable cells was calculated by dividing the number of live cells (as assessed by exclusion of the trypan blue dye) by the total number of cells and multiplying by 100.

2.3.7 Neurite measurements

Undifferentiated NSC-34 cells are round and lack neuronal processes; therefore, neurite outgrowth was induced by reducing FBS concentration of the supporting media from 10 to 3% (v/v), a concentration shown to reduce serum withdrawal-associated cell death (Matusica *et al.* 2008). After transfection, cells were allowed to grow for 96 h in differentiation media. β-tubulin-stained cells were examined using a Zeiss Axioplan 2 microscope with mounted AxioCam and a 20x objective lens. ≥ 15 images were taken of cells from each condition per individual experimental replicate, and an average of 121.4 cells were counted to assess the percentage of cells bearing at least one neurite, and 59.4 neurites measured to calculate mean length. Cells in direct contact with five or more other cells and neurites less than 10 µm were excluded from the analyses. Neurite measurements were calculated using ImageJ by manually plotting points along the length of a cell's longest neurite. Abnormal neurites were scored as those with axonal swellings, that completely reverted back on themselves, or that diverted off at a distinct angle greater than 30˚ at least 10 µm from the base of the projection (Locatelli *et al.* 2012).

2.3.8 Secretion assays

For C2C12 cell experiments, the media was discarded two days post-magnetofection, and the cells carefully washed three times with 0.5 ml pre-warmed PBS. 1 ml serum-free DMEM was added to the cells, which were then left in the incubator for 8 h. The cell media was spun at 1,500 x *g* for 3 min and the supernatant re-spun at 4,000 x *g* for 10 min. The supernatant was then concentrated using VIVAspin columns (MWCO 10 kDa, Sartorius) at 4,000 x *g* for 20 min. 1.5% (v/v) protease inhibitor cocktail was added to the concentrated media, which was then frozen at -80˚C for Western blotting. Meanwhile, protein was also extracted from the cells as described above. The secretion assay was performed three times independently. For the WHEP-deletion secretion study, the cytoplasmic form of human GlyRS (wild type or P234KY mutant) was cloned into the pcDNA6-V5/His vector to produce the 685 residue protein with a V5 tag and a His_6 tag at the C-terminus. To create the WHEP domain-deleted GlyRS, 69 residues were removed from the N-terminus. GlyRS constructs were transiently transfected into COS7 cells, and 24 h post-transfection, the cell media was separated from the cells and used in Western blot analysis to evaluate GlyRS secretion.

2.4 *Drosophila*-specific methods

2.4.1 *Drosophila* genetics

Coding sequences of *Drosophila* $gars^{WT}$, $gars^{P234KY}$, $gars^{G240R}$, and $gars^{\Delta WHEP\text{-}P234KY}$ were amplified using primers containing KpnI sites, subcloned into pUAST, and injected into embryos. We wish to thank the following for stocks/reagents: *1032-GAL4*, *Act5C-GAL4*, *elav-GAL4*, *how-GAL4*, and $plexB^{KG00878}$ (BDSC, Indiana University), *BG487-GAL4*, and

C57-GAL4 (Vivian Budnik), *UAS-plexB* (Alex Kolodkin), *nrv2-GAL4* (Paul Salvaterra), and *69B-GAL4* (Clive Wilson).

2.4.2 Behavioural assays

All stocks were cultured on standard molasses/maize meal and agar medium in plastic vials or bottles at 25˚C. Adult viability assays were conducted by crossing GAL4 driver stocks to lines harbouring *gars* overexpression or to w^{1118} for controls. Embryos were then counted and lined on apple juice plates with yeast, and the development of the larvae was noted. Fresh yeast was added daily. Two days post-eclosion the number of surviving adult flies was counted for each genotype. Measurement of motor function involved placing individual age-matched larvae at the centre of a 0.7% (w/v) agar plate and counting the forward body wall contractions exhibited in 2 min.

2.4.3 Larval NMJ analysis

Larvae for branching and bouton counts were reared, dissected, and processed as previously described with analysis of hemisegment A2 (Schuster *et al.* 1996). Ectopic branch contact analysis was performed by looking at L3 larval hemisegments A1 to A3. For immunohistochemistry, anti-discs large (DLG, Developmental Studies Hybridoma Bank, DSHB), anti-HRP (Jackson), anti-Bruchpilot (DSHB), and anti-HA (Santa Cruz) were all used at 1/100, with the secondary antibodies, AlexaFluor 488 goat anti-rabbit and AlexaFluor 633 goat anti-mouse (Invitrogen) at 1/1000. Z-stacks were taken using a Leica SP5 laser confocal microscope and analysis performed using ImageJ and Photoshop (Adobe).

2.5 Mouse-specific methods

2.5.1 Genotyping *Gars* mice

Ear biopsies were taken from young mice and the DNA extracted as described above. *Gars*$^{C201R/+}$ mice were differentiated from wild type by PCR followed by sequencing. Genotyping of *Gars*$^{Nmf249/+}$ mice was performed using a common forward primer with wild type- and mutant-specific reverse primers (Table 2.8) in separate reactions. Cycling conditions: 95˚C for 3 min, 35 x [95˚C 30 sec, 64˚C 30 sec, 72˚C 1 min], 72˚C 2 min. PCR products were separated on a 1.5% (w/v) agarose gel.

Genotype	Forward primer 5'-3'	Reverse primer 5'-3'
Gars^{C201R}	ATACATGCCTGTGGTGAGCA	CTGAGCCATCTCTCCAGGAC
Gars^{Nmf249}	GCCTTGTTCTGTAACGTTTGCAC	CCAGGCATATTTCCTCCATATTT
Gars^{+}	GCCTTGTTCTGTAACGTTTGCAC	CCAGGCATATTTCCTCCAGG

Table 2.8. Primers used to genotype *Gars* mice.

2.5.2 NMJ Visualisation and scoring

Mice were sacrificed, muscles dissected, and NMJs immunohistochemically labelled and observed as previously described (Murray *et al.* 2008). Muscles were dissected in chilled PBS and fixed in freshly prepared 4% (w/v) PFA in PBS for 15 min. Muscles were permeabilised with 2% (v/v) Triton X-100 in PBS for 30 min, blocked in 4% (w/v) bovine serum albumin and 1% (v/v) Triton X-100 in PBS for 30 min, and then incubated overnight at 4˚C in blocking solution with primary antibodies against neurofilament (2H3, 1/50, DSHB) and synaptic vesicles (SV2, 1/100, DSHB). PBS was used to wash the muscles three times for 1 h before exposure to 5 mg/ml tetramethylrhodamine α-bungarotoxin (Cambridge Bioscience) in PBS for 10 min to label post-synaptic AChRs. Muscles were incubated with AlexaFluor 488 secondary antibody (goat anti-mouse, 1/250, Invitrogen) in PBS, washed three times in PBS for 1 h, and mounted in Mowiol on glass slides with coverslips for subsequent imaging using a Zeiss LSM 510 META laser

scanning microscope or Zeiss Axioplan 2 microscope. Only NMJs with clearly visible pre-synaptic axons and terminals were scored. The first to fourth deep lumbrical muscles from the left hind-paw were dissected and scored. ≥ 40 NMJs were scored per mouse for innervation, perforation, and occupancy counts, and ≥ 14 for NMJ area measurements. ≥ 4 mice per genotype were scored at each time point. The region circumscribed by post-synaptic staining was measured using ImageJ to assess NMJ area. For occupancy counts, NMJs were categorised as previously described (Comley *et al.* 2011).

3. A new *Caenorhabditis elegans* model for SMA

With permission from Oxford University Press, the text and figures in this chapter are adapted from the published article Sleigh JN, Buckingham SD, Esmaeili B, Viswanathan M, Cuppen E, Westlund BM, Sattelle DB. 2011. A novel Caenorhabditis elegans *allele,* smn-1(cb131)*, mimicking a mild form of spinal muscular atrophy, provides a convenient drug screening platform highlighting new and pre-approved compounds.* Hum Mol Genet *20: 245-60. As the first author of the above publication, I took the lead on writing the sections that are included in this thesis.*

3.1 Introduction

Over the past few years, gene therapy strategies to restore SMN protein levels have shown great promise in mouse models of SMA (Passini & Cheng 2011). Using viral vectors to augment *SMN* expression, and antisense oligonucleotides or bifunctional RNAs to correct endogenous *SMN2* splicing, a number of research groups have been able to drastically improve motor function, body weight, and survival (from two weeks to over a year in some cases) in disease model mice (Dominguez *et al.* 2011, Foust *et al.* 2010, Glascock *et al.* 2012, Hua *et al.* 2011, Osman *et al.* 2012, Passini *et al.* 2011, Porensky *et al.* 2012, Valori *et al.* 2010). Consequently, the National Institutes of Health and other funding bodies have highlighted SMA as being one of the neurogenetic diseases that is closest to being cured. Nevertheless, these technologies have yet to be proven safe and efficacious in humans, and given that SMA has no available treatment, other options may prove beneficial in the short term.

Many compounds have shown potential to increase SMN protein levels and improve disease phenotypes in cell and animal models of SMN depletion (Fuller *et al.*

2010). A number of these have made it into pilot and early clinical trials (Kinali *et al.* 2002, Liang *et al.* 2008, Mercuri *et al.* 2004, Miller *et al.* 2001, Russman *et al.* 2003, Tzeng *et al.* 2000, Weihl *et al.* 2006); however, even the most promising, including phenylbutyrate and valproic acid, had only negligible or short-lived benefits sometimes with undesirable side effects (Brichta *et al.* 2006, Mercuri *et al.* 2007, Rak *et al.* 2009, Swoboda *et al.* 2010, Tsai *et al.* 2007). From mouse studies, it is evident that early intervention leads to the best outcome (Butchbach *et al.* 2010, Foust *et al.* 2010, Hammond *et al.* 2010, Hua *et al.* 2011, Lutz *et al.* 2011, Narver *et al.* 2008). Hence, the timing of therapy delivery may have played a factor in these trials. This highlights a critical role for pre-clinical model systems in informing clinical trials. The considerable ethical hurdles required to allow clinical trials in pre-symptomatic neonates will only be overcome if there is a clear scientific rationale based on proven efficacy before disease onset, for example, in mice.

The approach of screening libraries containing drugs approved for human use has successfully highlighted potential pharmacological agents for the treatment of several neurodegenerative disorders including amyotrophic lateral sclerosis and Huntington's disease (Barber *et al.* 2009, Desai *et al.* 2006). Interestingly, a number of drugs used to treat various other diseases have shown off-label effects that may prove beneficial to SMA patients (Jarecki *et al.* 2005, Riessland *et al.* 2010). Thus, screening pre-approved compounds for potential as SMA therapeutics may accelerate the identification and development of drugs helpful in treating the disease. The majority of laboratories working on treatments for SMA are focusing on gene therapy strategies; however, if these were to have limited success in patients, it is important that other avenues remain to be pursued.

For speed and economy of testing, invertebrate organisms offer convenient models for both chemical and genetic screening (Jones *et al.* 2005, Simpson *et al.* 2012, Sleigh &

Sattelle 2010, Westlund *et al.* 2004). The nematode *C. elegans* is ideal in this regard, with its benefits of rapid lifecycle (Figure 3.1), substantial reproductive capacity, ease of large-scale culture, and potential for automated behavioural analysis (Buckingham & Sattelle 2008, Buckingham & Sattelle 2009). *C. elegans* can be quickly dispensed into 96-well plates containing chemical compounds and screened for alteration of easily scorable phenotypes. Several drugs used in the clinic to treat neurodegenerative disease are also effective in *C. elegans* models (Braungart *et al.* 2004, Gaud *et al.* 2004, Marvanova & Nichols 2007). This small invertebrate is thus a powerful tool with which to triage compounds from large chemical libraries prior to validation in vertebrate models. Indeed, a *C. elegans* model of Duchenne muscular dystrophy was recently used to screen and identify compounds that caused improvement of muscle strength in the dystrophic mouse model (Giacomotto *et al.* 2009).

C. elegans possesses a single gene, *smn-1*, orthologous to *SMN1* that is expressed throughout development and in a number of cell types including neurons and body wall muscles (Miguel-Aliaga *et al.* 1999). Like human SMN, SMN-1 has been shown to self-oligomerise and bind to the *C. elegans* orthologue of Gemin2 (Burt *et al.* 2006, Miguel-Aliaga *et al.* 1999). Disruption of endogenous SMN-1 function using RNAi results in various phenotypic defects including locomotor dysfunction and sterility (Miguel-Aliaga *et al.* 1999), and a null mutant, *smn-1(ok355)*, displays a range of morphological and physiological defects including abnormal germline migration and severely reduced swimming (thrashing) rate (Briese *et al.* 2009). The *smn-1(ok355)* mutant animals appear normal during early development due to maternal loading of SMN-1 protein and mRNA, but rapidly deteriorate in later larval stages (Briese *et al.* 2009). The *smn-1(ok355)* deletion is homozygous lethal and so must be maintained using a chromosomal balancer, limiting the ease with which the mutant can be used for large-scale screening.

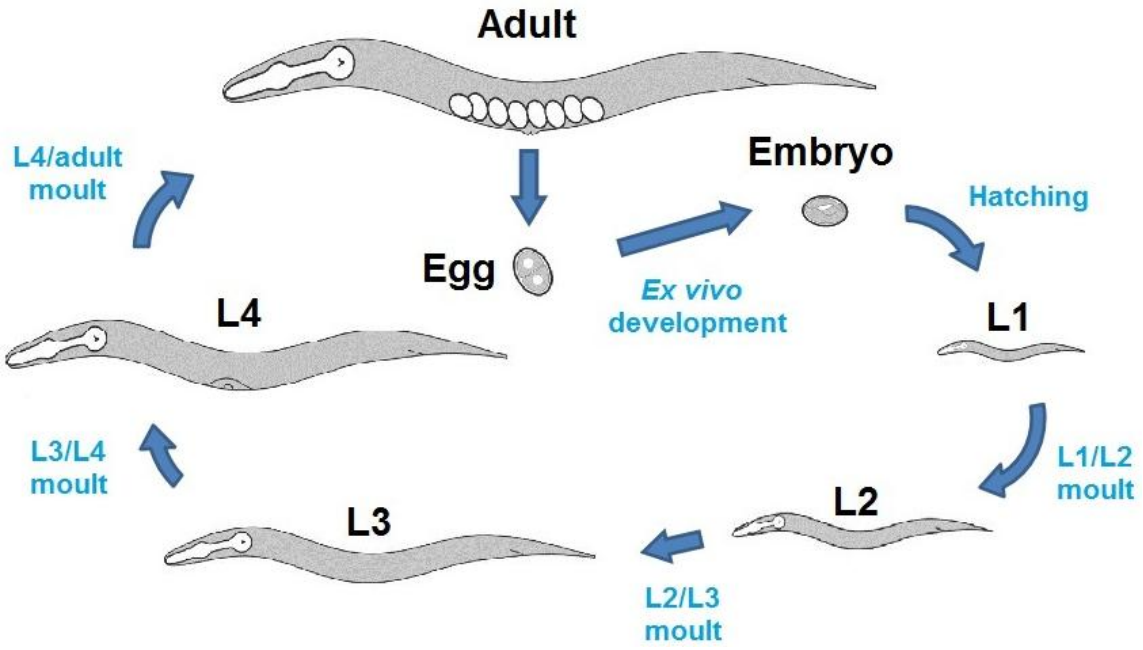

Figure 3.1. The *C. elegans* life cycle. The life cycle of *C. elegans* consists of an embryonic stage, four larval stages (L1-L4), and adulthood. At the end of each larval stage, a new, stage-specific cuticle is produced and the old one disposed of during moulting. At 23.5˚C, it takes ≈ 72 h for a newly laid egg to reach adulthood. If conditions are not optimal for growth, for example there is no food or the worms are overcrowded, early stage larvae (L1/L2) can enter an arrested state called dauer. For simplicity, this part of the cycle has been omitted as it is not relevant to the work presented in this thesis. Figure adapted from Wood (1988).

3.1.1 Aims of chapter 3

The *smn-1* null mutant has been used in a large-scale screen (Dimitriadi *et al.* 2010); however, neuromuscular defects manifest suddenly and progress rapidly, making screening of the locomoter phenotype difficult. A milder and fertile allele with a robust defect in thrashing would obviate the need for a balancer chromosome and the expensive equipment needed to separate genotypes. The goal of work in this chapter was to characterise a recently isolated allele, *smn-1(cb131),* which encodes an amino acid substitution closely resembling a change in SMN found in a patient with a less severe form of the disease, in the hope of developing a *C. elegans* model for SMN-1 dysfunction that would facilitate

screening. I aimed to assay a range of phenotypes to see how the point mutant compared with the already available null mutant. An automated screening system able to measure thrashing rate of worms in 96-well plates was available to me (Buckingham & Sattelle 2009). I wanted to test the ability of the software to accurately measure rate of locomotion and then screen a small library of 1,040 diverse compounds, including many with known human therapeutic profiles and nerve/muscle activity, for amelioration of the *smn-1(cb131)* thrashing defect with the goal of expediting the development of drugs for the treatment of SMA.

3.2 Results

3.2.1 The reduced growth and lifespan of the *smn-1(cb131)* allele

smn-1(cb131) (strain LL2073), isolated in a reverse genetic screen for *smn-1* mutants, contains a novel point mutation in exon 2 that alters a highly conserved amino acid residue (D27N) in the SMN-1 protein (Figure 3.2). This same residue (D44V) is mutated in a patient with type III SMA, a less severe, but still debilitating, form of the disease (Sun *et al.* 2005). This alteration in human SMN affects N-terminal self-association, Gemin2 binding, snRNP assembly activity, and protein stability *in vitro* (Ogawa *et al.* 2007). Recently, the D44 residue of SMN was shown to interact with R213 of Gemin2, which likely explains why the D44V mutation causes impaired Gemin2 binding and leads to a defect in snRNP biogenesis (Zhang *et al.* 2011).

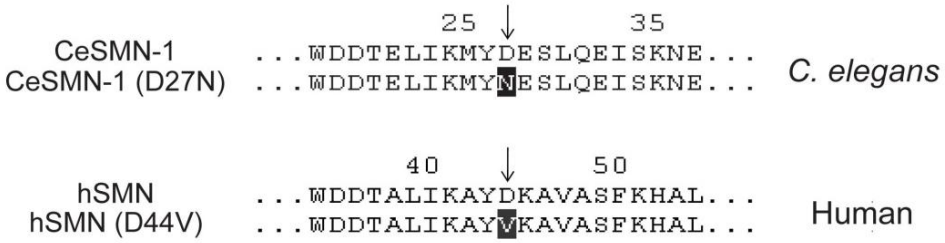

Figure 3.2. *smn-1(cb131)* harbours a novel point mutation that mimics a substitution seen in a SMA type III patient. In *C. elegans* SMN-1 (CeSMN-1), aspartic acid (D) at residue 27 is mutated to asparagine (N). In human SMN (hSMN), D is mutated to valine (V) at residue 44. Figure taken with permission from Oxford University Press from Sleigh *et al.* (2011a).

There does not appear to be any gross change in the rate of development of *smn-1(cb131)* compared to wild type up to 4 days post-L1 (larval stage 1, Figure 3.3). The developmental stage of mutant and wild type animals was scored 24, 48 and 72 h after eggs were laid and no difference between strains was seen at any time point (data not shown). However, 3-5 days post-L1 the mutant body length was significantly shorter than wild type, with the growth of *smn-1(cb131)* animals appearing to cease between 2 and 3 days post-L1 while wild type continued to grow (Figure 3.4A). The median and mean values of *smn-1(cb131)* body length were within 11 μm of each other on days 3-5. *smn-1(cb131)* also displayed a significantly reduced lifespan with median survival of 15 days compared to 17 days for wild type at 23.5˚C (Figure 3.4B). During lifespan assays mutant animals stopped moving around the plate sooner than wild type, indicating an accelerated age-associated decline in movement.

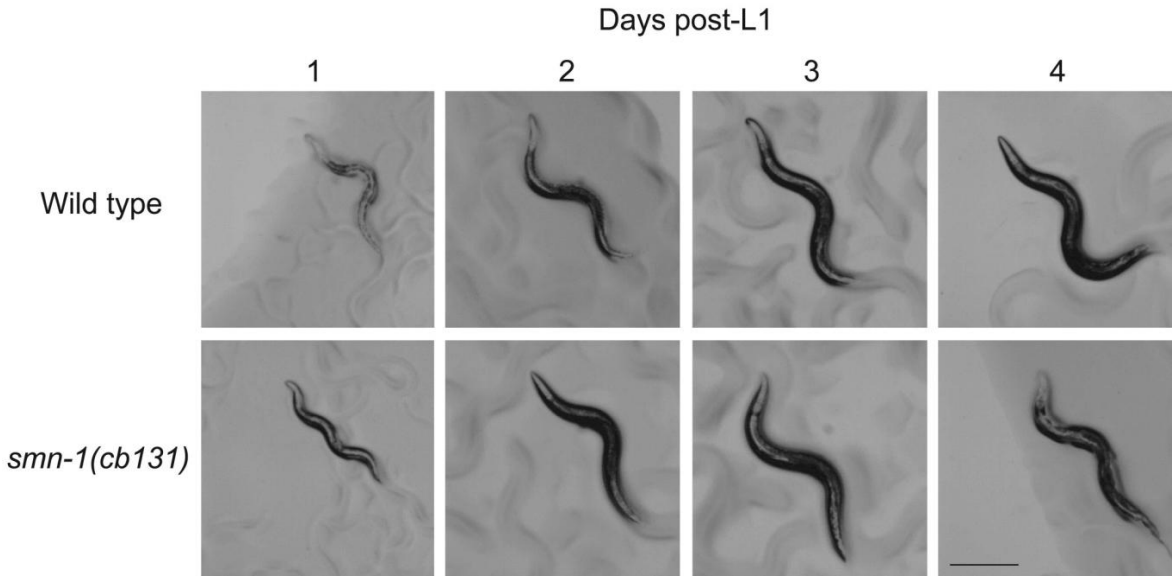

Figure 3.3. Developmental comparison of *smn-1(cb131)* with wild type. There is no obvious developmental difference between *smn-1(cb131)* and wild type. The strain is indicated on the left and the number of days post-L1 of the age-synchronised animals above. For all images the head is on the left and the tail on the right. Scale bar = 400 μm. Figure taken with permission from Oxford University Press from Sleigh *et al.* (2011a).

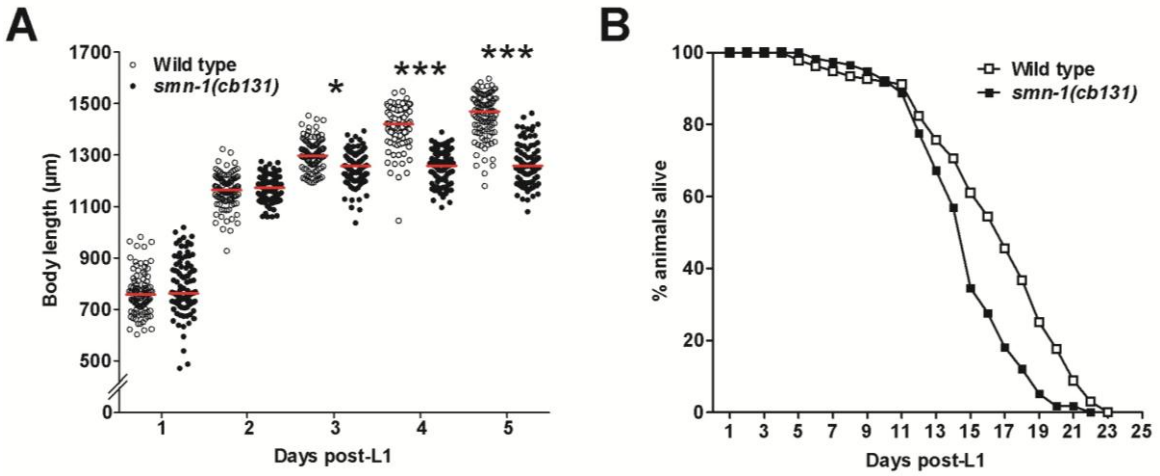

Figure 3.4. *smn-1(cb131)* displays defects in body length and survival. (A) *smn-1(cb131)* grows at a similar rate to wild type up to two days post-L1; however, after 3-5 days they have a significantly shorter body length. *smn-1(cb131)* animals were 95.9 ± 1.6%, 88.7 ± 0.6% and 87.0 ± 0.6% the length of wild type animals on days 3, 4 and 5, respectively. 100 animals/strain/time point were assayed over three independent experiments. Red lines indicate the median value. $P < 0.001$, Kruskal-Wallis test. * $P < 0.05$; *** $P < 0.001$, Dunn's multiple comparison test. **(B)** *smn-1(cb131)* (n = 115) has a median survival of 15 days and wild type (n = 136) 17 days at 23.5˚C. $P < 0.001$, Log-rank (Mantel-Cox) test; $P < 0.001$, Gehan-Breslow-Wilcoxon test. Data points represent the percentage of age-synchronised animals found alive each day post-synchronisation. Data from three independent assays are presented. In each experiment, wild type animals lived longer than mutant with $P < 0.001$, $P = 0.002$ and $P = 0.119$, Log-rank (Mantel-Cox) test. Figure taken with permission from Oxford University Press from Sleigh *et al.* (2011a).

3.2.2 Defects in egg-laying and hatching

On food, age-synchronised young adult *smn-1(cb131)* animals laid ≈ 50% of the number of eggs as wild type (Figure 3.5A). Since food cues play an important role in egg-laying behaviour (McGovern *et al.* 2007), the response of *smn-1(cb131)* to the absence of food was also assessed. As expected, wild type animals laid considerably fewer eggs without food. *smn-1(cb131)* animals also laid significantly fewer eggs suggesting that the egg-

laying defect was not a result of a deficit in food chemosensation or sensory processing of food cues.

There was also no difference in the number of eggs retained in the uterus of mutant and wild type animals (Figure 3.5B), which was confirmed by sodium hypochlorite bleaching of the cuticle and counting of the number of released eggs (data not shown). Due to increased egg retention, egg-laying defective mutants usually bloat and show an enhanced tendency for internal hatching of larvae (Trent *et al.* 1983), but this was not common in *smn-1(cb131)*, which could mean that the defect is perhaps pre-egg-laying, i.e. in the generation of embryos, maybe due to a sperm or oocyte defect. Brood size assays confirmed that egg production is affected; *smn-1(cb131)* animals laid fewer eggs over a lifetime than wild type (Figure 3.5C). During the retention assay there was an indication that some mutant uteri were less well organised than in wild type, with less distinct egg boundaries. Also, some mutant animals expelled an amorphous substance from the vulva into the medium. On plates, ≈ 5-10% of eggs laid were unusually circular, discoloured, or large. Eggs laid by *smn-1(cb131)* mutants hatched at a slightly lower frequency than those laid by wild type (Figure 3.5D).

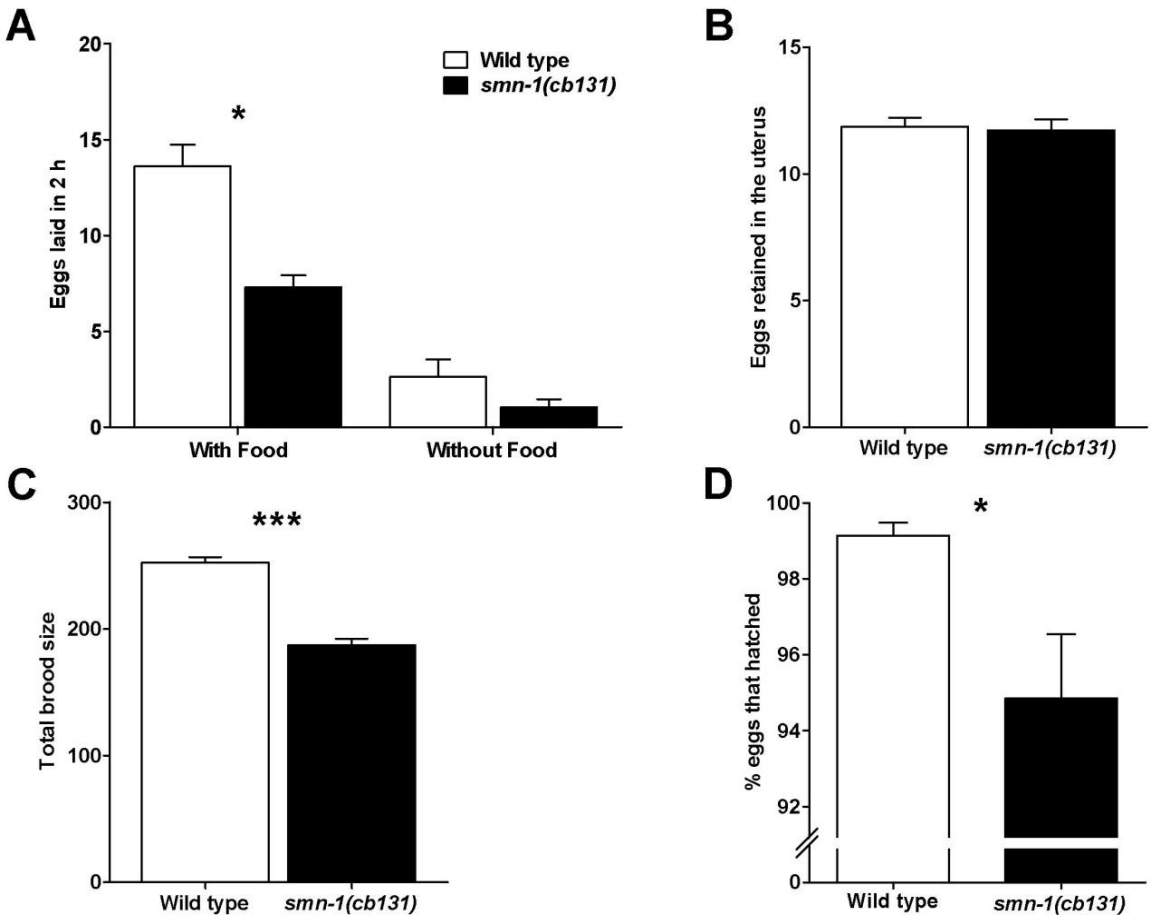

Figure 3.5. *smn-1(cb131)* is defective at egg-laying. (A) In 2 h at 23.5˚C, age-synchronised young adult *smn-1(cb131)* animals laid approximately half the number of eggs as wild type on food. However, they responded normally to food cues, laying fewer eggs without food. 23-24 animals/strain were assayed for each condition over three independent experiments. $P < 0.001$, Kruskal-Wallis test. * $P < 0.05$, Dunn's multiple comparison test. **(B)** There was no difference in the number of eggs retained in the uterus of wild type and *smn-1(cb131)* young adults. 30 animals/strain were assayed over three independent experiments. An unpaired *t*-test was used to assess significance. **(C)** The total brood size of *smn-1(cb131)* animals was reduced. 30 animals/strain were assayed over three independent experiments. *** $P < 0.001$, unpaired *t*-test with Welch's correction. **(D)** The percentage of mutant eggs laid by young adults that failed to hatch is six times that of wild type (5.14% and 0.86%, respectively). Hatching percentages were calculated for individual sets of ≥ 50 eggs. 650 eggs/strain were assayed over seven independent experiments. * $P < 0.05$, unpaired *t*-test with Welch's correction. Figure taken with permission from Oxford University Press from Sleigh *et al.* (2011a).

3.2.3 Pharyngeal pumping rate is unchanged but motility is defective

The *C. elegans* pharynx, a neuromuscular pump used to ingest and break up food, pumps back and forth in an easily-quantifiable manner. Similarly, when placed in liquid, *C. elegans* thrash back and forth at a regular rate. Pharyngeal pumping and thrashing assays are thus simple, robust methods for assessing neuromuscular function. *smn-1(ok355)* null mutants (strain LM99) show a dramatic and progressive decline in pharyngeal pumping and thrashing rates at the L2/L3 stage that continues until death a few days later (Briese *et al.* 2009, Dimitriadi *et al.* 2010). Pharyngeal pumping and thrashing rates of *smn-1(cb131)* animals were thus assessed.

To assay pharyngeal pumping rates, animals were filmed for 10 s and videos were played back in slow motion to enable accurate counting. Mutant pumping rates were indistinguishable from wild type from 1 to 10 days post-L1 (Figure 3.6A). Thrashing assays were performed in PBS on 1-5 consecutive days post-L1. Similar to wild type, *smn-1(cb131)* animals showed a gradual reduction in thrashing rate over time; however, no striking decline, as seen in the null mutant, was observed (Figure 3.6B). Nevertheless, *smn-1(cb131)* did consistently thrash at a significantly reduced rate compared to wild type animals at all times tested, indicating a robust motility defect.

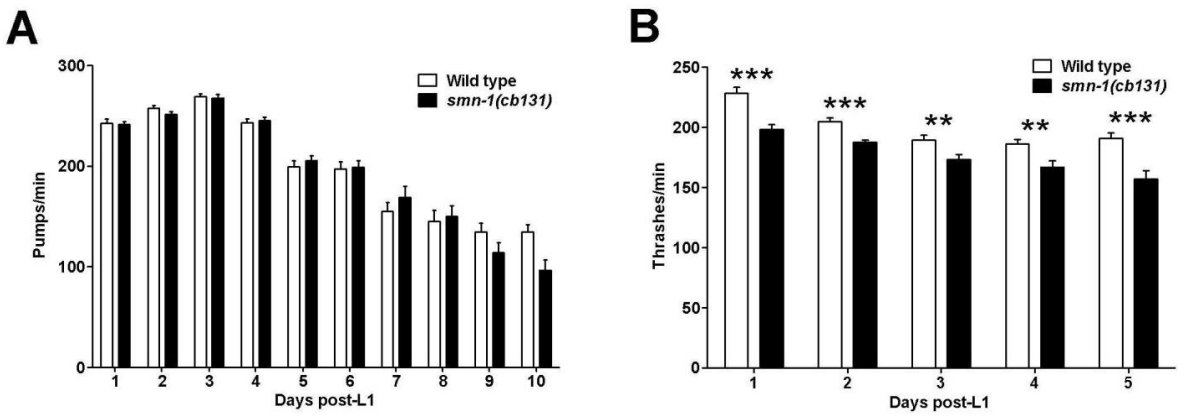

Figure 3.6. Thrashing but not pharyngeal pumping rate is reduced in *smn-1(cb131)*. (A) Pharyngeal pumping rates of wild type and *smn-1(cb131)* 1-10 days post-larval L1 stage. *smn-1(cb131)* pumping rates are indistinguishable from wild type at all time points. ≥ 24 animals/strain/time point were assayed over three independent experiments. $P < 0.001$, Kruskal-Wallis test. **(B)** Thrashing rates of wild type and *smn-1(cb131)* after 10 min in PBS 1-5 days post-L1. *smn-1(cb131)* consistently thrashes at a slower rate than age-synchronised wild type. *smn-1(cb131)* animals thrashed at 86.8 ± 5.0%, 93.1 ± 5.4%, 91.6 ± 5.2%, 90.0 ± 8.5% and 82.9 ± 3.0% of the rate of wild type on days 1-5, respectively. ≥ 22 animals/strain/time point were assayed over three independent experiments. $P < 0.001$, Kruskal-Wallis test. * $P < 0.05$; ** $P < 0.01$; *** $P < 0.001$, Dunn's multiple comparison test. Figure taken with permission from Oxford University Press from Sleigh *et al.* (2011a).

3.2.4 Synaptic neurotransmission is deficient in *smn-1(cb131)* animals

In order to determine the cause of the motility defect, muscle and nervous system architecture in young adults were examined. The musculature of wild type and *smn-1(cb131)* animals was assessed by Nomarski microscopy (Figure 3.7A, B) and by fluorescence microscopy of phalloidin staining of F-actin (Figure 3.7C, D). No obvious differences in muscle size, structure or orientation were seen, suggesting that the motility defect of *smn-1(cb131)* is unlikely to be due to muscle degeneration. To perform neuron counts and to observe the morphology of the nervous system, *smn-1(cb131)* animals were crossed with a strain expressing pan-neuronal *GFP*, *F25B3.3::GFP* (Altun-Gultekin *et al.*

2001), producing *smn-1(cb131); F25B3.3::GFP* (strain LM123), which was confirmed by sequencing. Using White *et al.* as a guide (White *et al.* 1986), GFP-positive neuron cell bodies in the ventral nerve cord, which includes cholinergic and gamma-aminobutyric acid (GABA)-ergic neurons that control locomotion, were counted (Figure 3.7E). No difference was seen between *smn-1(cb131)* and control animals, a result similar to that seen for the null mutant (Briese *et al.* 2009). The nervous systems of the two strains were then examined in more detail for subtle abnormalities that may account for the motility defect. The organisation of both the ventral and dorsal nerve cords were inspected, as well as neuronal trajectories, but no obvious differences in morphology were seen.

Since the structure of the neuromuscular system was not grossly affected, synaptic transmission efficiency of *smn-1(cb131)* was assessed using the acetylcholinesterase inhibitor pyridostigmine bromide. Pyridostigmine bromide disrupts the enzymatic breakdown of acetylcholine and its subsequent clearance from the synaptic cleft, causing neurotransmitter accumulation and thus muscle hypercontraction. It has been used for many years to treat post-synaptic myasthenic disorders (Argov 2009), and for this reason was chosen for paralysis assays. The time taken for *C. elegans* to paralyse in the presence of the drug gives an indication of whether synaptic neurotransmission at the NMJ is altered. The mutant appears to be relatively resistant to the drug (Figure 3.7F), suggesting that synaptic transmission is defective in *smn-1(cb131)* animals.

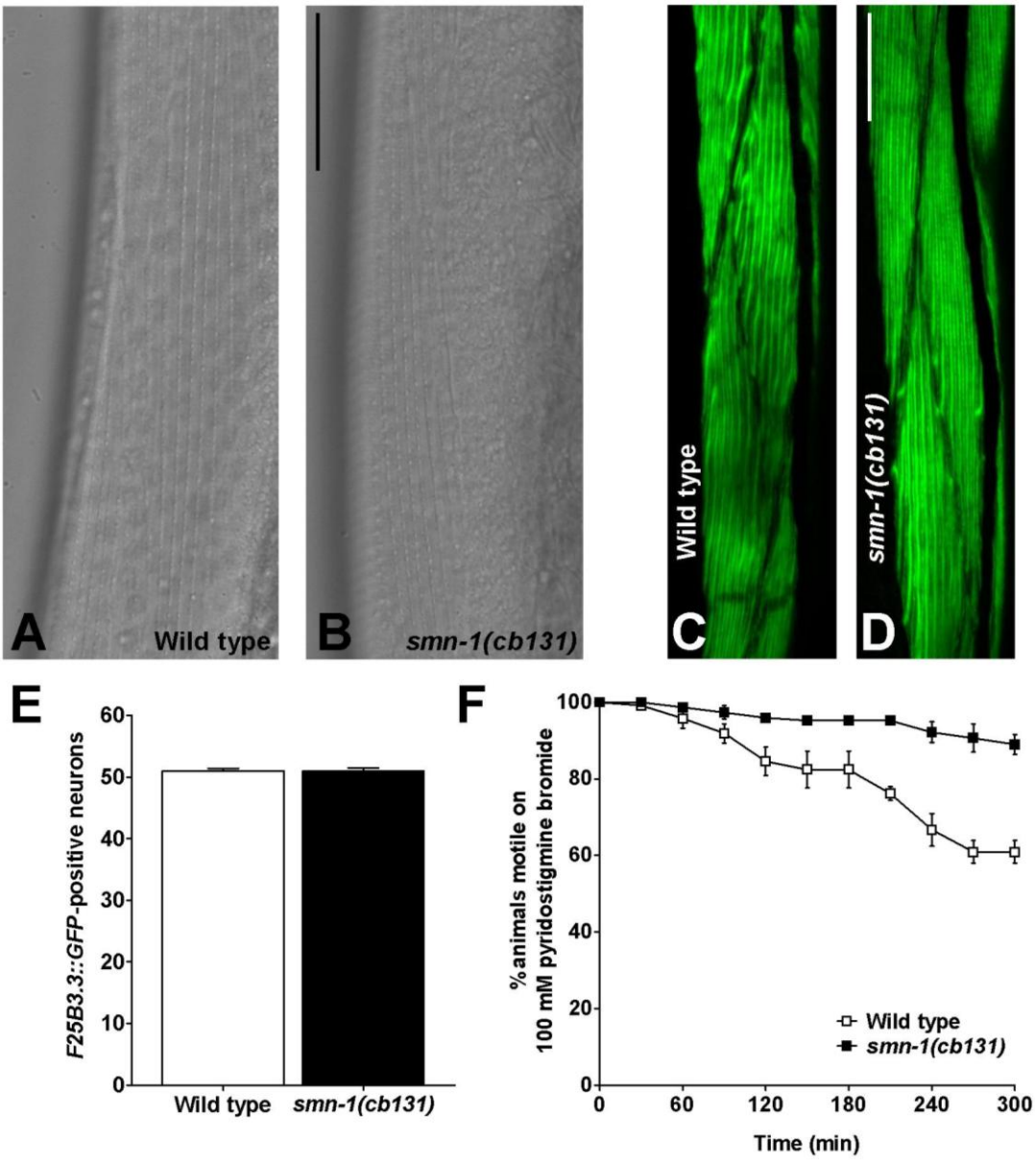

Figure 3.7. *smn-1(cb131)* animals have no gross structural defects in muscles or neurons, but display impaired synaptic transmission. (A, B) Nomarski and (**C, D)** fluorescence microscopy of phalloidin staining of wild type (A, C) and *smn-1(cb131)* (B, D) muscle structure. *smn-1(cb131)* muscle size, structure, and orientation are all similar to wild type. For all images the head is situated upwards and images are taken of regions anterior to the vulva. Scale bars = 25 µM. **(E)** *smn-1(cb131)* animals display no reduction in the number of neuron cell bodies in the ventral nerve cord. GFP-positive cells expressing the pan-neuronal marker *F25B3.3::GFP* were counted from and including VA2 (anterior) to VD11 (posterior). 30 young adults/strain were assayed over three independent experiments. An unpaired *t*-test was used to assess significance. **(F)** *smn-1(cb131)* animals are resistant to the acetylcholinesterase inhibitor pyridostigmine bromide. Data points represent the percentage of age-synchronised young adults found moving on 100 mM

plates at 30 min intervals over a period of 6 h. P < 0.001, Log-rank (Mantel-Cox) test; P < 0.001, Gehan-Breslow-Wilcoxon test. Data from three independent assays are presented P = 0.0011, P = 0.128 and P = 0.0026, Log-rank (Mantel-Cox) test. Figure taken with permission from Oxford University Press from Sleigh *et al.* (2011a).

3.2.5 *smn-1(cb131)* defects are specific to the point mutation

To confirm that *smn-1(cb131)* is indeed an allele of *smn-1*, and that defects seen in the strain are due to the mutation in *smn-1*, a complementation test was performed (Brenner 1974). *smn-1(cb131)* was combined *in trans* with *smn-1(ok355)* by crossing *smn-1(cb131)* males with *smn-1(ok355)/hT2[qIs48]* hermaphrodites, producing *smn-1(cb131) smn-1(ok355)* (strain LM124) progeny. The thrashing rate of these animals was significantly slower than wild type and homozygous *smn-1(cb131)* animals at the young adult stage (Figure 3.8). This suggests that the product of neither allele restores wild type function, meaning that they do not complement and are therefore likely to be alleles of the same gene. However, for complementation testing to work both alleles must be recessive. *smn-1(ok355)* is reccessive as it is a deletion. To provide evidence that *smn-1(cb131)* is recessive, *smn-1(ok355)/hT2[qIs48]* and *smn-1(cb131)/hT2[qIs48]* (strain LM125) animals were also assayed for thrashing (Figure 3.8). If *cb131* were a dominant mutation the thrashing rate of *smn-1(cb131)/hT2[qIs48]* animals would be expected to be similar to *smn-1(cb131)*, due to the presence of the mutated allele, and less than *smn-1(ok355)/hT2[qIs48]*, because of the absence of *cb131*. Neverthless, this was not the case, suggesting that *cb131* is recessive. *smn-1(cb131)/hT2[qIs48]* animals were allowed to lay eggs before assaying so as to be able to subsequently differentiate them from any self-progeny of *smn-1(ok355)/hT2[qIs48]* hermaphrodites, which produce *smn-1(ok355)* null mutants.

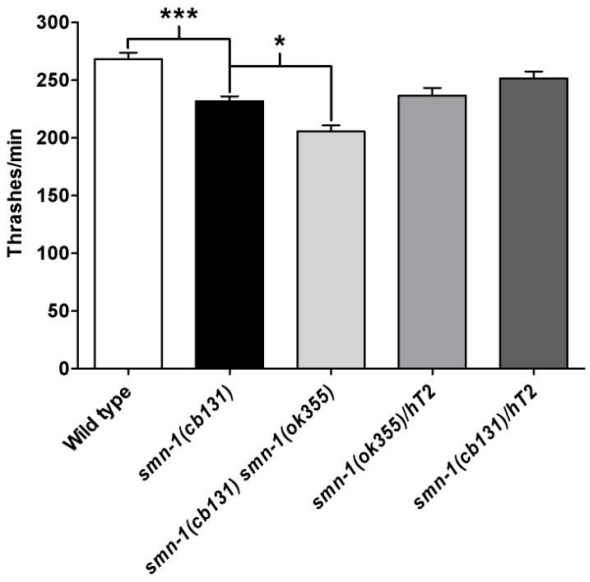

Figure 3.8. *smn-1(cb131)* thrashing defects are specifc to the point mutation. *smn-1(cb131)* males were crossed with *smn-1(ok355)/hT2[qIs48]* hermaphrodites and assayed for motility to test for genetic complementation. *smn-1(cb131) smn-1(ok355)* progeny thrashed significantly slower than wild type, suggesting that the mutations do not complement and are thus both alleles of *smn-1*. *smn-1(cb131)/hT2[qIs48]* animals thrash faster than both *smn-1(ok355)/hT2[qIs48]* and *smn-1(cb131)*, suggesting that *cb131* is not a dominant mutation. 32 animals/strain were assayed over four independent experiments. $P < 0.001$, Kruskal-Wallis test. * $P < 0.05$; *** $P < 0.001$, Dunn's multiple comparison test. Figure taken with permission from Oxford University Press from Sleigh *et al.* (2011a).

3.2.6 Evaluating an automated *smn-1(cb131)* thrashing assay

To determine if the *smn-1(cb131)* thrashing defect could be used as the basis of an *in vivo* chemical library screen, thrashing rates of wild type and *smn-1(cb131)* animals were measured using an automated phenotyping system, developed for measuring the effects of chemicals on locomotion (Buckingham & Sattelle 2009). Synchronised young adults (two days post-L1) were assayed at various time points in liquid suspension from 10 min to 6 h. Young adults were used because thrashing rates of larvae cannot be accurately determined with the software, and assaying a day later would allow sufficient time for progeny of the age-synchronised nematodes to reach a size that confounds quantification of thrashing of

the parent generation. Similar to the results of the manual assay, the automated assay was able to detect a significant difference between wild type and *smn-1(cb131)* animals; the mutants consistently thrashed at a slower rate at all time points in solution (Figure 3.9).

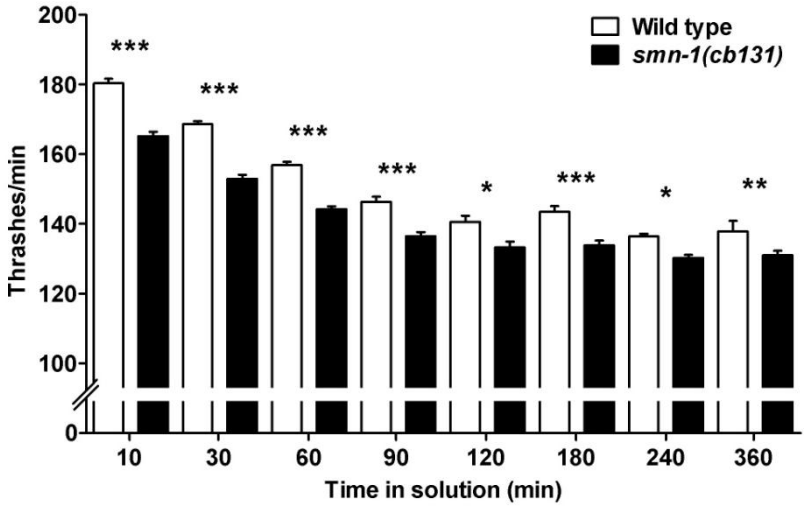

Figure 3.9. Automated assessment of thrashing rates. Two days post-L1, a significant difference was seen between wild type and mutant animals at all time points in PBS. ≥ 69 wells/strain/time point were assayed over three independent experiments. $P < 0.001$, Kruskal-Wallis test. * $P < 0.05$; ** $P < 0.01$; *** $P < 0.001$, Dunn's multiple comparison test. Figure taken with permission from Oxford University Press from Sleigh *et al.* (2011a).

3.2.7 Screening of a chemical library identifies six compounds

The National Institute of Neurological Disorders and Stroke (NINDS) chemical compound library was used to screen *smn-1(cb131)* animals for amelioration of the motility defect. Before screening, the robustness of the automated system to differences in the number of worms per well and volumes of liquid was confirmed using wild type animals (Figure 3.10). The NINDS library consists of 1,040 compounds covering a wide range of drug classes (listed at http://www.msdiscovery.com/), the majority of which are approved for use in humans by the US Food and Drug Administration (FDA) (Abbott 2002, Heemskerk

et al. 2002, Piccioni *et al.* 2004). An overview of the entire screening process can be seen in Figure 3.11A. In brief, for the primary screen 2-25 age-synchronised *smn-1(cb131)* young adult animals were dispensed into each well of 96-well plates containing library compounds dissolved in DMSO at 1 mM (10 µM compound and 1% (v/v) DMSO after addition of liquid and nematodes). Thrashing rates were measured using the previously described automated phenotyping system 4 and 6 h after addition of the animals (Buckingham & Sattelle 2009). The top 64 compounds (Figure 3.11B) that increased thrashing rate at both time points included 48 pre-approved compounds, and comprised various receptor agonists (e.g. cholinergic, GABAergic, glutamatergic, and serotonergic), and muscle relaxants (both skeletal and smooth). These 64 compounds were re-tested in triplicate on both wild type and *smn-1(cb131)* animals in dose-response format at concentrations ranging from <0.1-50 µM in order to highlight the most promising for further study. Six compounds, including four pre-approved drugs, were selected based on dose-dependence, a non-linear regression coefficient (R^2) > 0.1, and a point along the line of regression ≥ 7.3 at both 4 and 6 h. The six compounds were aklavin hydrochloride, 4-aminopyridine (4-AP), gaboxadol hydrochloride, metaraminol bitartrate, N-acetylneuraminic acid (Neu5Ac), and zidovudine.

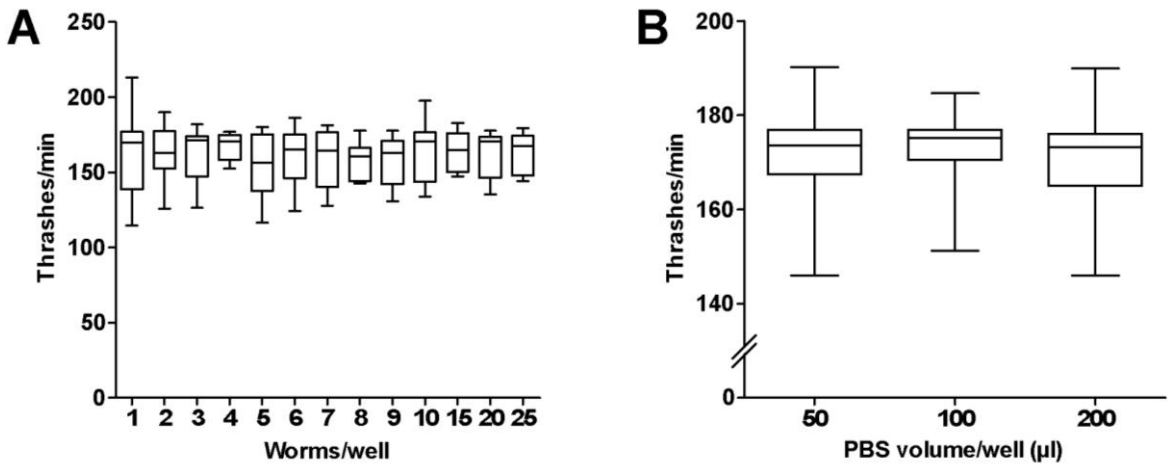

Figure 3.10. The automated thrashing software is robust to the number of worms per well and volume of PBS used. (A) Thrashing rate is unaffected by the number of worms/well. 9 wells/worm number were assayed over three independent experiments. P = 0.982, one-way ANOVA. **(B)** The volume of PBS in each well also has no bearing on thrashing rate. 48 wells/PBS volume were assayed over three independent experiments. P = 0.289, Kruskal-Wallis test. The boxes in both graphs represent the median and interquartile range, and the whiskers depict the range.

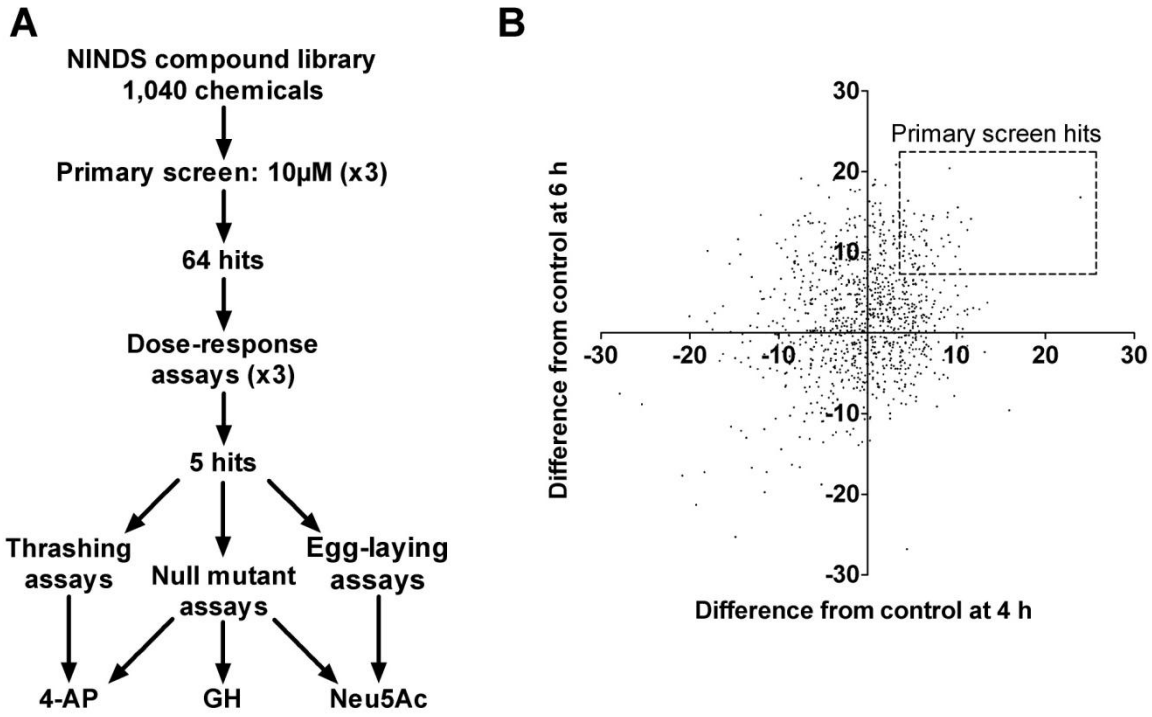

Figure 3.11. Screening overview and primary screen hits. (A) Flow diagram highlighting the screening process. Briefly, the NINDS library comprising 1,040 compounds was independently screened three times at 10 μM for amelioration of the *smn-1(cb131)* thrashing defect. This primary screen highlighted 64 compounds, on which dose-response assays were subsequently performed. Six drugs were identified and then assayed for their ability to improve the various defects of *smn-1(cb131)* and the null mutant, *smn-1(ok355)*. 4-AP, 4-aminopyridine; GH, gaboxadol hydrochloride; Neu5Ac, N-acetylneuraminic acid. **(B)** Primary screen hit compounds. A scatter graph of the 1,040 chemicals showing the median difference in thrashing rate from control at 4 and 6 h. Data represent absolute values. Figure taken with permission from Oxford University Press from Sleigh *et al.* (2011a).

3.2.8 Validation of the top six compounds

In order to identify which, if any, of the six compounds could robustly and significantly improve motility of *smn-1(cb131)*, additional thrashing assays were performed. The most effective concentration for each compound from the dose-response assays was used. This was 25 μM for 4-AP, gaboxadol hydrochloride and Neu5Ac, 12.5 μM for metaraminol bitartrate and 6.25 μM for zidovudine. Unfortunately, aklavin hydrochloride was

unavailable for purchase. Compounds used in these assays were obtained from a source independent of the NINDS library manufacturer. Age-synchronised young adults were assayed in the presence of compounds at 1.5, 2, 2.5, and 3 h (Figure 3.12A). 4-AP significantly improved *smn-1(cb131)* motility at all time points and had no effect on wild type. However, it also increased thrashing frequency of *unc-63(x26)* (strain ZZ26) after 1.5-2.5 h, which was included to test the specificity of the drugs for the *smn-1(cb131)* mutation. Disturbed expression of *unc*-63, a nicotinic AChR subunit found in both muscles and neurons, results in locomotor dysfunction (Culetto *et al.* 2004, Kaas *et al.* 2010, Sleigh 2010). *unc-63(x26)* was thus included as a control because it encodes a point mutation in *unc-63*, which is important for synaptic transmission (Culetto *et al.* 2004), that results in a mild motility defect (Kaas *et al.* 2010).

The top 5 available compounds were also tested for their ability to improve the *smn-1(cb131)* egg-laying defect. In brief, L4 stage animals were transferred to new plates containing compounds at 50 μM and left to mature overnight. Eggs from these age-synchronised animals were then transferred to new drug plates, placed at 23.5˚C for 72 ± 1 h, and the number of eggs laid by young adults in 2 h was assessed. Drugs were also added at the same final concentration to the food used to seed the plates; only zidovudine visually affected the growth of the bacterial lawn, causing small distinct clusters of food to form and the lawn to take on a slightly darker appearance. No compound significantly affected wild type egg-laying (Figure 3.12B); however, Neu5Ac significantly increased the number of eggs laid by *smn-1(cb131)* by 26.1 ± 6.0%. Gaboxadol hydrochloride also appeared to improve egg-laying, albeit not reaching significance.

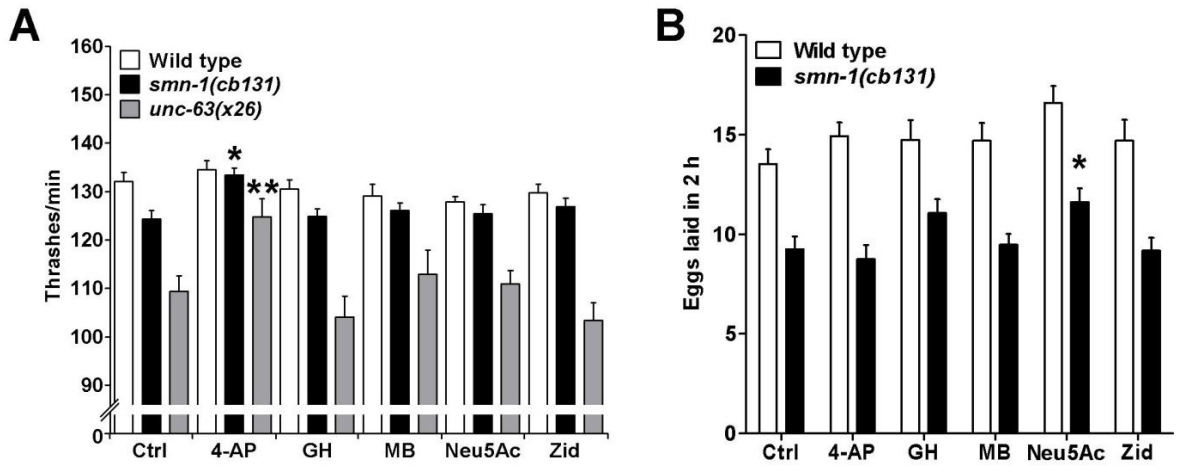

Figure 3.12. 4-AP rescues *smn-1(cb131)* motility and Neu5Ac improves egg-laying. (A) 4-AP significantly rescued thrashing frequency of *smn-1(cb131)* after 1.5, 2, 2.5, and 3 h in solution, did not affect wild type, and improved *unc-63(x26)* thrashing from 1.5-2.5 h. Graphs for all four time points were similar so only that of 2.5 h is presented. 21-22 wells/strain were assayed for each treatment over four independent experiments. $P < 0.001$, Kruskal-Wallis test. **(B)** Animals were exposed to the top six compounds from hatching and the number of eggs laid in 2 h as young adults assayed. None of the compounds had a significant effect on the number of eggs laid by wild type animals ($P = 0.2523$, Kruskal-Wallis test), whereas Neu5Ac significantly increased the number of eggs laid by *smn-1(cb131)* compared to PBS control. 39-40 animals/strain were assayed for each treatment over four independent experiments. $P = 0.0112$, Kruskal-Wallis test. * $P < 0.05$; ** $P < 0.01$, Dunn's multiple comparison test. Ctrl = control, 4-AP, 4-aminopyridine; GH, gaboxadol hydrochloride; MB, metaraminol bitartrate; Neu5Ac, N-acetylneuraminic acid; Zid, zidovudine. Figure taken with permission from Oxford University Press from Sleigh *et al.* (2011a).

3.2.9 Efficacy of compounds in the *smn-1* null mutant

The top five compounds were tested for their ability to rescue lifespan, body length, and pharyngeal pumping, all of which are severely reduced, in the null mutant, *smn-1(ok355)* (Briese *et al.* 2009). Animals heterozygous for the balancer chromosome and the *smn-1* deletion that were raised from hatching on 50 μM drug plates were allowed to lay eggs for 5 h on new drug plates and removed. The homozygous *smn-1* progeny were then assayed for survival each day until death and for body length and pumping at various time points.

No compound significantly affected *smn-1(ok355)* lifespan, although zidovudine did extend the median survival from 6 to 7 days, which approached significance (data not shown). In the body length assays, no compound had a significant effect 1-2 days post-L1; however, after 3 days, both 4-AP and gaboxadol hydrochloride caused significant rescue (Figure 3.13A). 4-AP also significantly improved pharyngeal pumping rate of the *smn-1* null mutant 3 and 4 days post-L1, while Neu5Ac significantly improved pumping on day 4 (Figure 3.13B).

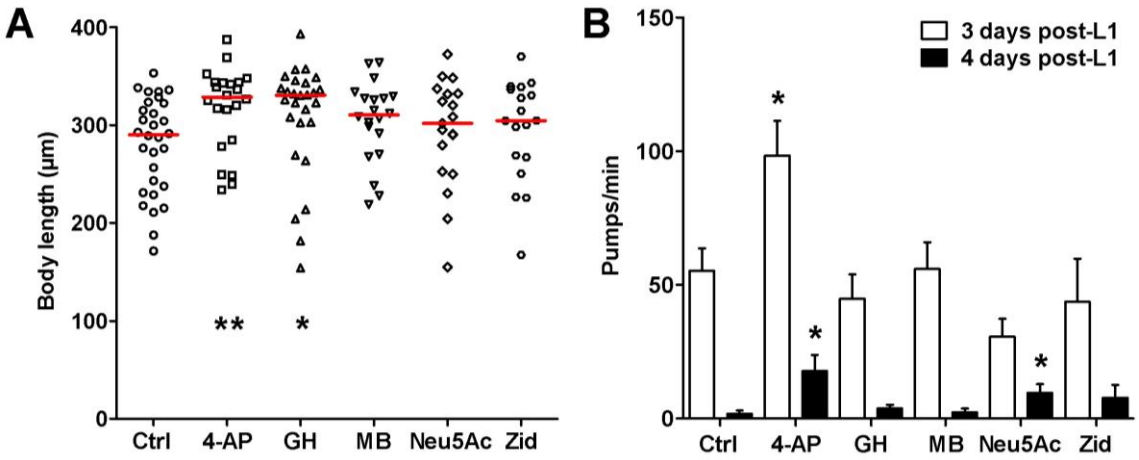

Figure 3.13. 4-AP partially rescues both body length and pharyngeal pumping defects of *smn-1(ok355)*. Null mutant animals were raised on plates containing compounds from birth and assayed for effects on body length and pharyngeal pumping. **(A)** 3 days post-L1 4-AP and gaboxadol hydrochloride (GH) both significantly improved body length. 18-30 animals/treatment were assayed over three independent experiments. Red lines indicate the median value. P = 0.0458, Kruskal-Wallis test. **(B)** 4-AP improved pharyngeal pumping rate both 3 and 4 days post-L1, while Neu5Ac improved function at 4 days. 15-30 animals/strain were assayed on each day over three independent experiments. At 3 days P = 0.0029 and 4 days P = 0.0443, Kruskal-Wallis test. * $P < 0.05$; ** $P < 0.01$, Dunn's multiple comparison test. Figure taken with permission from Oxford University Press from Sleigh *et al.* (2011a).

3.3 Discussion

SMA is one of the primary genetic causes of infant mortality and there is no effective treatment. In the last three years or so, we have seen a renaissance period for SMA therapeutics, with the successful application of gene therapy strategies to restore SMN protein levels in mouse models. However, these treatments are not 100% effective; not all mice respond to therapy with the same extension in lifespan, vascular necrosis of the extremities becomes evident in some of the longer-lived animals, wild type levels of survival have yet to be accomplished, and there is an issue of the immune response to viral vector capsids. Thus, small molecule compounds that can be taken orally could perhaps be used in combination with and complement gene therapy strategies.

3.3.1 *smn-1(cb131)* is a non-lethal mutant, suited to screening

Reduced *smn-1* expression in *C. elegans* by means of RNAi causes a multitude of defects, including reduced motility, severely diminished fertility, and ultimately, larval lethality, indicating that SMN is essential in *C. elegans*, as it is in all other organisms (Miguel-Aliaga *et al.* 1999). Recently, a null mutant, *smn-1(ok355)*, was generated that shows comparable defects (Briese *et al.* 2009). The homozygous null displays larval lethality, arresting at the L2/L3 stage, and a rapid degeneration of motility and neuromuscular function, thought to coincide with depletion of maternally loaded SMN-1 protein and mRNA (Briese *et al.* 2009). Since *smn-1(ok355)* is homozygous lethal and must be maintained using a balancer chromosome, this allele is technically demanding for screening on a large scale. Unlike *smn-1(ok355)*, *smn-1(cb131)* is a milder allele of *smn-1* that is fertile and produces progeny that reach adulthood (Figure 3.2). Since all animals are homozygous for the mutation there is no requirement for elaborate or costly equipment to isolate large numbers of a particular genotype (Pulak 2006). *smn-1(cb131)* mutant animals

display readily quantifiable defects including diminished body length (Figure 3.4A), lifespan (Figure 3.4B), egg-laying (Figure 3.5), and in particular motility (Figure 3.6B), which are specific to the point mutation in *smn-1* (Figure 3.8); however, these defects are much less severe than in *smn-1(ok355)* and therefore enable the study of SMN-1 function into adulthood.

Animals bearing the *smn-1 cb131* mutation lay significantly fewer eggs (Figure 3.5A). This defect is unlikely to be caused by a deficiency in chemosensation as fewer eggs were laid in the absence of food, similar to what is seen in wild type animals. Usually, egg-laying-defective mutants lay fewer eggs and consequently retain more in the uterus (Trent *et al.* 1983); however, this was not observed in *smn-1(cb131)* animals, which behaved similar to wild type in this regard (Figure 3.5B). This, coupled with observations of minor germline disorganisation, an increased percentage of embryonic lethality, and reduced total brood sizes (Figure 3.5C-D), suggests that the *cb131* mutation reduces egg viability and decreases fertility. This situation is mirrored by *smn-1* RNAi, where syncytial germ cells quickly fail to proliferate and differentiate before the somatic gonad and behavioural phenotypes are affected, indicating that the germline is perhaps amongst the most susceptible tissues to *SMN* mutation (Miguel-Aliaga *et al.* 1999). Consistent with this, in *Drosophila*, SMN is required for the differentiation and maintenance of the male germline (Grice & Liu 2011).

Unlike the null mutant, *smn-1(cb131)* does not display a rapidly progressive decline in neuromuscular function. Interestingly, thrashing but not the pharyngeal pumping ability of *smn-1(cb131)* is defective, suggesting that these tissues are differentially affected by the *cb131* mutation. This may reflect a disparity in the requirements of SMN-1 in different muscle types. There are striking biochemical (Ardizzi & Epstein 1987, Krause *et al.* 1990) and physiological (Avery & Horvitz 1989) differences between body wall and

pharyngeal muscles. In particular, *C. elegans* pharyngeal muscle is capable of myogenic activity; the pharynx continues pumping despite laser ablation of the entire nervous system innervating the structure, similar to cardiac myocytes (Avery & Horvitz 1989). These differences may underlie the disparate susceptibility to altered SMN-1 function. Since the frequency of pharyngeal pumping is unaffected in *smn-1(cb131)* animals, it is unlikely that the observable phenotypic defects are caused by lack of food. This is supported by the observation that *cb131* adults do not display the pale, starved appearance seen in the *ok355* null mutant animals (Briese *et al.* 2009). Differential vulnerability of muscles to SMN loss is a disease hallmark and has been reported in a number of mouse models (Ling *et al.* 2012, Murray *et al.* 2008, Ruiz *et al.* 2010, Voigt *et al.* 2010).

To find an explanation for the motility defect of *smn-1(cb131)*, body wall musculature and nervous system morphology were assessed (Figure 3.7A-E). No gross structural defects in either tissue were seen. Synaptic function was thus assessed using the acetylcholinesterase inhibitor pyridostigmine bromide (Figure 3.7F). The *smn-1(cb131)* animals took longer to paralyse on plates containing the drug, suggesting that synaptic transmission between cholinergic ventral nerve cord motor neurons and body wall muscles is disrupted (Miller *et al.* 1996, Nguyen *et al.* 1995). Neurotransmission also appears to be affected in *Drosophila smn* mutants (Chan *et al.* 2003) and mouse models of SMA (Kong *et al.* 2009, Ling *et al.* 2010, Mentis *et al.* 2011, Park *et al.* 2010, Ruiz *et al.* 2010, Torres-Benito *et al.* 2011). Given that the ventral nerve cord neuron number is unaltered and that muscle structure appears unaffected, this deficiency at the synapse may be the principal cause of the motility defect. Interestingly, mutations that affect cholinergic neurotransmission have also been shown to result in impairment of egg-laying (Schafer *et al.* 1996), which is a phenotype seen in *smn-1(cb131)* animals (Figure 3.5A). Furthermore, two *C. elegans* neuronal, RNA-binding splicing factors that localise to the nucleus, UNC-

75 and EXC-7, have also been implicated in synaptic transmission, providing a link between RNA processing and synaptic transmission (Loria *et al.* 2003), which may be particularly relevant to SMA (Bäumer *et al.* 2010).

3.3.2 Chemical screening using *C. elegans*

The NINDS library consists of 1,040 chemicals from a range of drug classes, the majority of which have known targets and are approved for use in humans by the FDA (Abbott 2002, Heemskerk *et al.* 2002, Piccioni *et al.* 2004). If such a compound should be found to be efficacious for the treatment of a disease, it may furnish a faster route from the laboratory to the clinic. The ease with which large collections of drugs can be screened, coupled with the speed and low cost of using *C. elegans*, provides an efficient combination for highlighting compounds with therapeutic potential (Sleigh & Sattelle 2010). Vital to this utility for drug screening, ≈ 60% of human genes have a *C. elegans* orthologue, suggesting that many biochemical pathways are conserved (Culetto & Sattelle 2000, Harris *et al.* 2004). It is not feasible to perform large-scale screens on mouse models of disease, so invertebrates like *C. elegans* offer a first-pass filter to identify putative novel targets and drug leads *in vivo*. Various compounds enhance *SMN* expression *in cellulo* by upregulating *SMN2* transcription or increasing the number of *SMN2* transcripts containing exon 7 (Andreassi *et al.* 2004, Andreassi *et al.* 2001, Brichta *et al.* 2003, Lunn *et al.* 2004); however, limitations of toxicity or rapid metabolism can often restrict their utility. Screening drugs in live models can help to eliminate compounds with systemic toxic properties. The development of a high-throughput, whole-animal chemical screen on a genetic model of SMA is likely to be more powerful and advantageous than a screen only focused on identifying compounds with specific effects of increasing *SMN* expression levels, in that it may identify drugs that target pathways not directly related to SMN, thus

highlighting novel potential pharmacological agents. This aspect of whole-animal *in vivo* screening is particularly useful for diseases like SMA, where the pathophysiology is not yet fully established. The use of a *C. elegans* Duchenne muscular dystrophy model serves as a prime example of the utility of the nematode for highlighting potential therapeutic agents (Carre-Pierrat *et al.* 2006, Gaud *et al.* 2004, Giacomotto *et al.* 2009).

3.3.3 Identification of compounds with potential to treat SMA

Through screening of the NINDS collection of chemical compounds with subsequent validation assays, two FDA-approved drugs, 4-AP and gaboxadol hydrochloride, and one novel compound, Neu5Ac, were highlighted that rescued at least one aspect of *smn-1* phenotypic dysfunction and thus may be of interest for further study (Figure 3.14). No compound significantly improved the lifespan of the null mutant, but given the extreme nature of the model this is unsurprising. Importantly for candidate drugs with potential to treat SMA, all three are able to cross the blood-brain barrier (Lemeignan *et al.* 1984, Wafford & Ebert 2006, Wang *et al.* 2007).

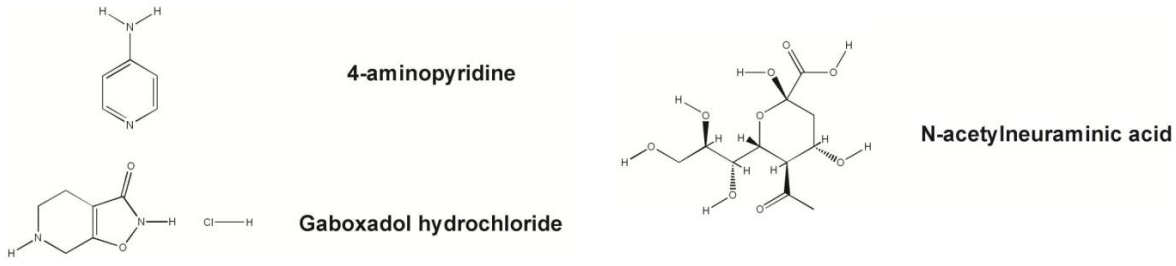

Figure 3.14. Chemical structures of drugs that rescue the *smn-1* phenotype. The chemical structures of 4-AP, gaboxadol hydrochloride, and Neu5Ac are presented. Structures were found at http://pubchem.ncbi.nlm.nih.gov/. Figure taken with permission from Oxford University Press from Sleigh *et al.* (2011a).

4-AP is a dose-dependent potassium channel blocker that can restore conductance along focally demyelinated neurons and prolong action potential duration by blocking potassium channels and perhaps opening calcium channels (Sherratt *et al.* 1980, Targ & Kocsis 1985, Thesleff 1980, Thomsen & Wilson 1983, Wu *et al.* 2009). It therefore has potential for the treatment of neuromuscular disorders and injuries in which synaptic transmission is affected. Indeed, 4-AP has shown efficacy in models of neurological disease (Franciosi *et al.* 2006, Pinter *et al.* 1997), and positive results have been obtained in early human trials of 4-AP for the treatment of multiple sclerosis (Goodman *et al.* 2008, Goodman *et al.* 2009, van Diemen *et al.* 1993) and spinal cord injury (Wolfe *et al.* 2001). Here, 4-AP rescued *smn-1(cb131)* motility to wild type levels (Figure 3.12A), and improved growth and neuromuscular function of the null mutant (Figure 3.13), making it the most promising candidate from the study. Wild type thrashing was unaffected, indicating that 4-AP was not simply causing a hyperthrash effect as a result of stress. *unc-63(x26)* motility was also improved by 4-AP, demonstrating that the positive effect on *cb131* thrashing was not specific to the *smn-1* mutation; however, this does not diminish its potential. Given the action of 4-AP and that *smn-1(cb131)* displays a synaptic transmission defect, it is unsurprising that 4-AP improved motility of the model.

Neurotransmission defects have been previously reported in other models of SMA (Torres-Benito *et al.* 2012). SMNΔ7 mice display a ≈ 50% reduction in quantal content, i.e. the number of synaptic vesicles released from lower motor neuron terminals upon stimulation, in several different muscles (Kong *et al.* 2009, Ruiz *et al.* 2010). However, there is debate as to whether such a reduction, given the relatively large neuromuscular transmission safety factor of rodents (Wood & Slater 2001), would alone account for the motor impairment of these mice (Ling *et meral.* 2010). Nevertheless, many NMJs in young Olig2-Cre SMA mice, which have selectively depleted Smn levels in motor neuron

progenitor cells, do fail to activate muscle fibres and display an increase in neurotransmission failures (Park *et al.* 2010). Furthermore, when performing electrophysiological recordings in SMNΔ7 mice, the authors of one paper state that they may have underestimated the decrease in quantal content due to the exclusion of recordings from muscle fibers with unstable membrane potentials or those lacking evoked neurotransmitter release (Ruiz *et al.* 2010). It is unclear exactly what role synaptic transmission deficiencies at the NMJ are playing in SMA pathology; nevertheless, functional and structural connectivity between lower motor neurons and muscle fibres is undeniably affected by the disease. Moreover, the central sensory to motor synapses also appear to be impaired due to lower motor neuron dysfunction (Gogliotti *et al.* 2012, Ling *et al.* 2010, Mentis *et al.* 2011, Park *et al.* 2010). It is therefore possible that drugs like 4-AP, which serve to modulate or stabilise dysfunctional synapses, have potential to improve the condition of SMA patients.

Gaboxadol hydrochloride is a potent agonist of a specific extra-synaptic, δ-containing $GABA_A$ receptor subtype, $\alpha_4\beta_3\delta$ (Adkins *et al.* 2001, Brown *et al.* 2002). A late-stage investigational treatment for insomnia, gaboxadol has been shown to activate extra-synaptic receptors in relay neurons of the ventrobasal thalamus (Jia *et al.* 2005, Wafford & Ebert 2006). In *C. elegans*, GABA acts as both an excitatory and inhibitory neurotransmitter (McIntire *et al.* 1993), making it difficult to suggest a potential mechanism of action in the nematode.

Neu5Ac is a common, negatively charged monosaccharide often found as a terminal component of glycoproteins and glycolipids (gangliosides) on the surface of many animal cells (Schauer 2009). Cleaved from gangliosides by sialidases, it also transiently exists in small quantities in free monomeric form in organs and tissues (Iijima *et al.* 2004). Interestingly, gangliosides most commonly containing Neu5Ac have been shown to

display multiple neurotrophic effects in several neuronal populations including cholinergic and dopaminergic neurons (Hadjiconstantinou & Neff 1998, Mocchetti 2005). Given the seemingly neuroprotective and neurorestorative properties of gangliosides, they have been explored as potential therapies for neurological disease with reasonable success (Schneider *et al.* 2010, Svennerholm *et al.* 2002); however, the molecular mechanism(s) are not fully known. Recently, a novel function of Neu5Ac as a scavenger of toxic hydrogen peroxide (H_2O_2) both in free form and as part of a glycochain was highlighted (Iijima *et al.* 2007, Iijima *et al.* 2004). The ability of Neu5Ac to inhibit cell death caused by H_2O_2 in a dose-dependent manner is hypothesised to be a novel defence mechanism against oxidative damage (Iijima *et al.* 2004). This suggests a possible mode of action by which Neu5Ac could ameliorate the egg-laying defect of *smn-1(cb131)* and pharyngeal pumping deficiency of the null mutant. *C. elegans* do not possess endogenous sialic acid (Bacic *et al.* 1990), consequently any benefit caused by Neu5Ac administration is unlikely to be attributed to increased incorporation into gangliosides. Instead, the enhanced presence of a scavenger of reactive oxygen species may reduce the chances of oxidative cellular damage, which has been implicated in SMA (Araki *et al.* 2003, Hayashi *et al.* 2002, Wan *et al.* 2008).

In summary, in this chapter I describe a novel *C. elegans smn-1* point mutant, which displays various mild phenotypic defects, that is well suited to large-scale screening. Using this model, I illustrate the utility of a milder, fertile *smn-1* allele, identifying three candidate compounds with potential for further study in vertebrate models for the treatment of SMA.

4. Functional analysis of chondrolectin isoforms in SMA

4.1 Introduction

In spite of having identified the SMA disease gene in 1995 (Lefebvre *et al.* 1995), and subsequently a range of cellular pathways and processes in which the SMN protein is involved (Chang *et al.* 2008, Dimitriadi *et al.* 2010, Fischer *et al.* 1997, Grice & Liu 2011, Pagliardini *et al.* 2000, Pellizzoni *et al.* 2001b, Pellizzoni *et al.* 1998, Rossoll *et al.* 2003), the direct mechanistic link between low SMN levels and the characteristic lower motor neuron pathology is yet to be determined. Lower motor neurons may have a greater constitutive requirement for snRNP biogenesis and could thus be more susceptible to defects in splicing. Alternatively, defective splicing of a motor neuron-specific gene or subset of genes may contribute to neuronal fragility (Burghes & Beattie 2009, Sleigh *et al.* 2011b, Workman *et al.* 2012). Despite evidence connecting low SMN protein levels to diminished snRNP formation (Gabanella *et al.* 2007, Wan *et al.* 2005, Workman *et al.* 2009) and altered intra-nuclear snRNP mobility (Clelland *et al.* 2012), convincing evidence in an SMA-relevant tissue of a downstream functional deficit in gene splicing at or before symptom onset, such as that seen upon mutation of a mouse U2 snRNA (major spliceosome) gene (Jia *et al.* 2012), remains elusive. Thus, an attractive alternative hypothesis is that SMN depletion disrupts a non-canonical, lower motor neuron-specific function (Briese *et al.* 2005, Fallini *et al.* 2012). In harmony with this, work in *Drosophila* suggests that the role of SMN in snRNP biogenesis can be separated from motility and survival defects caused by SMN deficiency (Praveen *et al.* 2012). A similar dissociation of snRNP biogenesis and an axon-specific function of SMN has been reported in zebrafish (Carrel *et al.* 2006).

In order to determine whether defects in splicing are indeed involved in disease, longitudinal, exon-level microarrays were performed on spinal cords of SMNΔ7 (Le *et al.* 2005) and *Smn*$^{-/-}$; *SMN2* (Monani *et al.* 2000) mouse models of severe SMA at pre- and late-symptomatic stages (Bäumer *et al.* 2009). In both models, the vast majority of alternative splicing events occurred late in disease, suggesting that they are unlikely to play a major causative role in pathology. Furthermore, all transcript alterations were to known, physiologically-occurring isoforms, indicating that at least some of the observed changes are perhaps a secondary response to cellular stress. Nevertheless, a small number of transcripts were altered compared to control mice at the pre-symptomatic stage; therefore, these genes may have a particularly crucial function for motor neuron integrity in SMA (Bäumer *et al.* 2009). Alternatively, these changes could be actively contributing to disease progression, or may simply reflect compensatory mechanisms to preserve motor neuron function.

One of the early affected genes, *Chodl*, encodes the protein chondrolectin, which within mouse and human spinal cords, specifically localises to motor neurons (Bäumer *et al.* 2009, Enjin *et al.* 2010, Wootz *et al.* 2010). There are three isoforms of mouse chondrolectin, Chodl-001-003, that differ only in their C-terminus (Figure 4.1A, B). In the SMA mouse spinal cord there was preferential loss of *Chodl-001* expression with relative sparing of *Chodl-002*, a pattern not observed in skeletal muscle or kidney. *Chodl* expression had previously been identified as being misregulated in late stage, moribund SMNΔ7 mouse spinal cord (Zhang *et al.* 2008).

Human chondrolectin is a monomeric transmembrane protein with a C-type lectin-like domain in its relatively long extracellular portion (Weng *et al.* 2002). Mouse *Chodl* is 92.3% identical to its human counterpart, and, in addition to motor neuron expression, can be found in a number of tissues in the adult mouse including skeletal muscle, testes, and

brain (Weng *et al.* 2003). *Chodl* appears to be a marker for motor neurons with fast electrophysiological properties (Enjin *et al.* 2010), and elevated expression correlates with reduced survival time of patients with lung cancer, possibly due to growth-promotion and enhanced cell invasiveness (Masuda *et al.* 2011). The precise function of chondrolectin is yet to be determined; however, recent work in the zebrafish (*D. rerio*) suggests that the fine-tuning of *Chodl* expression is vital for motor axon growth (Zhong *et al.* 2012).

4.1.1 Aims of chapter 4

The main aim of chapter 4 was to begin to deduce the reason for the differential expression of *Chodl* isoforms in the SMA mouse spinal cord (Bäumer *et al.* 2009), and be able to comment on the role of splicing in disease. Using the mouse NSC-34 motor neuronal cell line, which has been used in numerous SMA studies due to experimental tractability and genetic pathways in common with primary neuronal cultures and animal models (Acsadi *et al.* 2009, Ahmad *et al.* 2012, Hensel *et al.* 2012, Wen *et al.* 2010), I wanted to perform *Chodl* isoform expression studies in Smn-depleted cells. At the time of experimental conception, no role had been assigned to chondrolectin; hence, I also hoped to comment on its constitutive cellular function.

4.2 Results

4.2.1 NSC-34 cells provide a good system for *Chodl* isoform expression studies

Mouse *Chodl* encodes three isoforms that share exons 1-5, but differ in their 3' terminal exon and 3' untranslated region usage (Figure 4.1A). All three proteins possess an N-terminal signal peptide, a carbohydrate recognition domain, a transmembrane domain, and a short cytoplasmic tail (Weng *et al.* 2003), only the latter of which varies between the

three proteins, suggesting that any functional differences are mediated through this region (Figure 4.1B). Given that *Chodl* is abnormally spliced at pre-symptomatic stages in SMA mouse spinal cord (Bäumer *et al.* 2009), I wanted to study the effects of the individual isoforms in mouse neuronal cells with depleted Smn levels. I confirmed the presence of genomic *Chodl* DNA in the motor neuronal NSC-34 cell line (Figure 4.1C), but was unable to detect *Chodl* mRNA *via* RT-PCR in either undifferentiated or differentiated cells using primers common to all isoforms (Figure 4.1D). This was confirmed by qPCR, but not Western blotting because the three chondrolectin antibodies tested (Santa Cruz sc-67391, Abcam ab76710, and Weng *et al.* 2003) were insensitive to the mouse protein (data not shown). Therefore, NSC-34 cells provide a physiologically-relevant cellular environment in which to deplete Smn protein without affecting the splicing of endogenous *Chodl*. Using this model, I can individually express the three *Chodl* isoforms, assess their effects on cellular viability and neurite outgrowth, and be sure that the observed results are due to the transfected isoform because the cDNA vectors only express a single protein.

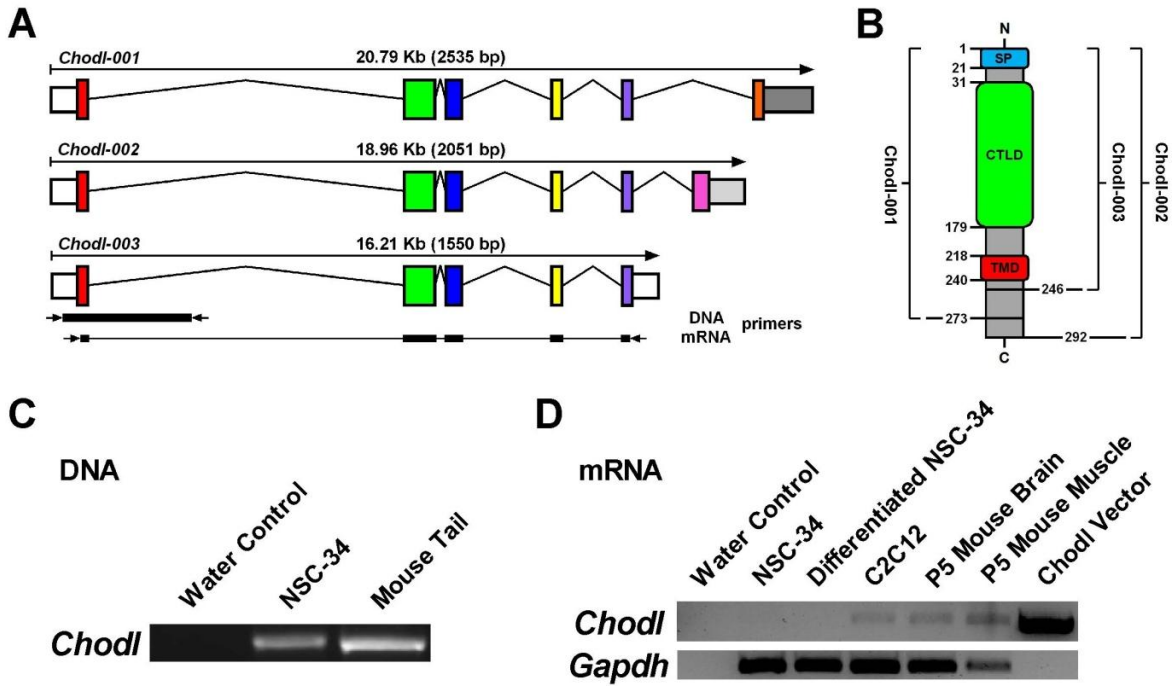

Figure 4.1. NSC-34 cells provide a good model for *Chodl* expression studies. (A) *Chodl* encodes three isoforms that share exons 1-5 (colour coded), but terminate in different 3' exons and untranslated regions. The location of primer sets used in parts C and D of this figure are labeled below *Chodl-003*. The figure is not to scale, and is based on information from Ensembl (www.ensembl.org) and UCSC Genome Browsers (www.genome.ucsc.edu). **(B)** Protein structure of the three Chodl isoforms based on information from Ensembl and SMART (smart.embl-heidelberg.de). All three proteins possess an N-terminal signal peptide (SP), a C-type lectin-like domain (CTLD), a transmembrane domain (TMD), and a short cytoplasmic tail at the C-terminus that differs between the three isoforms. Numbers represent amino acid position and the figure is not to scale. **(C)** *Chodl* genomic DNA is present in NSC-34 cells and mouse tail, shown by standard PCR. **(D)** *Chodl* expression is below detection in undifferentiated and differentiated (4 days) NSC-34 cells as assessed by RT-PCR with *Gapdh* as the loading control. *Chodl* expression was detected in mouse myoblastic C2C12 cells and P5 mouse brain and skeletal muscle.

4.2.2 Smn siRNAs reduce *Smn* expression and cell viability

Three siRNAs targeting different regions of *Smn* mRNA were tested for their ability to reduce *Smn* expression (Figure 4.2). All three successfully reduced Smn mRNA and

protein levels (Figure 4.2A, B, C). However, the initial concentrations of transfection reagent (Lipofectamine at 1.5 µl/well) and siRNAs (100 nm) significantly decreased cell viability in control treatments, as assessed by the MTT assay (Figure 4.2D). Consequently, Lipofectamine concentration was reduced to 1 µl/well, and siRNAs 74016 and 74017 were tested at 25 and 50 nm (Figure 4.3). Smn siRNA 74018 was not used in subsequent experiments because at 100 nm it only reduced Smn to ≈ 40% of control levels. Smn siRNAs 74016 and 74017 both depleted Smn protein to ≈ 40 and 20% of control siRNA at 25 and 50 nm, respectively (Figure 4.3A, B). Smn protein reduction was also confirmed by immunofluorescence (Figure 4.3C). Decreasing Lipofectamine and control siRNA concentrations abrogated the negative effects on viability (Figure 4.3D). This concentration optimisation revealed that the viability of cells with depleted Smn levels was significantly reduced (siRNA 74016), which has been previously shown in NSC-34 cells and a range of other lines including induced pluripotent stem cell-derived motor neurons from SMA patients (Ilangovan *et al.* 2003, Parker *et al.* 2008, Sareen *et al.* 2012, Trülzsch *et al.* 2007). At 50 nm, siRNA 74016 consistently depleted Smn to disease-relevant levels (≈ 20-40%) (Helmken *et al.* 2003, Piepers *et al.* 2011), and reduced cellular viability; therefore, 74016 was used in all subsequent experiments and will be known hereafter simply as Smn siRNA. SMA is a disease of SMN reduction, not complete absence; hence, it is important that Smn is not overly depleted. Reducing Smn to a level below that of the disease state would disrupt the constitutive housekeeping function of the protein and provide little insight into the relative vulnerability of neuronal cells.

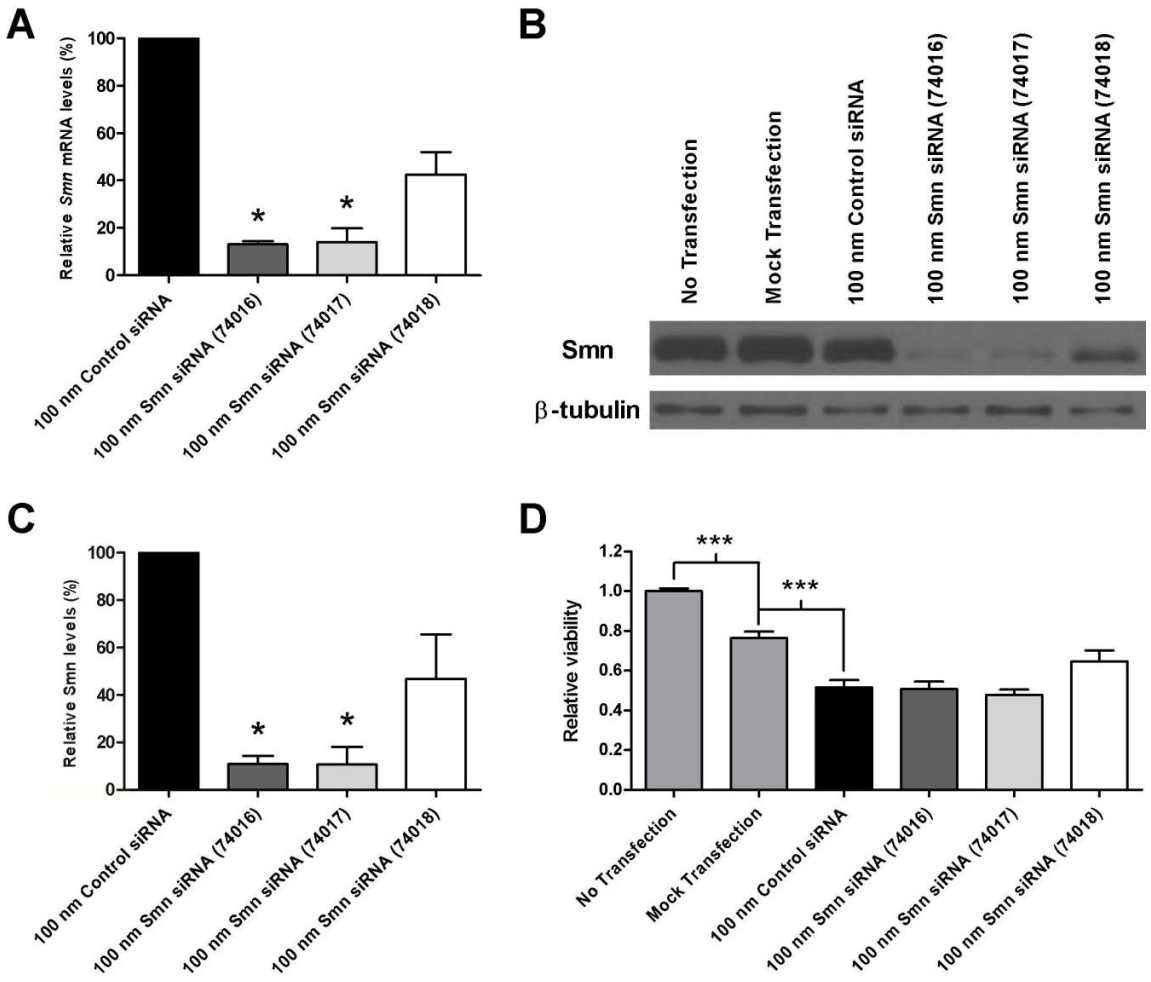

Figure 4.2. Lipofectamine and control siRNA diminish viability when too concentrated. (A) At 100 nm, three different siRNAs targeting Smn (74016, 74017, and 74018) were able to reduce *Smn* mRNA levels compared to control siRNA at 72 h post-transfection, as assessed by qPCR. *Gapdh* was used as the reference gene. Data were collected from three independent experiments. P = 0.0311, Kruskal-Wallis test. **(B)** A representative Western blot indicating that the reduction in *Smn* mRNA translates into Smn protein depletion. **(C)** Densitometric analysis of Western blots from three independent experiments reveals that Smn protein is reduced to similar levels as the mRNA. P = 0.0393, Kruskal-Wallis test. **(D)** At 1.5 µl/well, Lipofectamine (Mock Transfection) significantly reduces viability in the MTT assay compared to No Transfection. Similarly, at 100 nm, control siRNA significantly affects viability compared to Mock Transfection. Consequently, reagent concentrations were reduced for subsequent experiments (Figure 4.3). Three data points/condition were collected from each of three independent experiments. $P < 0.001$, one-way ANOVA. * $P < 0.05$; *** $P < 0.001$, Bonferroni's/Dunn's multiple comparison test.

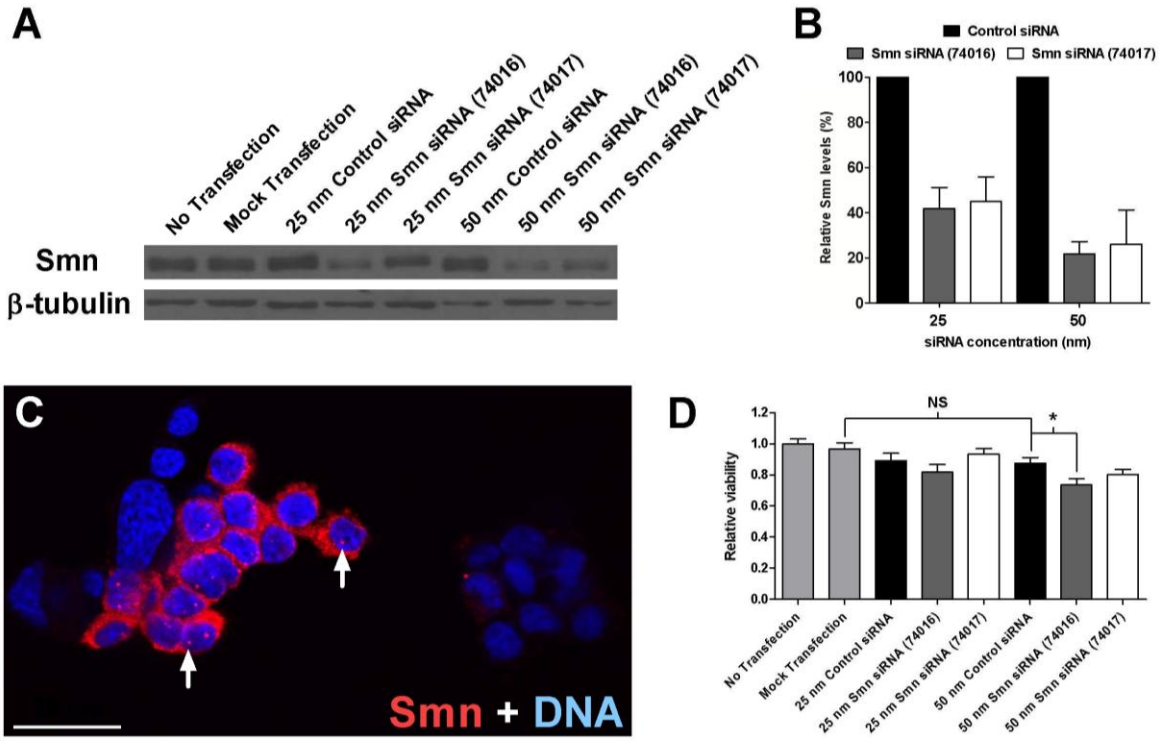

Figure 4.3. siRNAs targeting *Smn* decrease protein levels leading to reduced cell viability. (A) A representative Western blot showing that at 25 and 50 nm, Smn siRNAs 74016 and 74017 are both able to reduce Smn protein levels 72 h post-transfection. **(B)** Densitometric analysis of Western blots from three independent experiments reveals that at 25 and 50 nm, Smn siRNAs are able to reduce Smn protein levels to ≈ 40 and 20% of control, respectively. **(C)** A representative immunofluorescence image depicting cells in which Smn protein has been depleted. Arrows point to nuclear gems, SMN-enriched nuclear foci, indicating the specificity of the antibody for Smn. Scale bar = 30 µm. **(D)** At 50 nm, Smn siRNA 74016 significantly reduces cell viability in an MTT assay compared to control siRNA. Reducing the concentration of Lipofectamine from 1.5 to 1 µl/well and siRNAs from 100 to 50 nm abrogates the negative effects on viability seen in Figure 4.2. Three data points/condition were collected from each of three independent experiments. $P < 0.001$, one-way ANOVA. NS, not significant. * $P < 0.05$, Bonferroni's multiple comparison test.

4.2.3 The reduced cell viability is caused by Smn depletion and not an off-target effect of the siRNA

It is possible that the diminished viability seen upon Smn siRNA administration was not due to the reduced Smn levels, but a non-specific, off-target effect or even a contaminant. Consequently, a cDNA vector was created to transiently express eGFP-tagged *Smn* insensitive to siRNA knockdown. Using site-directed mutagenesis, three synonymous base pair changes were introduced into the siRNA target sequence of the encoded Smn (Figure 4.4A). Cellular viability was completely rescued when Smn siRNA was co-transfected with the mutated vector (Figure 4.4B). I determined by Western blot that endogenous Smn was decreased, but total Smn levels were restored to normal due to exogenous Smn-eGFP (Figure 4.4C, D). *Smn-eGFP* expression was also confirmed by live fluorescence microscopy (Figure 4.4E), and showed a similar subcellular localisation to that previously reported (Acsadi *et al.* 2009). Relative viability is significantly dependent on Smn levels, indicating that the reduced viability seen upon Smn siRNA treatment was indeed due to Smn protein depletion (Figure 4.4F).

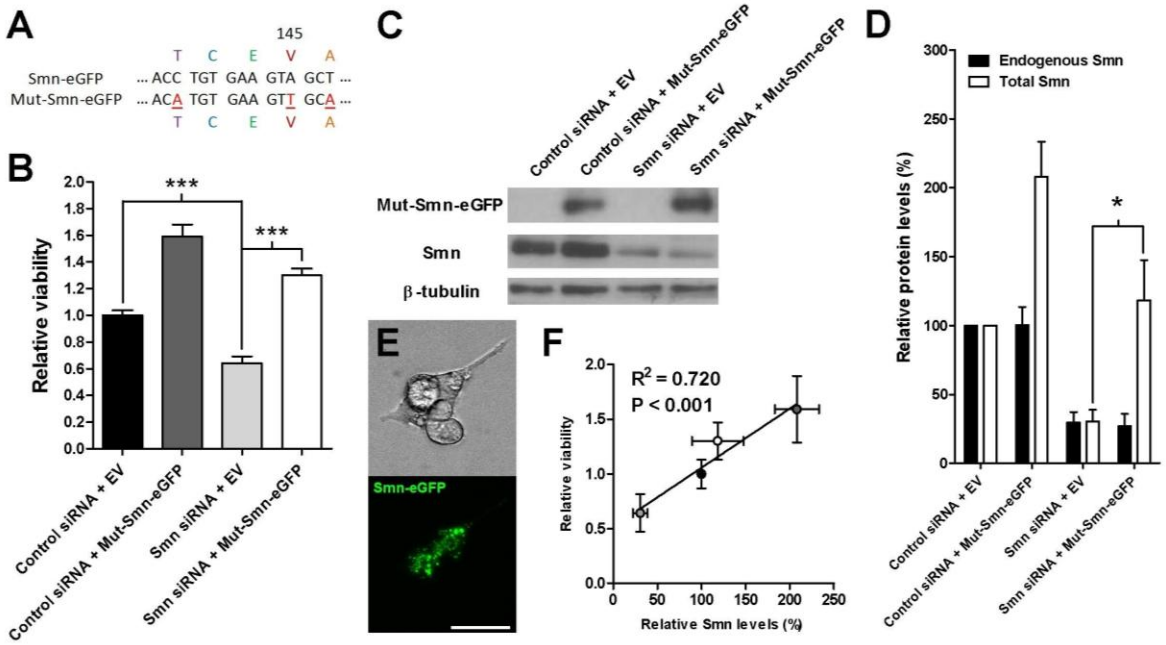

Figure 4.4. The reduced cellular viability is caused by Smn protein depletion. (A) Site-directed mutagenesis was used to incorporate three synonymous base pair changes into a cDNA vector to express siRNA-insensitive *Smn-eGFP* (Mut-Smn-eGFP). Mutated base pairs are underlined and highlighted in red. The coloured letters above and below the nucleotides represent the encoded amino acids. 145 denotes the amino acid position within the protein. **(B)** Co-transfection of Smn siRNA with Mut-Smn-eGFP was able to significantly rescue the decreased viability at 72 h post-transfection. Three data points/condition were collected from each of four independent experiments. EV, empty vector. $P < 0.001$, one-way ANOVA. **(C)** A representative Western blot showing successful depletion of endogenous Smn protein, and transfection of the Mut-Smn-eGFP vector. **(D)** Densitometric analysis of Western blots from four independent experiments reveals that total Smn is significantly restored using the siRNA-insensitive vector. $P = 0.001$, Kruskal-Wallis test. **(E)** Successful vector transfection was also confirmed by live fluorescence microscopy for eGFP. Scale bar = 15 µm. **(F)** Viability is significantly dependent upon Smn protein levels indicating that the reduced viability seen upon Smn siRNA treatment is indeed due to diminished Smn and not an off-target effect of the siRNA. $R^2 = 0.720$, $P < 0.001$, linear regression. * $P < 0.05$; *** $P < 0.001$, Bonferroni's/Dunn's multiple comparison test.

4.2.4 *Chodl-001* expression exacerbates the viability defect

Chodl-001 is significantly downregulated in the spinal cord of SMA mice, while *Chodl-002* levels are unaffected (Bäumer *et al.* 2009). This could be a physiological response to diminished Smn levels. If this is indeed the case, isoform 001 expression may be suppressed due to a compounding negative effect on cells within the spinal cord when Smn availability is low. I hypothesised that if this were true, the combination of *Chodl-001* expression and *Smn* knockdown would result in a further decrease in viability over and above that caused by Smn depletion alone. To test this, I created a cDNA vector able to transiently express *Chodl-001* with a 3xFLAG tag (Figure 4.6A). As with the previous experiment, DNA concentration required optimisation (Figure 4.5). Once accomplished, I observed that *Chodl-001* expression in cells with normal Smn levels had no effect on viability (Figure 4.6B). However, in cells with reduced Smn levels, expression of *Chodl-001* significantly exacerbated the viability defect caused by Smn depletion, and this was independent of a further reduction in Smn levels (Figure 4.6C, D).

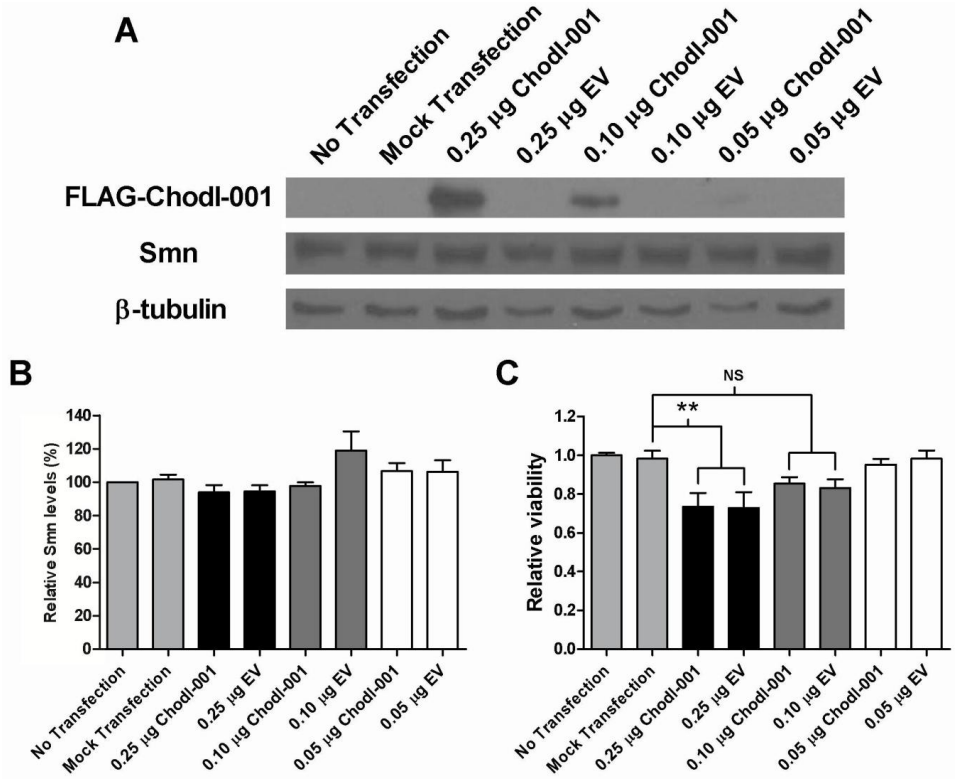

Figure 4.5. Optimisation of DNA vector concentration. (A) A representative Western blot showing successful transfection of *Chodl-001* DNA at 0.25, 0.10, and 0.05 µg DNA/well at 72 h post-transfection. **(B)** Densitometric analysis of Western blots from three independent experiments reveals that *Chodl-001* expression has no effect on Smn protein levels. P = 0.0856, Kruskal-Wallis test. **(C)** 0.10 µg/well DNA had no effect on cell viability; thus, this concentration was chosen for subsequent experiments. Three data points/condition were collected from each of three independent experiments. P < 0.001, one-way ANOVA. ** P < 0.01, Bonferroni's multiple comparison test.

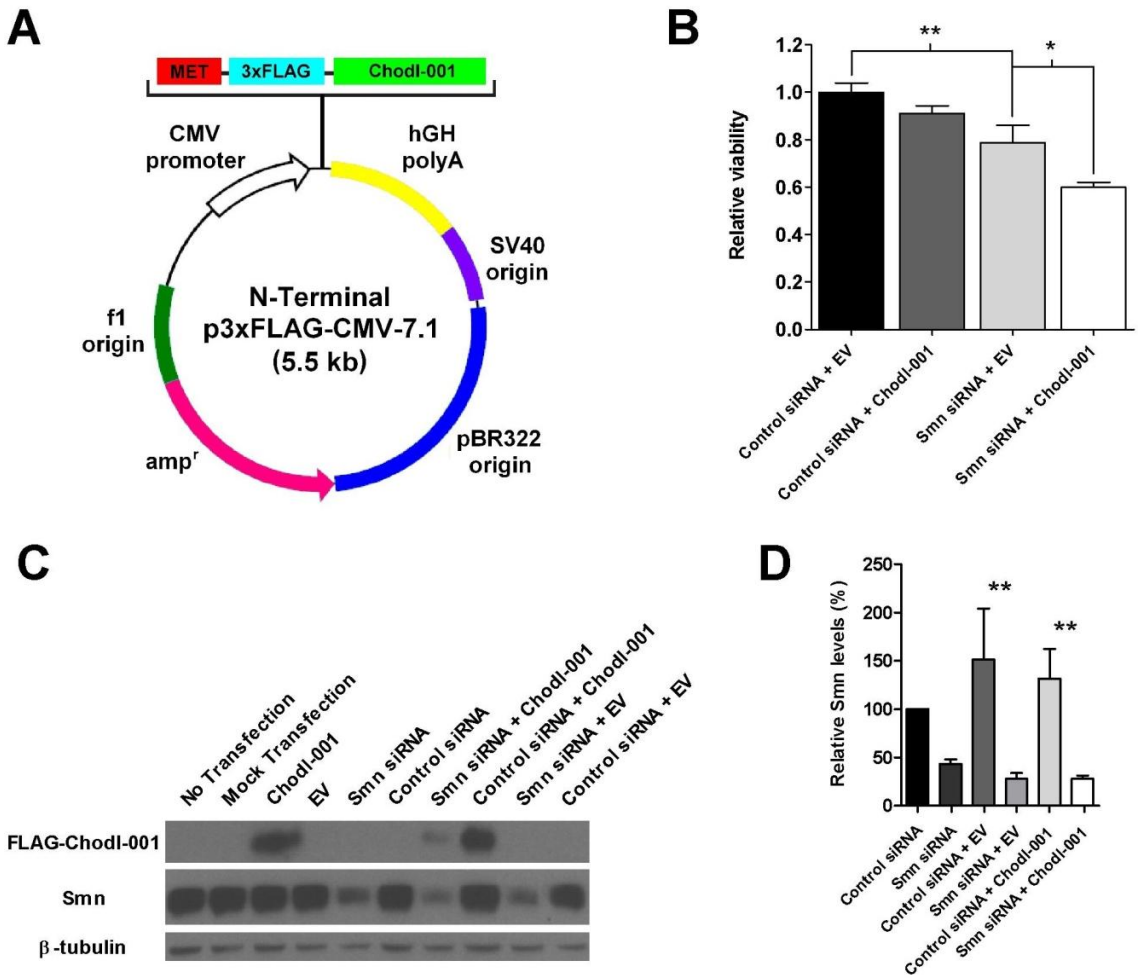

Figure 4.6. *Chodl-001* expression exacerbates the viability defect caused by Smn depletion. (A) A map of the p3xFLAG-CMV-7.1 vector used to express *Chodl-001*. The size of the vector with insert is ≈ 5.5 kb. Figure adapted from the Sigma Aldrich website. **(B)** *Chodl-001* expression in Smn-depleted cells exacerbates the viability defect caused by *Smn* knockdown at 96 h post-transfection. Two data points/condition were collected from each of six independent experiments. $P < 0.001$, one-way ANOVA. **(C)** A representative Western blot showing successful reduction of endogenous Smn, and expression of *Chodl-001*. An antibody against FLAG was used to detect Chodl-001 because the three Chodl antibodies tested were insensitive to the mouse protein. **(D)** Densitometric analysis of Western blots from at least five independent experiments reveals that the effect of Chodl-001 in Smn-depleted cells is independent of a further decrease in Smn. $P < 0.001$, one-way ANOVA. * $P < 0.05$; ** $P < 0.01$, Bonferroni's multiple comparison test.

Vast overexpression of any gene is likely to be detrimental to cell viability. Consequently, I wanted to confirm that the effect of Chodl-001 was not simply due to

overwhelming the cells with an abundance of protein, or perhaps even a vector artifact. Hence, using the same expression vector (kindly provided by Esther B. Becker (Becker *et al.* 2009)), I expressed *transient receptor potential cation channel, type C3* (*TRPC3*), a gene not highlighted by exon- or gene-level microarrays in the original study on SMA mice (Bäumer *et al.* 2009). *TRPC3* expression had no effect on viability, whereas the effect caused by Chodl-001 in Smn-depleted cells was repeated (Figure 4.7A). Western blotting confirmed that there was no difference in Smn protein levels between the vector treatments, indicating that the result was not caused by differences in *Smn* expression (Figure 4.7B, C). Importantly, expression of *TRPC3* was greater than *Chodl-001*, suggesting that the difference in viability was not due to Chodl-001 being more abundant than TRPC3 (Figure 4.7D, E).

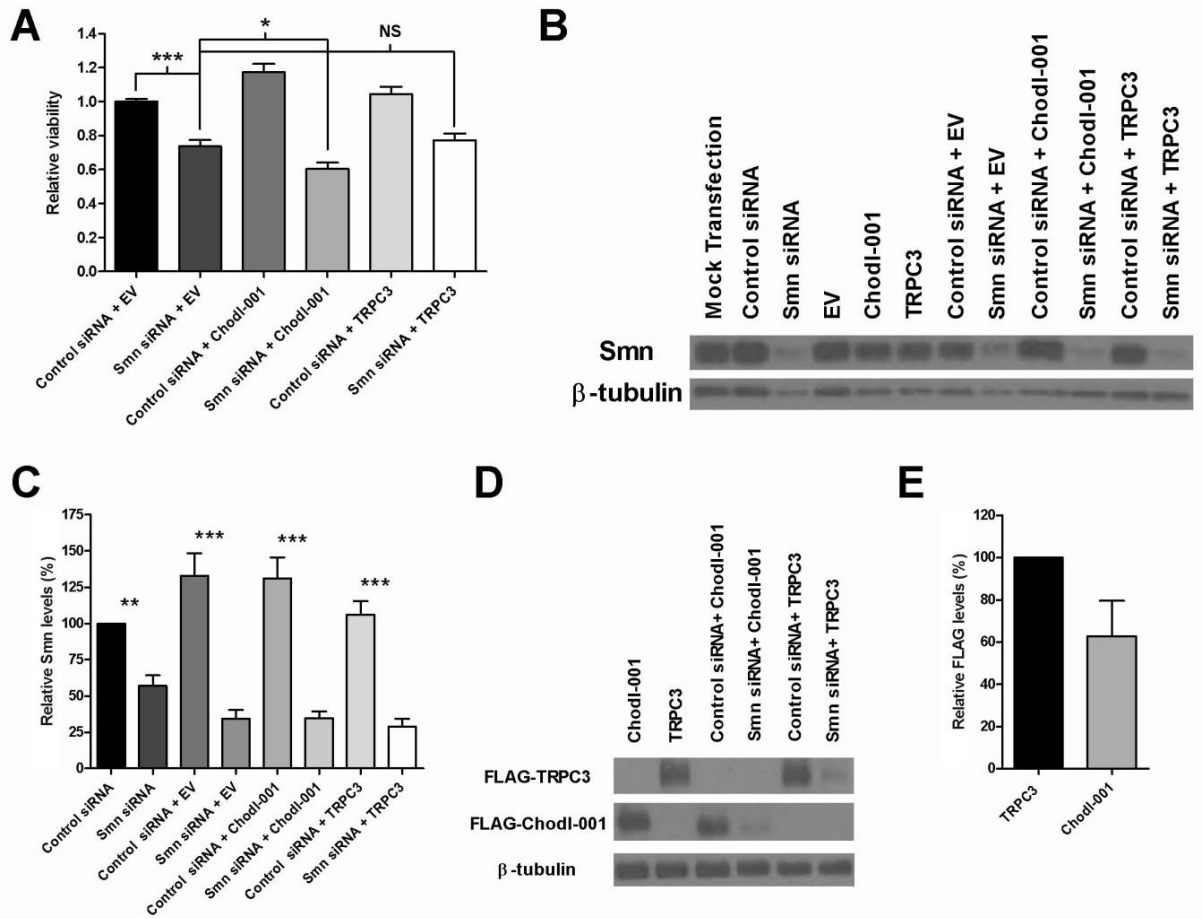

Figure 4.7. The exacerbated viability is specific to Chodl-001. (A) *TRPC3* expression has no effect on the viability of cells with reduced Smn levels at 96 h post-transfection, whereas the result of decreased viability caused by *Chodl-001* expression was repeated. Two data points/condition were collected from each of ten independent experiments. $P < 0.001$, one-way ANOVA. **(B)** A representative Western blot showing successful reduction of Smn. **(C)** Densitometric analysis of Western blots from eight independent experiments reveals that the decreased viability caused by Chodl-001 is not due to differences in Smn depletion. $P < 0.001$, one-way ANOVA. **(D)** A representative Western blot showing successful FLAG detection. **(E)** Densitometric analysis of Western blots from ten independent experiments comparing FLAG density between TRPC3 and Chodl-001 reveals that *TRPC3* was more highly expressed, suggesting that the observed effects on viability were not simply due to massive *Chodl-001* expression. * $P < 0.05$; ** $P < 0.01$; *** $P < 0.001$, Bonferroni's multiple comparison test.

4.2.5 Distinct effects of Chodl-001-003 on cell survival

Since the levels of *Chodl-002* are unaffected in SMA mouse spinal cord, I hypothesised that isoform 002 expression in cells with reduced Smn levels would have no impact on viability. *Chodl-003* expression was not assessed in the original study because its entire sequence is common to all three isoforms; therefore, I was unable to predict the impact it would have. However, my hypothesis that Chodl-002 does not affect cell viability was correct. In fact, cell viability was slightly improved in the presence of Chodl isoforms 002 and 003 (Figure 4.8A). The differential effects of the three isoforms improves confidence in my Chodl-001 result, not only because the variation makes it unlikely that the result is due to a non-specific phenomenon, but because I was able to reproduce the result for a third time, with experimental treatments being assigned to different wells for each of the three sets of experiments.

Since the MTT assay uses mitochondrial function as a proxy for cell viability (Denizot & Lang 1986, Mosmann 1983), alterations in mitochondrial metabolism could confound results. Consequently, I performed trypan blue exclusion experiments (Figure 4.8B). Calculating the percentage of live cells, I was able to replicate the MTT result and show that Chodl-001 significantly reduced cell survival, while Chodl-002 and Chodl-003 significantly increased survival of cells with reduced Smn levels. The MTT and trypan blue results significantly correlate, suggesting that Chodl affects the survival of cells and not metabolic activity (Figure 4.8C). Both Smn and FLAG protein levels were similar between treatments, indicating that this result was independent of transfection differences (Figure 4.8D, E).

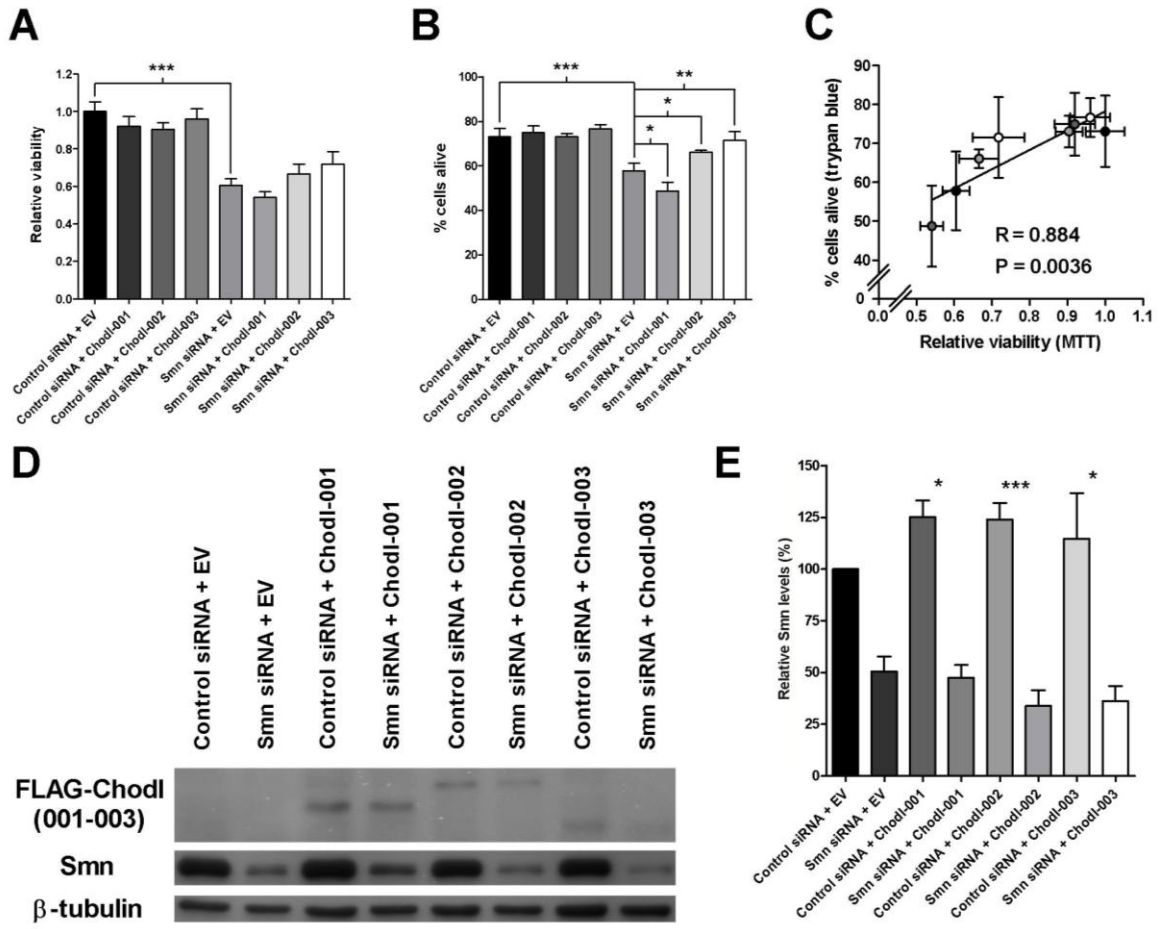

Figure 4.8. Differential effects of Chodl isoforms on cell viability. (A) Chodl isoforms 001-003 have differential effects on cell viability at 96 h post-transfection. Three data points/condition were collected from each of seven independent experiments. $P < 0.001$, one-way ANOVA. **(B)** Trypan blue experiments indicate that Chodl-001 significantly reduces survival in cells with diminished Smn levels, whereas Chodl-002 and Chodl-003 significantly improve survival. One to three data points/condition were collected from each of three independent experiments. $P < 0.001$, one-way ANOVA. **(C)** The results of the MTT and trypan blue experiments significantly correlate signifying that Chodl isoforms affect cell survival and not metabolic activity. $R = 0.884$, $P = 0.0036$, Pearson's product-moment correlation coefficient. **(D)** A representative Western blot showing successful Smn depletion and FLAG detection. *Chodl* isoforms were expressed at similar levels. **(E)** Densitometric analysis of Western blots from five independent experiments reveals that differences in Smn levels do not account for the differential effects of Chodl isoforms on cell survival. $P < 0.001$, Kruskal-Wallis test. * $P < 0.05$; ** $P < 0.01$; *** $P < 0.001$, Bonferroni's/Dunn's multiple comparison test.

Work in zebrafish suggests that the single *D. rerio* isoform of *Chodl* must be expressed in a discrete concentration window for efficient motor axon outgrowth; too little Chodl causes stunted axonal growth and reduced muscle innervation, and too much also results in shorter processes (Zhong *et al.* 2012). I wanted to determine whether Chodl levels are also important for the viability of NSC-34 cells, so I doubled the DNA concentration from 0.1 to 0.2 µg/well (Figure 4.9). This abrogated the differential effects of the Chodl isoforms in Smn-depleted cells, such that all three negatively affected viability (Figure 4.9A). Similar to the result at the lower DNA concentration (Figure 4.6A, 4.7A, 4.8A, B), no changes were observed in cells with normal Smn levels, indicating that the effects of Chodl are dependent on the availability of Smn.

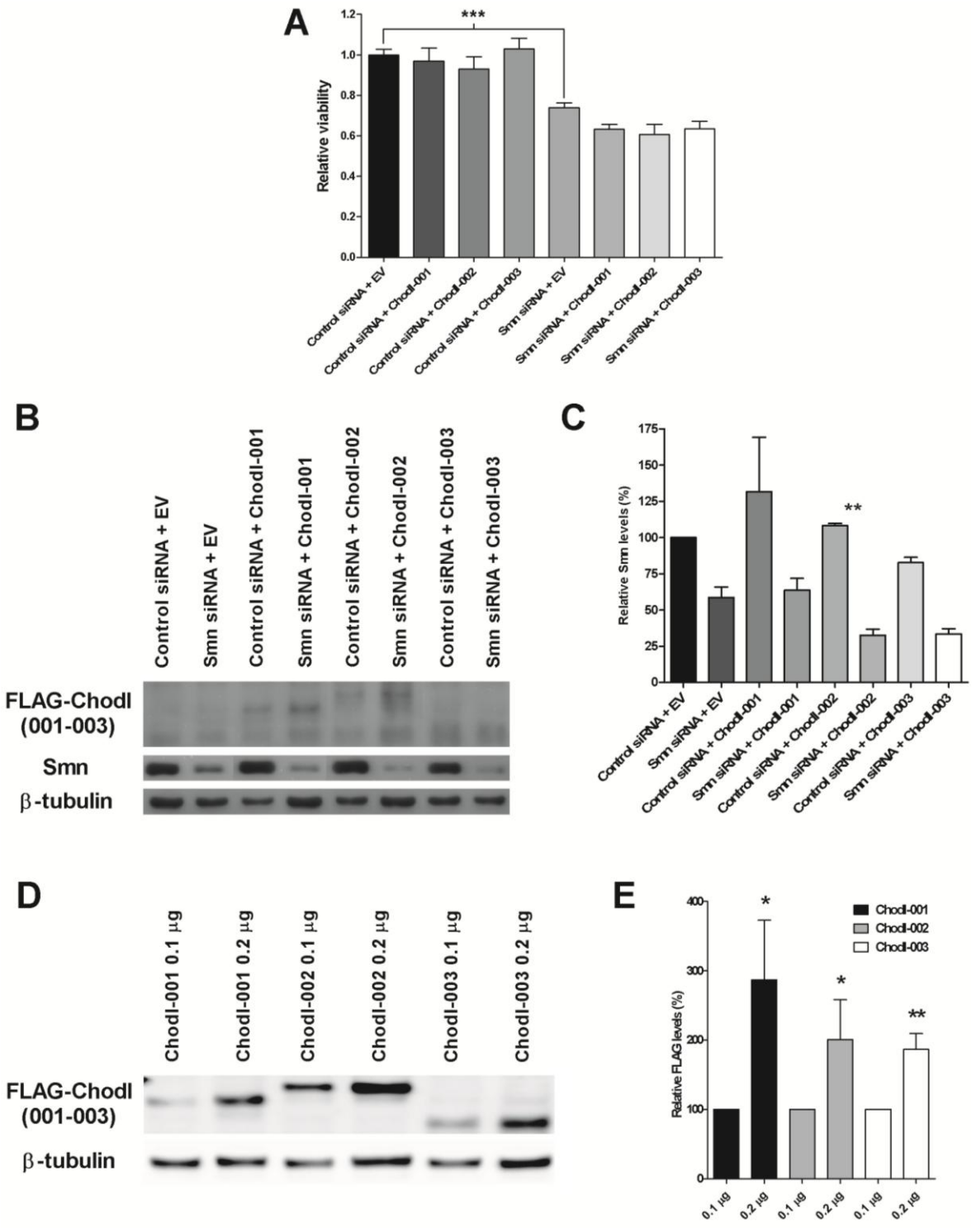

Figure 4.9. Doubling Chodl concentration abrogates the differential effects of the three isoforms. (A) Upon doubling of DNA concentration, Chodl-002 and Chodl-003 no longer improved viability at 96 h post-transfection. Three data points/condition were collected from each of three independent experiments. $P < 0.001$, one-way ANOVA. **(B)** A representative Western blot showing successful Smn depletion and FLAG detection. *Chodl* isoforms were expressed at similar levels. **(C)** Densitometric analysis of Western blots from three independent experiments confirms *Smn* knockdown. $P = 0.0036$, Kruskal-Wallis test. **(D)** A

representative Western blot showing that doubling the DNA concentration of the Chodl vectors leads to increased FLAG detection. **(E)** Densitometric analysis of Western blots from five independent experiments confirms the increase in Chodl protein levels. $P < 0.001$, Kruskal-Wallis test. * $P < 0.05$; ** $P < 0.01$; *** $P < 0.001$, Bonferroni's/Dunn's multiple comparison test.

4.2.6 Chodl isoforms also differentially affect neurite outgrowth

As zebrafish chondrolectin appears to be involved in axonal growth and development (Zhong *et al.* 2012), I investigated what effect individual isoforms had on neurite outgrowth in NSC-34 cells. *Smn* knockdown is known to affect NSC-34 neurite outgrowth, both reducing the percentage of cells bearing neurites and average neurite length (Kwon *et al.* 2011). Similar phenotypes have been described in induced pluripotent stem cell-derived motor neurons from SMA patients (Chang *et al.* 2011), other primary and immortal neuronal cells with reduced Smn levels (Jablonka *et al.* 2007, Ning *et al.* 2010, Nölle *et al.* 2011, Shafey *et al.* 2008, van Bergeijk *et al.* 2007), animal models (Liu *et al.* 2011, McWhorter *et al.* 2003), and severe SMA patient spinal cords (Šimić *et al.* 2008).

NSC-34 cells were differentiated using media with 3% (v/v) serum, and both the percentage of neurite-bearing cells and average neurite length were calculated (Figure 4.10). Upon *Smn* knockdown, the percentage of cells with at least one neurite and the mean neurite length were significantly reduced (Figure 4.10A, B, C, D). Expression of the three individual *Chodl* isoforms had no effect on neurite formation in cells with normal Smn levels; however, *Chodl-002* expression did significantly decrease neurite length, with the neurites of cells expressing *Chodl-001* exhibiting a trend towards decreased length. This parallels the result in zebrafish in that *Chodl* expression did not completely abrogate axon outgrowth, but lead to shorter, stunted axons (Zhong *et al.* 2012). When DNA concentration was doubled, both isoform 001 and 002 significantly reduced neurite length (Figure 4.11A, B).

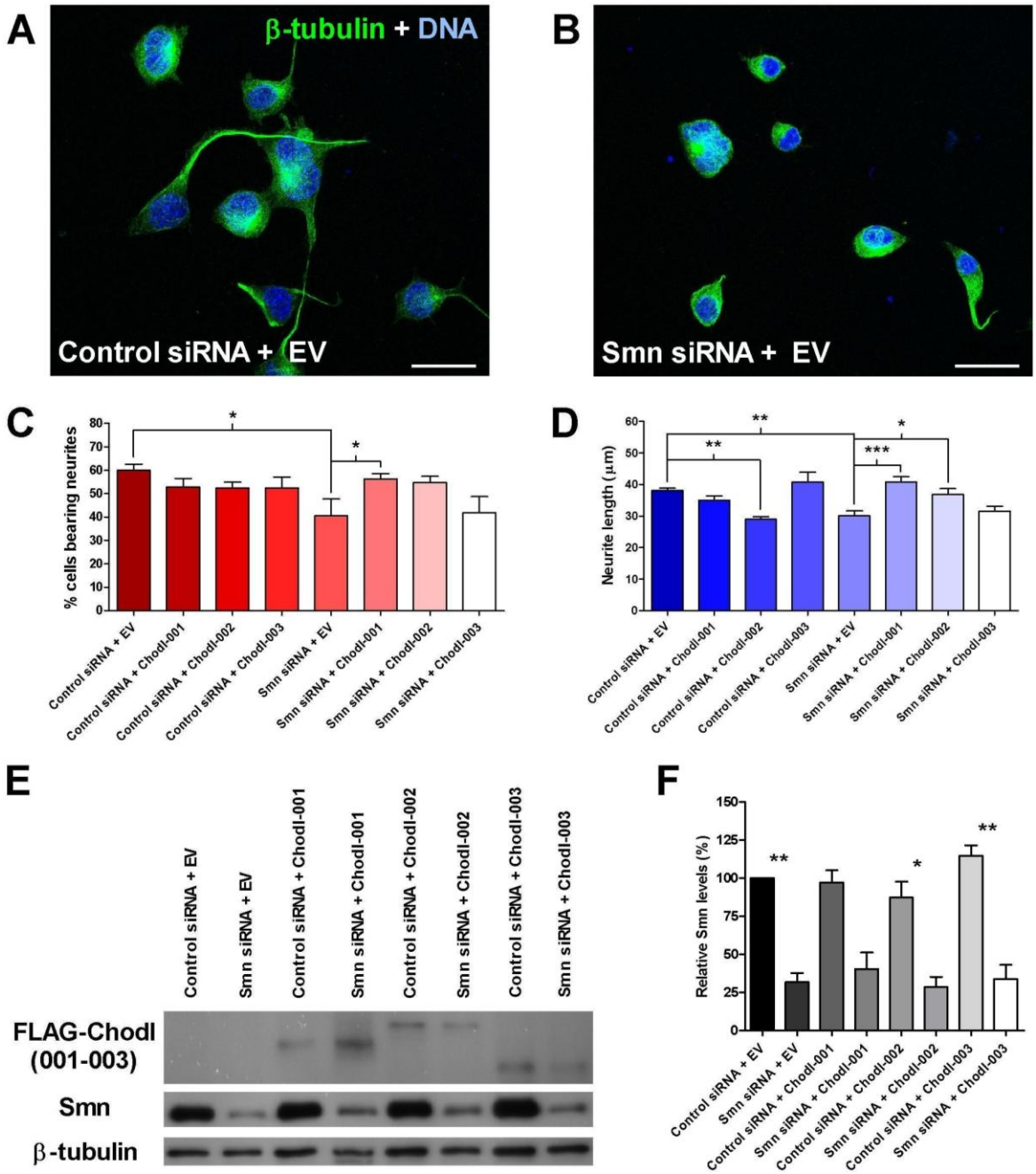

Figure 4.10. Chodl-001 and Chodl-002 improve neurite defects caused by Smn depletion. (A, B) Representative images of NSC-34 cells in 3% (v/v) serum differentiation media with normal (A) and depleted (B) Smn. Scale bars = 30 μm. **(C)** *Chodl* isoform expression has no effect on the percentage of cells bearing neurites that have normal Smn levels; however, in Smn-depleted cells, Chodl-001 is able to significantly rescue the defect caused by *Smn* knockdown. Percentages were calculated for one to three replicates/condition from each of three independent experiments. At least five replicates were included for each condition. P = 0.0546, Kruskal-Wallis test. * P < 0.05, Dunn's multiple comparison test. **(D)** *Chodl-002*

expression reduces neurite length in cells with normal Smn levels, while both Chodl-001 and Chodl-002 rescue length in Smn-depleted cells. Mean lengths were calculated for one to three replicates/condition from each of three independent experiments. At least five replicates were included for each condition. $P < 0.001$, one-way ANOVA. * $P < 0.05$; ** $P < 0.01$; *** $P < 0.001$, Bonferroni's multiple comparison test. **(E)** A representative Western blot showing successful Smn depletion and FLAG detection. *Chodl* isoforms were expressed at similar levels. **(F)** Densitometric analysis of Western blots from three independent experiments reveals that differences in Smn levels do not account for the differential effects of Chodl isoforms on neurite outgrowth. $P < 0.001$, Kruskal-Wallis test. * $P < 0.05$; ** $P < 0.01$, Dunn's multiple comparison test.

In cells with reduced Smn levels, expression of *Chodl-001* at 0.1 µg/well significantly rescued neurite production and length, while *Chodl-002* increased the percentage of neurite-bearing cells (not significant) and significantly improved neurite length (Figure 4.10C, D). At twice the DNA concentration, the rescue effects of Chodl-001 and Chodl-002 on neurite production, and Chodl-001 on neurite length were abrogated; however, neurite length remained significantly improved by isoform 002 (Figure 4.11A, B). Isoform 003 appeared to have no effect on either phenotype, at either concentration, irrespective of Smn availability (Figure 4.10C, D, 4.11A, B). When measuring neurite lengths, some extensive processes were counted that may have skewed the results. Consequently, neurite measurements were also combined for each experimental treatment and the overall mean and median values plotted, but the same trends in the data were observed (data not shown). Moreover, counts were similar between controls at the different DNA concentrations. Western blotting suggests that the differential effects of Chodl isoforms on neurite growth were not caused by discrepancies in *Smn* knockdown or vector expression levels (Figure 4.10E, F, 4.11C, D). I also calculated the percentage of cells bearing abnormal neurites (see methods), but observed no differences (Figure 4.12). In summary, my observations suggest that chondrolectin isoforms differentially affect neurite outgrowth dependent upon their expression level and Smn availability.

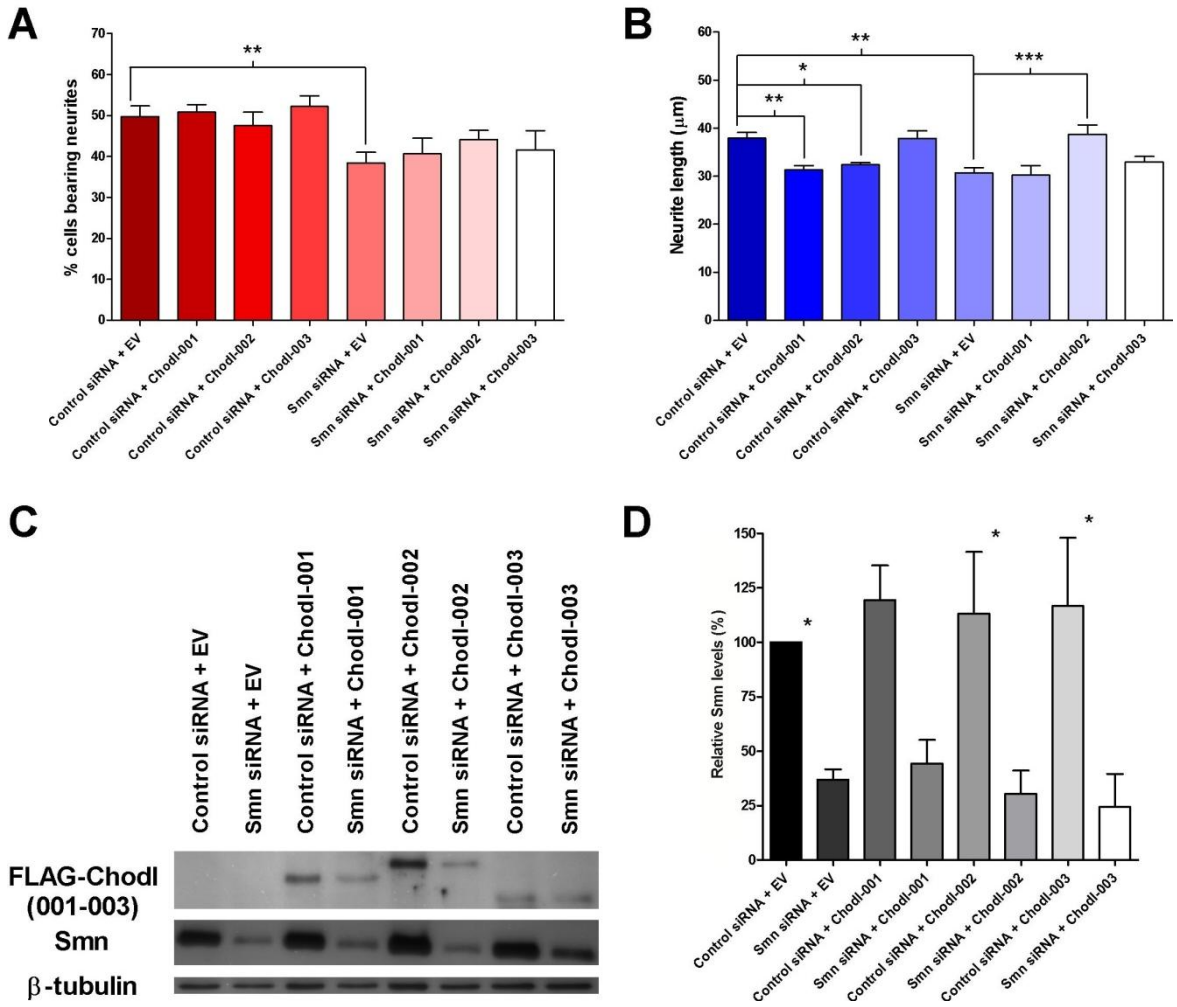

Figure 4.11. Fine-tuning of Chodl levels is important for neurite outgrowth. (A, B) Doubling the concentration of Chodl isoforms abrogates the effects in Smn-depleted cells of Chodl-001 and Chodl-002 on the percentage of neurite-bearing cells, and of Chodl-001 on neurite length; however, *Chodl-002* expression still significantly rescues neurite length. In cells with normal Smn levels, the increased amounts of Chodl-001 and Chodl-002 exacerbate the associated length deficiency observed at the lower concentration. A, $P = 0.0137$; B, $P < 0.001$, one-way ANOVA. * $P < 0.05$; ** $P < 0.01$; *** $P < 0.001$, Bonferroni's multiple comparison test. **(C)** A representative Western blot showing successful Smn depletion and FLAG detection. *Chodl* isoforms were expressed at similar levels. **(D)** Densitometric analysis of Western blots from three independent experiments reveals that differences in Smn levels do not account for the differential effects of Chodl isoforms on neurite outgrowth. $P = 0.0121$, Kruskal-Wallis test. * $P < 0.05$, Dunn's multiple comparison test.

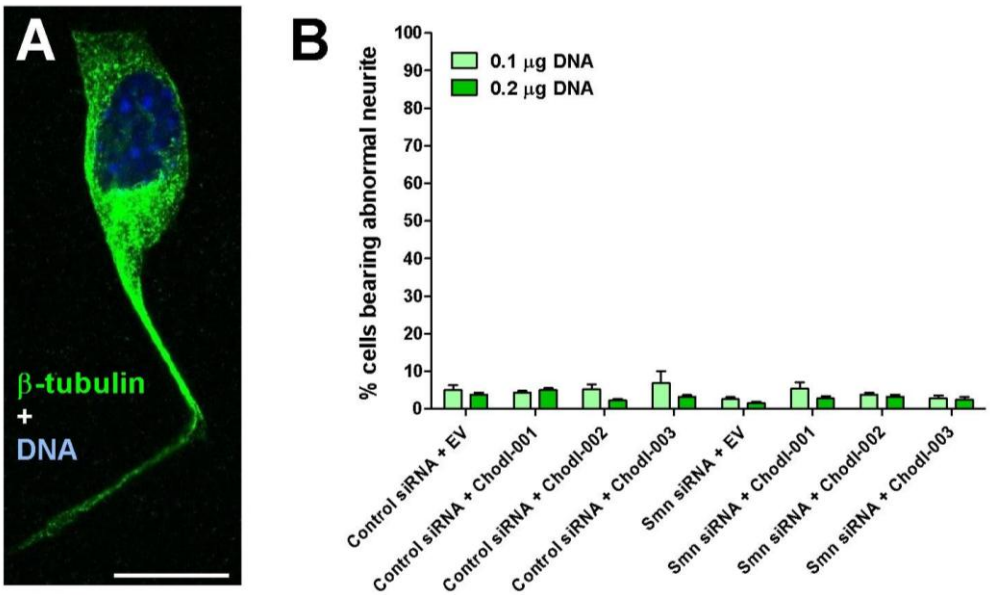

Figure 4.12. *Chodl* expression has no effect on neurite structure. (A) An example abnormal neurite (bent at an odd angle, see methods). Scale bar = 20 μm. **(B)** *Chodl* expression has no effect on the percentage of cells bearing at least one abnormal neurite. P = 0.451, Kruskal-Wallis test.

4.3 Discussion

Chondrolectin is alternatively spliced at early, pre-symptomatic stages in SMA mouse spinal cord, suggesting that disruption of this or associated pathways may be playing an important role in the disease (Bäumer *et al.* 2009). *Chodl* is expressed in motor neurons of zebrafish, mice, and humans (Bäumer *et al.* 2009, Enjin *et al.* 2010, Wootz *et al.* 2010, Zhong *et al.* 2012), which is indicative of an evolutionary conserved role for its protein product. Definition of its role in neuronal cells and deduction of why isoform expression is affected in SMA mice may provide important clues about the disease mechanism that links SMN depletion to lower motor neuron loss. Here, I have used a mouse motor neuronal cell line to show that Chodl isoforms differentially affect cell survival and neurite outgrowth, and that this is dependent on both Chodl concentration and Smn availability.

4.3.1 *Chondrolectin* dysregulation: contributor to pathology or compensatory mechanism?

It has been hypothesised that SMA is caused by a general deficiency in splicing, or mis-regulation of one or a few key motor neuron-specific genes. Indeed, splice-site pairing is reduced two-fold in SMA patient fibroblasts (Fox-Walsh & Hertel 2009), and defective splicing, such as increased intron-inclusion, has been reported in a number of systems (Boulisfane *et al.* 2011, Campion *et al.* 2010, Zhang *et al.* 2008). Nonetheless, defective splicing of a motor neuronal gene at or before disease onset has yet to be identified. To address this, exon-specific microarrays were performed on SMA mouse spinal cord; however, the vast majority of alternative splicing events were a late feature of disease and all changes were to known isoforms (Bäumer *et al.* 2009). Furthermore, despite minor-class snRNPs appearing to be more sensitive to SMN depletion (Gabanella *et al.* 2007, Praveen *et al.* 2012, Workman *et al.* 2009, Zhang *et al.* 2008), genes processed by the minor spliceosome did not appear to be preferentially affected (Bäumer *et al.* 2009, Zhang *et al.* 2008). The expression of physiological alternative splice isoforms in late-stage, severely moribund SMA mice is probably a secondary, non-specific response to systemic stress such as hypoxia. This is supported by the abnormalities observed in largely unaffected tissues such as the kidneys (Bäumer *et al.* 2009, Zhang *et al.* 2008). Accordingly, oxygen levels have been shown to modulate *SMN2* splicing and disease severity in SMNΔ7 mice (Bebee *et al.* 2012), and there is evidence to suggest that mitochondrial stress can cause an imbalance in isoform expression profiles in neuronal cells in particular (Maracchioni *et al.* 2007).

Nevertheless, the differences seen in SMA spinal cord at pre-symptomatic stages may reflect pathways actively contributing to disease progression, or early compensatory mechanisms. In order to deconvolute the downregulation of *Chodl-001* but maintenance of

Chodl-002, I investigated what effect the isoforms had on the survival of neuronal cells with reduced Smn levels (Figure 4.6, 4.7, 4.8). From P1 to P13, *Chodl* dysregulation gets progressively worse, correlating with the deteriorating health of the SMA mice (Bäumer *et al.* 2009), but this is consistent with both cause and effect. I thus hypothesised that if *Chodl-001* downregulation was playing a causative role in pathology, adding the protein into Smn-depleted cells could potentially rescue viability. Conversely, if the abnormal splicing of *Chodl* is simply an adjustment to Smn depletion, then perhaps *Chodl-001* expression becomes detrimental to the motor neurons under conditions of low Smn, whereas *Chodl-002* does not. In cells with reduced Smn levels, I observed a further reduction in viability when *Chodl-001* was expressed, while *Chodl-002* caused a subtle improvement (Figure 4.8A, B). This suggests that *Chodl* dysregulation is not a consequence of mis-splicing, but may simply reflect an early compensatory mechanism to reduce the negative impact of Smn depletion on neuronal survival. Consistent with this, depriving mild SMA mice of food also leads to abnormal splicing of *Chodl* in the spinal cord (Sahashi *et al.* 2012). Importantly, chondrolectin isoforms had no effect on the viability of cells with normal Smn levels (Figure 4.8). Doubling the expression levels abolished the positive effects of *Chodl-002* and *Chodl-003* on Smn-depleted cells, such that all three isoforms had a negative impact on viability (Figure 4.9), consistent with the normally low expression of *Chodl*, and mirroring effects seen in zebrafish (Zhong *et al.* 2012).

4.3.2 How do Chodl isoforms exert their differential effects?

Chondrolectin is a monomeric transmembrane protein with a C-type lectin-like domain (CTLD) (Weng *et al.* 2003, Weng *et al.* 2002). These domains typify proteins belonging to the C-type lectin (CLEC) superfamily of proteins (Zelensky & Gready 2005). The majority

of vertebrate CLECs act as recognition molecules within the immune system, because their CTLDs are able to bind to carbohydrates in a calcium-dependent manner. Non-classical CLECs, on the other hand, are able to interact with proteins and other molecules, and therefore possess functions outside the immune system. Chondrolectin is not the first CLEC to be implicated in axonal pathfinding - *C. elegans* CLEC-38 has been shown to function in migrating axons to promote synapse assembly (Kulkarni *et al.* 2008). Given that *Chodl* is expressed in developing motor nerves and has been implicated in axonal pathfinding, it is likely that its CTLD interacts with extracellular proteins rather than carbohydrates. Any differences between the three isoforms, however, are expected to be mediated through the short cytoplasmic tail, as the extracellular portions are identical (Figure 4.1A, B). Using a mouse skeletal muscle cDNA library to identify potential interacting proteins, the cytoplasmic domain of Chodl-001 was shown to bind with the β-subunit of rab geranylgeranyl transferase (Rabggtb) (Claessens *et al.* 2008). Rabggtb isoprenylates Rab GTPases that are then involved in vesicle trafficking of transmembrane proteins from the Golgi to the cell surface (Farnsworth *et al.* 1994, Simons & Zerial 1993). *Rabggtb* is expressed widely during early gestation, but by about embryonic day 13.5 (E13.5) is more restricted to the liver and spinal cord (Chinpaisal *et al.* 1997). Given this expression pattern, Rabggtb could be interacting with chondrolectin in motor neurons during early development. To begin to resolve what role the different Chodl isoforms are playing and how they exert their distinct effects on the nervous system, the neuronal cytoplasmic protein interaction profiles of the three isoforms should be examined. It is also vital to identify proteins that are able to bind to the CTLD of Chodl.

4.3.3 Chondrolectin and nervous system development

In whole mouse embryos, *Chodl* expression is tightly regulated during early embryonic development; mRNA levels gradually increase from E7 to E15 and then begin to decline by E17 (Weng *et al.* 2003). *Chodl* is expressed at the base of the developing limb bud and in spinal cord motor neurons at E10.5 and E11.5, a time when the motor axons are reaching and invading the bud region and a number of pathfinding decisions are made (Enjin *et al.* 2010, Shou *et al.* 2005). Given the pattern and timing of expression, it is possible that Chodl is playing an integral role in the development of the nervous system, in particular, in motor axon guidance. Corroborating this, work in zebrafish suggests that Chodl is vital for the interaction of motor axons with the horizontal myoseptum, an early developmental choice point (Zhong *et al.* 2012). Moreover, *Chodl* overexpression increases cellular invasion in a number of different cell lines, concordant with an outgrowth phenotype (Masuda *et al.* 2011). Nonetheless, increased expression of the single *Chodl* isoform in zebrafish results in abnormal axonal growth similar to morpholino knockdown (Zhong *et al.* 2012). Similarly, I report that expression of *Chodl-001* and *Chodl-002* in differentiated NSC-34 cells with normal Smn levels results in reduced neurite outgrowth, the severity of which correlates with DNA concentration (Figure 4.10, 4.11). The percentage of cells bearing neurites was unaffected by *Chodl* expression, similar to the observation in zebrafish that *Chodl* overexpression did not cause failure of axon outgrowth. Together, these results suggest that in cells with normal SMN levels, chondrolectin is involved in the outgrowth and elongation of neuronal process, not their initial generation, and that the fine-tuning of Chodl levels is vital for efficient neuronal growth and development.

4.3.4 Chondrolectin and neurite outgrowth in Smn-depleted cells

SMN depletion results in neurite and axon outgrowth defects in a number of different cell lines and animal models (Chang *et al.* 2011, Jablonka *et al.* 2007, Kwon *et al.* 2011, Liu *et al.* 2011, McWhorter *et al.* 2003, Ning *et al.* 2010, Nölle *et al.* 2011, Shafey *et al.* 2008, van Bergeijk *et al.* 2007, Ymlahi-Ouazzani *et al.* 2010). Furthermore, knockdown of *SMN* in astroglioma cells causes defective migration (Caraballo-Miralles *et al.* 2012), and the spinal motor neurons of severe SMA patients have been shown to be deficient in migration, axonal outgrowth, and ability to increase motor unit territory (Hausmanowa-Petrusewicz 1988, Šimić *et al.* 2008). Smn reduction in NSC-34 cells is no different (Figure 4.10, 4.11); both the percentage of cells bearing neurites and neurite length were significantly reduced. Given that individual knockdown of *Chodl* and *Smn* produces a similar phenotype of defective axonal pathfinding in zebrafish (McWhorter *et al.* 2003, Zhong *et al.* 2012), it is possible that the downregulation of *Chodl-001* in SMA mouse spinal cord is contributing to or even mediating subtle nervous system defects that destabilise the motor neurons. I expressed the different *Chodl* isoforms in Smn-depleted NSC-34 cells to determine whether I could rescue the neurite outgrowth and length defects. Individual expression of *Chodl-001* at the lower concentration was able to significantly improve the percentage of neurite-bearing cells (Figure 4.10C), while individual expression of *Chodl-001* or *Chodl-002* was able to significantly increase neurite length (Figure 4.10D). Doubling the DNA concentration abrogated the positive effect of Chodl-001 on neurite generation and length (Figure 4.11A, B); once again, it therefore appears that the level of *Chodl* expression is integral to proper function.

If Chodl isoforms improve neurite outgrowth in an environment with low Smn, why is *Chodl-001* expression suppressed in SMA mouse spinal cord? Considering the results from the cell survival experiments, it is possible that *Chodl-001* is downregulated in order to preserve the viability of motor neurons due to a compounding toxic effect of

Chodl-001 when Smn is sparse. This dysregulation of *Chodl*, which becomes progressively more prominent during early postnatal development, could conceivably lead to the subsequent destabilisation and degeneration of neuronal cells early after birth. Consistent with this, no major defects in axonal architecture are seen at embryonic stages in mouse models of SMA (McGovern *et al.* 2008, Murray *et al.* 2010), a time when *Chodl* dysregulation is just beginning to occur, whereas at P1, pathways involved in postnatal maturation of the spinal cord appear to be disrupted (Bäumer *et al.* 2009). Moreover, Chodl can be found in adult spinal cord motor neurons (Bäumer *et al.* 2009), suggesting that besides axonal outgrowth and development, chondrolectin may also function in motor neuron maintenance. Taken together, the cellular viability and neuronal outgrowth experiments suggest that the dysregulation of *Chodl* may be both a contributor to pathology and a compensatory mechanism, but is unlikely to be due to aberrant splicing.

In summary, the different chondrolectin isoforms appear to play distinct roles in cell survival and neurite outgrowth depending on their abundance and Smn availability. This work hints that the dysregulation of *Chodl* seen at pre-symptomatic stages in SMA mice may be a compensatory response to low Smn levels, and that, in turn, this contributes to subtle nervous system defects that underlie the lower motor neuron degeneration seen in SMA.

5. A potential toxic gain-of-function mechanism in CMT2D

5.1 Introduction

The aminoacyl-tRNA synthetases (ARSs) are an ancient class of enzymes that charge specific amino acids to their cognate tRNAs, thereby ensuring the fidelity of the genetic code during protein translation. In addition to aminoacylation, a number of secondary, non-canonical functions have been ascribed to the ARSs, the disruption of which is thought to contribute to the specific pathology observed in a number of human diseases (Antonellis & Green 2008, Park *et al.* 2008). Mutations in several genes encoding ARSs have been implicated in Charcot-Marie-Tooth (CMT) diseases (Antonellis *et al.* 2003, Jordanova *et al.* 2006, Latour *et al.* 2010, McLaughlin *et al.* 2010), a heterogeneous set of conditions characterised by distal motor and sensory dysfunction leading to progressive muscle atrophy in the hands and feet (Reilly *et al.* 2011). Dominant mutations in *GARS* cause CMT disease type 2D (Antonellis *et al.* 2003). Through two translation start sites, *GARS* encodes mitochondrial and cytoplasmic isoforms of the non-redundant, homodimeric enzyme, glycyl-tRNA synthetase (GlyRS), which specifically ligates glycine to its tRNA. GlyRS has been detected in healthy mouse and human serum (Park *et al.* 2012), and can exist as a monomer that is inactive for aminoacylation (Nangle *et al.* 2007), indicating that GlyRS may also possess a non-canonical function. Nevertheless, it remains elusive how mutations in this widely expressed gene lead to the susceptibility of neurons seen in CMT2D patients.

Two mouse models of CMT2D, $Gars^{Nmf249/+}$ and $Gars^{C201R/+}$, result from dominant amino acid substitutions in *Gars* equivalent to *P234KY* and *C157R* seen in patients, respectively (Achilli *et al.* 2009, Seburn *et al.* 2006). In common with the human disease, these mice exhibit motor and sensory deficits with reduced body weight. Marked NMJ

degeneration and axon loss is seen in *Gars*$^{Nmf249/+}$ by 3-4 weeks, which precedes frequent, genetic background-dependent mortality at 6-8 weeks. *Gars*$^{C201R/+}$ animals display only mild muscle weakness and partial loss of innervation with normal lifespan, which is the phenotype most similar to human CMT2D.

CMT2D-associated mutations are all located downstream of the 54 amino acid mitochondrial targeting sequence and tend to cluster at the dimer interface (Cader *et al.* 2007, He *et al.* 2011, Nangle *et al.* 2007, Xie *et al.* 2007). GlyRS possesses three functional domains common to mitochondrial and cytoplasmic isoforms: a highly conserved N-terminal helix-turn-helix WHEP domain of unclear function, a catalytic core, and a C-terminal anticodon-binding domain. Human and mouse phenotypes do not correlate with aminoacylation function (Achilli *et al.* 2009, Nangle *et al.* 2007, Seburn *et al.* 2006, Stum *et al.* 2010), and a 50% reduction in *Gars* mRNA levels results in no overt phenotype or NMJ pathology in an mRNA-null allele, *Gars*$^{XM256/+}$ (Seburn *et al.* 2006). Together, these results argue against a simple loss-of-function or haploinsufficiency disease mechanism. The recent demonstration that wild type *Gars* transgene overexpression is unable to rescue CMT2D mice confirms a toxic gain-of-function of mutant GlyRS as the disease trigger (Motley *et al.* 2011). Consistent with this, CMT-associated *GARS* mutations and deletion of the WHEP domain cause the same localised conformational opening of the GlyRS protein, potentially providing new binding sites for neomorphic interactions (He *et al.* 2011).

With the extensive knowledge of its nervous system, its short life cycle (Figure 5.1), and a large number of available genetic techniques, *Drosophila melanogaster* is well placed for the study of human neuromuscular disorders (Lloyd & Taylor 2010, Reiter & Bier 2002). The *Drosophila gars* gene (also known as *aats-gly*) encodes a protein that shares 60% identity with human GlyRS, and most patient mutations affect amino acids

conserved in the fly (Motley *et al.* 2010). Using mosaic analysis with a repressible cell marker (MARCM), homozygous null *gars* mutations were shown to affect branching of olfactory bulb and mushroom body neurons, revealing the importance of protein translation in axonal and dendritic arborisation (Chihara *et al.* 2007). However, this recessive loss-of-function model does not reflect well human CMT - a dominant disorder where mutant *GARS* is expressed in all tissues.

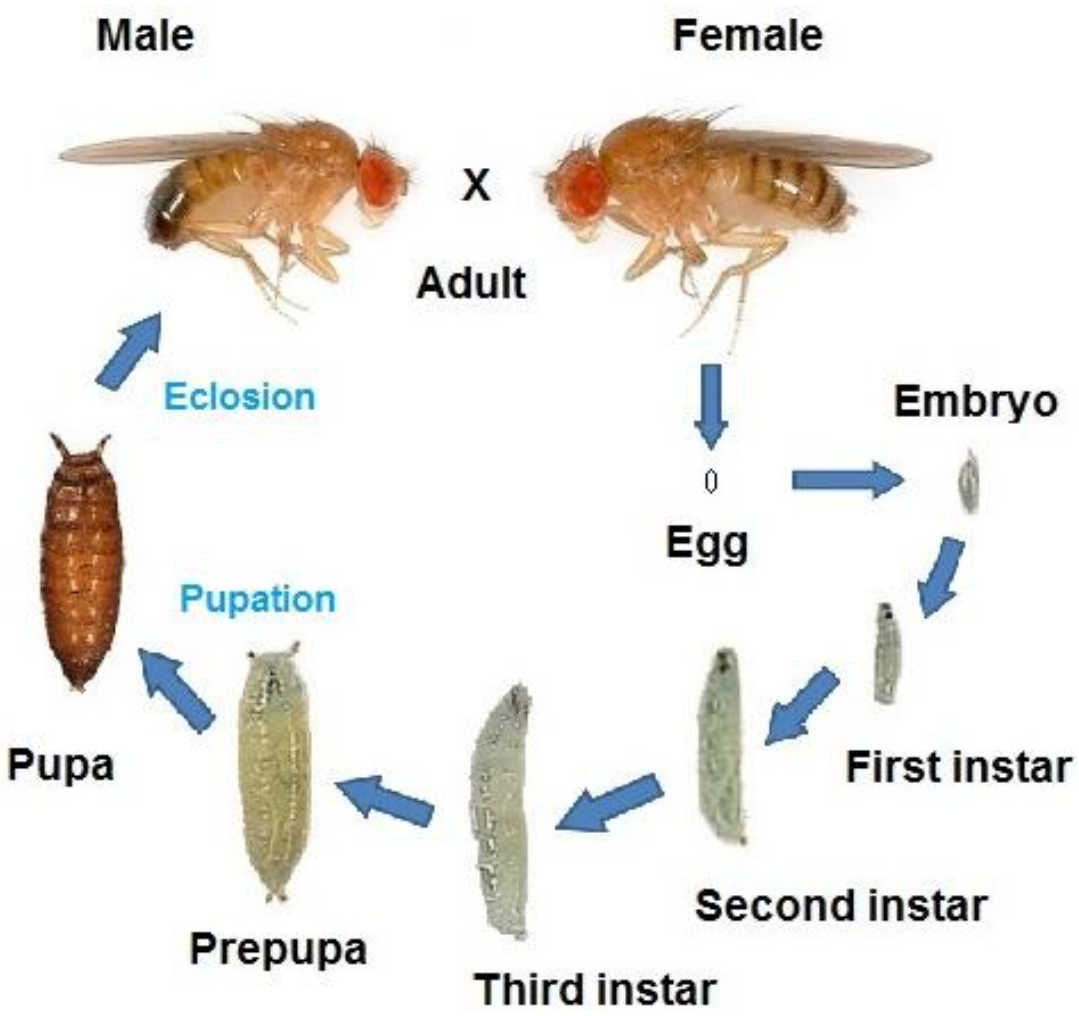

Figure 5.1. The *Drosophila* life cycle. At 25˚C, *Drosophila* transition from newly laid eggs to adults in ≈ 10 days. Developing from eggs, embryos then grow through three larval stages (first to third instar), pupate, and finally eclose from pupal cases as adults.

5.1.1 Aims of chapter 5

Using a novel fly model generated by Dr. Stuart J. Grice and both existing mouse models of the disease, the objective of this chapter was to identify novel features of disease pathology and the GlyRS toxic gain-of-function.

The work presented in this chapter was the result of collaboration with Dr. Stuart J. Grice. Data from experiments using Drosophila *were generated by Dr. Grice (except for the qPCR work). However, as the author of this thesis, I statistically analysed the fly data, designed the graphs and figures, and wrote all of the associated text.*

5.2 Results

5.2.1 Mutant GlyRS causes selective motor defects

Since there is no indication of a specific role for the mitochondrial form of GlyRS in CMT2D, UAS-cytoplasmic constructs to express wild type and mutant *Drosophila gars* were created, focusing on the *P234KY* mutation. The equivalent *Drosophila* and human mutations correspond to *P278KY* in *Gars*$^{Nmf249/+}$ mice (Seburn *et al.* 2006). Residue P234 is in 'kissing contact' with I280 mutated in human disease, as well as residue C201 mutated in the second *Gars* mouse (Achilli *et al.* 2009, He *et al.* 2011, Nangle *et al.* 2007). We tested the effects of GlyRS^{WT} and GlyRS^{P234KY} on adult viability, larval motor function and muscle morphology, and overall development using tissue-specific drivers (Figure 5.2): neuron (*elav-GAL4*, *nrv2-GAL4*), glia (*repo-GAL4*), muscle (*how-GAL4*, *MHC-GAL4* and *C57-GAL4*) and *Drosophila* disc tissue (*69B-GAL4*). *UAS-gars*^{P234KY} had the greatest effect on survival when expressed ubiquitously (strong, *Act5C-GAL4*; weak, *1032-GAL4*) or in muscle, with a small contribution from neurons and glia (Figure 5.2A).

Importantly, ubiquitous and muscle-specific *UAS-gars*^{WT} expression had no such effect (Figure 5.2B). When *gars*^{P234KY} was expressed in all tissues or restricted to muscle, it significantly reduced motor function, as scored by counting the number of body wall muscle contractions of late stage larvae (Figure 5.2C); however, mutant larvae developed normally, survived through each moult, and displayed no obvious muscle degeneration (Figure 5.2D). *gars*^{P234KY} larvae can reach the pupal stage, but many then fail to eclose, becoming trapped in their pupal cases (Figure 5.2E, F). The few escapers show movement defects, fail to expand their wings, and do not survive beyond one week (Figure 5.2G). The human *G240R* mutation in *Drosophila gars* had similar pathogenic effects to *P234KY* (Figure 5.2B). These data show a clear dominant neuromuscular-specific, toxic gain-of-function of mutant but not wild type GlyRS.

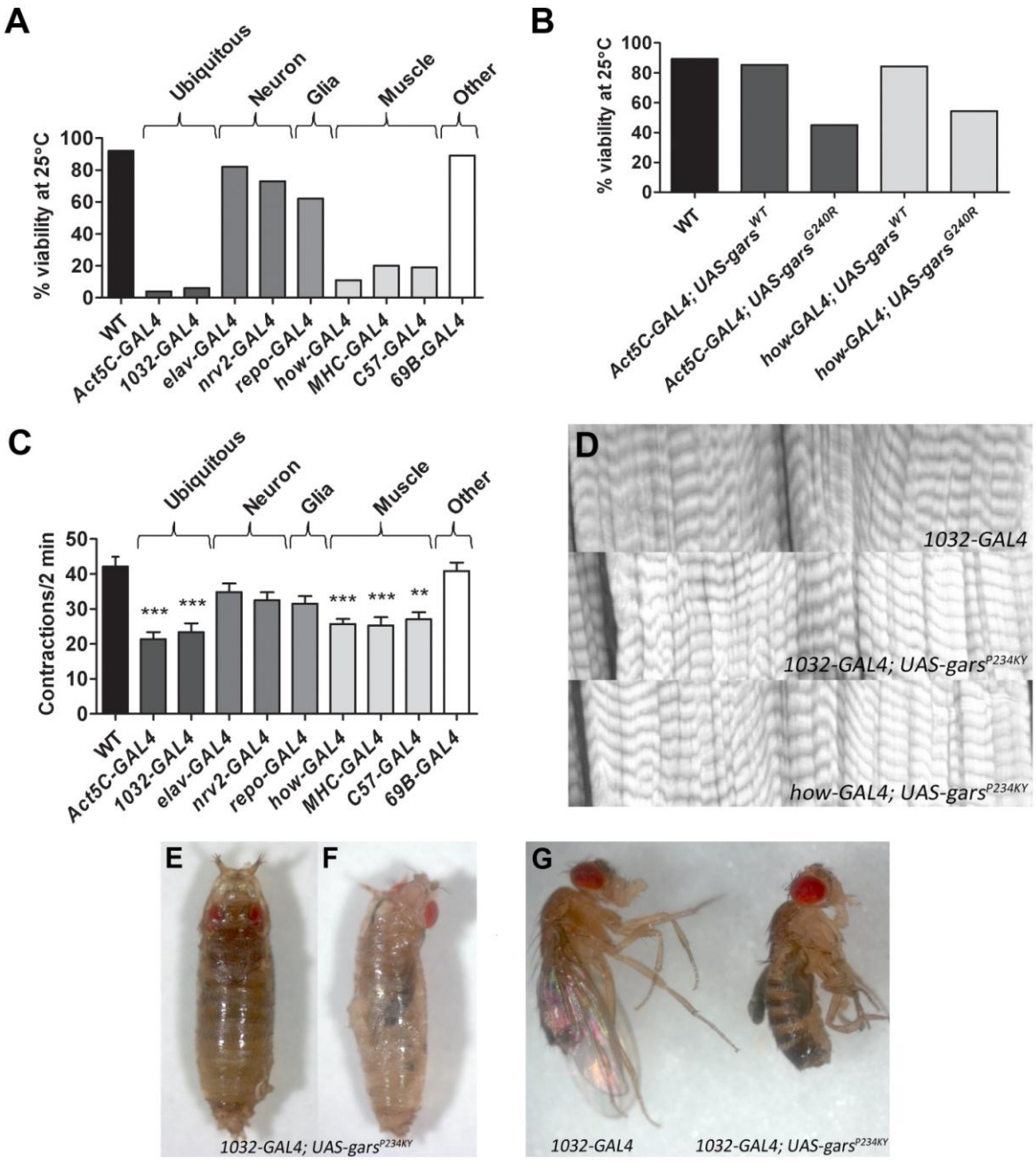

Figure 5.2. Dominant toxic effects from mutant GlyRS can lead to non-cell autonomous motor defects in *Drosophila*. (A) The percentage of flies surviving at 25˚C with ubiquitous, neuron, glia, muscle, and disc expression of $gars^{P234KY}$ using the GAL4/UAS bipartite system. Each genotype was scored two days post-eclosion. The most severe defects were generated by ubiquitous $gars^{P234KY}$ expression, with muscle expression a close second. 300 flies/genotype were scored over three independent experiments. **(B)** Ubiquitous expression of wild type *gars* has no effect on viability, whereas a second mutation, *G240R*, causes a comparable effect to *P234KY*. **(C)** Analysis of the number of body wall muscle contractions in 2 min of third instar larvae at 25˚C. Similar to the viability experiments, ubiquitous and muscle-specific mutant

gars expression resulted in the greatest defect in motor function. 20 flies/genotype were scored. $P < 0.001$, Kruskal-Wallis test. ** $P < 0.01$ and *** $P < 0.001$, Dunn's multiple comparison test with wild type. **(D)** Larvae expressing $gars^{P234KY}$ ubiquitously or in muscle are able to develop through each moult, and display no obvious defects in muscle structure. **(E, F)** Mutant $gars^{P234KY}$ flies reach the pupal stage but fail to eclose and often become trapped in their pupal cases. **(G)** The few flies that escape and reach adulthood display defects in motility and wing expansion, and survive for less than a week. The data for this figure were generated by Dr. Stuart J. Grice.

5.2.2 Branching defects precede pre-synaptic GlyRS build-up and bouton retraction

To explore how mutant *gars* expression affects the neuromuscular system, we examined larval NMJs. The abdominal ventrolateral muscles 6 and 7 of *Drosophila* larvae are innervated by segmental nerve d (SNd). SNd defasciculates, projects toward, and innervates muscles 6 and 7 in a highly stereotypical manner (Peron *et al.* 2009). Wild type NMJs grow by adding circular synaptic specialisations called boutons that resemble beads on a string (Johansen *et al.* 1989), where both pre- and post-synaptic regions closely overlap (Figure 5.3A). In early larval stages, the main nerve trunks of *1032-GAL4; UAS-*$gars^{P234KY}$ larvae appear to pathfind normally, but NMJs display irregular additional branches (Figure 5.3B, D). The difference in bouton number per NMJ between wild type and mutant larvae increases with age, suggesting that the mutant NMJs are unstable (Figure 5.3C, E). We also saw more pre-synaptic ghost boutons and accumulation of synaptic debris (Figure 5.3C, F), both of which are linked to defective clearance and retraction of undifferentiated boutons at the synapse (Fuentes-Medel *et al.* 2009). Moreover, mutant pre-synaptic terminals can be seen on the muscle without the corresponding post-synaptic anchoring.

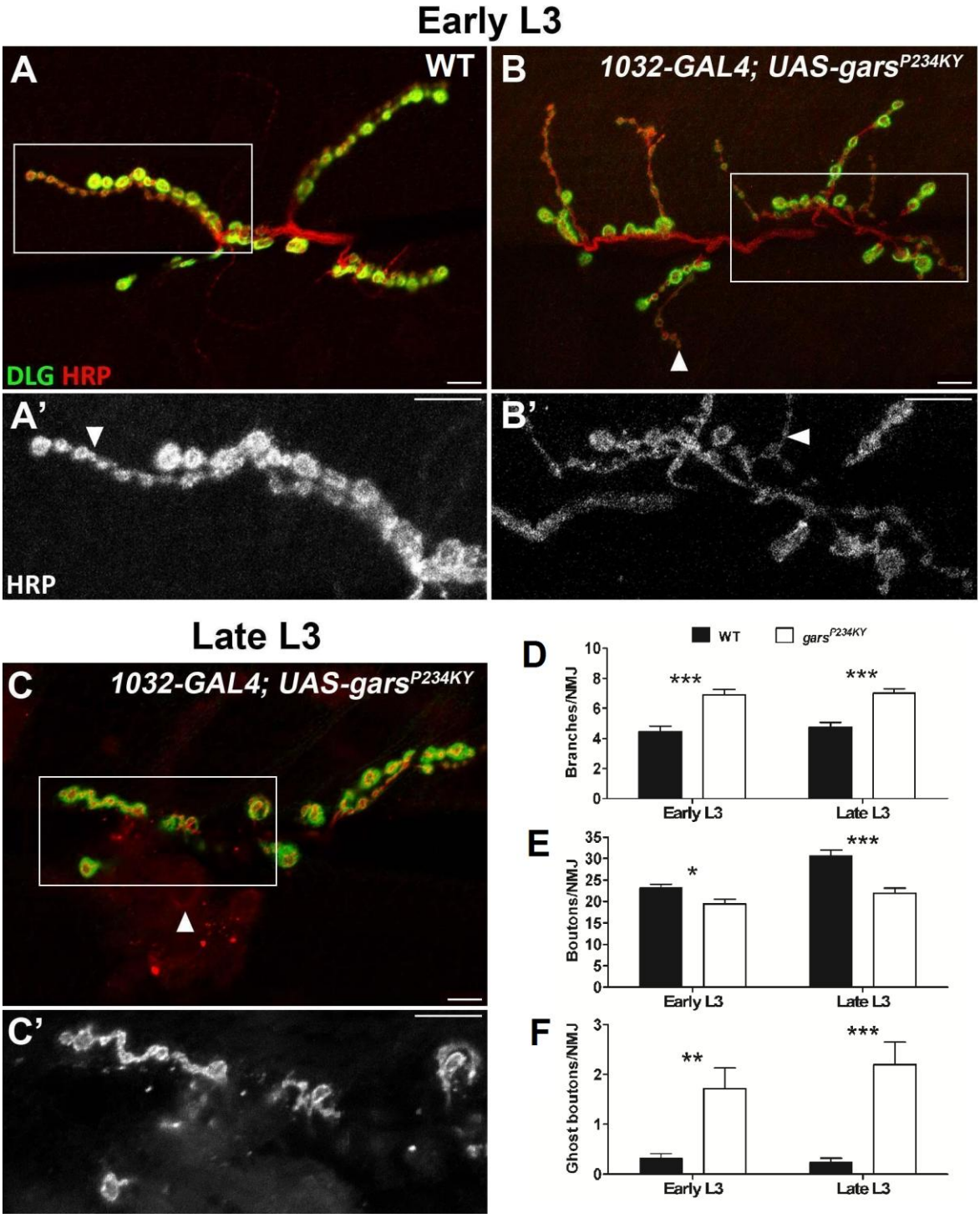

Figure 5.3. Mutant *gars*^{P234KY} expression causes increased NMJ branching and synaptic growth abnormalities. (A) An example NMJ from abdominal ventrolateral muscles 6 and 7 in an early L3 wild type larva. The synapses consist of boutons that grow in lines resembling beads on a string (arrowhead). Post-synaptic apparatus is visualised with anti-DLG (green) and nerves with anti-HRP (red). A' is a magnified view from the box found in A. **(B)** Early L3 *1032-GAL4; UAS-gars*^{P234KY} larvae display NMJs with abnormal

extra branches (arrowheads). **(C)** Late L3 *1032-GAL4; UAS-gars*^{P234KY} larval NMJs are reduced in size. The decrease in NMJ area correlates with an increase in ghost bouton (arrowhead) number and synaptic debris. **(D, E, F)** *1032-GAL4; UAS-gars*^{P234KY} NMJs exhibit increased branching (D, $P < 0.001$, one-way ANOVA), decreased bouton number (E, $P < 0.001$, one-way ANOVA), and increased ghost bouton number (F, $P < 0.001$, Kruskal-Wallis test). NMJ analysis was performed on hemisegment A2, 23-25 NMJs/genotype/stage were scored, and * $P < 0.05$; ** $P < 0.01$; *** $P < 0.001$, Bonferroni's or Dunn's multiple comparison test. Scale bars = 10 μm. The data for this figure were generated by Dr. Stuart J. Grice.

To further understand the NMJ pathology, we monitored changes in the localisation of mutant GlyRS in motor neurons and muscles of *1032-GAL4; UAS-gars*^{P234KY} larvae. At early third instar, GlyRS^{P234KY} protein can be seen in the muscle. As the larvae age, mutant GlyRS localises to pre-synaptic regions of the NMJ (Figure 5.4A). These regions correspond to degenerate parts of the NMJ and areas with pre-synaptic ghost boutons. GlyRS^{P234KY} colocalises with the pre-synaptic neuronal membrane (labelled with anti-HRP) at the bouton, but not more proximally up or in the axon. To understand the origin of the accumulating pre-synaptic mutant GlyRS, *gars*^{P234KY} was driven exclusively in muscle (*MHC-GAL4*, Figure 5.4B) or neuron (*nrv2-GAL4*, Figure 5.4C). Pre-synaptic GlyRS accumulation was observed when *gars*^{P234KY} was expressed in muscle, but not neuron, suggesting that mutant GlyRS originating in muscle is able to cross the synaptic cleft and interact with the pre-synapse. Wild type GlyRS did not do this. The *Drosophila* NMJ adapts in response to growth and activity by adding or pruning boutons and branches at the outer periphery of the synapse. The GlyRS build-up and subsequent synaptic defects appear to be associated with such regions.

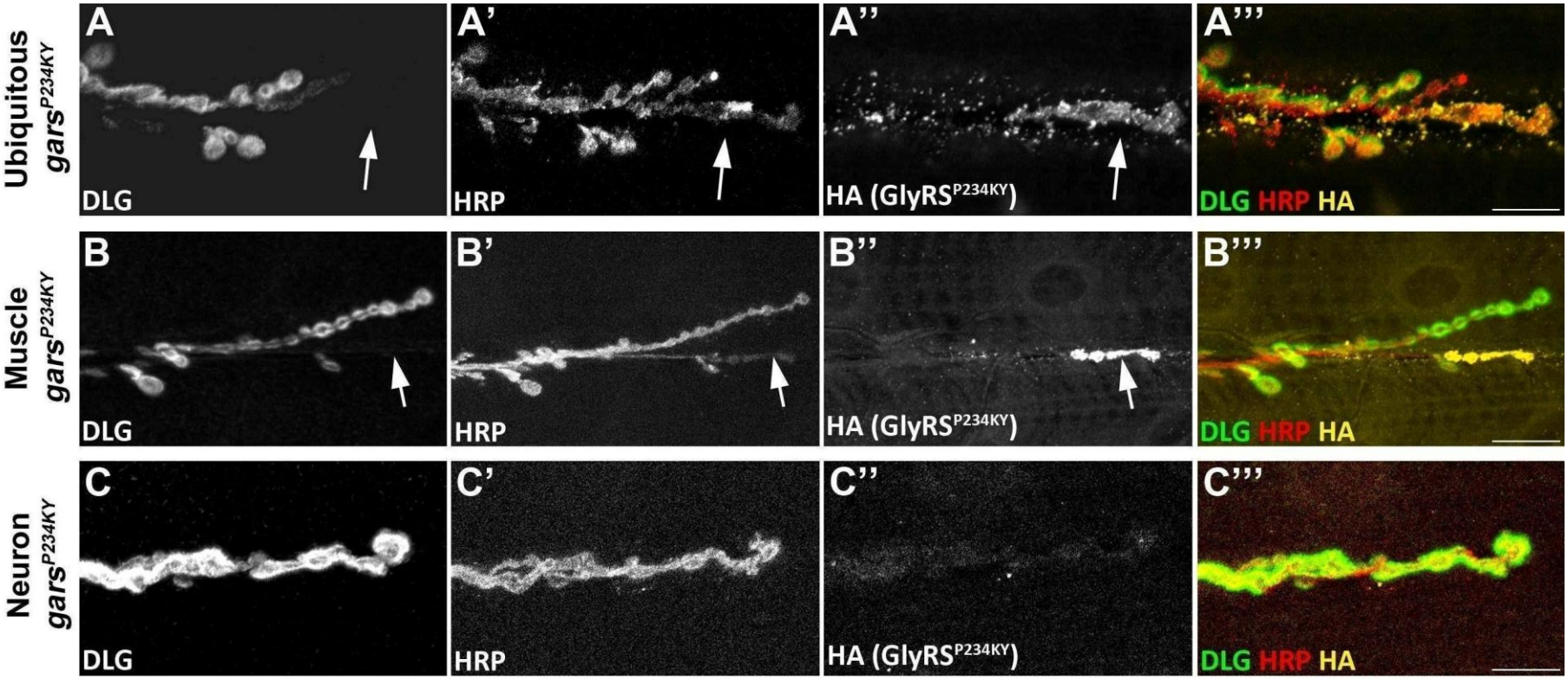

Figure 5.4. Muscle-expressed mutant GlyRS accumulates at the pre-synapse. (A) A pictorial projection of an example NMJ from a larva expressing ubiquitous *gars*^{P234KY} (*1032-GAL4*). Note the lack of post-synapse (DLG) associated with the nerve (HRP, i.e. die-back, arrow). This region has an enrichment of GlyRS^{P234KY} that colocalises with the pre-synaptic component of the synapse. **(B, C)** Muscle (*how-GAL4*, B), but not neuron (*nrv2-GAL4*, C), expression of *gars*^{P234KY} also leads to synaptic die-back (arrow) and GlyRS^{P234KY} build-up at the pre-synapse.

Human GlyRS was recently shown to be secreted by macrophages and to be present in human and mouse serum (Park *et al.* 2012). Secretion of several other ARSs has also been demonstrated (Park *et al.* 2008). We expressed wild type and *P234KY* human *GARS* constructs (fused with eGFP) in C2C12 myoblast cells and found that both encoded proteins are secreted into the media (Figure 5.5A). We also investigated the determinant on GlyRS that directs the protein for secretion. A candidate is the N-terminal helix-turn-helix WHEP domain, which is appended to GlyRS in metazoans and is dispensable for the aminoacylation activity of GlyRS (Xie *et al.* 2007). Deletion of the WHEP domain resulted in a loss of GlyRS secretion in the context of both the wild type and mutant protein (Figure 5.5B), suggesting that the WHEP domain is required for this process. With this in sight, we investigated the importance of GlyRS secretion to the mutant $gars^{P234KY}$ phenotype by generating a WHEP-deletion fly: $UAS\text{-}gars^{\Delta WHEP\text{-}P234KY}$. Under ubiquitous or muscle-specific induction of $gars^{\Delta WHEP\text{-}P234KY}$, we found that removal of the WHEP domain resulted in a robust amelioration of the fly viability defect (Figure 5.5C). Furthermore, NMJ structure was rescued and the pre-synaptic localisation of mutant GlyRS was abrogated (Figure 5.5D).

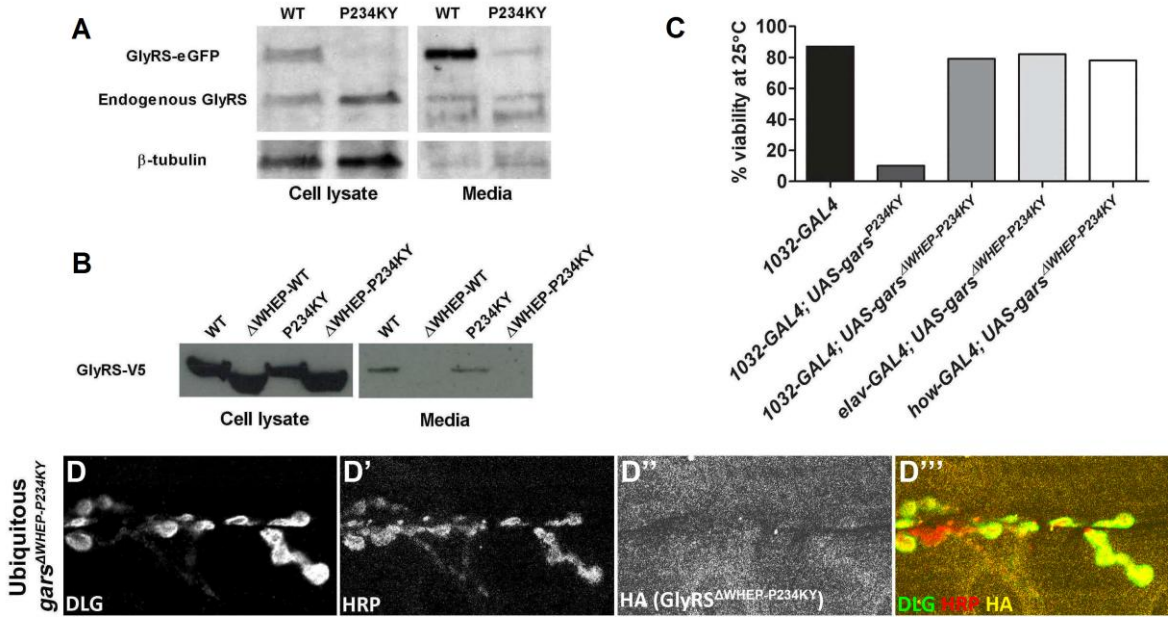

Figure 5.5. The WHEP domain is required for pre-synaptic build-up of muscle-secreted mutant GlyRS. (A) Both wild type and P234KY mutant human GlyRS are secreted from C2C12 cells into the media. **(B)** The WHEP domain is vital for the secretion of both wild type and P234KY mutant human GlyRS from COS7 cells. **(C)** Expression of *gars*$^{\Delta WHEP\text{-}P234KY}$ has no effect on fly viability. **(D)** The WHEP domain is required for the pre-synaptic accumulation of mutant GlyRS. Scale bars = 10 µm. The data for panels A, B, C, F, and G of this figure were generated by Dr. Stuart J. Grice. Weiwei He and Xiang-Lei Yang performed the experiments presented in panel E.

5.2.3 Semaphorin-plexin pathways mediate the GlyRS neuron-associated defects

In order to discover the causative mechanism of the mutant GlyRS toxic gain-of-function, we studied the aberrant branching and maturation defects that precede the subsequent NMJ die-back. In addition to the over-elaboration of the native synapse, we also discovered ectopic branching. *Drosophila* muscles 6 and 7 have flanking neurons, including the transverse nerve (TN) that completely bypasses 6 and 7, and segmental nerve b (SNb) innervating muscles 12 and 13 (Figure 5.6A). In ubiquitous and muscle-specific *gars*^{P234KY} larvae, the number of ectopic contacts and branches from the TN and SNb are significantly increased (Figure 5.6B, C, D). *Bruchpilot* is also expressed at these contacts, which

encodes an active zone-associated protein (Figure 5.6D). *gars*^{P234KY} branching defects were non-cell autonomous and highly specific, as shown by expressing *gars*^{P234KY} exclusively in the abdominal ventrolateral muscles 6 and 7 using *BG487-GAL4* (Figure 5.6E). Ectopic branching still occurs from the TN even though GlyRS^{P234KY} is not being produced in the muscles where the TN forms native synapses. This suggests that a muscle-secreted factor is attracting or failing to repel accessory branches and synaptic contacts. Overall, the phenotype closely resembles that reported in the plexin B receptor (*plexB*) hypomorphic mutant, *plexB*^{KG00878}, which also display larval viability defects (Carrillo *et al.* 2010). Plexins are receptors that function during semaphorin signalling, a process that governs fidelity during axon guidance and synapse formation (Tran *et al.* 2007). *plexB* is expressed by *Drosophila* motor neurons and Plexin B binds to the secreted chemorepulsive molecule Semaphorin-2a (Sema-2a), an interaction that is vital for preventing unwanted contact with off-target muscles (Ayoob *et al.* 2006, Bates & Whitington 2007, Matthes *et al.* 1995). We examined the larval NMJ and innervation patterns in *plexB* homozygous loss-of-function flies in comparison to *gars* flies. As previously described, we found almost identical branching defects and ectopic *Bruchpilot* expression (Figure 5.6F).

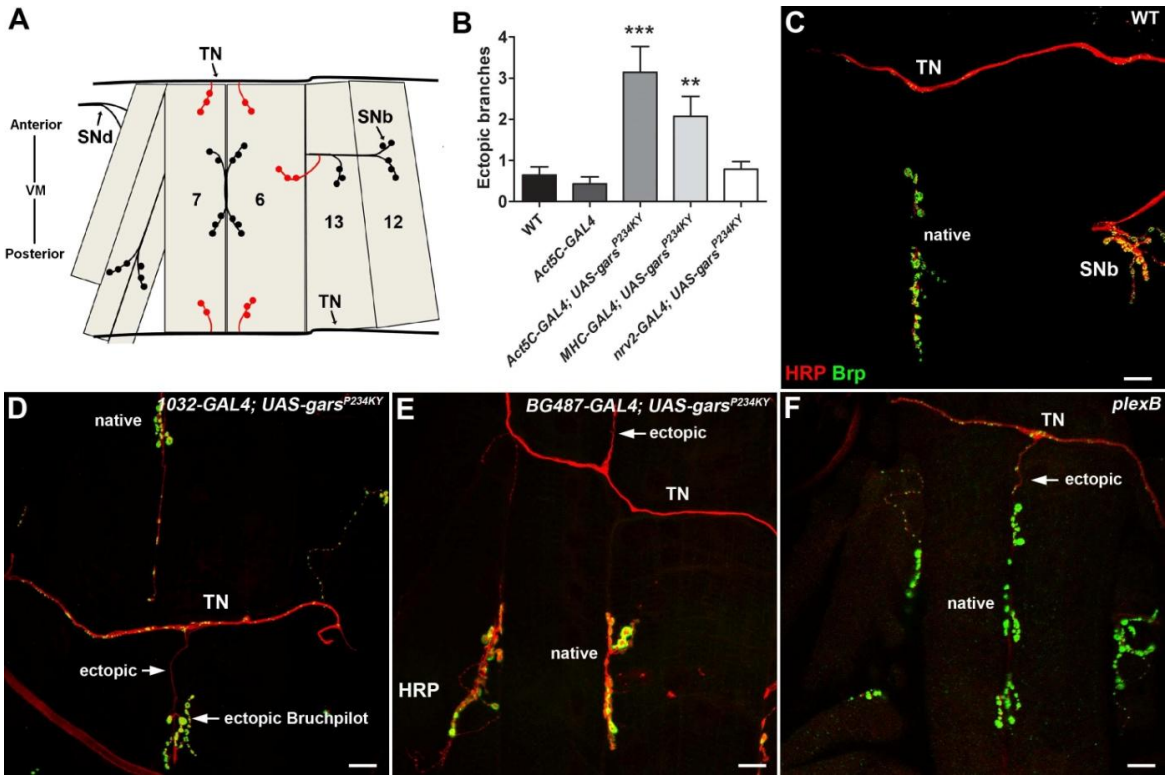

Figure 5.6. Mutant *gars*^{P234KY} expression causes ectopic axonal branching and synapse formation. (A) A schematic of the ventral body wall muscles in one hemisegment, showing segmental nerves b (SNb) and d (SNd), and the transverse nerve (TN). The ectopic synaptic contacts often observed on muscles 6 and 7 in *gars*^{P234KY} flies are shown in red. VM, ventral midline. Figure adapted from Carrillo *et al.* (2010). **(B)** *Act5C-GAL4; UAS-gars*^{P234KY} and *MHC-GAL4; UAS-gars*^{P234KY} larvae have increased frequency of ectopic contacts in L3 larvae. 14 flies/genotype were scored. $P < 0.001$, Kruskal-Wallis test. ** $P < 0.01$ and *** $P < 0.001$, Dunn's multiple comparison test with wild type. **(C)** In wild type, the SNb and the TN innervate their normal target muscles. **(D)** In *gars*^{P234KY} flies, ectopic axons and synaptic contacts can be observed from the SNb and the TN. **(E)** *gars*^{P234KY} expression in muscles 6 and 7 using *BG487-GAL4*, leads to ectopic branching from the TN. **(F)** The mutant *gars* flies phenocopy homozygous *plexB*^{KG00878} mutants. Scale bars = 10 µm. The data for this figure were generated by Dr. Stuart J. Grice.

In support of disrupted Plexin B signalling, gene expression studies in *Drosophila* larvae revealed that *sema-2a* levels are increased while *plexB* levels remain constant in mutant *gars*^{P234KY} compared to control larvae (Figure 5.7A). The increase in *sema-2a* gene expression is only small and likely represents a secondary reactive change to disruption of

semaphorin signalling. We next investigated expression changes of three genes involved in the vertebrate semaphorin-plexin system in the lumbrical muscles of *Gars*$^{C201R/+}$ mice. Sema3A is a secreted protein that serves to repel a variety of axonal populations that possess its co-receptor neuropilin-1 (Nrp1), whereas Sema3C is a chemoattractant for axons (Bagnard *et al.* 1998, Bagnard *et al.* 2000, Pasterkamp *et al.* 1998, Schwarting *et al.* 2000). We saw significant reductions in expression of *Sema3A* and *Sema3C*, but not *Nrp1*, at P15-16 in mutant *Gars*$^{C201R/+}$ mice (Figure 5.7B); however, by one month, these changes were no longer present (Figure 5.7C). An increase in levels of Sema3C, an attractant, might be expected to have similar consequences to a reduction in *Drosophila* Sema-2a, a repellent; although due to the downregulation of *Sema3a* it is difficult to interpret these expression changes. Nevertheless, these data show that mutant GlyRS impacts semaphorin-plexin signalling.

Collectively, this suggests that in *gars*^{P234KY} larvae, a muscle-secreted factor is affecting Plexin B signalling leading to the observed branching defects and extensive phenocopy of the *plexB* hypomorphic larvae. This is unlikely to be caused by Sema-2a since, at least at the transcript level, expression is increased. Instead, we hypothesise that the muscle-secreted factor is mutant GlyRS, which binds to Plexin B on the pre-synaptic terminal, where it appears to accumulate. To investigate this further, we looked to modify the *gars* phenotype with a heterozygous *plexB*^{KG00878} mutant and using the GAL4/UAS system to overexpress *plexB*. *plexB*^{KG00878} heterozygous flies display only a minimal reduction in viability when compared to wild type controls, as do *1032-GAL4; UAS-plexB* overexpressors (Figure 5.7D). However, when mutant *gars*^{P234KY} is expressed either ubiquitously or in muscle in tandem with the heterozygous *plexB*^{KG00878} mutation, there is a significant amelioration of the viability defect (Figure 5.7D). Moreover, we find a significant reduction in the pre-synaptic accumulation of GlyRS when Plexin B levels are

reduced (Figure 5.7E). Ubiquitous *plexB* overexpression has no effect on either phenotype, but this may simply be due to there being no additional GlyRS available to interact with the excess Plexin B receptors. Together, these results suggest that interaction of mutant GlyRS with Plexin B modifies the GlyRS toxic gain-of-function.

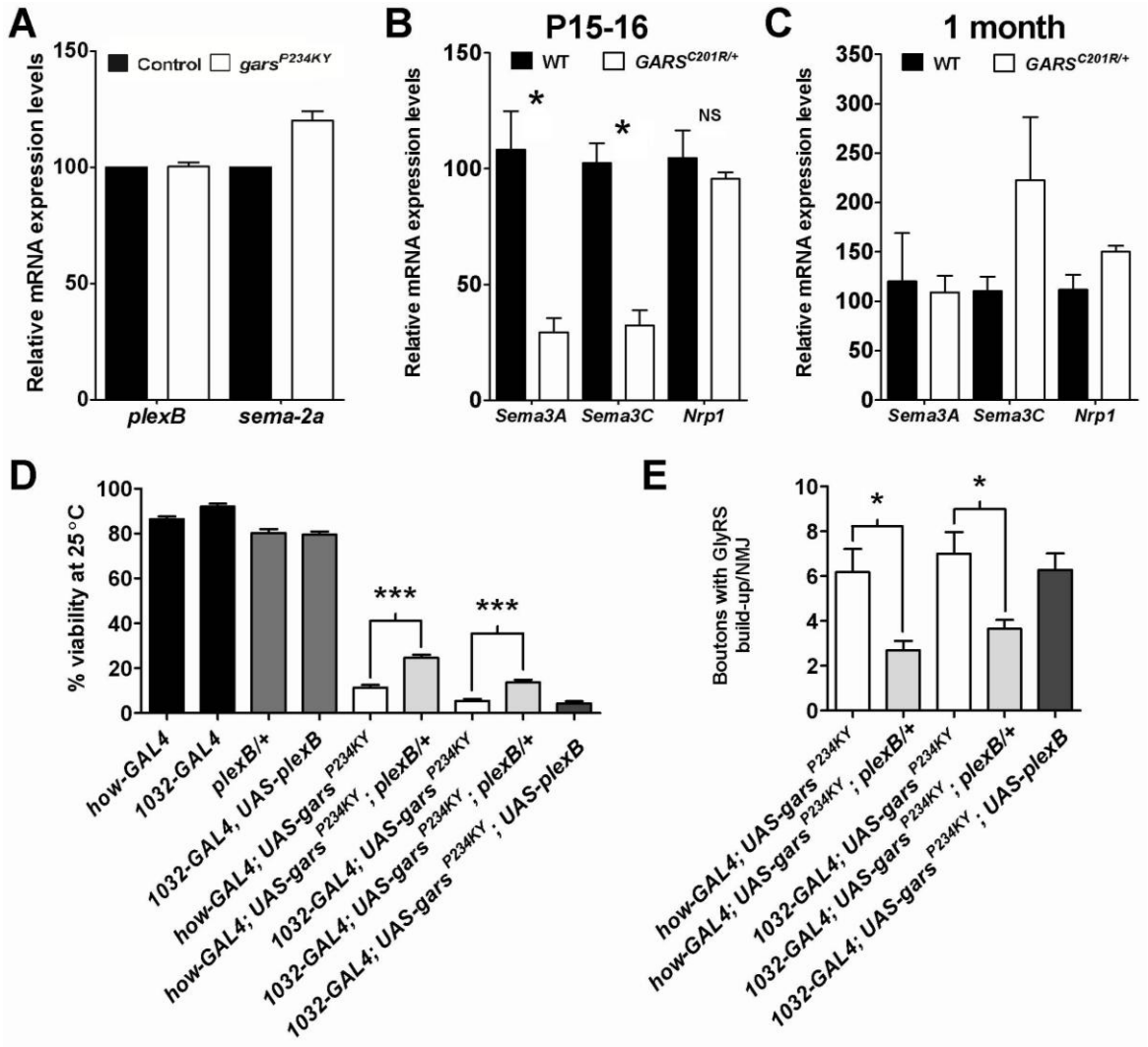

Figure 5.7. Semaphorin-plexin signalling pathways mediate the mutant GlyRS toxic gain-of-function. **(A)** Relative to *1032-GAL4* control, *sema-2a* expression is increased in *1032-GAL4; UAS-gars*^{P234KY} third instar larvae, as assessed by qPCR (n = 3). *Act5C* was used as the reference gene. **(B)** At P15-16, expression of *Sema3A* and *Sema3C*, but not *Nrp1*, is significantly downregulated in *Gars*$^{C201R/+}$ mouse muscle. P = 0.0078, Kruskal-Wallis test. * P < 0.05, Dunn's multiple comparison test. **(C)** By 1 month, these effects are no longer observed. P = 0.353, Kruskal-Wallis test. *Gapdh* was used as the reference gene for qPCR in B and

C. **(D, E)** Analysis of the effects of *plexB* expression levels on mutant GlyRS toxicity. Crossing $gars^{P234KY}$ flies with $plexB^{KG00878}$ heterozygotes significantly alleviates the viability defect (D, $P < 0.001$, one-way ANOVA, *** $P < 0.001$, Bonferroni's multiple comparison test) and reduces the number of boutons with aggregated GlyRS protein (E, $P < 0.001$, Kruskal-Wallis test, * $P < 0.05$, Dunn's multiple comparison test). The data for panels D and E of this figure were generated by Dr. Stuart J. Grice.

5.2.4 NMJ maturation defects precede denervation in *Gars* mice

Although many genes and pathways are conserved between *Drosophila* and humans, mouse models are better placed to answer fundamental questions about how human neuromuscular function and development are affected by disease. Consequently, we also looked at NMJ architecture in the two *Gars* mouse mutants. At one month, NMJs are severely denervated in the lower leg muscles of $Gars^{Nmf249/+}$ mice (Seburn *et al.* 2006). A similar, but milder, degeneration is observed in $Gars^{C201R/+}$ mice (Achilli *et al.* 2009). In order to determine whether developmental abnormalities precede this denervation, as observed in our fly model, we performed a longitudinal assessment of $Gars^{C201R/+}$ NMJ maturation in the lumbrical muscles of the hind paw (Figure 5.8). These muscles were chosen because they are thin and flat distal muscles that can be labelled in whole-mount and visualised without sectioning. As vertebrate NMJs develop during the first few postnatal weeks, a number of structural and functional alterations occur (Sanes & Lichtman 1999). At birth, NMJs are innervated by multiple motor axons, post-synaptic AChRs form a simple plaque shape, and a foetal subunit can be found in the AChRs. By two weeks of age in the mouse, NMJs become singly innervated through synapse elimination, the plaques are transitioning to a pretzel-like conformation, and the γ-subunit of the foetal AChR (Chrng) is replaced by the adult ε-subunit (Chrne). We observed impaired synapse elimination at P15-16 in the $Gars^{C201R/+}$ mice that persisted into adulthood (Figure 5.8A, B, C). Mutant mice also had significantly fewer perforations per

NMJ at P15-16 and one month, indicative of reduced complexity, and therefore delayed development to the pretzel conformation (Figure 5.8D, E). At P15-16, *Gars*$^{C201R/+}$ mice show significantly lower expression of the adult AChR subunit (Figure 5.8F). By one month, the adult subunit is expressed at similar levels to wild type, however, downregulation of foetal subunit expression is impeded (Figure 5.8G).

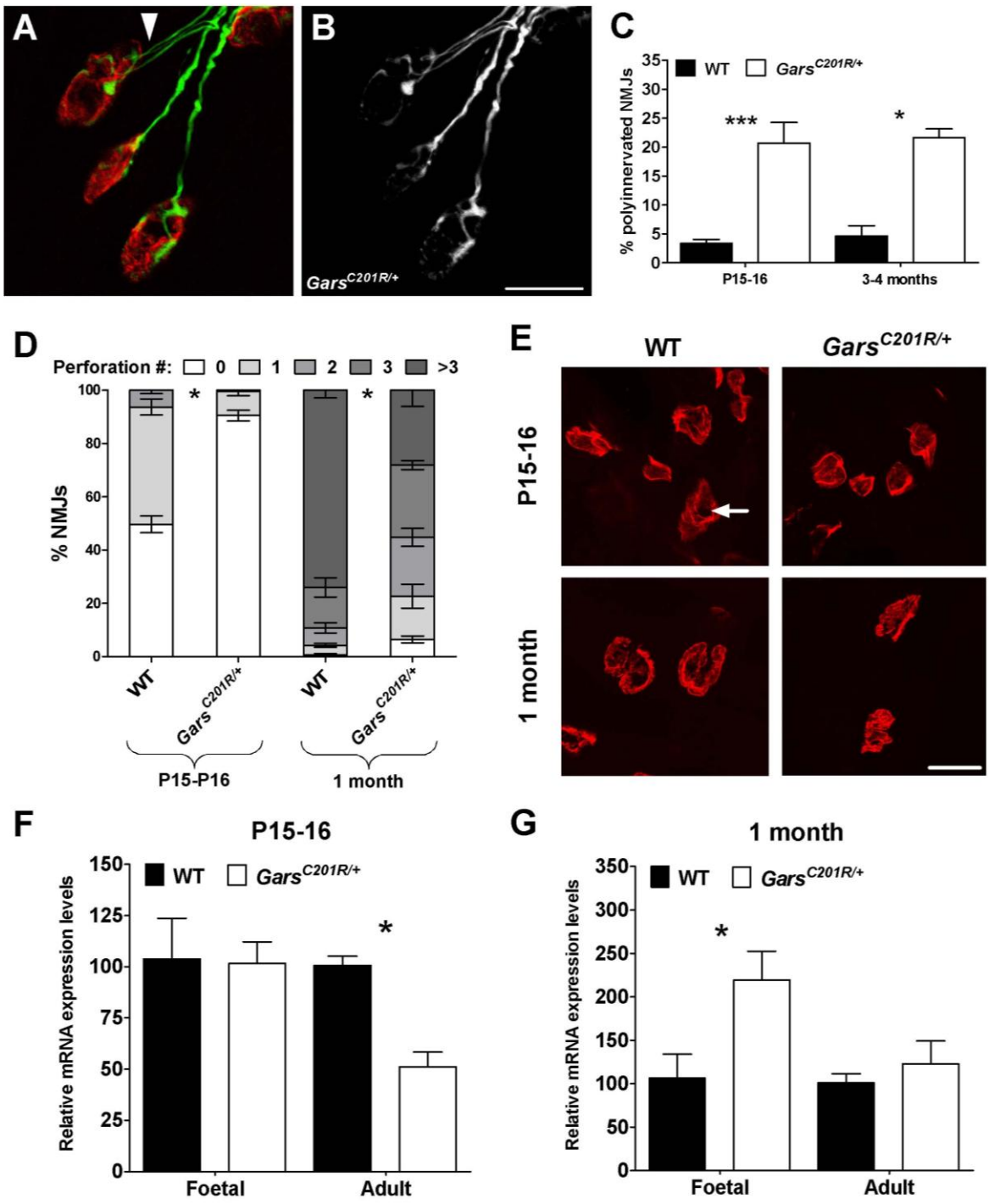

Figure 5.8. NMJ development is delayed in *Gars*$^{C201R/+}$ mice. (A, B) An example polyinnervated NMJ (arrowhead) from a P15 *Gars*$^{C201R/+}$ mouse lumbrical muscle. AChRs are stained red and neuronal tissue in green. **(C)** *Gars*$^{C201R/+}$ mice have significantly more polyinnervated NMJs than wild type at P15-16, a delay in maturation that persists into adulthood (3-4 months). $P < 0.001$, Kruskal-Wallis test. **(D)** Mutant NMJs have significantly fewer perforations in the post-synapse at P15-16 and 1 month, indicative of hindered

progression from the plaque to pretzel conformation. $P < 0.01$, Kruskal-Wallis test. **(E)** Example NMJs from wild type and mutant mice at P15-16 and 1 month. Note the reduced complexity and slight reduction in size. The arrow highlights a perforation. **(F, G)** At P15-16, *Gars*$^{C201R/+}$ mice show a delay in expression of the adult AChR subunit (*Chrne*) as assessed by qPCR. $P = 0.0523$, Kruskal-Wallis test. At 1 month, *Chrne* expression has caught up, but foetal subunit (*Chrng*) expression persists. *Gapdh* was used as the reference gene. $P = 0.0956$, Kruskal-Wallis test. * $P < 0.05$; *** $P < 0.001$, Dunn's multiple comparison test. Scale bars = 10 μm. ≥ 4 mice/genotype were assayed for C and D, and 2-6 for F and G.

We then assessed the innervation status of NMJs in the *Gars*$^{C201R/+}$ mice (Figure 5.9A, B, C). As has been reported for *Gars*$^{Nmf249/+}$ mutants at P7 (Seburn *et al.* 2006), we found no denervation at P15-16 in *Gars*$^{C201R/+}$. However, by 3-4 months, we saw significantly more partially innervated NMJs and some complete denervation (Figure 5.9C). The region circumscribed by the post-synapse was also assessed and the average NMJ area shown to be smaller than wild type at one and 3-4 months, while no difference was seen at P15-16 (Figure 5.9D). Given the smaller size of the mutant mice, this difference is likely a result of body size.

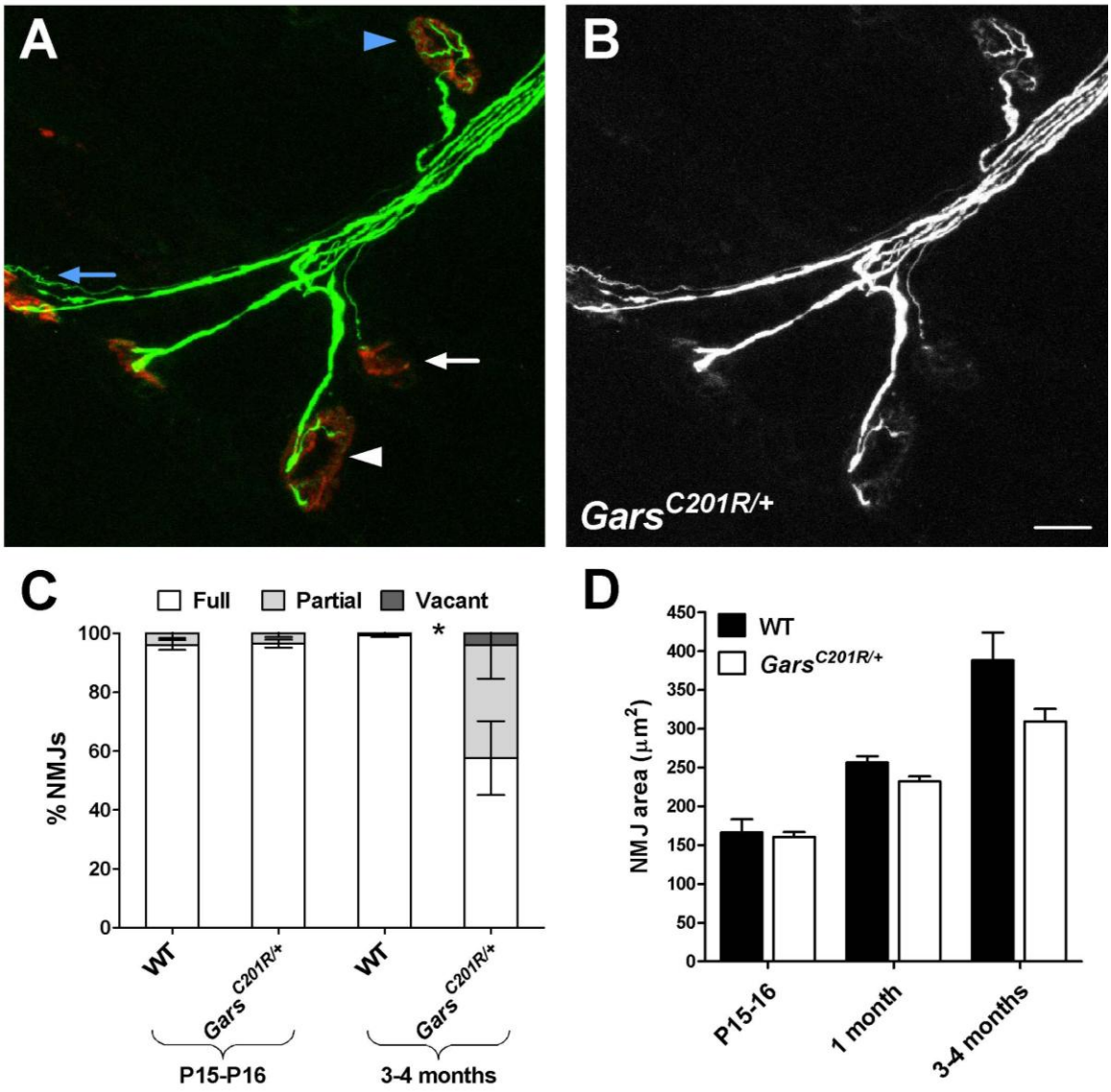

Figure 5.9. Mild denervation succeeds the delay in NMJ maturation. (A, B) Examples of fully occupied (blue arrowhead), partially occupied (white arrowhead), almost vacant (white arrow), and polyinnervated (blue arrow) NMJs from a lumbrical muscle of a 3 month old *Gars*$^{C201R/+}$ mouse. Scale bar = 10 μm. **(C)** At P15-16, a time when the development of the mutant NMJ is perturbed (Figure 5.8), no denervation is seen. However, at 3-4 months, there is a significant increase in the number of partially innervated NMJs with some total denervation, suggesting that maturation defects precede subtle die-back. P = 0.0466, Kruskal-Wallis test. * P < 0.05, Dunn's multiple comparison test. **(D)** There is a small reduction in NMJ area of mutant mice, which becomes more distinct with time, although does not reach significance. P = 0.0035, Kruskal-Wallis test. ≥ 4 mice/genotype were assayed.

For comparison, we also analysed NMJs from *Gars*$^{Nmf249/+}$ mice (Figure 5.10). At one month, the more severe *Gars* mutant displays significant polyinnervation (mean percentage = 25.75), the extent of which supersedes that seen at any time point in the *C201R* allele (mean percentages = 20.71 and 21.62 for P15-16 and 1 month, respectively) (Figure 5.10A). Furthermore, the extent of denervation was also greater (Figure 5.10B), as was the reduction in NMJ area (Figure 5.10C). Thus, we have confirmed both at the structural and molecular levels that *Gars* mice display defects in NMJ maturation that precede degeneration. Moreover, these defects broadly correlate with the severity of the *Gars* model.

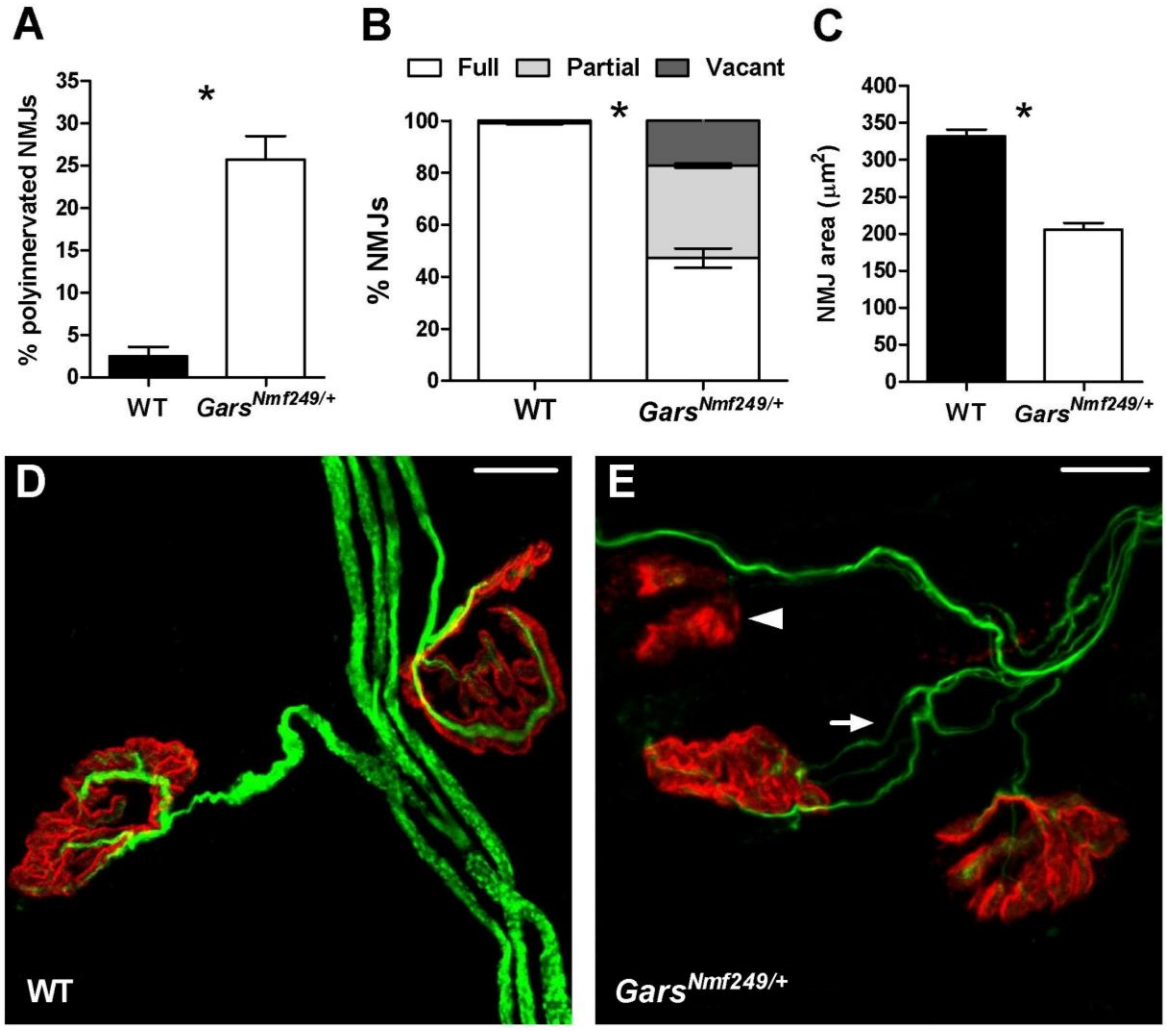

Figure 5.10. *Gars* mouse NMJ defects correlate with mutant severity. (A, B, C) At 1 month, the more severe mutant mouse, *Gars*$^{Nmf249/+}$, displays significantly more NMJs that are polyinnervated (A), denervated (B), and smaller (C) than wild type. The degree of *Gars*$^{Nmf249/+}$ polyinnervation is greater than that seen in *Gars*$^{C201R/+}$ mice at P15-16 and 3-4 months (Figure 5.8C). Similarly, denervation and the reduction in NMJ size are also more severe (Figure 5.9C, D). * $P < 0.05$, Mann-Whitney *U* test. ≥ 4 mice/genotype were assayed. **(D, E)** Example NMJs from 1 month old wild type and *Gars*$^{Nmf249/+}$ mice. A denervated (arrowhead) and polyinnervated (arrow) NMJ can be seen in the mutant muscle. Differences in post-synaptic complexity and size are evident between genotypes. Neuronal atrophy can also be seen in the mutant mouse. Scale bars = 10 μm.

5.3 Discussion

Aminoacyl-tRNA synthetases are modular proteins with unique domains, enabling multiple protein interactions and therefore diverse functions beyond translation, including cytokine activity, apoptosis signalling, and transcription control (Antonellis & Green 2008, Guo *et al.* 2010). This provides novel paths to toxic gain-of-function mechanisms in disease. Here, we show that neuromuscular developmental defects precede denervation in a new fly model of mutant *gars* expression and CMT2D mice, and that two non-canonical properties of mutant GlyRS likely contribute to pathology - secretion from muscle and an interaction with the semaphorin-plexin pathway.

ARS secretion is well described; TyrRS (tyrosine, *YARS*) and TrpRS (tryptophan, *WARS*) bind and signal through extracellular receptors to exert cytokine function and regulate angiogenesis, respectively (Wakasugi & Schimmel 1999, Zhou *et al.* 2010), while secreted LysRS (lysine, *KARS*) is involved in the immune response (Park *et al.* 2005). More recently, the Fas ligand-stimulated secretion of GlyRS from macrophages was reported (Park *et al.* 2012). Our data indicate that several cell types are able to secrete both wild type and mutant GlyRS *in vitro*, and that this is dependent upon the WHEP domain (Figure 5.5A, B). Importantly, flies expressing mutant *gars* lacking the WHEP domain ($gars^{\Delta WHEP\text{-}P234KY}$) do not show pre-synaptic GlyRS localisation or disease pathology, indicating the importance of GlyRS secretion to pathogenesis (Figure 5.5C, D).

Secretion of GlyRS is a novel mechanism through which the observed toxic gain-of-function effects may occur. In the fly, we observe greater toxicity through exclusive expression of mutant *gars* in muscle compared to neurons or glia, indicating a non-cell autonomous effect on the nervous system (Figure 5.2A, C, 5.4). Consistent with this, specific localised ectopic branching and NMJ degeneration are seen when mutant *gars* is expressed in just larval abdominal ventrolateral muscles 6 and 7 (Figure 5.6E).

Nevertheless, there does appear to be a small contribution to pathology from *gars* expression in non-muscle tissue, as evidenced by the minor viability and neuromuscular function defects seen upon neuron and glia *gars* expression, and the distinction in pathology caused by ubiquitous and muscle drivers (Figure 5.2A, C). Furthermore, mutant forms of the protein fail to localise to the neurites in immortal neuronal cells (Antonellis *et al.* 2006, Nangle *et al.* 2007). Together, this suggests that cell autonomous effects are also involved in the disease process. Since both wild type and mutant GlyRS can be secreted and to approximately the same degree (Figure 5.5), this characteristic of the protein is unlikely to account for the majority of the observed pathology.

Developing motor neurons selectively target muscle through reciprocal communication mediated by chemoattractants and repellents such as the semaphorins (Tran *et al.* 2007). In the fly, as the receptor for the secreted chemorepulsive molecule Sema-2A, Plexin B plays a crucial role in the process of off-target motor neuron withdrawal (Ayoob *et al.* 2006, Hu *et al.* 2001, Matthes *et al.* 1995, Winberg *et al.* 1998). The response to Sema-2A is further modulated by pre-synaptic electrical activity (Carrillo *et al.* 2010). In our *Drosophila* model, it is perhaps the specific activation of Plexin B by mutant but not wild type GlyRS that is the critical gain-of-function endowed by disease mutations. The conformational opening of the GlyRS protein caused by disease-associated *GARS* mutations is a candidate area for this neomorphic interaction (Hu *et al.* 2011). It is possible that through this region, muscle-secreted mutant GlyRS binds to Plexin B and thus competes with the endogenous ligand Sema-2A disrupting off-target motor neuron elimination. Hence, we observe ectopic branching, mimicking the effects of *plexB* knock-out to a remarkable degree (Figure 5.6F). In mice, molecules involved in synapse elimination are largely unknown, but reciprocal activity between the motor nerve and muscle is a major contributor (Sanes & Lichtman 1999, Turney & Lichtman 2012). We

find defective synapse elimination in CMT2D mice with persistent polyinnervation at two weeks (Figure 5.8C), and subsequent NMJ degeneration evident at 3-4 months (Figure 5.9C).

Plexins are the receptors and signal transduction machinery of semaphorins. They act alone in the fly, but typically with co-receptors such as neuropilin-1 in vertebrates (Tran *et al.* 2007). There are several signalling cascades that plexins initiate to control axon guidance, synapse formation, or collapse. It is important to consider the potential consequences of GlyRS-Plexin B binding relevant to neuromuscular degeneration. For example, the antagonism of Plexin B, and hence blocking of Sema-2A may result in multiple unstable branches prone to degeneration. Consistent with this, pruning and maturation in the fly and mouse CMTD models precede the neurodegeneration (Figure 5.3, 5.8, 5.9). Alternatively, GlyRS may agonise and activate other Plexin B signalling cascades to destabilise the neuromuscular synapse. Finally, Plexin B may only serve as a docking site to enable mutant GlyRS to be endocytosed, thereby providing access to pre-synaptic subcellular compartments previously out of reach. We find that *plexB* reduction (heterozygous flies) and overexpression (GAL4/UAS) have no major effect on fly viability or NMJ structure (Figure 5.7D and data not shown). However, reducing Plexin B levels ameliorates the muscle-driven mutant *gars* neurodegenerative phenotype, and partially abrogates the phenotype of clear pre-synaptic mutant GlyRS accumulation (Figure 5.7D, E). It appears that the mutant GlyRS cannot be cleared from the bouton as we do not observe muscle-secreted GlyRS more proximally in the axon. Live imaging studies will be required to explore this further.

Since semaphorins and plexins are expressed from an early stage, an important remaining question is why the developmental program is not disrupted in any significant way. It is unknown whether GlyRS secretion occurs from immature muscle. Also, we

found that GlyRS secretion and action occurs over a short range (Figure 5.6E). Therefore, secretion and uptake of GlyRS may only occur to a sufficient degree to cause toxicity in a more mature NMJ where differentiated muscle and nerve are in close apposition. Furthermore, in the mouse, semaphorin expression is high prenatally and as such may out-compete GlyRS binding and prevent toxicity, although this is difficult to prove because it likely depends on gene expression levels, the degree of GlyRS and semaphorin secretion, and the relative competition between them.

It seems plausible to consider that accumulation of mutant GlyRS in the pre-synaptic terminal is deleterious to NMJ viability. It is interesting that neuronal *gars* expression does not lead to GlyRS accumulation in a similar manner and suggests that secreted GlyRS ends up in an otherwise inaccessible subcellular region. Future experiments will be needed to clarify the fate of mutant GlyRS taken up by the pre-synapse. Our current data have provided a new disease paradigm, although it remains to be established whether other tRNA synthetase neuropathies share similar pathogenic mechanisms.

6. Conclusions and future directions

During my DPhil, I have worked on two neuromuscular conditions: spinal muscular atrophy (SMA), which is caused by recessive mutations in the *survival motor neuron 1* (*SMN1*) gene, and Charcot-Marie-Tooth disease type 2D (CMT2D), which results from dominant mutations in *GARS*, the gene encoding glycyl-tRNA synthetase (GlyRS). Despite having different modes of inheritance, both diseases share a common conundrum - why do mutations in their respective housekeeping genes result in such a detrimental effect on the lower motor nerves? In addition to performing a drug screen for compounds able to improve motility of a novel *C. elegans* model for SMA, I have attempted to improve understanding of the mechanisms that underlie SMA and CMT2D. To reflect the diversity of my three experimental chapters, I will now highlight the major findings from my thesis and discuss directions for future research under three distinct headings, followed by a final summary section.

6.1 Functionally stabilising the NMJ may prove beneficial to SMA patients

The first aim of my DPhil was to characterise a novel *C. elegans smn-1* allele, *smn-1(cb131)*, with a point mutation in a highly conserved residue of exon 2 (Figure 3.2), and compare it to the already available *smn-1* null mutant. I showed that in solution *smn-1(cb131)* has a mild motility defect (Figure 3.6), which is likely caused by inefficient synaptic transmission. The time to paralysis in the presence of an acetylcholinesterase inhibitor, which is used in humans, was greater than wild type, indicating an impaired response to acetylcholine at the mutant NMJ (Figure 3.7). Using automated software, I screened a small library of chemical compounds for substances able to ameliorate the thrashing defect of *smn-1(cb131),* in the first large-scale drug screen performed on an *in*

vivo model of SMA. The most promising compound that I identified was the potassium channel blocker 4-aminopyridine, which, in accord with the basis of the defect in motility, is able to enhance neuromuscular transmission. Not only did 4-AP rescue the motility defect of *smn-1(cb131)* (Figure 3.12), but it also improved neuromuscular function and growth of the *smn-1* null mutant (Figure 3.13), further validating my screening approach.

The *C. elegans* NMJ is a cholinergic synapse like its human counterpart; however, there are a number of developmental, functional, and structural differences that could diminish the utility of using the worm for studying neuromuscular disease. The principal developmental difference is that rather than lower motor neurons migrating towards and contacting muscles, worm NMJs form when specialised muscle cell projections called arms migrate towards nerves (Dixon & Roy 2005, Sulston & Horvitz 1977, Sulston *et al.* 1983, White *et al.* 1986). Muscle membrane extensions have been observed in other experimental systems, but unlike in the nematode, these are not maintained once NMJs form (Misgeld *et al.* 2002, Ritzenthaler *et al.* 2000, Uhm *et al.* 2001). Moreover, the NMJs form along axons, rather than at their termini, and are thus known as *en passe* synapses (Broadie & Richmond 2002). At the structural level, *C. elegans* NMJs display little post-synaptic membrane specialisation or folding (Jin 2005), have small and relatively simple active zones (Jin 2005), and can form between single nerves and multiple different muscle cells (Liu *et al.* 2007, White *et al.* 1986). However, perhaps most pertinent is the functional distinction: in order to coordinate the classic sinusoidal movement, worm body wall muscles receive input from both excitatory cholinergic and inhibitory GABAergic motor neurons. Two different neurotransmitters require more than one type of post-synaptic receptor; *C. elegans* therefore possesses two distinct pentameric AChRs, and one GABA receptor at the NMJ (Richmond & Jorgensen 1999). The nicotine-sensitive AChRs (N-AChRs) are composed of five ACR-16 subunits (Touroutine *et al.* 2005), the

levamisole-sensitive receptors (L-AChRs) consist of five different subunits (Boulin *et al.* 2008), and the GABA receptor is made from two isoforms of UNC-49 (Bamber *et al.* 2005). These major differences notwithstanding, *C. elegans* has proven time and again that it is a useful model for studying basic neurobiology and neurotransmission. This is perhaps unsurprising given the major conservation of genes integral to the function of ion channels and cholinergic synapses (Rand 2007, Salkoff *et al.* 2005). For this very reason, a drug that has shown efficacy in human patients with defective neurotransmission was identified in my compound screen using *smn-1(cb131)*.

The NMJ is an early site of pathology in SMA models (Boon *et al.* 2009, Kariya *et al.* 2008, Murray *et al.* 2008). In SMA mice, reduced post-synaptic complexity, pre-synaptic neurofilament accumulation, and denervation have all been reported during the first two postnatal weeks (Kariya *et al.* 2008, Kong *et al.* 2009, Murray *et al.* 2008). As have developmental delays in the plaque-to-pretzel transition and foetal-to-adult AChR subunit switching. However, the situation is much less clear in humans and due to the subtle differences between human and mouse NMJs, the observations in SMA mice may not perfectly represent what is occurring at patient synapses. Of the most widely used model organisms, the NMJ of the mouse is most similar to that of our own. Nevertheless, there are a number of instances where deletion of a mouse neuromuscular synaptic gene leads to a more severe disease phenotype than that seen when the human homologue is missing (Feng *et al.* 1999, Missias *et al.* 1997, Witzemann *et al.* 1996). This may be due to differences in alternative splicing, in expression of compensatory genes, or in the genetic redundancy between humans and mice (Barbosa-Morais *et al.* 2012, Merkin *et al.* 2012). Alternatively, a potential lack of congruence could result from structural differences: human NMJs are on average smaller in size than the mouse synapse, are often located on larger muscle fibres, and have longer post-synaptic junctional folds with deeper gutters

(Marques *et al.* 2000). Nevertheless, new evidence from pre- and post-natal severe SMA samples indicates that NMJ pathology is indeed a feature of the human disease. Martínez-Hernández and colleagues recently reported that pre-natal NMJs in type I SMA samples display AChR clustering defects, abnormal pre-synaptic accumulation of synaptic vesicles, and structural abnormalities at the nerve terminus (Martínez-Hernández *et al.* 2012). Furthermore, there was a post-natal persistance of the foetal AChR subunit. This work indicates that the neuromuscular pathology observed in SMA mice mirrors that of severe SMA patients, and that defects in the development and structure of the NMJ are indeed a feature of the human disease.

SMN depletion also appears to affect neuromuscular transmission efficiency in SMA mice (Kong *et al.* 2009, Ling *et al.* 2010, Mentis *et al.* 2011, Park *et al.* 2010, Ruiz *et al.* 2010, Torres-Benito *et al.* 2011) and pateints (Wadman *et al.* 2012). It is therefore possible that drugs able to modulate this process or stabilise the synapse could prove beneficial to SMA patients. 4-AP is able to facilitate neurotransmission by blocking potassium channels and prolonging action potential duration (Thesleff 1980, Thomsen & Wilson 1983). It has also been reported that 4-AP may affect neurotransmission by increasing pre-synaptic calcium influx into neurons (Wu *et al.* 2009). Intracellular calcium in SMNΔ7 mice nerve terminals is significantly higher than controls leading to an increase in asynchronous synaptic vesicle release (Ruiz *et al.* 2010). It is unclear what effect 4-AP would have on these altered calcium dynamics. Nonetheless, a clinical trial has recently been initiated to test the long and short term effects of 4-AP in ambulatory SMA patients (http://clinicaltrials.gov/ct2/show/NCT01645787). Dependent on the outcome of this trial, a range of different drugs, including novel analogues based on the structure of 4-AP and distinct compounds able to modify synaptic transmission via different mechanisms (for instance acetylcholinesterase inhibitors such as physostigmine able to prolong the effects

of acetylcholine in the synaptic cleft), could also be tested. Drugs acting on neurotransmission are not going to cure SMA, especially the more severe forms of the disease where non-motor neuronal pathology is observed. Nevertheless, they could aid mobility of patients with moderate disease severity. Indeed, anecdotal evidence suggests that pyridostigmine may improve stamina of SMA type III patients (Wadman *et al.* 2012). Consequently, 4-AP and similar drugs should be tested in a less severe model, such as the $Smn^{2B/-}$ mouse (Bowerman *et al.* 2009), in order to assess efficacy before clinical trials.

6.2 Chondrolectin isoforms differentially affect survival and neurite outgrowth of Smn-depleted cells

In my second experimental chapter, I set out to investigate the role of chondrolectin (Chodl) protein isoforms in SMA. At pre-symptomatic stages in SMA mouse spinal cord, *Chodl* isoform 001 (*Chodl-001*) expression is downregulated, whereas *Chodl-002* levels remain unperturbed (Bäumer *et al.* 2009). Given the early time point of this dysregulation, I hypothesised that the alternative splicing of *Chodl* may be actively contributing to pathology or could simply reflect a compensatory mechanism. Using a mouse motor neuronal cell line, I showed that expression of isoform 001 in Smn-depleted cells exacerbates defective survival, while *Chodl-002* slightly improves cell viability, and that this was dependent on Chodl concentration and Smn availability (Figure 4.8). Chondrolectin is involved in motor axon outgrowth in zebrafish (Zhong *et al.* 2012), thus I also determined the effects of isoform expression on neurite generation and length in the cell line. Similar to zebrafish, the fine-tuning of Chodl levels appears to be important for growth and elongation but not the generation of neurites (Figure 4.10, 4.11). In cells with reduced Smn levels, Chodl isoforms also affected neurite outgrowth, with Chodl-001 and Chodl-002 partially rescuing neurite defects at the lower concentration tested. It is perhaps

counterintuitive that *Chodl-001* is downregulated when it is able to rescue a Smn-depletion phenotype; however, since its expression becomes toxic to cells with low Smn levels, it may be a compensatory response in the SMA mouse spinal cord to preserve motor neuron viability, which has a knock-on effect on neuronal processes. Hence, the alternative splicing of *Chodl* could both be a compensatory mechanism and, as a consequence, a contributor to pathology, but is unlikely to be due to mis-splicing. As a result, it is important that scientists continue to research the non-canonical roles of the SMN protein, and the effect that disturbance of these functions has on SMA pathology.

To determine whether *Chodl* dysregulation is actively contributing to SMA pathology, *in vivo* validation experiments are required. Upon *Smn* knockdown using morpholinos, zebrafish display axon outgrowth defects similar to those observed when Chodl is depleted (McWhorter *et al.* 2003). If the defects seen upon Smn depletion act through Chodl, then restoration of *Chodl* expression may ameliorate the neuronal phenotype. This can be determined by co-injection of *Smn* morpholinos and *Chodl* RNA into zebrafish embryos. If this yields a positive result with the single zebrafish Chodl isoform, then the three individual mouse proteins could also be tested to see whether they corroborate the findings in the mouse motor neuronal cell line. Since Chodl possesses a transmembrane domain and is involved in axonal outgrowth, it is likely to localise to the surface of neuronal cells. Determining the expression patterns of the different *Chodl* isoforms in immortalised cell lines and primary neuronal cultures, and identifying the extracellular binding partners will be important to elucidating protein function. As will ascertaining the differences that the short cytoplasmic tails of the three isoforms mediate.

6.3 A potential mechanism for the neuronal-specificity of CMT2D

In addition to my work on SMA, in the final year of my DPhil I began researching into CMT2D in collaboration with Dr. Stuart J. Grice. Together, we have been working to describe pathways in the disease that may account for the neuronal specificity observed in CMT2D patients. Stuart generated a new *Drosophila* model that expresses wild type or dominant mutant forms of the fly GlyRS gene, *gars*. Using the GAL4/UAS system to drive expression of exogenous *gars* in a tissue-specific fashion, we were able to show that mutant $GlyRS^{P234KY}$, but not wild type, causes dominant toxic effects on fly viability and the larval nervous system, with no observable changes in muscle structure (Figure 5.2, 5.3). Intriguingly, muscle-specific expression of mutant *gars* caused defects similar in severity to the ubiquitous driver, while there was only a small contribution from neurons and glia, suggesting a possible non-cell autonomous disease mechanism. Looking in detail at the larval NMJ, we found that mutant *gars* expression caused an excessive branching at the synapse, in addition to reduced bouton number, and build up of synaptic debris and ghost boutons (Figure 5.3). As the larvae age, when *gars* is expressed in muscle there is a build-up of mutant $GlyRS^{P234KY}$ in boutons at the pre-synaptic side of the NMJ, but not more proximally up the axon, indicating that mutant protein originating in the muscle is able to cross the synaptic cleft (Figure 5.4). This protein accumulation corresponds to degenerate regions of the NMJ. We then determined that both wild type and mutant human GlyRS can be secreted from C2C12 muscle cells and that secretion is contingent upon the WHEP domain of the protein (Figure 5.5). Consistent with this, removal of the WHEP domain from mutant *Drosophila* GlyRS dramatically ameliorates the viability defect caused by $gars^{P234KY}$ expression, and prevents the pre-synaptic localisation of the protein. We also looked at NMJs from mutant *Gars* mice, and showed that they display analogous phenotypes of delayed maturation with subsequent denervation (Figure 5.8, 5.9, 5.10). Studying the aberrant branching and maturation defects that precede die-back in

Drosophila, we found an ectopic branching phenotype similar to that caused by reduced levels of the axonal guidance protein Plexin B (Figure 5.6). In combination with evidence of disturbed semaphorin-plexin gene expression in both flies and mice (Figure 5.7), this led us to hypothesise that defective axonal pathfinding may be playing a role in disease. We thus crossed heterozygous *PlexB* flies with the *gars* mutants to see whether this would modify the disease phenotype. Interestingly, reducing Plexin B levels resulted in amelioration of the phenotype and reduced pre-synaptic accumulation of mutant protein (Figure 5.7). Taken together, our data hint at a possible disease mechanism - secreted mutant GlyRS is able to exert its toxic gain-of-function by binding to Plexin B, thereby disturbing axon guidance cues leading to aberrant neuronal branching and loss of NMJ viability.

Dissecting disease mechanisms in humans is not feasible. We must therefore make use of model organisms to better understand basic biological processes and decipher how and why these are disrupted in disease. Using multiple models to study a disorder is a powerful approach because commonalities between organisms are more likely to be pertinent to the human condition. That being said, it is challenging to draw meaningful parallels between results generated from experiments on organisms separated by millions of years of evolution, and then relate them to humans. My chapter on CMT2D studying the NMJs of *Drosophila* larvae and mice highlights this point.

The main difference between the *Drosophila* larval neuromuscular synapse and those of humans and mice is that the fly NMJ is glutaminergic, whereas the principal neurotransmitter in mammals is acetylcholine. As a consequence, different post-synaptic receptors are required. Two glutamate receptors with distinct subunit complements including either GluRIIA or GluRIIB are found at the fly NMJ (Featherstone *et al.* 2005, Marrus *et al.* 2004, Qin *et al.* 2005), whereas mice and humans only transiently express

more than one type of AChR during early postnatal development (Sanes & Lichtman 1999). It is therefore not possible to equate the delay in adult subunit and persistent foetal subunit expression seen in $Gars^{C201R/+}$ mice (Figure 5.8F, G) with a *gars* mutant fly phenotype. Similarly contrasting with what is seen in mammals, *Drosophila* muscle fibres can be innervated by more than one axon and there is no process of synapse elimination during development (Hoang & Chiba 2001, Wu *et al.* 2010). Nevertheless, in the light of the similarities in NMJ over-elaboration (Figure 5.3) and ectopic branching phenotypes (Figure 5.6) of the *gars* mutant flies with defective synapse elimination in the *Gars* mice (Figure 5.8, 5.10), the parallels between the *gars* and *plexB* mutant flies (Figure 5.6), and the comparable gene expression changes between mutant flies and mice (Figure 5.7), it is an enticing prospect that there is a common disease mechanism involving semaphorin-plexin signalling.

The structure of the *Drosophila* larval NMJ is fundamentally similar to the mammalian synapse; pre-synaptic active zones are in close juxtaposition to post-synaptic receptor clusters (Prokop & Meinertzhagen 2006), the post-synaptic muscle membrane displays multiple invaginations (Atwood *et al.* 1993, Jia *et al.* 1993), and glial cells encapsulate and support the synapse (Freeman & Doherty 2006). However, differences in the initial set up of the neuromuscular system are evident. In mammals, primitive aneural AChRs cluster in the central region of muscles prior to the arrival of lower motor nerves (Lin *et al.* 2001, Yang *et al.* 2001). This pre-patterning, which is believed to serve as guide for incoming neurons (Kummer *et al.* 2006), is absent in *Drosophila* (Prokop *et al.* 1996, Qin *et al.* 2005, Schmid *et al.* 2006). Instead, fly motor nerves seek out and target muscles without the aid of the post-synapse, although upon connection reciprocal interactions are required for subsequent differentiation as in mammals (Wu *et al.* 2010). The pattern of the *Drosophila* neuromuscular system appears to be more stereotyped than in mice and

humans, with innervation, arborisation, and synaptic strength being largely equivalent from fly to fly. Moreover, the growth of the fly synapse is different from mammalian NMJs in that discrete, button-like axonal termini known as boutons are added to the periphery like beads on a string (Johansen *et al.* 1989), whereas mammalian NMJs develop from a plaque-like structure to a more complex pretzel shape, while increasing in size in a continuous manner. In spite of this, the bouton loss in mutant *gars* larvae (Figure 5.3) appears to be analogous to the denervation seen in the two mouse mutants (Figure 5.9, 5.10).

We must be cautious when using a dual-organism approach to model human neuromuscular disorders that we do not overstate results and make erroneous comparisons. Nevertheless, given the overarching similarities in NMJ structure and function, and considerable genetic conservation between flies, mice, and humans, common mechanisms can be observed. The potential mechanism outlined in chapter 5 is far from being confirmed. In *Drosophila*, we need to show that mutant GlyRS is able to bind to Plexin B, and that, because $GlyRS^{WT}$ also appears to be secreted, it does this with a higher affinity than the wild type protein. Our work and that of others showing that wild type GlyRS is secreted by a number of different cell types opens up a whole new area of research to determine possible non-canonical functions of the protein. In the mouse, we need to assess whether there is a similar pre-synaptic build-up of mutant but not wild type protein, and then determine what GlyRS is binding to. It is also vital to understand what is happening to the mutant protein once it binds to the surface of the motor neurons. For instance, are Plexin B pathways being agonised or antagonised, or is GlyRS being internalised and interacting with non-semaphorin-plexin pathways. Furthermore, to firm up the hypothesis of a non-cell autonomous mechanism, we would have to express mutant *Gars* exclusively

in mouse muscle using the Cre-loxP recombination system analogous to the GAL4/UAS system in flies.

6.4 How do mutations in widely expressed genes lead to motor neuron diseases?

SMA, CMT2D, some forms of amyotrophic lateral sclerosis, spinal and bulbar muscular atrophy (SBMA), and SMA with respiratory distress, are but a few diseases caused by mutations in widely expressed genes that result in selective neuronal pathology. Since the mode of inheritance of such disorders can be dominant (CMT2D), recessive (SMA), or X-linked (SBMA), and because the disease genes encode proteins implicated in a wide range of cellular processes, it is unlikely that they share a single causative pathway. Nevertheless, common themes, such as disturbed RNA processing (Bäumer *et al.* 2010), may serve to explain the general susceptibility of the motor nerves. In this thesis, I aimed to address the cause of this neuronal vulnerability in SMA and CMT2D using a variety of model systems. Through experiments on chondrolectin presented in chapter 4 and a large body of data from many other laboratories (see section 1.1.4.2), it appears that in addition to its general housekeeping role in snRNP biogenesis, SMN may have evolved a secondary motor neuron-specific function. Similarly, although CMT2D is caused by a dominant toxic gain-of-function, the observation in chapter 5 that wild type GlyRS can be secreted from muscle cells and possibly at the fly NMJ, suggests that it may also have acquired a novel non-canonical function in the neuromuscular system independent of its tRNA charging capacity. Together, data generated from this thesis conform to the idea that proteins encoded by widely expressed genes with functions in critical processes such as RNA biology are capable of acquiring nervous system-specific functions in evolution, thereby challenging the idea that single genes encode one protein with one function, and providing a possible explanation for neuronal susceptibility seen in disease.

An alternative, but not mutually exclusive, cause of the vulnerability of the motor nerves may simply be that they are victims of their own unusual and specialised architecture. Lower motor nerves are highly polarised structures that can reach up to over a metre in length, and are thought to connect to up to 1,000 individual muscle fibres. Furthermore, due to their extensive dendritic arbours, lower motor nerves are able to form an even greater number of synaptic connections with distinct molecular identities. The upper motor neurons that connect the lower motor neurons to the brain, share these features of polarity, a large number of synaptic contacts, and long, thin axons. Given their structure and function, these motor nerves need to compartmentalise different mRNAs and proteins to distinct regions of the cell, and are required to respond rapidly to internal and external stimuli. Consequently, asymmetric targeting of mRNAs from the nucleus to specific cellular compartments of motor nerves for local translation is a highly regulated process, and one that is perhaps particularly prone to fault. As highlighted in chapter 1, there is indeed evidence that axonal RNA transport is disturbed in SMA; depletion of Smn in mouse primary neuron cultures leads to reduced levels of *β-actin* and *cpg15* mRNA at the growth cone, and diminished amounts of poly(A) mRNA in axons (Akten *et al.* 2011, Fallini *et al.* 2011, Rossoll *et al.* 2003). In the case of *β-actin*, this leads to reduced local translation and less protein at the growth cone correlating with reduced growth cone size and shorter axons (Rathod *et al.* 2012, Rossoll *et al.* 2003). This suggests that disturbing the balance and localisation of mRNA or proteins within these cells may play an important part in the disease process. Consistent with this, mutation of genes encoding the kinesin and dynactin motor proteins involved in the active transport of RNA granules along microtubules has also been associated with motor neuron disorders (James & Talbot 2006, Puls *et al.* 2003).

In conclusion, throughout this thesis, I have used a variety of model systems to explore therapeutic interventions and disease mechanisms in two forms of spinal muscular atrophy. There are no available treatments for either disease, and we do not understand why both result in the specific degeneration of motor neurons despite being caused by mutations in widely and constitutively expressed genes with housekeeping functions. Nevertheless, in three years, I have made a small but solid contribution to the collective knowledge of both disorders, and through my thesis work, have improved the understanding of pathological mechanisms underlying the selective neuronal susceptibility seen in both disorders. In the future, it will remain crucial to use a range of cellular and animal models, each with their own experimental advantages, in order to one day make these spinal muscular atrophies and other neuromuscular disorders curable.

References

Abbott A. 2002. Neurologists strike gold in drug screen effort. *Nature* 417: 109

Achilli F, Bros-Facer V, Williams HP, Banks GT, AlQatari M, *et al.* 2009. An ENU-induced mutation in mouse glycyl-tRNA synthetase (GARS) causes peripheral sensory and motor phenotypes creating a model of Charcot-Marie-Tooth type 2D peripheral neuropathy. *Dis Model Mech* 2: 359-73

Ackermann B, Kröber S, Torres-Benito L, Borgmann A, Peters M, *et al.* 2013. Plastin 3 ameliorates spinal muscular atrophy via delayed axon pruning and improves neuromuscular junction functionality. *Hum Mol Genet*

Acsadi G, Lee I, Li X, Khaidakov M, Pecinova A, *et al.* 2009. Mitochondrial dysfunction in a neural cell model of spinal muscular atrophy. *J Neurosci Res* 87: 2748-56

Adkins CE, Pillai GV, Kerby J, Bonnert TP, Haldon C, *et al.* 2001. *α4β3δ* $GABA_A$ receptors characterized by fluorescence resonance energy transfer-derived measurements of membrane potential. *J Biol Chem* 276: 38934-9

Ahmad S, Wang Y, Shaik GM, Burghes AH, Gangwani L. 2012. The zinc finger protein ZPR1 is a potential modifier of spinal muscular atrophy. *Hum Mol Genet* 21: 2745-58

Akten B, Kye MJ, Hao le T, Wertz MH, Singh S, *et al.* 2011. Interaction of survival of motor neuron (SMN) and HuD proteins with mRNA cpg15 rescues motor neuron axonal deficits. *Proc Natl Acad Sci U S A* 108: 10337-42

Alfonso A, Grundahl K, Duerr JS, Han HP, Rand JB. 1993. The *Caenorhabditis elegans unc-17* gene: a putative vesicular acetylcholine transporter. *Science* 261: 617-9

Altun-Gultekin Z, Andachi Y, Tsalik EL, Pilgrim D, Kohara Y, Hobert O. 2001. A regulatory cascade of three homeobox genes, *ceh-10*, *ttx-3* and *ceh-23*, controls cell fate specification of a defined interneuron class in *C. elegans*. *Development* 128: 1951-69

Anagnostou E, Miller SP, Guiot MC, Karpati G, Simard L, *et al.* 2005. Type I spinal muscular atrophy can mimic sensory-motor axonal neuropathy. *J Child Neurol* 20: 147-50

Andreassi C, Angelozzi C, Tiziano FD, Vitali T, De Vincenzi E, *et al.* 2004. Phenylbutyrate increases *SMN* expression *in vitro*: relevance for treatment of spinal muscular atrophy. *Eur J Hum Genet* 12: 59-65

Andreassi C, Jarecki J, Zhou J, Coovert DD, Monani UR, *et al.* 2001. Aclarubicin treatment restores SMN levels to cells derived from type I spinal muscular atrophy patients. *Hum Mol Genet* 10: 2841-9

Antonellis A, Ellsworth RE, Sambuughin N, Puls I, Abel A, *et al.* 2003. Glycyl tRNA synthetase mutations in Charcot-Marie-Tooth disease type 2D and distal spinal muscular atrophy type V. *Am J Hum Genet* 72: 1293-9

Antonellis A, Green ED. 2008. The role of aminoacyl-tRNA synthetases in genetic diseases. *Annu Rev Genomics Hum Genet* 9: 87-107

Antonellis A, Lee-Lin SQ, Wasterlain A, Leo P, Quezado M, *et al.* 2006. Functional analyses of glycyl-tRNA synthetase mutations suggest a key role for tRNA-charging enzymes in peripheral axons. *J Neurosci* 26: 10397-406

Araki S, Hayashi M, Tamagawa K, Saito M, Kato S, *et al.* 2003. Neuropathological analysis in spinal muscular atrophy type II. *Acta Neuropathol* 106: 441-8

Ardizzi JP, Epstein HF. 1987. Immunochemical localization of myosin heavy chain isoforms and paramyosin in developmentally and structurally diverse muscle cell types of the nematode *Caenorhabditis elegans*. *J Cell Biol* 105: 2763-70

Argov Z. 2009. Management of myasthenic conditions: nonimmune issues. *Curr Opin Neurol* 22: 493-7

Atwood HL, Govind CK, Wu CF. 1993. Differential ultrastructure of synaptic terminals on ventral longitudinal abdominal muscles in *Drosophila* larvae. *J Neurobiol* 24: 1008-24

Avery L, Horvitz HR. 1989. Pharyngeal pumping continues after laser killing of the pharyngeal nervous system of *C. elegans*. *Neuron* 3: 473-85

Ayoob JC, Terman JR, Kolodkin AL. 2006. *Drosophila* Plexin B is a Sema-2a receptor required for axon guidance. *Development* 133: 2125-35

Bacic A, Kahane I, Zuckerman BM. 1990. *Panagrellus redivivus* and *Caenorhabditis elegans*: evidence for the absence of sialic acids. *Exp Parasitol* 71: 483-8

Bagnard D, Lohrum M, Uziel D, Püschel AW, Bolz J. 1998. Semaphorins act as attractive and repulsive guidance signals during the development of cortical projections. *Development* 125: 5043-53

Bagnard D, Thomasset N, Lohrum M, Püschel AW, Bolz J. 2000. Spatial distributions of guidance molecules regulate chemorepulsion and chemoattraction of growth cones. *J Neurosci* 20: 1030-5

Balabanian S, Gendron NH, MacKenzie AE. 2007. Histologic and transcriptional assessment of a mild SMA model. *Neurol Res* 29: 413-24

Bamber BA, Richmond JE, Otto JF, Jorgensen EM. 2005. The composition of the GABA receptor at the *Caenorhabditis elegans* neuromuscular junction. *Br J Pharmacol* 144: 502-9

Barber SC, Higginbottom A, Mead RJ, Barber S, Shaw PJ. 2009. An *in vitro* screening cascade to identify neuroprotective antioxidants in ALS. *Free Radic Biol Med* 46: 1127-38

Barbosa-Morais NL, Irimia M, Pan Q, Xiong HY, Gueroussov S, *et al.* 2012. The evolutionary landscape of alternative splicing in vertebrate species. *Science* 338: 1587-93

Bassell GJ, Zhang H, Byrd AL, Femino AM, Singer RH, *et al.* 1998. Sorting of *β-actin* mRNA and protein to neurites and growth cones in culture. *J Neurosci* 18: 251-65

Bates KE, Whitington PM. 2007. Semaphorin 2a secreted by oenocytes signals through plexin B and plexin A to guide sensory axons in the *Drosophila* embryo. *Dev Biol* 302: 522-35

Bäumer D, Lee S, Nicholson G, Davies JL, Parkinson NJ, *et al.* 2009. Alternative splicing events are a late feature of pathology in a mouse model of spinal muscular atrophy. *PLoS Genet* 5: e1000773

Bäumer D, Ansorge O, Almeida M, Talbot K. 2010. The role of RNA processing in the pathogenesis of motor neuron degeneration. *Expert Rev Mol Med* 12: e21

Bebee TW, Dominguez CE, Samadzadeh-Tarighat S, Akehurst KL, Chandler DS. 2012. Hypoxia is a modifier of *SMN2* splicing and disease severity in a severe SMA mouse model. *Hum Mol Genet* 21: 4301-13

Béchade C, Rostaing P, Cisterni C, Kalisch R, La Bella V, *et al.* 1999. Subcellular distribution of survival motor neuron (SMN) protein: possible involvement in nucleocytoplasmic and dendritic transport. *Eur J Neurosci* 11: 293-304

Becker EB, Oliver PL, Glitsch MD, Banks GT, Achilli F, *et al.* 2009. A point mutation in TRPC3 causes abnormal Purkinje cell development and cerebellar ataxia in moonwalker mice. *Proc Natl Acad Sci U S A* 106: 6706-11

Bergin A, Kim G, Price DL, Sisodia SS, Lee MK, Rabin BA. 1997. Identification and characterization of a mouse homologue of the spinal muscular strophy-determining gene, *survival motor neuron*. *Gene* 204: 47-53

Bertrandy S, Burlet P, Clermont O, Huber C, Fondrat C, *et al.* 1999. The RNA-binding properties of SMN: deletion analysis of the zebrafish orthologue defines domains conserved in evolution. *Hum Mol Genet* 8: 775-82

Bevan AK, Hutchinson KR, Foust KD, Braun L, McGovern VL, *et al.* 2010. Early heart failure in the SMNΔ7 model of spinal muscular atrophy and correction by postnatal scAAV9-SMN delivery. *Hum Mol Genet* 19: 3895-905

Boon KL, Xiao S, McWhorter ML, Donn T, Wolf-Saxon E, *et al.* 2009. Zebrafish *survival motor neuron* mutants exhibit presynaptic neuromuscular junction defects. *Hum Mol Genet* 18: 3615-25

Boulin T, Gielen M, Richmond JE, Williams DC, Paoletti P, Bessereau JL. 2008. Eight genes are required for functional reconstitution of the *Caenorhabditis elegans* levamisole-sensitive acetylcholine receptor. *Proc Natl Acad Sci U S A* 105: 18590-5

Boulisfane N, Choleza M, Rage F, Neel H, Soret J, Bordonne R. 2011. Impaired minor tri-snRNP assembly generates differential splicing defects of U12-type introns in lymphoblasts derived from a type I SMA patient. *Hum Mol Genet* 20: 641-8

Bowerman M, Anderson CL, Beauvais A, Boyl PP, Witke W, Kothary R. 2009. SMN, profilin IIa and plastin 3: a link between the deregulation of actin dynamics and SMA pathogenesis. *Mol Cell Neurosci* 42: 66-74

Braungart E, Gerlach M, Riederer P, Baumeister R, Hoener MC. 2004. *Caenorhabditis elegans* MPP^+ model of Parkinson's disease for high-throughput drug screenings. *Neurodegener Dis* 1: 175-83

Brenner S. 1974. The genetics of *Caenorhabditis elegans*. *Genetics* 77: 71-94

Brichta L, Hofmann Y, Hahnen E, Siebzehnrubl FA, Raschke H, *et al.* 2003. Valproic acid increases the SMN2 protein level: a well-known drug as a potential therapy for spinal muscular atrophy. *Hum Mol Genet* 12: 2481-9

Brichta L, Holker I, Haug K, Klockgether T, Wirth B. 2006. *In vivo* activation of *SMN* in spinal muscular atrophy carriers and patients treated with valproate. *Ann Neurol* 59: 970-5

Briese M, Esmaeili B, Fraboulet S, Burt EC, Christodoulou S, *et al.* 2009. Deletion of *smn-1*, the *Caenorhabditis elegans* ortholog of the spinal muscular atrophy gene, results in locomotor dysfunction and reduced lifespan. *Hum Mol Genet* 18: 97-104

Briese M, Esmaeili B, Sattelle DB. 2005. Is spinal muscular atrophy the result of defects in motor neuron processes? *Bioessays* 27: 946-57

Broadie KS, Richmond JE. 2002. Establishing and sculpting the synapse in *Drosophila* and *C. elegans*. *Curr Opin Neurobiol* 12: 491-8

Brown N, Kerby J, Bonnert TP, Whiting PJ, Wafford KA. 2002. Pharmacological characterization of a novel cell line expressing human *α4β3δ* $GABA_A$ receptors. *Br J Pharmacol* 136: 965-74

Bruckner JJ, Gratz SJ, Slind JK, Geske RR, Cummings AM, *et al.* 2012. Fife, a *Drosophila* Piccolo-RIM homolog, promotes active zone organization and neurotransmitter release. *J Neurosci* 32: 17048-58

Buckingham SD, Sattelle DB. 2008. Strategies for automated analysis of *C. elegans* locomotion. *Invert Neurosci* 8: 121-31

Buckingham SD, Sattelle DB. 2009. Fast, automated measurement of nematode swimming (thrashing) without morphometry. *BMC Neurosci* 10: 84

Budnik V, Salinas PC. 2011. Wnt signaling during synaptic development and plasticity. *Curr Opin Neurobiol* 21: 151-9

Bühler D, Raker V, Lührmann R, Fischer U. 1999. Essential role for the tudor domain of SMN in spliceosomal U snRNP assembly: implications for spinal muscular atrophy. *Hum Mol Genet* 8: 2351-7

Burghes AH. 1997. When is a deletion not a deletion? When it is converted. *Am J Hum Genet* 61: 9-15

Burghes AH, Beattie CE. 2009. Spinal muscular atrophy: why do low levels of survival motor neuron protein make motor neurons sick? *Nat Rev Neurosci* 10: 597-609

Burt EC, Towers PR, Sattelle DB. 2006. *Caenorhabditis elegans* in the study of SMN-interacting proteins: a role for SMI-1, an orthologue of human Gemin2 and the identification of novel components of the SMN complex. *Invert Neurosci* 6: 145-59

Butchbach ME, Singh J, Thorsteinsdóttir M, Saieva L, Slominski E, *et al.* 2010. Effects of 2,4-diaminoquinazoline derivatives on *SMN* expression and phenotype in a mouse model for spinal muscular atrophy. *Hum Mol Genet* 19: 454-67

Cader MZ, Ren J, James PA, Bird LE, Talbot K, Stammers DK. 2007. Crystal structure of human wildtype and S581L-mutant glycyl-tRNA synthetase, an enzyme underlying distal spinal muscular atrophy. *FEBS Lett* 581: 2959-64

Campion Y, Neel H, Gostan T, Soret J, Bordonne R. 2010. Specific splicing defects in *S. pombe* carrying a degron allele of the *survival of motor neuron* gene. *EMBO J* 29: 1817-29

Caraballo-Miralles V, Cardona-Rossinyol A, Garcera A, Villalonga P, Soler RM, *et al.* 2012. SMN deficiency attenuates migration of U87MG astroglioma cells through the activation of RhoA. *Mol Cell Neurosci* 49: 282-9

Carre-Pierrat M, Mariol MC, Chambonnier L, Laugraud A, Heskia F, *et al.* 2006. Blocking of striated muscle degeneration by serotonin in *C. elegans*. *J Muscle Res Cell Motil* 27: 253-8

Carrel TL, McWhorter ML, Workman E, Zhang H, Wolstencroft EC, *et al.* 2006. Survival motor neuron function in motor axons is independent of functions required for small nuclear ribonucleoprotein biogenesis. *J Neurosci* 26: 11014-22

Carrillo RA, Olsen DP, Yoon KS, Keshishian H. 2010. Presynaptic activity and CaMKII modulate retrograde semaphorin signaling and synaptic refinement. *Neuron* 68: 32-44

Chan YB, Miguel-Aliaga I, Franks C, Thomas N, Trülzsch B, *et al.* 2003. Neuromuscular defects in a *Drosophila survival motor neuron* gene mutant. *Hum Mol Genet* 12: 1367-76

Chang HC, Dimlich DN, Yokokura T, Mukherjee A, Kankel MW, *et al.* 2008. Modeling spinal muscular atrophy in *Drosophila*. *PLoS One* 3: e3209

Chang KJ, Wang CC. 2004. Translation initiation from a naturally occurring non-AUG codon in *Saccharomyces cerevisiae*. *J Biol Chem* 279: 13778-85

Chang T, Zheng W, Tsark W, Bates S, Huang H, *et al.* 2011. Brief report: phenotypic rescue of induced pluripotent stem cell-derived motoneurons of a spinal muscular atrophy patient. *Stem Cells* 29: 2090-3

Chihara T, Luginbuhl D, Luo L. 2007. Cytoplasmic and mitochondrial protein translation in axonal and dendritic terminal arborization. *Nat Neurosci* 10: 828-37

Chinpaisal C, Lee CH, Wei LN. 1997. Studies of the mouse Rab geranylgeranyl transferase β subunit: gene structure, expression and regulation. *Gene* 184: 237-43

Cifuentes-Diaz C, Frugier T, Tiziano FD, Lacene E, Roblot N, *et al.* 2001. Deletion of murine *SMN* exon 7 directed to skeletal muscle leads to severe muscular dystrophy. *J Cell Biol* 152: 1107-14

Cifuentes-Diaz C, Nicole S, Velasco ME, Borra-Cebrian C, Panozzo C, *et al.* 2002. Neurofilament accumulation at the motor endplate and lack of axonal sprouting in a spinal muscular atrophy mouse model. *Hum Mol Genet* 11: 1439-47

Claessens A, Weyn C, Merregaert J. 2008. The cytoplasmic domain of chondrolectin interacts with the β-subunit of Rab geranylgeranyl transferase. *Cell Mol Biol Lett* 13: 250-9

Clelland AK, Bales AB, Sleeman JE. 2012. Changes in intranuclear mobility of mature snRNPs provide a mechanism for splicing defects in spinal muscular atrophy. *J Cell Sci* 125: 2626-37

Collins CA, DiAntonio A. 2007. Synaptic development: insights from *Drosophila*. *Curr Opin Neurobiol* 17: 35-42

Comley LH, Fuller HR, Wishart TM, Mutsaers CA, Thomson D, *et al.* 2011. ApoE isoform-specific regulation of regeneration in the peripheral nervous system. *Hum Mol Genet* 20: 2406-21

Coovert DD, Le TT, McAndrew PE, Strasswimmer J, Crawford TO, *et al.* 1997. The survival motor neuron protein in spinal muscular atrophy. *Hum Mol Genet* 6: 1205-14

Culetto E, Baylis HA, Richmond JE, Jones AK, Fleming JT, *et al.* 2004. The *Caenorhabditis elegans unc-63* gene encodes a levamisole-sensitive nicotinic acetylcholine receptor α subunit. *J Biol Chem* 279: 42476-83

Culetto E, Sattelle DB. 2000. A role for *Caenorhabditis elegans* in understanding the function and interactions of human disease genes. *Hum Mol Genet* 9: 869-77

Cuppen E, Gort E, Hazendonk E, Mudde J, van de Belt J, *et al.* 2007. Efficient target-selected mutagenesis in *Caenorhabditis elegans*: toward a knockout for every gene. *Genome Res* 17: 649-58

Del Bo R, Locatelli F, Corti S, Scarlato M, Ghezzi S, *et al.* 2006. Coexistence of CMT-2D and distal SMA-V phenotypes in an Italian family with a *GARS* gene mutation. *Neurology* 66: 752-4

Denizot F, Lang R. 1986. Rapid colorimetric assay for cell growth and survival. Modifications to the tetrazolium dye procedure giving improved sensitivity and reliability. *J Immunol Methods* 89: 271-7

Desai UA, Pallos J, Ma AA, Stockwell BR, Thompson LM, *et al.* 2006. Biologically active molecules that reduce polyglutamine aggregation and toxicity. *Hum Mol Genet* 15: 2114-24

DiDonato CJ, Chen XN, Noya D, Korenberg JR, Nadeau JH, Simard LR. 1997. Cloning, characterization, and copy number of the murine *survival motor neuron* gene: homolog of the spinal muscular atrophy-determining gene. *Genome Res* 7: 339-52

Dietzl G, Chen D, Schnorrer F, Su KC, Barinova Y, *et al.* 2007. A genome-wide transgenic RNAi library for conditional gene inactivation in *Drosophila*. *Nature* 448: 151-6

Dimitriadi M, Hart AC. 2010. Neurodegenerative disorders: insights from the nematode *Caenorhabditis elegans*. *Neurobiol Dis* 40: 4-11

Dimitriadi M, Sleigh JN, Walker A, Chang HC, Sen A, *et al.* 2010. Conserved genes act as modifiers of invertebrate SMN loss of function defects. *PLoS Genet* 6: e1001172

Dixon SJ, Roy PJ. 2005. Muscle arm development in *Caenorhabditis elegans*. *Development* 132: 3079-92

Dominguez E, Marais T, Chatauret N, Benkhelifa-Ziyyat S, Duque S, *et al.* 2011. Intravenous scAAV9 delivery of a codon-optimized *SMN1* sequence rescues SMA mice. *Hum Mol Genet* 20: 681-93

Dubourg O, Azzedine H, Yaou RB, Pouget J, Barois A, *et al.* 2006. The G526R glycyl-tRNA synthetase gene mutation in distal hereditary motor neuropathy type V. *Neurology* 66: 1721-6

Duffy JB. 2002. GAL4 system in *Drosophila*: a fly geneticist's Swiss army knife. *Genesis* 34: 1-15

Emery AE. 1991. Population frequencies of inherited neuromuscular diseases - a world survey. *Neuromuscul Disord* 1: 19-29

Enjin A, Rabe N, Nakanishi ST, Vallstedt A, Gezelius H, *et al.* 2010. Identification of novel spinal cholinergic genetic subtypes disclose *Chodl* and *Pitx2* as markers for fast motor neurons and partition cells. *J Comp Neurol* 518: 2284-304

Eskuri JM, Stanley CM, Moore SA, Mathews KD. 2012. Infantile onset CMT2D/dSMA V in monozygotic twins due to a mutation in the anticodon-binding domain of *GARS*. *J Peripher Nerv Syst* 17: 132-4

Fallini C, Bassell GJ, Rossoll W. 2010. High-efficiency transfection of cultured primary motor neurons to study protein localization, trafficking, and function. *Mol Neurodegener* 5: 17

Fallini C, Bassell GJ, Rossoll W. 2012. Spinal muscular atrophy: the role of SMN in axonal mRNA regulation. *Brain Res* 1462: 81-92

Fallini C, Zhang H, Su Y, Silani V, Singer RH, *et al.* 2011. The survival of motor neuron (SMN) protein interacts with the mRNA-binding protein HuD and regulates localization of poly(A) mRNA in primary motor neuron axons. *J Neurosci* 31: 3914-25

Fan L, Simard LR. 2002. Survival motor neuron (SMN) protein: role in neurite outgrowth and neuromuscular maturation during neuronal differentiation and development. *Hum Mol Genet* 11: 1605-14

Farnsworth CC, Seabra MC, Ericsson LH, Gelb MH, Glomset JA. 1994. Rab geranylgeranyl transferase catalyzes the geranylgeranylation of adjacent cysteines in the small GTPases Rab1A, Rab3A, and Rab5A. *Proc Natl Acad Sci U S A* 91: 11963-7

Featherstone DE, Rushton E, Rohrbough J, Liebl F, Karr J, *et al.* 2005. An essential *Drosophila* glutamate receptor subunit that functions in both central neuropil and neuromuscular junction. *J Neurosci* 25: 3199-208

Feldkötter M, Schwarzer V, Wirth R, Wienker TF, Wirth B. 2002. Quantitative analyses of *SMN1* and *SMN2* based on real-time lightCycler PCR: fast and highly reliable carrier testing and prediction of severity of spinal muscular atrophy. *Am J Hum Genet* 70: 358-68

Feng G, Krejci E, Molgo J, Cunningham JM, Massoulié J, Sanes JR. 1999. Genetic analysis of collagen Q: roles in acetylcholinesterase and butyrylcholinesterase assembly and in synaptic structure and function. *J Cell Biol* 144: 1349-60

Fischer U, Liu Q, Dreyfuss G. 1997. The SMN-SIP1 complex has an essential role in spliceosomal snRNP biogenesis. *Cell* 90: 1023-9

Foust KD, Wang X, McGovern VL, Braun L, Bevan AK, *et al.* 2010. Rescue of the spinal muscular atrophy phenotype in a mouse model by early postnatal delivery of SMN. *Nat Biotechnol* 28: 271-4

Fox-Walsh KL, Hertel KJ. 2009. Splice-site pairing is an intrinsically high fidelity process. *Proc Natl Acad Sci U S A* 106: 1766-71

Franciosi S, Ryu JK, Choi HB, Radov L, Kim SU, McLarnon JG. 2006. Broad-spectrum effects of 4-aminopyridine to modulate amyloid β_{1-42}-induced cell signaling and functional responses in human microglia. *J Neurosci* 26: 11652-64

Francis JW, Sandrock AW, Bhide PG, Vonsattel JP, Brown RH, Jr. 1998. Heterogeneity of subcellular localization and electrophoretic mobility of survival motor neuron (SMN) protein in mammalian neural cells and tissues. *Proc Natl Acad Sci U S A* 95: 6492-7

Freeman MR, Doherty J. 2006. Glial cell biology in *Drosophila* and vertebrates. *Trends Neurosci* 29: 82-90

Frugier T, Tiziano FD, Cifuentes-Diaz C, Miniou P, Roblot N, *et al.* 2000. Nuclear targeting defect of SMN lacking the C-terminus in a mouse model of spinal muscular atrophy. *Hum Mol Genet* 9: 849-58

Fuentes-Medel Y, Logan MA, Ashley J, Ataman B, Budnik V, Freeman MR. 2009. Glia and muscle sculpt neuromuscular arbors by engulfing destabilized synaptic boutons and shed presynaptic debris. *PLoS Biol* 7: e1000184

Fujino T, Wu Z, Lin WC, Phillips MA, Nedivi E. 2008. cpg15 and cpg15-2 constitute a family of activity-regulated ligands expressed differentially in the nervous system to promote neurite growth and neuronal survival. *J Comp Neurol* 507: 1831-45

Fuller HR, Barišić M, Šešo-Šimić D, Špeljko T, Morris GE, Šimić G. 2010. Treatment strategies for spinal muscular atrophy. *Transl Neurosci* 1: 308-21

Gabanella F, Butchbach ME, Saieva L, Carissimi C, Burghes AH, Pellizzoni L. 2007. Ribonucleoprotein assembly defects correlate with spinal muscular atrophy severity and preferentially affect a subset of spliceosomal snRNPs. *PLoS One* 2: e921

Gabanella F, Carissimi C, Usiello A, Pellizzoni L. 2005. The activity of the spinal muscular atrophy protein is regulated during development and cellular differentiation. *Hum Mol Genet* 14: 3629-42

Gaud A, Simon JM, Witzel T, Carre-Pierrat M, Wermuth CG, Ségalat L. 2004. Prednisone reduces muscle degeneration in dystrophin-deficient *Caenorhabditis elegans*. *Neuromuscul Disord* 14: 365-70

Giacomotto J, Pertl C, Borrel C, Walter MC, Bulst S, *et al.* 2009. Evaluation of the therapeutic potential of carbonic anhydrase inhibitors in two animal models of dystrophin deficient muscular dystrophy. *Hum Mol Genet* 18: 4089-101

Giagtzoglou N, Ly CV, Bellen HJ. 2009. Cell adhesion, the backbone of the synapse: "vertebrate" and "invertebrate" perspectives. *Cold Spring Harb Perspect Biol* 1: a003079

Giavazzi A, Setola V, Simonati A, Battaglia G. 2006. Neuronal-specific roles of the survival motor neuron protein: evidence from survival motor neuron expression patterns in the developing human central nervous system. *J Neuropathol Exp Neurol* 65: 267-77

Glascock JJ, Osman EY, Wetz MJ, Krogman MM, Shababi M, Lorson CL. 2012. Decreasing disease severity in symptomatic, *Smn*$^{-/-}$; *SMN2*$^{+/+}$, spinal muscular atrophy mice following scAAV9-SMN delivery. *Hum Gene Ther* 23: 330-5

Glinka M, Herrmann T, Funk N, Havlicek S, Rossoll W, *et al.* 2010. The heterogeneous nuclear ribonucleoprotein-R is necessary for axonal *β-actin* mRNA translocation in spinal motor neurons. *Hum Mol Genet* 19: 1951-66

Goda Y, Davis GW. 2003. Mechanisms of synapse assembly and disassembly. *Neuron* 40: 243-64

Gogliotti RG, Quinlan KA, Barlow CB, Heier CR, Heckman CJ, Didonato CJ. 2012. Motor neuron rescue in spinal muscular atrophy mice demonstrates that sensory-motor defects are a consequence, not a cause, of motor neuron dysfunction. *J Neurosci* 32: 3818-29

Gong WJ, Golic KG. 2003. Ends-out, or replacement, gene targeting in *Drosophila*. *Proc Natl Acad Sci U S A* 100: 2556-61

Goodman AD, Brown TR, Cohen JA, Krupp LB, Schapiro R, *et al.* 2008. Dose comparison trial of sustained-release fampridine in multiple sclerosis. *Neurology* 71: 1134-41

Goodman AD, Brown TR, Krupp LB, Schapiro RT, Schwid SR, *et al.* 2009. Sustained-release oral fampridine in multiple sclerosis: a randomised, double-blind, controlled trial. *Lancet* 373: 732-8

Grice SJ, Liu JL. 2011. Survival motor neuron protein regulates stem cell division, proliferation, and differentiation in *Drosophila*. *PLoS Genet* 7: e1002030

Grice SJ, Sleigh JN, Liu JL, Sattelle DB. 2011. Invertebrate models of spinal muscular atrophy: insights into mechanisms and potential therapeutics. *Bioessays* 33: 956-65

Guo M, Yang XL, Schimmel P. 2010. New functions of aminoacyl-tRNA synthetases beyond translation. *Nat Rev Mol Cell Biol* 11: 668-74

Hadjiconstantinou M, Neff NH. 1998. GM1 ganglioside: *in vivo* and *in vitro* trophic actions on central neurotransmitter systems. *J Neurochem* 70: 1335-45

Hammond SM, Gogliotti RG, Rao V, Beauvais A, Kothary R, Didonato CJ. 2010. Mouse *survival motor neuron* alleles that mimic *SMN2* splicing and are inducible rescue embryonic lethality early in development but not late. *PLoS One* 5: e15887

Hao le T, Wolman M, Granato M, Beattie CE. 2012. Survival motor neuron affects plastin 3 protein levels leading to motor defects. *J Neurosci* 32: 5074-84

Harris TW, Chen N, Cunningham F, Tello-Ruiz M, Antoshechkin I, *et al.* 2004. WormBase: a multi-species resource for nematode biology and genomics. *Nucleic Acids Res* 32: D411-7

Hausmanowa-Petrusewicz I. 1988. Electrophysiological findings in childhood spinal muscular atrophies. *Rev Neurol (Paris)* 144: 716-20

Hayashi M, Araki S, Arai N, Kumada S, Itoh M, *et al.* 2002. Oxidative stress and disturbed glutamate transport in spinal muscular atrophy. *Brain Dev* 24: 770-5

He W, Zhang HM, Chong YE, Guo M, Marshall AG, Yang XL. 2011. Dispersed disease-causing neomorphic mutations on a single protein promote the same localized conformational opening. *Proc Natl Acad Sci U S A* 108: 12307-12

Heemskerk J, Tobin AJ, Bain LJ. 2002. Teaching old drugs new tricks. Meeting of the Neurodegeneration Drug Screening Consortium, 7-8 April 2002, Washington, DC, USA. *Trends Neurosci* 25: 494-6

Heier CR, Satta R, Lutz C, Didonato CJ. 2010. Arrhythmia and cardiac defects are a feature of spinal muscular atrophy model mice. *Hum Mol Genet* 19: 3906-18

Helmken C, Hofmann Y, Schoenen F, Oprea G, Raschke H, *et al.* 2003. Evidence for a modifying pathway in SMA discordant families: reduced SMN level decreases the amount of its interacting partners and Htra2-beta1. *Hum Genet* 114: 11-21

Hensel N, Ratzka A, Brinkmann H, Klimaschewski L, Grothe C, Claus P. 2012. Analysis of the fibroblast growth factor system reveals alterations in a mouse model of spinal muscular atrophy. *PLoS One* 7: e31202

Hoang B, Chiba A. 2001. Single-cell analysis of *Drosophila* larval neuromuscular synapses. *Dev Biol* 229: 55-70

Hsieh-Li HM, Chang JG, Jong YJ, Wu MH, Wang NM, *et al.* 2000. A mouse model for spinal muscular atrophy. *Nat Genet* 24: 66-70

Hu H, Marton TF, Goodman CS. 2001. Plexin B mediates axon guidance in *Drosophila* by simultaneously inhibiting active Rac and enhancing RhoA signaling. *Neuron* 32: 39-51

Hua Y, Sahashi K, Rigo F, Hung G, Horev G, *et al.* 2011. Peripheral SMN restoration is essential for long-term rescue of a severe spinal muscular atrophy mouse model. *Nature* 478: 123-6

Hubers L, Valderrama-Carvajal H, Laframboise J, Timbers J, Sanchez G, Côté J. 2011. HuD interacts with survival motor neuron protein and can rescue spinal muscular atrophy-like neuronal defects. *Hum Mol Genet* 20: 553-79

Ibba M, Soll D. 2000. Aminoacyl-tRNA synthesis. *Annu Rev Biochem* 69: 617-50

Iijima R, Takahashi H, Ikegami S, Yamazaki M. 2007. Characterization of the reaction between sialic acid (N-acetylneuraminic acid) and hydrogen peroxide. *Biol Pharm Bull* 30: 580-2

Iijima R, Takahashi H, Namme R, Ikegami S, Yamazaki M. 2004. Novel biological function of sialic acid (N-acetylneuraminic acid) as a hydrogen peroxide scavenger. *FEBS Lett* 561: 163-6

Ilangovan R, Marshall WL, Hua Y, Zhou J. 2003. Inhibition of apoptosis by Z-VAD-fmk in SMN-depleted S2 cells. *J Biol Chem* 278: 30993-9

Jablonka S, Bandilla M, Wiese S, Bühler D, Wirth B, *et al.* 2001. Co-regulation of survival of motor neuron (SMN) protein and its interactor SIP1 during development and in spinal muscular atrophy. *Hum Mol Genet* 10: 497-505

Jablonka S, Beck M, Lechner BD, Mayer C, Sendtner M. 2007. Defective Ca^{2+} channel clustering in axon terminals disturbs excitability in motoneurons in spinal muscular atrophy. *J Cell Biol* 179: 139-49

Jablonka S, Holtmann B, Meister G, Bandilla M, Rossoll W, *et al.* 2002. Gene targeting of Gemin2 in mice reveals a correlation between defects in the biogenesis of U snRNPs and motoneuron cell death. *Proc Natl Acad Sci U S A* 99: 10126-31

Jablonka S, Schrank B, Kralewski M, Rossoll W, Sendtner M. 2000. Reduced survival motor neuron (*Smn*) gene dose in mice leads to motor neuron degeneration: an animal model for spinal muscular atrophy type III. *Hum Mol Genet* 9: 341-6

James PA, Cader MZ, Muntoni F, Childs AM, Crow YJ, Talbot K. 2006. Severe childhood SMA and axonal CMT due to anticodon binding domain mutations in the *GARS* gene. *Neurology* 67: 1710-2

James PA, Talbot K. 2006. The molecular genetics of non-ALS motor neuron diseases. *Biochim Biophys Acta* 1762: 986-1000

Jan LY, Jan YN. 1976. L-glutamate as an excitatory transmitter at the *Drosophila* larval neuromuscular junction. *J Physiol* 262: 215-36

Jarecki J, Chen X, Bernardino A, Coovert DD, Whitney M, *et al.* 2005. Diverse small-molecule modulators of *SMN* expression found by high-throughput compound screening: early leads towards a therapeutic for spinal muscular atrophy. *Hum Mol Genet* 14: 2003-18

Javaherian A, Cline HT. 2005. Coordinated motor neuron axon growth and neuromuscular synaptogenesis are promoted by CPG15 *in vivo*. *Neuron* 45: 505-12

Jia F, Pignataro L, Schofield CM, Yue M, Harrison NL, Goldstein PA. 2005. An extrasynaptic $GABA_A$ receptor mediates tonic inhibition in thalamic VB neurons. *J Neurophysiol* 94: 4491-501

Jia XX, Gorczyca M, Budnik V. 1993. Ultrastructure of neuromuscular junctions in *Drosophila*: comparison of wild type and mutants with increased excitability. *J Neurobiol* 24: 1025-44

Jia Y, Mu JC, Ackerman SL. 2012. Mutation of a U2 snRNA gene causes global disruption of alternative splicing and neurodegeneration. *Cell* 148: 296-308

Jin Y. 2005. Synaptogenesis. *WormBook*: 1-11

Jodelka FM, Ebert AD, Duelli DM, Hastings ML. 2010. A feedback loop regulates splicing of the spinal muscular atrophy-modifying gene, *SMN2*. *Hum Mol Genet* 19: 4906-17

Johansen J, Halpern ME, Johansen KM, Keshishian H. 1989. Stereotypic morphology of glutamatergic synapses on identified muscle cells of *Drosophila* larvae. *J Neurosci* 9: 710-25

Johnson CD, Russell RL. 1983. Multiple molecular forms of acetylcholinesterase in the nematode *Caenorhabditis elegans*. *J Neurochem* 41: 30-46

Jones AK, Sattelle DB. 2004. Functional genomics of the nicotinic acetylcholine receptor gene family of the nematode, *Caenorhabditis elegans*. *Bioessays* 26: 39-49

Jones AK, Buckingham SD, Sattelle DB. 2005. Chemistry-to-gene screens in *Caenorhabditis elegans*. *Nat Rev Drug Discov* 4: 321-30

Jordanova A, Irobi J, Thomas FP, Van Dijck P, Meerschaert K, *et al.* 2006. Disrupted function and axonal distribution of mutant tyrosyl-tRNA synthetase in dominant intermediate Charcot-Marie-Tooth neuropathy. *Nat Genet* 38: 197-202

Jung H, O'Hare CM, Holt CE. 2011. Translational regulation in growth cones. *Curr Opin Genet Dev* 21: 458-64

Jung H, Yoon BC, Holt CE. 2012. Axonal mRNA localization and local protein synthesis in nervous system assembly, maintenance and repair. *Nat Rev Neurosci* 13: 308-24

Kaas B, Vaidya AR, Leatherman A, Schleidt S, Kohn RE. 2010. Technical report: exploring the basis of congenital myasthenic syndromes in an undergraduate course, using the model organism, *Caenorhabditis elegans*. *Invert Neurosci* 10: 17-23

Kariya S, Park GH, Maeno-Hikichi Y, Leykekhman O, Lutz C, *et al.* 2008. Reduced SMN protein impairs maturation of the neuromuscular junctions in mouse models of spinal muscular atrophy. *Hum Mol Genet* 17: 2552-69

Kerr DA, Nery JP, Traystman RJ, Chau BN, Hardwick JM. 2000. Survival motor neuron protein modulates neuron-specific apoptosis. *Proc Natl Acad Sci U S A* 97: 13312-7

Khatri IA, Chaudhry US, Seikaly MG, Browne RH, Iannaccone ST. 2008. Low bone mineral density in spinal muscular atrophy. *J Clin Neuromuscul Dis* 10: 11-7

Kinali M, Mercuri E, Main M, De Biasia F, Karatza A, *et al.* 2002. Pilot trial of albuterol in spinal muscular atrophy. *Neurology* 59: 609-10

Kolson DL, Russell RL. 1985. A novel class of acetylcholinesterase, revealed by mutations, in the nematode *Caenorhabditis elegans*. *J Neurogenet* 2: 93-110

Kong L, Wang X, Choe DW, Polley M, Burnett BG, *et al.* 2009. Impaired synaptic vesicle release and immaturity of neuromuscular junctions in spinal muscular atrophy mice. *J Neurosci* 29: 842-51

Krause M, Fire A, Harrison SW, Priess J, Weintraub H. 1990. CeMyoD accumulation defines the body wall muscle cell fate during *C. elegans* embryogenesis. *Cell* 63: 907-19

Kroiss M, Schultz J, Wiesner J, Chari A, Sickmann A, Fischer U. 2008. Evolution of an RNP assembly system: a minimal SMN complex facilitates formation of UsnRNPs in *Drosophila melanogaster*. *Proc Natl Acad Sci U S A* 105: 10045-50

Kulkarni G, Li H, Wadsworth WG. 2008. CLEC-38, a transmembrane protein with C-type lectin-like domains, negatively regulates UNC-40-mediated axon outgrowth and promotes presynaptic development in *Caenorhabditis elegans*. *J Neurosci* 28: 4541-50

Kummer TT, Misgeld T, Sanes JR. 2006. Assembly of the postsynaptic membrane at the neuromuscular junction: paradigm lost. *Curr Opin Neurobiol* 16: 74-82

Kwon JE, Kim EK, Choi EJ. 2011. Stabilization of the survival motor neuron protein by ASK1. *FEBS Lett* 585: 1287-92

Latour P, Thauvin-Robinet C, Baudelet-Mery C, Soichot P, Cusin V, *et al.* 2010. A major determinant for binding and aminoacylation of tRNA(Ala) in cytoplasmic Alanyl-tRNA synthetase is mutated in dominant axonal Charcot-Marie-Tooth disease. *Am J Hum Genet* 86: 77-82

Le TT, Pham LT, Butchbach ME, Zhang HL, Monani UR, *et al.* 2005. SMNΔ7, the major product of the centromeric survival motor neuron (*SMN2*) gene, extends survival in mice with spinal muscular atrophy and associates with full-length SMN. *Hum Mol Genet* 14: 845-57

Lefebvre S, Burglen L, Reboullet S, Clermont O, Burlet P, *et al.* 1995. Identification and characterization of a spinal muscular atrophy-determining gene. *Cell* 80: 155-65

Lefebvre S, Burlet P, Liu Q, Bertrandy S, Clermont O, *et al.* 1997. Correlation between severity and SMN protein level in spinal muscular atrophy. *Nat Genet* 16: 265-9

Lemeignan M, Millart H, Lamiable D, Molgo J, Lechat P. 1984. Evaluation of 4-aminopyridine and 3,4-diaminopyridine penetrability into cerebrospinal fluid in anesthetized rats. *Brain Res* 304: 166-9

Liang WC, Yuo CY, Chang JG, Chen YC, Chang YF, *et al.* 2008. The effect of hydroxyurea in spinal muscular atrophy cells and patients. *J Neurol Sci* 268: 87-94

Lin W, Burgess RW, Dominguez B, Pfaff SL, Sanes JR, Lee KF. 2001. Distinct roles of nerve and muscle in postsynaptic differentiation of the neuromuscular synapse. *Nature* 410: 1057-64

Ling KK, Gibbs RM, Feng Z, Ko CP. 2012. Severe neuromuscular denervation of clinically relevant muscles in a mouse model of spinal muscular atrophy. *Hum Mol Genet* 21: 185-95

Ling KK, Lin MY, Zingg B, Feng Z, Ko CP. 2010. Synaptic defects in the spinal and neuromuscular circuitry in a mouse model of spinal muscular atrophy. *PLoS One* 5: e15457

Liu H, Beauvais A, Baker AN, Tsilfidis C, Kothary R. 2011. Smn deficiency causes neuritogenesis and neurogenesis defects in the retinal neurons of a mouse model of spinal muscular atrophy. *Dev Neurobiol* 71: 153-69

Liu Q, Chen B, Hall DH, Wang ZW. 2007. A quantum of neurotransmitter causes minis in multiple postsynaptic cells at the *Caenorhabditis elegans* neuromuscular junction. *Dev Neurobiol* 67: 123-8

Liu Q, Dreyfuss G. 1996. A novel nuclear structure containing the survival of motor neurons protein. *EMBO J* 15: 3555-65

Liu Q, Fischer U, Wang F, Dreyfuss G. 1997. The spinal muscular atrophy disease gene product, SMN, and its associated protein SIP1 are in a complex with spliceosomal snRNP proteins. *Cell* 90: 1013-21

Lloyd TE, Taylor JP. 2010. Flightless flies: *Drosophila* models of neuromuscular disease. *Ann N Y Acad Sci* 1184: e1-20

Locatelli D, d'Errico P, Capra S, Finardi A, Colciaghi F, *et al.* 2012. Spinal muscular atrophy pathogenic mutations impair the axonogenic properties of axonal-survival of motor neuron. *J Neurochem* 121: 465-74

Loria PM, Duke A, Rand JB, Hobert O. 2003. Two neuronal, nuclear-localized RNA binding proteins involved in synaptic transmission. *Curr Biol* 13: 1317-23

Lorson CL, Androphy EJ. 2000. An exonic enhancer is required for inclusion of an essential exon in the SMA-determining gene *SMN*. *Hum Mol Genet* 9: 259-65

Lorson CL, Hahnen E, Androphy EJ, Wirth B. 1999. A single nucleotide in the *SMN* gene regulates splicing and is responsible for spinal muscular atrophy. *Proc Natl Acad Sci U S A* 96: 6307-11

Lunn MR, Root DE, Martino AM, Flaherty SP, Kelley BP, *et al.* 2004. Indoprofen upregulates the survival motor neuron protein through a cyclooxygenase-independent mechanism. *Chem Biol* 11: 1489-93

Lunn MR, Wang CH. 2008. Spinal muscular atrophy. *Lancet* 371: 2120-33

Lutz CM, Kariya S, Patruni S, Osborne MA, Liu D, *et al.* 2011. Postsymptomatic restoration of SMN rescues the disease phenotype in a mouse model of severe spinal muscular atrophy. *J Clin Invest* 121: 3029-41

Mailman MD, Heinz JW, Papp AC, Snyder PJ, Sedra MS, *et al.* 2002. Molecular analysis of spinal muscular atrophy and modification of the phenotype by *SMN2*. *Genet Med* 4: 20-6

Maracchioni A, Totaro A, Angelini DF, Di Penta A, Bernardi G, *et al.* 2007. Mitochondrial damage modulates alternative splicing in neuronal cells: implications for neurodegeneration. *J Neurochem* 100: 142-53

Marques MJ, Conchello JA, Lichtman JW. 2000. From plaque to pretzel: fold formation and acetylcholine receptor loss at the developing neuromuscular junction. *J Neurosci* 20: 3663-75

Marrus SB, Portman SL, Allen MJ, Moffat KG, DiAntonio A. 2004. Differential localization of glutamate receptor subunits at the *Drosophila* neuromuscular junction. *J Neurosci* 24: 1406-15

Martínez-Hernández R, Bernal S, Also-Rallo E, Alías L, Barceló M, *et al.* 2012. Synaptic defects in type I spinal muscular atrophy in human development. *J Pathol* (Epub)

Marvanova M, Nichols CD. 2007. Identification of neuroprotective compounds of *Caenorhabditis elegans* dopaminergic neurons against 6-OHDA. *J Mol Neurosci* 31: 127-37

Masuda K, Takano A, Oshita H, Akiyama H, Tsuchiya E, *et al.* 2011. Chondrolectin is a novel diagnostic biomarker and a therapeutic target for lung cancer. *Clin Cancer Res* 17: 7712-22

Matthes DJ, Sink H, Kolodkin AL, Goodman CS. 1995. Semaphorin II can function as a selective inhibitor of specific synaptic arborizations. *Cell* 81: 631-9

Matusica D, Fenech MP, Rogers ML, Rush RA. 2008. Characterization and use of the NSC-34 cell line for study of neurotrophin receptor trafficking. *J Neurosci Res* 86: 553-65

McAndrew PE, Parsons DW, Simard LR, Rochette C, Ray PN, *et al.* 1997. Identification of proximal spinal muscular atrophy carriers and patients by analysis of SMN^T and SMN^C gene copy number. *Am J Hum Genet* 60: 1411-22

McGovern M, Yu L, Kosinski M, Greenstein D, Savage-Dunn C. 2007. A role for sperm in regulation of egg-laying in the nematode *C. elegans*. *BMC Dev Biol* 7: 41

McGovern VL, Gavrilina TO, Beattie CE, Burghes AH. 2008. Embryonic motor axon development in the severe SMA mouse. *Hum Mol Genet* 17: 2900-9

McIntire SL, Jorgensen E, Kaplan J, Horvitz HR. 1993. The GABAergic nervous system of *Caenorhabditis elegans*. *Nature* 364: 337-41

McLaughlin HM, Sakaguchi R, Liu C, Igarashi T, Pehlivan D, *et al.* 2010. Compound heterozygosity for loss-of-function lysyl-tRNA synthetase mutations in a patient with peripheral neuropathy. *Am J Hum Genet* 87: 560-6

McWhorter ML, Monani UR, Burghes AH, Beattie CE. 2003. Knockdown of the survival motor neuron (Smn) protein in zebrafish causes defects in motor axon outgrowth and pathfinding. *J Cell Biol* 162: 919-31

Meister G, Bühler D, Pillai R, Lottspeich F, Fischer U. 2001. A multiprotein complex mediates the ATP-dependent assembly of spliceosomal U snRNPs. *Nat Cell Biol* 3: 945-9

Mentis GZ, Blivis D, Liu W, Drobac E, Crowder ME, *et al.* 2011. Early functional impairment of sensory-motor connectivity in a mouse model of spinal muscular atrophy. *Neuron* 69: 453-67

Mercuri E, Bertini E, Messina S, Pelliccioni M, D'Amico A, *et al.* 2004. Pilot trial of phenylbutyrate in spinal muscular atrophy. *Neuromuscul Disord* 14: 130-5

Mercuri E, Bertini E, Messina S, Solari A, D'Amico A, *et al.* 2007. Randomized, double-blind, placebo-controlled trial of phenylbutyrate in spinal muscular atrophy. *Neurology* 68: 51-5

Merkin J, Russell C, Chen P, Burge CB. 2012. Evolutionary dynamics of gene and isoform regulation in Mammalian tissues. *Science* 338: 1593-9

Miguel-Aliaga I, Chan YB, Davies KE, van den Heuvel M. 2000. Disruption of SMN function by ectopic expression of the human *SMN* gene in *Drosophila*. *FEBS Lett* 486: 99-102

Miguel-Aliaga I, Culetto E, Walker DS, Baylis HA, Sattelle DB, Davies KE. 1999. The *Caenorhabditis elegans* orthologue of the human gene responsible for spinal muscular atrophy is a maternal product critical for germline maturation and embryonic viability. *Hum Mol Genet* 8: 2133-43

Miller KG, Alfonso A, Nguyen M, Crowell JA, Johnson CD, Rand JB. 1996. A genetic selection for *Caenorhabditis elegans* synaptic transmission mutants. *Proc Natl Acad Sci U S A* 93: 12593-8

Miller RG, Moore DH, Dronsky V, Bradley W, Barohn R, *et al.* 2001. A placebo-controlled trial of gabapentin in spinal muscular atrophy. *J Neurol Sci* 191: 127-31

Misgeld T, Burgess RW, Lewis RM, Cunningham JM, Lichtman JW, Sanes JR. 2002. Roles of neurotransmitter in synapse formation: development of neuromuscular junctions lacking choline acetyltransferase. *Neuron* 36: 635-48

Missias AC, Mudd J, Cunningham JM, Steinbach JH, Merlie JP, Sanes JR. 1997. Deficient development and maintenance of postsynaptic specializations in mutant mice lacking an 'adult' acetylcholine receptor subunit. *Development* 124: 5075-86

Mocchetti I. 2005. Exogenous gangliosides, neuronal plasticity and repair, and the neurotrophins. *Cell Mol Life Sci* 62: 2283-94

Monani UR, Lorson CL, Parsons DW, Prior TW, Androphy EJ, *et al.* 1999. A single nucleotide difference that alters splicing patterns distinguishes the SMA gene *SMN1* from the copy gene *SMN2*. *Hum Mol Genet* 8: 1177-83

Monani UR, Pastore MT, Gavrilina TO, Jablonka S, Le TT, *et al.* 2003. A transgene carrying an A2G missense mutation in the *SMN* gene modulates phenotypic severity in mice with severe (type I) spinal muscular atrophy. *J Cell Biol* 160: 41-52

Monani UR, Sendtner M, Coovert DD, Parsons DW, Andreassi C, *et al.* 2000. The human centromeric *survival motor neuron* gene (*SMN2*) rescues embryonic lethality in *Smn*$^{-/-}$ mice and results in a mouse with spinal muscular atrophy. *Hum Mol Genet* 9: 333-9

Mosmann T. 1983. Rapid colorimetric assay for cellular growth and survival: application to proliferation and cytotoxicity assays. *J Immunol Methods* 65: 55-63

Motley WW, Seburn KL, Nawaz MH, Miers KE, Cheng J, *et al.* 2011. Charcot-Marie-Tooth-linked mutant GARS is toxic to peripheral neurons independent of wild-type GARS levels. *PLoS Genet* 7: e1002399

Motley WW, Talbot K, Fischbeck KH. 2010. *GARS* axonopathy: not every neuron's cup of tRNA. *Trends Neurosci* 33: 59-66

Mudge SJ, Williams JH, Eyre HJ, Sutherland GR, Cowan PJ, Power DA. 1998. Complex organisation of the 5'-end of the human glycine tRNA synthetase gene. *Gene* 209: 45-50

Munsat TL, Davies KE. 1992. International SMA consortium meeting. (26-28 June 1992, Bonn, Germany). *Neuromuscul Disord* 2: 423-8

Murray LM, Comley LH, Thomson D, Parkinson N, Talbot K, Gillingwater TH. 2008. Selective vulnerability of motor neurons and dissociation of pre- and post-synaptic pathology at the

neuromuscular junction in mouse models of spinal muscular atrophy. *Hum Mol Genet* 17: 949-62

Murray LM, Lee S, Bäumer D, Parson SH, Talbot K, Gillingwater TH. 2010. Pre-symptomatic development of lower motor neuron connectivity in a mouse model of severe spinal muscular atrophy. *Hum Mol Genet* 19: 420-33

Mutsaers CA, Wishart TM, Lamont DJ, Riessland M, Schreml J, *et al.* 2011. Reversible molecular pathology of skeletal muscle in spinal muscular atrophy. *Hum Mol Genet* 20: 4334-44

Nangle LA, Zhang W, Xie W, Yang XL, Schimmel P. 2007. Charcot-Marie-Tooth disease-associated mutant tRNA synthetases linked to altered dimer interface and neurite distribution defect. *Proc Natl Acad Sci U S A* 104: 11239-44

Narver HL, Kong L, Burnett BG, Choe DW, Bosch-Marce M, *et al.* 2008. Sustained improvement of spinal muscular atrophy mice treated with trichostatin A plus nutrition. *Ann Neurol* 64: 465-70

Nguyen M, Alfonso A, Johnson CD, Rand JB. 1995. *Caenorhabditis elegans* mutants resistant to inhibitors of acetylcholinesterase. *Genetics* 140: 527-35

Nicole S, Desforges B, Millet G, Lesbordes J, Cifuentes-Diaz C, *et al.* 2003. Intact satellite cells lead to remarkable protection against *Smn* gene defect in differentiated skeletal muscle. *J Cell Biol* 161: 571-82

Ning K, Drepper C, Valori CF, Ahsan M, Wyles M, *et al.* 2010. PTEN depletion rescues axonal growth defect and improves survival in SMN-deficient motor neurons. *Hum Mol Genet* 19: 3159-68

Nölle A, Zeug A, van Bergeijk J, Tonges L, Gerhard R, *et al.* 2011. The spinal muscular atrophy disease protein SMN is linked to the Rho-kinase pathway via profilin. *Hum Mol Genet* 20: 4865-78

Ogawa C, Usui K, Aoki M, Ito F, Itoh M, *et al.* 2007. Gemin2 plays an important role in stabilizing the survival of motor neuron complex. *J Biol Chem* 282: 11122-34

Ogino S, Wilson RB. 2002. Genetic testing and risk assessment for spinal muscular atrophy (SMA). *Hum Genet* 111: 477-500

Okuda T, Haga T, Kanai Y, Endou H, Ishihara T, Katsura I. 2000. Identification and characterization of the high-affinity choline transporter. *Nat Neurosci* 3: 120-5

Olesen J, Gustavsson A, Svensson M, Wittchen HU, Jonsson B. 2012. The economic cost of brain disorders in Europe. *Eur J Neurol* 19: 155-62

Oprea GE, Kröber S, McWhorter ML, Rossoll W, Muller S, *et al.* 2008. Plastin 3 is a protective modifier of autosomal recessive spinal muscular atrophy. *Science* 320: 524-7

Osman EY, Yen PF, Lorson CL. 2012. Bifunctional RNAs targeting the intronic splicing silencer N1 increase SMN levels and reduce disease severity in an animal model of spinal muscular atrophy. *Mol Ther* 20: 119-26

Otter S, Grimmler M, Neuenkirchen N, Chari A, Sickmann A, Fischer U. 2007. A comprehensive interaction map of the human survival of motor neuron (SMN) complex. *J Biol Chem* 282: 5825-33

Pagliardini S, Giavazzi A, Setola V, Lizier C, Di Luca M, *et al.* 2000. Subcellular localization and axonal transport of the survival motor neuron (SMN) protein in the developing rat spinal cord. *Hum Mol Genet* 9: 47-56

Park GH, Maeno-Hikichi Y, Awano T, Landmesser LT, Monani UR. 2010. Reduced survival of motor neuron (SMN) protein in motor neuronal progenitors functions cell autonomously to cause spinal muscular atrophy in model mice expressing the human centromeric (*SMN2*) gene. *J Neurosci* 30: 12005-19

Park MC, Kang T, Jin D, Han JM, Kim SB, *et al.* 2012. Secreted human glycyl-tRNA synthetase implicated in defense against ERK-activated tumorigenesis. *Proc Natl Acad Sci U S A* 109: E640-7

Park SG, Kim HJ, Min YH, Choi EC, Shin YK, *et al.* 2005. Human lysyl-tRNA synthetase is secreted to trigger proinflammatory response. *Proc Natl Acad Sci U S A* 102: 6356-61

Park SG, Schimmel P, Kim S. 2008. Aminoacyl tRNA synthetases and their connections to disease. *Proc Natl Acad Sci U S A* 105: 11043-9

Parker GC, Li X, Anguelov RA, Toth G, Cristescu A, Acsadi G. 2008. Survival motor neuron protein regulates apoptosis in an *in vitro* model of spinal muscular atrophy. *Neurotox Res* 13: 39-48

Parks AL, Cook KR, Belvin M, Dompe NA, Fawcett R, *et al.* 2004. Systematic generation of high-resolution deletion coverage of the *Drosophila melanogaster* genome. *Nat Genet* 36: 288-92

Passini MA, Bu J, Richards AM, Kinnecom C, Sardi SP, *et al.* 2011. Antisense oligonucleotides delivered to the mouse CNS ameliorate symptoms of severe spinal muscular atrophy. *Sci Transl Med* 3: 72ra18

Passini MA, Cheng SH. 2011. Prospects for the gene therapy of spinal muscular atrophy. *Trends Mol Med* 17: 259-65

Pasterkamp RJ, De Winter F, Holtmaat AJ, Verhaagen J. 1998. Evidence for a role of the chemorepellent semaphorin III and its receptor neuropilin-1 in the regeneration of primary olfactory axons. *J Neurosci* 18: 9962-76

Patel AA, Steitz JA. 2003. Splicing double: insights from the second spliceosome. *Nat Rev Mol Cell Biol* 4: 960-70

Pearn J. 1978. Incidence, prevalence, and gene frequency studies of chronic childhood spinal muscular atrophy. *J Med Genet* 15: 409-13

Pellizzoni L. 2007. Chaperoning ribonucleoprotein biogenesis in health and disease. *EMBO Rep* 8: 340-5

Pellizzoni L, Baccon J, Charroux B, Dreyfuss G. 2001a. The survival of motor neurons (SMN) protein interacts with the snoRNP proteins fibrillarin and GAR1. *Curr Biol* 11: 1079-88

Pellizzoni L, Charroux B, Dreyfuss G. 1999. SMN mutants of spinal muscular atrophy patients are defective in binding to snRNP proteins. *Proc Natl Acad Sci U S A* 96: 11167-72

Pellizzoni L, Charroux B, Rappsilber J, Mann M, Dreyfuss G. 2001b. A functional interaction between the survival motor neuron complex and RNA polymerase II. *J Cell Biol* 152: 75-85

Pellizzoni L, Kataoka N, Charroux B, Dreyfuss G. 1998. A novel function for SMN, the spinal muscular atrophy disease gene product, in pre-mRNA splicing. *Cell* 95: 615-24

Pellizzoni L, Yong J, Dreyfuss G. 2002. Essential role for the SMN complex in the specificity of snRNP assembly. *Science* 298: 1775-9

Peron S, Zordan MA, Magnabosco A, Reggiani C, Megighian A. 2009. From action potential to contraction: neural control and excitation-contraction coupling in larval muscles of *Drosophila*. *Comp Biochem Physiol A Mol Integr Physiol* 154: 173-83

Piccioni F, Roman BR, Fischbeck KH, Taylor JP. 2004. A screen for drugs that protect against the cytotoxicity of polyglutamine-expanded androgen receptor. *Hum Mol Genet* 13: 437-46

Piepers S, Cobben JM, Sodaar P, Jansen MD, Wadman RI, *et al.* 2011. Quantification of SMN protein in leucocytes from spinal muscular atrophy patients: effects of treatment with valproic acid. *J Neurol Neurosurg Psychiatry* 82: 850-2

Pinter MJ, Waldeck RF, Cope TC, Cork LC. 1997. Effects of 4-aminopyridine on muscle and motor unit force in canine motor neuron disease. *J Neurosci* 17: 4500-7

Porensky PN, Mitrpant C, McGovern VL, Bevan AK, Foust KD, *et al.* 2012. A single administration of morpholino antisense oligomer rescues spinal muscular atrophy in mouse. *Hum Mol Genet* 21: 1625-38

Praveen K, Wen Y, Matera AG. 2012. A *Drosophila* model of spinal muscular atrophy uncouples snRNP biogenesis functions of survival motor neuron from locomotion and viability defects. *Cell Rep* 1: 624-31

Prior TW, Snyder PJ, Rink BD, Pearl DK, Pyatt RE, *et al.* 2010. Newborn and carrier screening for spinal muscular atrophy. *Am J Med Genet A* 152A: 1608-16

Prokop A, Landgraf M, Rushton E, Broadie K, Bate M. 1996. Presynaptic development at the *Drosophila* neuromuscular junction: assembly and localization of presynaptic active zones. *Neuron* 17: 617-26

Prokop A, Meinertzhagen IA. 2006. Development and structure of synaptic contacts in *Drosophila*. *Semin Cell Dev Biol* 17: 20-30

Pulak R. 2006. Techniques for analysis, sorting, and dispensing of *C. elegans* on the COPAS flow-sorting system. *Methods Mol Biol* 351: 275-86

Puls I, Jonnakuty C, LaMonte BH, Holzbaur EL, Tokito M, Mann E, Floeter MK, Bidus K, Drayna D, Oh SJ, Brown RH Jr, Ludlow CL, Fischbeck KH. 2003. Mutant dynactin in motor neuron disease. *Nat Genet* 33: 455-6

Qin G, Schwarz T, Kittel RJ, Schmid A, Rasse TM, *et al.* 2005. Four different subunits are essential for expressing the synaptic glutamate receptor at neuromuscular junctions of *Drosophila*. *J Neurosci* 25: 3209-18

Rajendra TK, Gonsalvez GB, Walker MP, Shpargel KB, Salz HK, Matera AG. 2007. A *Drosophila melanogaster* model of spinal muscular atrophy reveals a function for SMN in striated muscle. *J Cell Biol* 176: 831-41

Rak K, Lechner BD, Schneider C, Drexl H, Sendtner M, Jablonka S. 2009. Valproic acid blocks excitability in SMA type I mouse motor neurons. *Neurobiol Dis* 36: 477-87

Rand JB. 2007. Acetylcholine. *WormBook*: 1-21

Rand JB, Russell RL. 1985. Properties and partial purification of choline acetyltransferase from the nematode *Caenorhabditis elegans*. *J Neurochem* 44: 189-200

Rathod R, Havlicek S, Frank N, Blum R, Sendtner M. 2012. Laminin induced local axonal translation of *β-actin* mRNA is impaired in SMN-deficient motoneurons. *Histochem Cell Biol* (Epub)

Reilly MM, Murphy SM, Laura M. 2011. Charcot-Marie-Tooth disease. *J Peripher Nerv Syst* 16: 1-14

Reiter LT, Bier E. 2002. Using *Drosophila melanogaster* to uncover human disease gene function and potential drug target proteins. *Expert Opin Ther Targets* 6: 387-99

Reiter LT, Potocki L, Chien S, Gribskov M, Bier E. 2001. A systematic analysis of human disease-associated gene sequences in *Drosophila melanogaster*. *Genome Res* 11: 1114-25

Richmond JE, Jorgensen EM. 1999. One GABA and two acetylcholine receptors function at the *C. elegans* neuromuscular junction. *Nat Neurosci* 2: 791-7

Riessland M, Ackermann B, Förster A, Jakubik M, Hauke J, *et al.* 2010. SAHA ameliorates the SMA phenotype in two mouse models for spinal muscular atrophy. *Hum Mol Genet* 19: 1492-506

Ritzenthaler S, Suzuki E, Chiba A. 2000. Postsynaptic filopodia in muscle cells interact with innervating motoneuron axons. *Nat Neurosci* 3: 1012-7

Rossoll W, Bassell GJ. 2009. Spinal muscular atrophy and a model for survival of motor neuron protein function in axonal ribonucleoprotein complexes. *Results Probl Cell Differ* 48: 289-326

Rossoll W, Jablonka S, Andreassi C, Kröning AK, Karle K, *et al.* 2003. Smn, the spinal muscular atrophy-determining gene product, modulates axon growth and localization of *β-actin* mRNA in growth cones of motoneurons. *J Cell Biol* 163: 801-12

Rossoll W, Kröning AK, Ohndorf UM, Steegborn C, Jablonka S, Sendtner M. 2002. Specific interaction of Smn, the spinal muscular atrophy determining gene product, with hnRNP-R and gry-rbp/hnRNP-Q: a role for Smn in RNA processing in motor axons? *Hum Mol Genet* 11: 93-105

Rossor AM, Kalmar B, Greensmith L, Reilly MM. 2012. The distal hereditary motor neuropathies. *J Neurol Neurosurg Psychiatry* 83: 6-14

Rubin GM, Yandell MD, Wortman JR, Gabor Miklos GL, Nelson CR, *et al.* 2000. Comparative genomics of the eukaryotes. *Science* 287: 2204-15

Rudnik-Schöneborn S, Goebel HH, Schlote W, Molaian S, Omran H, *et al.* 2003. Classical infantile spinal muscular atrophy with SMN deficiency causes sensory neuronopathy. *Neurology* 60: 983-7

Rudnik-Schöneborn S, Heller R, Berg C, Betzler C, Grimm T, *et al.* 2008. Congenital heart disease is a feature of severe infantile spinal muscular atrophy. *J Med Genet* 45: 635-8

Ruggiu M, McGovern VL, Lotti F, Saieva L, Li DK, *et al.* 2012. A role for SMN exon 7 splicing in the selective vulnerability of motor neurons in spinal muscular atrophy. *Mol Cell Biol* 32: 126-38

Ruiz R, Casanas JJ, Torres-Benito L, Cano R, Tabares L. 2010. Altered intracellular Ca^{2+} homeostasis in nerve terminals of severe spinal muscular atrophy mice. *J Neurosci* 30: 849-57

Russman BS, Iannaccone ST, Samaha FJ. 2003. A phase 1 trial of riluzole in spinal muscular atrophy. *Arch Neurol* 60: 1601-3

Sahashi K, Hua Y, Ling KK, Hung G, Rigo F, *et al.* 2012. TSUNAMI: an antisense method to phenocopy splicing-associated diseases in animals. *Genes Dev* 26: 1874-84

Salkoff L, Wei AD, Baban B, Butler A, Fawcett G, *et al.* 2005. Potassium channels in *C. elegans*. *WormBook*: 1-15

Sanes JR, Lichtman JW. 1999. Development of the vertebrate neuromuscular junction. *Annu Rev Neurosci* 22: 389-442

Sanford JL, Mays TA, Rafael-Fortney JA. 2004. CASK and Dlg form a PDZ protein complex at the mammalian neuromuscular junction. *Muscle Nerve* 30: 164-71

Sareen D, Ebert AD, Heins BM, McGivern JV, Ornelas L, Svendsen CN. 2012. Inhibition of apoptosis blocks human motor neuron cell death in a stem cell model of spinal muscular atrophy. *PLoS One* 7: e39113

Satkauskas S, Bagnard D. 2007. Local protein synthesis in axonal growth cones: what is next? *Cell Adh Migr* 1: 179-84

Sauterer RA, Feeney RJ, Zieve GW. 1988. Cytoplasmic assembly of snRNP particles from stored proteins and newly transcribed snRNA's in L929 mouse fibroblasts. *Exp Cell Res* 176: 344-59

Schafer WR, Sanchez BM, Kenyon CJ. 1996. Genes affecting sensitivity to serotonin in *Caenorhabditis elegans*. *Genetics* 143: 1219-30

Schauer R. 2009. Sialic acids as regulators of molecular and cellular interactions. *Curr Opin Struct Biol* 19: 507-14

Schmid A, Qin G, Wichmann C, Kittel RJ, Mertel S, *et al.* 2006. Non-NMDA-type glutamate receptors are essential for maturation but not for initial assembly of synapses at *Drosophila* neuromuscular junctions. *J Neurosci* 26: 11267-77

Schneider JS, Sendek S, Daskalakis C, Cambi F. 2010. GM1 ganglioside in Parkinson's disease: results of a five year open study. *J Neurol Sci* 292: 45-51

Schrank B, Gotz R, Gunnersen JM, Ure JM, Toyka KV, *et al.* 1997. Inactivation of the *survival motor neuron* gene, a candidate gene for human spinal muscular atrophy, leads to massive cell death in early mouse embryos. *Proc Natl Acad Sci U S A* 94: 9920-5

Schuster CM. 2006. Glutamatergic synapses of *Drosophila* neuromuscular junctions: a high-resolution model for the analysis of experience-dependent potentiation. *Cell Tissue Res* 326: 287-99

Schuster CM, Davis GW, Fetter RD, Goodman CS. 1996. Genetic dissection of structural and functional components of synaptic plasticity. I. Fasciclin II controls synaptic stabilization and growth. *Neuron* 17: 641-54

Schwarting GA, Kostek C, Ahmad N, Dibble C, Pays L, Püschel AW. 2000. Semaphorin 3A is required for guidance of olfactory axons in mice. *J Neurosci* 20: 7691-7

Seburn KL, Nangle LA, Cox GA, Schimmel P, Burgess RW. 2006. An active dominant mutation of glycyl-tRNA synthetase causes neuropathy in a Charcot-Marie-Tooth 2D mouse model. *Neuron* 51: 715-26

Shababi M, Habibi J, Yang HT, Vale SM, Sewell WA, Lorson CL. 2010. Cardiac defects contribute to the pathology of spinal muscular atrophy models. *Hum Mol Genet* 19: 4059-71

Shafey D, MacKenzie AE, Kothary R. 2008. Neurodevelopmental abnormalities in neurosphere-derived neural stem cells from SMN-depleted mice. *J Neurosci Res* 86: 2839-47

Shaham S. 2006. Methods in Cell Biology (January 02, 2006). In the *C elegans* Research Community (ed.), WormBook. WormBook. doi/10.1895/wormbook.1.49.1, http://www.wormbook.org

Shanmugarajan S, Tsuruga E, Swoboda KJ, Maria BL, Ries WL, Reddy SV. 2009. Bone loss in survival motor neuron (*Smn$^{-/-}$ SMN2*) genetic mouse model of spinal muscular atrophy. *J Pathol* 219: 52-60

Sherratt RM, Bostock H, Sears TA. 1980. Effects of 4-aminopyridine on normal and demyelinated mammalian nerve fibres. *Nature* 283: 570-2

Shou S, Scott V, Reed C, Hitzemann R, Stadler HS. 2005. Transcriptome analysis of the murine forelimb and hindlimb autopod. *Dev Dyn* 234: 74-89

Shpargel KB, Matera AG. 2005. Gemin proteins are required for efficient assembly of Sm-class ribonucleoproteins. *Proc Natl Acad Sci U S A* 102: 17372-7

Šimić G, Mladinov M, Šešo-Šimić D, Jovanov Milosevic N, Islam A, *et al.* 2008. Abnormal motoneuron migration, differentiation, and axon outgrowth in spinal muscular atrophy. *Acta Neuropathol* 115: 313-26

Simons K, Zerial M. 1993. Rab proteins and the road maps for intracellular transport. *Neuron* 11: 789-99

Simpson KJ, Davis GM, Boag PR. 2012. Comparative high-throughput RNAi screening methodologies in *C. elegans* and mammalian cells. *N Biotechnol* 29: 459-70

Sivakumar K, Kyriakides T, Puls I, Nicholson GA, Funalot B, *et al.* 2005. Phenotypic spectrum of disorders associated with glycyl-tRNA synthetase mutations. *Brain* 128: 2304-14

Skre H. 1974. Genetic and clinical aspects of Charcot-Marie-Tooth's disease. *Clin Genet* 6: 98-118

Sleigh JN. 2010. Functional analysis of nematode nicotinic receptors. *Biosci Horizons* 3: 29-39

Sleigh JN, Buckingham SD, Esmaeili B, Viswanathan M, Cuppen E, *et al.* 2011a. A novel *Caenorhabditis elegans* allele, *smn-1(cb131)*, mimicking a mild form of spinal muscular atrophy, provides a convenient drug screening platform highlighting new and pre-approved compounds. *Hum Mol Genet* 20: 245-60

Sleigh JN, Gillingwater TH, Talbot K. 2011b. The contribution of mouse models to understanding the pathogenesis of spinal muscular atrophy. *Dis Model Mech* 4: 457-67

Sleigh JN, Sattelle DB. 2010. *C. elegans* models of neuromuscular diseases expedite translational research. *Transl Neurosci* 1: 214-27

Somers E, Stencel Z, Wishart TM, Gillingwater TH, Parson SH. 2012. Density, calibre and ramification of muscle capillaries are altered in a mouse model of severe spinal muscular atrophy. *Neuromuscul Disord* 22: 435-42

Stum M, McLaughlin HM, Kleinbrink EL, Miers KE, Ackerman SL, *et al.* 2010. An assessment of mechanisms underlying peripheral axonal degeneration caused by aminoacyl-tRNA synthetase mutations. *Mol Cell Neurosci* 46: 432-43

Sulston JE, Horvitz HR. 1977. Post-embryonic cell lineages of the nematode, *Caenorhabditis elegans*. *Dev Biol* 56: 110-56

Sulston JE, Schierenberg E, White JG, Thomson JN. 1983. The embryonic cell lineage of the nematode *Caenorhabditis elegans*. *Dev Biol* 100: 64-119

Sun Y, Grimmler M, Schwarzer V, Schoenen F, Fischer U, Wirth B. 2005. Molecular and functional analysis of intragenic *SMN1* mutations in patients with spinal muscular atrophy. *Hum Mutat* 25: 64-71

Svennerholm L, Brane G, Karlsson I, Lekman A, Ramstrom I, Wikkelso C. 2002. Alzheimer disease - effect of continuous intracerebroventricular treatment with GM1 ganglioside and a systematic activation programme. *Dement Geriatr Cogn Disord* 14: 128-36

Swoboda KJ, Scott CB, Crawford TO, Simard LR, Reyna SP, *et al.* 2010. SMA CARNI-VAL trial part I: double-blind, randomized, placebo-controlled trial of L-carnitine and valproic acid in spinal muscular atrophy. *PLoS One* 5

Talbot K, Ponting CP, Theodosiou AM, Rodrigues NR, Surtees R, *et al.* 1997. Missense mutation clustering in the *survival motor neuron* gene: a role for a conserved tyrosine and glycine rich region of the protein in RNA metabolism? *Hum Mol Genet* 6: 497-500

Targ EF, Kocsis JD. 1985. 4-aminopyridine leads to restoration of conduction in demyelinated rat sciatic nerve. *Brain Res* 328: 358-61

The *C. elegans* Sequencing Consortium. 1998. Genome sequence of the nematode *C. elegans*: a platform for investigating biology. *Science* 282: 2012-8

Theodosiou NA, Xu T. 1998. Use of FLP/FRT system to study *Drosophila* development. *Methods* 14: 355-65

Thesleff S. 1980. Aminopyridines and synaptic transmission. *Neuroscience* 5: 1413-9

Thomsen RH, Wilson DF. 1983. Effects of 4-aminopyridine and 3,4-diaminopyridine on transmitter release at the neuromuscular junction. *J Pharmacol Exp Ther* 227: 260-5

Torres-Benito L, Neher MF, Cano R, Ruiz R, Tabares L. 2011. SMN requirement for synaptic vesicle, active zone and microtubule postnatal organization in motor nerve terminals. *PLoS One* 6: e26164

Torres-Benito L, Ruiz R, Tabares L. 2012. Synaptic defects in spinal muscular atrophy animal models. *Dev Neurobiol* 72: 126-33

Touroutine D, Fox RM, Von Stetina SE, Burdina A, Miller DM III, Richmond JE. 2005. *acr-16* encodes an essential subunit of the levamisole-resistant nicotinic receptor at the *Caenorhabditis elegans* neuromuscular junction. *J Biol Chem* 280: 27013-21

Tran TS, Kolodkin AL, Bharadwaj R. 2007. Semaphorin regulation of cellular morphology. *Annu Rev Cell Dev Biol* 23: 263-92

Trent C, Tsuing N, Horvitz HR. 1983. Egg-laying defective mutants of the nematode *Caenorhabditis elegans*. *Genetics* 104: 619-47

Trülzsch B, Garnett C, Davies K, Wood M. 2007. Knockdown of *SMN* by RNA interference induces apoptosis in differentiated P19 neural stem cells. *Brain Res* 1183: 1-9

Tsai LK, Yang CC, Hwu WL, Li H. 2007. Valproic acid treatment in six patients with spinal muscular atrophy. *Eur J Neurol* 14: e8-9

Turner RJ, Lovato M, Schimmel P. 2000. One of two genes encoding glycyl-tRNA synthetase in *Saccharomyces cerevisiae* provides mitochondrial and cytoplasmic functions. *J Biol Chem* 275: 27681-8

Turney SG, Lichtman JW. 2012. Reversing the outcome of synapse elimination at developing neuromuscular junctions *in vivo*: evidence for synaptic competition and its mechanism. *PLoS Biol* 10: e1001352

Tzeng AC, Cheng J, Fryczynski H, Niranjan V, Stitik T, *et al.* 2000. A study of thyrotropin-releasing hormone for the treatment of spinal muscular atrophy: a preliminary report. *Am J Phys Med Rehabil* 79: 435-40

Uhm CS, Neuhuber B, Lowe B, Crocker V, Daniels MP. 2001. Synapse-forming axons and recombinant agrin induce microprocess formation on myotubes. *J Neurosci* 21: 9678-89

Valori CF, Ning K, Wyles M, Mead RJ, Grierson AJ, *et al.* 2010. Systemic delivery of scAAV9 expressing SMN prolongs survival in a model of spinal muscular atrophy. *Sci Transl Med* 2: 35ra42

van Bergeijk J, Rydel-Konecke K, Grothe C, Claus P. 2007. The spinal muscular atrophy gene product regulates neurite outgrowth: importance of the C terminus. *FASEB J* 21: 1492-502

van Diemen HA, Polman CH, van Dongen MM, Nauta JJ, Strijers RL, *et al.* 1993. 4-aminopyridine induces functional improvement in multiple sclerosis patients: a neurophysiological study. *J Neurol Sci* 116: 220-6

Viollet L, Bertrandy S, Bueno Brunialti AL, Lefebvre S, Burlet P, *et al.* 1997. cDNA isolation, expression, and chromosomal localization of the mouse *survival motor neuron* gene (*Smn*). *Genomics* 40: 185-8

Vitte JM, Davoult B, Roblot N, Mayer M, Joshi V, *et al.* 2004. Deletion of murine *Smn* exon 7 directed to liver leads to severe defect of liver development associated with iron overload. *Am J Pathol* 165: 1731-41

Voigt T, Meyer K, Baum O, Schümperli D. 2010. Ultrastructural changes in diaphragm neuromuscular junctions in a severe mouse model for spinal muscular atrophy and their prevention by bifunctional U7 snRNA correcting *SMN2* splicing. *Neuromuscul Disord* 20: 744-52

Wadman RI, Vrancken AF, van den Berg LH, van der Pol WL. 2012. Dysfunction of the neuromuscular junction in spinal muscular atrophy types 2 and 3. *Neurology* 79: 2050-5

Wafford KA, Ebert B. 2006. Gaboxadol - a new awakening in sleep. *Curr Opin Pharmacol* 6: 30-6

Wagh DA, Rasse TM, Asan E, Hofbauer A, Schwenkert I, *et al.* 2006. Bruchpilot, a protein with homology to ELKS/CAST, is required for structural integrity and function of synaptic active zones in *Drosophila*. *Neuron* 49: 833-44

Wakasugi K, Schimmel P. 1999. Two distinct cytokines released from a human aminoacyl-tRNA synthetase. *Science* 284: 147-51

Wan L, Battle DJ, Yong J, Gubitz AK, Kolb SJ, *et al.* 2005. The survival of motor neurons protein determines the capacity for snRNP assembly: biochemical deficiency in spinal muscular atrophy. *Mol Cell Biol* 25: 5543-51

Wan L, Ottinger E, Cho S, Dreyfuss G. 2008. Inactivation of the SMN complex by oxidative stress. *Mol Cell* 31: 244-54

Wang B, Downing JA, Petocz P, Brand-Miller J, Bryden WL. 2007. Metabolic fate of intravenously administered N-acetylneuraminic acid-6-^{14}C in newborn piglets. *Asia Pac J Clin Nutr* 16: 110-5

Weihl CC, Connolly AM, Pestronk A. 2006. Valproate may improve strength and function in patients with type III/IV spinal muscle atrophy. *Neurology* 67: 500-1

Wen HL, Lin YT, Ting CH, Lin-Chao S, Li H, Hsieh-Li HM. 2010. Stathmin, a microtubule-destabilizing protein, is dysregulated in spinal muscular atrophy. *Hum Mol Genet* 19: 1766-78

Weng L, Hubner R, Claessens A, Smits P, Wauters J, *et al.* 2003. Isolation and characterization of chondrolectin (*Chodl*), a novel C-type lectin predominantly expressed in muscle cells. *Gene* 308: 21-9

Weng L, Smits P, Wauters J, Merregaert J. 2002. Molecular cloning and characterization of human chondrolectin, a novel type I transmembrane protein homologous to C-type lectins. *Genomics* 80: 62-70

Westlund B, Stilwell G, Sluder A. 2004. Invertebrate disease models in neurotherapeutic discovery. *Curr Opin Drug Discov Devel* 7: 169-78

White JG, Southgate E, Thomson JN, Brenner S. 1986. The structure of the nervous system of the nematode *Caenorhabditis elegans*. *Phil Trans R Soc Lond B* 314: 1-340

Winberg ML, Noordermeer JN, Tamagnone L, Comoglio PM, Spriggs MK, *et al.* 1998. Plexin A is a neuronal semaphorin receptor that controls axon guidance. *Cell* 95: 903-16

Winkler C, Eggert C, Gradl D, Meister G, Giegerich M, *et al.* 2005. Reduced U snRNP assembly causes motor axon degeneration in an animal model for spinal muscular atrophy. *Genes Dev* 19: 2320-30

Wishart TM, Huang JP, Murray LM, Lamont DJ, Mutsaers CA, *et al.* 2010. SMN deficiency disrupts brain development in a mouse model of severe spinal muscular atrophy. *Hum Mol Genet* 19: 4216-28

Witzemann V, Schwarz H, Koenen M, Berberich C, Villarroel A, *et al.* 1996. Acetylcholine receptor ε-subunit deletion causes muscle weakness and atrophy in juvenile and adult mice. *Proc Natl Acad Sci U S A* 93: 13286-91

Wolfe DL, Hayes KC, Hsieh JT, Potter PJ. 2001. Effects of 4-aminopyridine on motor evoked potentials in patients with spinal cord injury: a double-blinded, placebo-controlled crossover trial. *J Neurotrauma* 18: 757-71

Wood SJ, Slater CR. 2001. Safety factor at the neuromuscular junction. *Prog Neurobiol* 64: 393-429

Wood WB. 1988. The Nematode *Caenorhabditis elegans*. Cold Spring Harbor Laboratory Press, Cold Spring Harbor, NY, 12-13.

Wootz H, Enjin A, Wallen-Mackenzie A, Lindholm D, Kullander K. 2010. Reduced VGLUT2 expression increases motor neuron viability in *Sod1*^{G93A} mice. *Neurobiol Dis* 37: 58-66

Workman E, Kolb SJ, Battle DJ. 2012. Spliceosomal small nuclear ribonucleoprotein biogenesis defects and motor neuron selectivity in spinal muscular atrophy. *Brain Res* 1462: 93-9

Workman E, Saieva L, Carrel TL, Crawford TO, Liu D, *et al.* 2009. A *SMN* missense mutation complements *SMN2* restoring snRNPs and rescuing SMA mice. *Hum Mol Genet* 18: 2215-29

Wu ZZ, Li DP, Chen SR, Pan HL. 2009. Aminopyridines potentiate synaptic and neuromuscular transmission by targeting the voltage-activated calcium channel β subunit. *J Biol Chem* 284: 36453-61

Wu H, Xiong WC, Mei L. 2010. To build a synapse: signaling pathways in neuromuscular junction assembly. *Development* 137: 1017-33

Xie W, Nangle LA, Zhang W, Schimmel P, Yang XL. 2007. Long-range structural effects of a Charcot-Marie-Tooth disease-causing mutation in human glycyl-tRNA synthetase. *Proc Natl Acad Sci U S A* 104: 9976-81

Yang X, Arber S, William C, Li L, Tanabe Y, *et al.* 2001. Patterning of muscle acetylcholine receptor gene expression in the absence of motor innervation. *Neuron* 30: 399-410

Ymlahi-Ouazzani Q, O JB, Paillard E, Ballagny C, Chesneau A, *et al.* 2010. Reduced levels of survival motor neuron protein leads to aberrant motoneuron growth in a *Xenopus* model of muscular atrophy. *Neurogenetics* 11: 27-40

Zelensky AN, Gready JE. 2005. The C-type lectin-like domain superfamily. *FEBS J* 272: 6179-217

Zhang H, Xing L, Rossoll W, Wichterle H, Singer RH, Bassell GJ. 2006. Multiprotein complexes of the survival of motor neuron protein SMN with Gemins traffic to neuronal processes and growth cones of motor neurons. *J Neurosci* 26: 8622-32

Zhang HL, Pan F, Hong D, Shenoy SM, Singer RH, Bassell GJ. 2003. Active transport of the survival motor neuron protein and the role of exon-7 in cytoplasmic localization. *J Neurosci* 23: 6627-37

Zhang R, So BR, Li P, Yong J, Glisovic T, *et al.* 2011. Structure of a key intermediate of the SMN complex reveals Gemin2's crucial function in snRNP assembly. *Cell* 146: 384-95

Zhang Z, Lotti F, Dittmar K, Younis I, Wan L, *et al.* 2008. SMN deficiency causes tissue-specific perturbations in the repertoire of snRNAs and widespread defects in splicing. *Cell* 133: 585-600

Zhong Z, Ohnmacht J, Reimer MM, Bach I, Becker T, Becker CG. 2012. Chondrolectin mediates growth cone interactions of motor axons with an intermediate target. *J Neurosci* 32: 4426-39

Zhou Q, Kapoor M, Guo M, Belani R, Xu X, *et al.* 2010. Orthogonal use of a human tRNA synthetase active site to achieve multifunctionality. *Nat Struct Mol Biol* 17: 57-61

Appendix 1 - List of publications produced during the DPhil

Sleigh JN*, Grice SJ*, Davies KE, Talbot K. 2012. Spinal muscular atrophy at the crossroads of basic science and therapy. *Neuromuscul Disord* 23: 96. * Equal contribution

Sleigh JN, Buckingham SD, Esmaeili B, Viswanathan M, Cuppen E, Westlund BM, Sattelle DB. 2011. A novel *Caenorhabditis elegans* allele, *smn-1(cb131)*, mimicking a mild form of spinal muscular atrophy, provides a convenient drug screening platform highlighting new and pre-approved compounds. *Hum Mol Genet* 20: 245-60

Grice SJ*, **Sleigh JN***, Liu JL, Sattelle DB. 2011. Invertebrate models of spinal muscular atrophy: insights into mechanisms and potential therapeutics. *Bioessays* 33: 956-65. * Equal contribution

Sleigh JN, Gillingwater TH, Talbot K. 2011. The contribution of mouse models to understanding the pathogenesis of spinal muscular atrophy. *Dis Model Mech* 4: 457-67

Sleigh JN, Sattelle DB. 2010. *C. elegans* models of neuromuscular diseases expedite translational research. *Transl Neurosci* 1: 214-27

Under review

Bogdanik LP, **Sleigh JN**, Tian C, Samuels ME, Bedard B, Seburn KL, Burgess RW. Loss of *Lrsam1*, a Charcot-Marie-Tooth disease-associated E3 ubiquitin ligase, sensitizes peripheral axons to degeneration in mice. *Dis Model Mech*

Turner BJ, Alfazema N, Sheean RK, **Sleigh JN**, Davies KE, Horne MK, Talbot K. Neuronal overexpression of SMN slows symptom onset and motor neuron loss inmouse models of ALS. *Hum Mol Genet*

In preparation

Sleigh JN, Oliver PL, Iglesias AB, Biba A, Becker T, Becker CG, Davies KE, Talbot K. Chondrolectin isoforms differentially affect neuronal survival and outgrowth in *in vitro* and *in vivo* models of spinal muscular atrophy.

Grice SJ*, **Sleigh JN***, Motley WW, He W, Yang XL, Burgess RW, Liu JL, Talbot K, Cader ZM. A novel toxic gain-of-function from Charcot-Marie-Tooth neuropathy mutations, subverting neurodevelopmental pathways to neurodegeneration. * Equal contribution.

Seburn KL, **Sleigh JN**, Spaulding EL, Burgess RW. Synaptic transmission defects at the neuromuscular junction in a mouse model of Charcot-Marie-Tooth disease type 2D (CMT2D).